九州大学学術情報リポジトリ
Kyushu University Institutional Repository

MULTISCALE ENTROPY ANALYSIS OF BRAIN COMPLEXITY USING SIMULTANEOUS EEG AND fNIRS

アンスワッタナク, タナート

https://hdl.handle.net/2324/4060010

出版情報：Kyushu University, 2019, 博士（システム生命科学）, 課程博士
バージョン：
権利関係：

KYUSHU UNIVERSITY

MULTISCALE ENTROPY ANALYSIS OF BRAIN COMPLEXITY USING SIMULTANEOUS EEG AND fNIRS

THANATE ANGSUWATANAKUL

Graduate School of Systems Life Sciences

Kyushu University

2020

ACKNOWLEDGEMENT

My study would not have been possible without the permission and the scholarship from Rangsit University.

First and most of all, I would like to express my gratitude and appreciation to my main supervisor, Prof. Keiji Iramina, I wholeheartedly thank him for his constructive suggestions, patience, and persistent support throughout my Ph.D. study. The willingness to give his time so generously has been really appreciated.

I would also like to extend my appreciation to Assist. Prof. Dr. Boonserm Kaewkamnerdpong and Dr. Kajornvut Ounjai, for the research concept and professional guidance regarding the data analysis.

Words cannot describe my appreciation to my family whose love and guidance are with me all the time. I would also like to express my gratitude to them for their love and support.

I am also grateful to my best friends: Assist. Prof. Yutthana Pititeeraphab, Assist. Prof. Tasawan Puttasakul and Dr. Jamie O'Reilly for continuous encouragement throughout my Ph.D. journey. This accomplishment would not have been possible without them.

Nobody has been more important to me in the pursuit of this study than Assoc. Prof. Nuntachai Thongpance, Assoc. Prof. Dr. Manas Sangworasil and Dr. Thapanee Khemanuwong. Their encouragement has consistently pushed my spirits up every time I was down.

TABLE OF CONTENTS

Page

ACKNOWLEDGEMENT ..... *ii*

TABLE OF CONTENTS ..... *iii*

LIST OF TABLES ..... *vi*

LIST OF FIGURES ..... *vii*

ABSTRACT ..... *ix*

CHAPTER 1 INTRODUCTION *1*

1.1 Introduction 1

1.2 Electroencephalography (EEG) as Measurement for Brain Complexity 2

1.2.1 General Principles of EEG 3

1.2.2 EEG Application in the Study of Memory 3

1.3 Functional Near-Infrared Spectroscopy (fNIRS) as Measurement for Brain Complexity 4

1.3.1 General Principles of fNIRS 7

1.3.2 fNIRS Application in the Study of Memory 9

1.4 Potential Application in the Study of Memory 11

1.4.1 Short Term and Long Term Memory 12

1.4.2 Working Memory and Its Capacity 14

1.5 Statement of the Problems 18

1.6 Research Objectives 21

1.7 Research Questions 21

1.8 Research Hypothesis 21

1.9 Conceptual Framework 22

CHAPTER 2 MATERIALS AND METHODS *24*

2.1 Introduction 24

2.2 Participants 24

2.3 Experimental Paradigm 25
2.4 Scene UNderstanding (SUN) Database 27
2.5 Scene Recognition Test 28
2.6 Customised Cap for Simultaneous EEG-fNIRS Measurement 28
2.7 Brain Complexity 30
2.7.1 Entropy 32
2.7.2 Multiscale Entropy (MSE) 33
2.8 Statistical Analysis 36
2.8.1 Wilcoxon signed-rank test 36
2.8.2 Pearson's correlation coefficient 37
2.9 Conclusion 39
CHAPTER 3 RESEARCH FINDINGS *41*
3.1 Introduction 41
3.2 Demographic Information 41
3.3 EEG Results 44
3.3.1 Pre-Processing Analysis 45
3.3.2 EEG Complexity Analysis 50
3.4 NIRS Results 52
3.4.1 Pre-processing Results 53
3.4.2 NIRS Complexity Analysis 57
3.5 MSE Topography and Statistical Analysis 61
3.5.1 MSE Topography 61
3.5.2 Statistical Analysis: Wilcoxon signed-rank test 67
3.5.3 Statistical Analysis: Correlations Coefficient 72
CHAPTER 4 DISCUSSION AND CONCLUSION *78*
REFERENCES *82*

APPENDIX A Consent form *93*

APPENDIX B Averaging graph of MSE graph with standard error *95*

APPENDIX C Comparision MSE graph among four groups *111*

APPENDIX D Participants' MSE topography *127*

APPENDIX E The results of Wilcoxon's signed rank test from SPSS *143*

APPENDIX F The scatter plot matrix of the correlation *171*

APPENDIX G Brain areas and brain functions *187*

LIST OF TABLES

Page

Table 1.1 Summary of fMRI, fNIRS and EEG Brain Signals' Characteristics 19

Table 2.1 Selection criteria of participants 25

Table 3.1 Demographic information of participants 42

Table 3.2 Pictures viewed per participant 43

Table 3.3 Results of the Wilcoxon Signed – Rank Test 68

Table 3.4 Results of the Pearson Correlation 75

LIST OF FIGURES

Page

Figure 1.1 Changes in memory capacity with age 15

Figure 1.2 Conceptual Framework 22

Figure 2.1 Timing diagram and the sequence of stimuli 26

Figure 2.2 Examples of indoor and outdoor images from SUN database 27

Figure 2.3 Customised cap for simultaneous EEG-fNIRS measurement 29

Figure 2.4 Schematic illustration of the coarse-graining procedure for scales 2 and 3. 35

Figure 2.5 Interpretation of Pearson's correlation coefficient 38

Figure 3.1 EEG recording and analysis 45

Figure 3.2 EEG channel location mapping 46

Figure 3.3 ICA: Eye blink & Eye Movement 47

Figure 3.4 EEG signal before and after the artifacts removal 48

Figure 3.5 FIR digital bandpass filter, 0.5 – 30 Hz 49

Figure 3.6 EEG output after bandpass filtering 50

Figure 3.7 Comparison among MSE graphs 50

Figure 3.8 Comparison among MSE graphs, RR – RF – FR – FF, at F7 51

Figure 3.9 fNIRS recording and analysis 52

Figure 3.10 Decomposition of NIRS signal 55

Figure 3.11 Reconstruction of NIRS signal 55

Figure 3.12 Comparison of raw signal, reconstruction signal and baseline 56

correction signal 56

Figure 3.13 Comparison of NIRS data groups: RR, RF, FR, and FF 57

Figure 3.14 Results of Hb.O2 and Hb.R displayed in MSE fNIRS graphs 58

Figure 3.15 MSE fNIRS for Hb.O2 59

Figure 3.16 MSE fNIRS for Hb.R 59

Figure 3.17 Comparison of MSE fNIRS in Hb.R at F7 60

Figure 3.18 Topography of EEG 61

Figure 3.19 Topography of fNIRS in Hb.O2 62

Figure 3.20 Topography of fNIRS in Hb.R. 63

Figure 3.21 Topography of differential MSE EEG 64

Figure 3.22 Topography of differential MSE Hb.O2 65

Figure 3.23 Topography of differential MSE Hb.R 66

Figure 3.24 Scatter plot matrix for Correlation of RR group with sample size of 1,163 pictures 72

Figure 3.25 Scatter plot matrix for Correlation of RF group with sample size 348 pictures 73

Figure 3.26 Scatter plot matrix for Correlation of FR group with sample size 1577 pictures 73

Figure 3.27 Scatter plot matrix for Correlation of FF group with sample size 651 pictures 74

MULTISCALE ENTROPY ANALYSIS OF BRAIN COMPLEXITY

USING SIMULTANEOUS EEG AND fNIRS

ABSTRACT

This study aims to apply multiscale entropy (MSE) to analyse brain activity in terms of brain complexity levels and to use simultaneous EEG - fNIRS recordings for brain functional analysis. The memory task is selected for demonstrating the potential of this multimodality approach since memory is a highly complex neurocognitive process, and the mechanisms governing selective retention of memories are not fully understood by other approaches. In this study, fifteen healthy participants with normal colour vision participated in the visual memory task, in which involves the executive decision on remembering or forgetting the visual stimuli by his/her own will. In a continuous stimulus set, 250 indoor/outdoor scenes were presented at random, between periods of fixation on a black background. The participants were instructed to make a binary choice indicating whether they wished to remember or forget the image; both stimulus and response times were stored for analysis. The participants then performed a scene recognition test to confirm whether or not they remembered the images. The results of Wilcoxon signed rank test revealed that participants intentionally memorising a visual scene demonstrate significantly greater brain complexity levels in the prefrontal and frontal lobe than when purposefully forgetting a scene; $p < 0.05$ (two-tailed). According to Pearson Correlation analysis, there is no relationship between EEG and NIRS, whereas Hb.O2 and Hb.R were positively correlated ($p < 0.05$) meaning that these two methods can be used for brain signal recording without interfering with one another and therefore simultaneous EEG and

fNIRS is considered suitable for brain measurement. This suggests that simultaneous EEG and fNIRS can be used for brain functional analysis and MSE might be the potential indicators for this multimodality approach.

Keywords: brain complexity, electroencephalography (EEG), functional near-infrared spectroscopy (fNIRS), multiscale entropy (MSE), simultaneous EEG and fNIRS

CHAPTER 1

INTRODUCTION

1.1 Introduction

Each neuroimaging modality has its own peculiarities, pros and cons. For example, electroencephalography (EEG) gives high temporal resolution but low spatial resolution, whereas functional near-infrared spectroscopy (fNIRS) offers high spatial resolution but relatively low temporal resolution (compared with EEG). Furthermore, fNIRS does not suffer from electromyographic (EMG) and blink artifacts. Combining the two modalities of EEG and fNIRS is therefore a complementary approach for brain function analysis with the strengths of each method supporting the weaknesses of the other. The simultaneous acquisition of EEG and fNIRS may therefore provide a more complete picture of brain activity than either of the two individual modalities. fNIRS should not be considered as a competitor of EEG, but rather as a pooling modality for cases in which one technique is insufficient.

For an in-depth understanding and insight of what is happening inside the human brain, both high spatial and high temporal resolution are likely to be beneficial. Research studies combining simultaneous EEG-fNIRS to examine memory functions are scant. However, there are a handful of published studies using simultaneous EEG and fNIRS to assess visual memory function (Aghajani, Garbey, & Omurtag, 2017; Putze, Hesslinger, Tse, Huang, Herff, Guan, & Schultz, 2014; Zama, Takahashi, & Shimada, 2019) employed bimodal recordings of EEG and fNIRS to measure and discriminate among levels of mental workload; reporting promising results for the accurate quantification of mental workload in real-world settings. In addition, Sun et

al. (2015) proposed a multimodal approach to evaluate EEG and fNIRS signals for affective state detection. Their results indicated that simultaneous EEG and fNIRS improves performance over fNIRS or EEG only. Despite using bimodal recordings of EEG and fNIRS, neither of these studies have explored the application of multiscale entropy (MSE) for signal analysis.

1.2 Electroencephalography (EEG) as Measurement for Brain Complexity

In general, EEG is regarded as a non-invasive, functional neuroimaging technique (Maturana-Candelas, Gómez, Poza, Pinto, & Hornero, 2019), which consists of measuring electrical activity from the brain using electrodes placed on the scalp. This has been applied widely in order to investigate neural activity underlying these processes. Since EEG can measure brain activity with high temporal resolution, it is suitable for capturing dynamic brain activity. Recording EEG remains the most effective technique for observing near-instantaneous neural responses to visual stimuli (Lin et al., 2010).

Furthermore, EEG devices are inexpensive and robust for the measurement of brain activity (Ullah, Ali, Rizwan, & Imran, 2011). However, the fundamental limitation of EEG is low spatial resolution due to the diffusion of electrical signals travelling between their intracranial source and electrodes on the scalp. The inverse square law of electric fields also limits the influence of sub-cortical structures on EEG waveforms. Generally, theta (4–7 Hz) and alpha (8–12 Hz) frequency ranges are dominant during working memory tasks (Moran, Campo, Maestu, Reilly, Dolan, & Strange, 2010). Increases in theta range spectral power have been associated with increasing difficulty of memory tasks (Scheeringa, Petersson, Oostenveld, Norris, Hagoort, & Bastiaansen, 2009).

In addition, Zhang et al. (2016) evaluated the modulation effects of mental workload on functional connectivity and found sustained and load-dependent theta power enhancement in the frontal midline region. In addition, Teng et al. (2018) compared EEG recorded during resting and active stages in elderly people, and they found that beta spectral power significantly decreased. This change may be a reflection of age-related changes in memory.

1.2.1 General Principles of EEG

The frequently used electroencephalography (EEG) primarily measure synchronous activation of a large population of neurons such as pyramidal cells, oriented perpendicularly to the scalp surface in response to exogenous stimulation.

Despite having several advantages, EEG methods present some limitations. One major limitation is that only scalp signals can be detected. These signals correspond to the integrated activity of various generators such as excitatory and inhibitory. In fact, the electric field recorded on the scalp cannot be used to discriminate the different generators. For this reason, several square centimetres of brain tissue must synchronously be activated to generate a signal that can be recorded at the scalp surface.

1.2.2 EEG Application in the Study of Memory

As mentioned above, EEG is regarded as one of neuroscientific methodologies used to gather electromagnetic signals and to measure electrical activity in the brain by using electrodes attached to the scalp. EEG has been commonly used for memory measurement, particularly to understand the neural activities during the working memory (WM) processes (Gevins, Smith, McEvoy, & Yu, 1997). Among the different

brain imaging techniques, EEG is considered as having an excellent temporal resolution, but a poor spatial one.

Since EEG can measure brain activity with high temporal resolution, it is suitable for capturing temporal changes in brain activity. Thus, with the use of EEG, it is possible to receive immediate feedback to visual stimuli (Lin et al., 2010). EEG devices are inexpensive and robust for the measurement of brain activity (Ullah, Ali, Rizwan, & Imran, 2011). Generally, theta (4–7 Hz) and alpha (8–12 Hz) frequencies are dominant during the working memory tasks. It was reported that the theta frequency shows an increase in power associated with a higher level of working memory tasks (Moran et al., 2010).

With reference to Zhang, Zhao, Bai, and Tian (2016), they evaluated the modulation effects of WM load on the functional connectivity of WM and found sustained and load dependent theta power in the frontal midline region throughout the WM delay period. In addition, Teng et al. (2018) investigated the brain activity for both resting state and task state. They found that EEG significantly decreased in beta band in the elderly people during the WM task.

To sum up, EEG measures the neural activities with an excellent temporal resolution (within a millisecond range), but suffers from poor spatial resolution due to volume conduction, thereby resulting in resolution limits in source localisation.

1.3 Functional Near-Infrared Spectroscopy (fNIRS) as Measurement for Brain Complexity

Functional near-infrared spectroscopy (fNIRS) is a promising tool for monitoring metabolic changes in the brain with good spatial but low temporal resolution as a result of the inherent hemodynamic delay. fNIRS is more robust when

confronted with electrical noise and motion-based muscle activity artifacts than EEG; consequently, it can be a practical alternative to EEG in a noisy environment (Shin et al., 2018). Additionally, fNIRS takes advantage of living tissue's particular absorption properties in the near-infrared range to measure changes in the local concentrations of oxy-haemoglobin (Hb.O2) and deoxy-haemoglobin (Hb.R) through the intact skull (Ranger, Johnston, Limperopoulos, Rennick, & du Plessis, 2011).

Near Infrared Spectroscopy (NIRS) is a relatively recent invention compared with EEG. It was developed in 1992 and presently multi-channel systems are commercially available (Ferrari, & Quaresima, 2012). As a neuroimaging tool, fNIRS offers a number of advantages. For example, it is non-invasive, easy to set up and does not require a large space (Ye, Tak, Jang, Jung, & Jang, 2009). Moreover, it offers a reasonable trade-off between temporal and spatial resolution (Huppert, Diamond, Franceschini, & Boas, 2009) improving on the spatial resolution of EEG. This method is also safe for use with neonates (Brooksby et al., 2005) and can be applied to observe brain function over extended periods.

To perform fNIRS, two near-infrared lights (650 and 1000 nm) are emitted through the scalp. Photodetectors track the diffusion of NIR light energy through the underlying brain tissue by measuring light intensity. This measurement relies on the absorption of light and light-scattering properties of the tissue. Changes in the metabolic activity of the brain induce haemodynamic responses that alter the rate of NIR light absorption. This influences the level of NIR light intensity measured, which provides an index of Hb.O2 and Hb.R concentrations (Bozkurt, Rosen, Rosen, & Onaral, 2005; Quaresima, Bisconti, & Ferrari, 2012). These are related to local neural function and the presumed cause of metabolic demand.

Functional near-infrared spectroscopy (fNIRS) was used by Borfeld et al. (2007) to study brain activity in infants. They found hemispheric asymmetry in the level of Hb.O2, with the left more active while the infants were watching an animation with speech. Schroeter et al. (2004) investigated brain functions during a Stroop test using fNIRS. They found a left-lateral difference in the haemodynamic responses of the prefrontal cortex that emerged with age.

Araki et al. (2015) used fNIRS to analyse brain function in children diagnosed as hyperactivity disorder in response to treatment with atomoxetine. Levels of Hb.O2 showed a significant decrease in the left ventrolateral prefrontal cortex. This neuroimaging modality has also been applied to investigate changes in brain activity following rehabilitation therapy in stroke patients.

According to Schreppel et al. (2008), fNIRS has been widely used to investigate the neural responses. They identified changes in several brain regions, including prefrontal cortex, occipital region, parietal regions and medial temporal areas. Using fNIRS, it has been found that differences in brain activity of the frontal cortex depend on the level of difficulty of tasks (Molteni et al., 2012). Additionally, Hb.O2 concentration during difficult tasks changes more when compared with easy tasks. This has been confirmed by research including a study by Sasabe and Hagiwara (2018), which characterised and compared oxygenated haemoglobin concentration changes in the brain using fNIRS measurements. Their analysis demonstrated a significant correlation between the number of false answers and the integral of Hb.O2, suggesting that Hb.O2 increases with task difficulty level.

Mirelman et al. (2014) also found a difficulty-related increase in frontal brain activity while doing two tasks during walking. Increased Hb.O2 in the frontal cortex

was maximal while the participants were walking and serially subtracting 7s followed by walking while counting forward, then the lowest while the participants were walking or standing without performing mental calculations. These kinds of studies rely on well-defined and separable task difficulties; if tasks are ill-defined or too similar, the analysis may be obscured.

1.3.1 General Principles of fNIRS

In general, fNIRS is used to measure changes in brain hemodynamics. It is performed by emitting near-infrared light into the scalp and detecting the transmitted light at certain positions. The difference between the emitted and received light intensities (due to absorption and scattering of photons) is determined by the tissue concentrations of Hb.O2 and Hb.R, and indirectly reflects brain activity (Yücel, Selb, Huppert, Franceschini, & Boas, 2017).

Furthermore, fNIRS emits two near-infrared lights, 650 – 1000 nm, to the brain and measures the diffusion of the NIR lights from brain tissue in terms of light intensity. The diffusion lights are reliant on absorption of light and light scattering in the brain. While the brain is activated, the hemodynamic changes during the activation time. That is why the intensity of the NIR lights can be changed. The changes of NIR light intensity can show the neural activity affecting Hb.O2 and Hb.R concentrations (Brooksby et al., 1990). As a visual measurement and non-invasive device, it is clearly safe and can be used with neonate to observe brain functions for a long period of time (Bozkurt, Rosen, Rosen, & Onaral, 2005).

As described previously, fNIRS suffers from a certain degree of errors in depth resolution. This is due to diffused transmission of light in NIR spectrum. This diffused transmission is the result of multiple scattering in tissue, which is generally contributed

to lipids and cellular organelles like mitochondria (Cope, 1991). Scattering phenomena can be concisely described as a result of macroscopic refractive index mismatch. Spectroscopy in the near infrared, used for measurement of changes in cerebral hemodynamic properties is done by emitting near infrared light into the scalp and receiving the transmitted part at certain positions (Haeussinger et al., 2011). The difference between emitted and received light intensities (due to absorption and scattering of photons) is determined by the difference in tissue concentration of the chromophores of interest, namely (Hb.O2) and (Hb.R) and reflects indirectly the actual activity of the brain.

It is generally accepted that the neuronal activity resulted from a sequence of events, commonly referred to as neurovascular coupling, produces changes in blood flow and oxygen consumption. The hemodynamic changes in the brain function region with increased neural activities are based on the assumption that the increase in blood flow associated with the increases in blood volume. In the meantime, more Hb.O2 can be carried into the nearby capillaries and veins while Hb.R is being washed out. The brain activities detected by fNIRS are often referred to assess the level of increase in Hb.O2 and decrease in Hb.R in the capillaries. Measuring the NIR light diffusely transmitted through tissue allows the mapping of hemoglobin changes associated with brain activities (Kim, Seo, Jeon, Lee, & Lee, 2017).

It should be noted that fNIRS provides some advantages that make it well situated to investigate the effects of physical activity on cognitive performance and cerebral oxygenation or hemodynamics. According to the advantages of fNIRS compared to other neuroimaging techniques such as fMRI and PET, fNIRS is considered as non-invasiveness; relatively good spatial ($\approx$ 1.0 – 3.0 cm) and temporal resolution (generally up to 10 Hz) (Herold, Wiegel, Scholkmann, & Mueller, 2018).

With a low noise level during operation, it also provides robustness against motion artifacts as well as the opportunity to conduct repeated measures in short time intervals (Bunce, Izzetoglu, Izzetoglu, Onaral, & Pourrezaei, 2006).

In contrast to EEG or a signal generated intrinsically by neurons, fNIRS measures changes in emitted light intensity after passage through a tissue of interest. These changes are due to absorption and scattering by local microvascular, Hb.O2 and Hb.R concentration variations in response to neuronal activation. Due to refraction, transmission of a light wave through a tissue can be described as a diffusion process, which occurs in all directions.

1.3.2 fNIRS Application in the Study of Memory

Encrypting, storage and retrieval comprise three fundamental stages in information processing and memory. They allow for the formation of new memory traces, the maintenance and the consolidation of these traces over time. Near Infrared Spectroscopy (NIRS) was developed to be fNIRS in 1992 and presently become multi-channel systems (Ferrari & Quaresima, 2012). Functional near-infrared spectroscopy (fNIRS) is a neuroimaging tool that offers a number of advantages. For example, it is non-invasive, easy to set up and does not occupy a large space (Ye, Tak, Jang, Jung, & Jang, 2009), high temporal resolution in addition to acceptable in spatial resolution (Huppert, Diamond, Franceschini, & Boas, 2009).

In many studies, fNIRS has been used for analysing brain functions and measuring brain activities. For example, Bortfeld, Wruck, and Boas (2007) studied brain activities in infants with NIRS. The Hb.O2 of left temporal region increased higher than the right side when infants watched animation with speech.

Schroeter et al. (2004) observed brain functions during the Stroop task with fNIRS. They found that the hemodynamic responses are different in left lateral prefrontal cortex with age. Araki et al. (2015) used fNIRS to analyse brain functions in AD/HD children for training and long-term treatment with atomoxetine. According to Hb.O2, the results showed a significant decrease in the left ventrolateral prefrontal cortex.

For rehabilitation task, fNIRS is also useful for measuring brain activities and brain imaging when stroke patients are treated with motor rehabilitation (Lin, Lin, Penney, & Chen, 2009). Lin et al. (2009) confirmed the consistent finding by fNIRS with fMRI and also reported that the brain activation measured by fNIRS based on the changes of Hb.O2 was more sensitive to detect brain activity compared to those from the BOLD signal of fMRI.

According to Schreppel et al. (2008), fNIRS has been widely used for memory measurement. It is supported by a study of Basso Moro, Cutini, Ursini, Ferrari, and Quaresima, (2013). Using a 16-channel fNIRS system, they examined human brain activation in the areas of the prefrontal cortex (PFC) during the encoding and retrieval processes (EP and RP, respectively) of 13 healthy participants while performing the "Logical Memory Test" (LMT) of the Wechsler Memory Scale. The results showed a heterogeneous Hb.O2 and Hb.R response over the mapped area during the EP and the RP, with a Hb.O2 progressive and prominent increment in ventrolateral PFC (VLPFC). This study has demonstrated that fNIRS has the potential to be adopted in patients with working memory deficits.

In terms of memory analysis with fNIRS, it is found that the difference of the brain activity in frontal cortex depends on a level of difficulty (Molteni et al., 2012).

In healthy people, the brain is more activated by difficult tasks. Additionally, Hb.O2 concentration during difficult tasks changes to a higher level when compared to easy tasks. To observe brain functions and activities from Hb concentration level, it requires the graph of Hb concentration of each participant. Therefore, it is applicable for different tasks especially a comparison between difficult and easy tasks, but worse if tasks are similar. This has been confirmed by several research studies such as a study of Duann et al. (2009) who studied brain frontal cortex activation during identification. The Hb.O2 concentration becomes greater while participants identify fragmented-letter than complete-letter.

Additionally, Mirelman et al. (2014) found an increase of frontal brain activation when doing two tasks while walking. The increased concentration of Hb.O2 in frontal cortex during walking while serially subtracting 7s was the highest level followed by walking while counting forward and the lowest level when walking or standing without mental calculation.

1.4 Potential Application in the Study of Memory

Memory plays a crucial role in human life and intimately involves a process of meaning-making by linking past, present, and future episodes that are differentially constructed in each individual. Memory can be classified into long-term memory and short-term, also called working memory (Morris & Jones, 1990). Long-term memory, in which informative knowledge is held indefinitely, encrypts information semantically for storage. In contrast, short-term memory, stores information for a short period of time and is generally used for fast response activities. Short-term or working memory is the cognitive system that holds and processes information.

Simply put, it is how the mind temporarily manipulates and stores information during tasks that require background knowledge and thinking processes. It has been investigated in previous functional neuroimaging studies, which identified the prefrontal cortex (PFC) as the most relevant area of activation (Braver et al., 1997). In vision, the information needs to enter working memory before being stored into long-term memory. Memory also changes through time; some grow stronger and last, whereas others fade.

Memories, regarded as the melodies of life are cognitive activities associated with the ability to manipulate and store information. It is therefore considered as central to the functioning of the mind, involved with general abilities and outcomes such as intelligence and educational attainment and linked to sensory processes (Lindenberger & Baltes, 1994).

1.4.1 Short Term and Long Term Memory

The formation of a memory begins with the registration of information in the brief sensory stage. A sensory memory then allows a perception such as a visual pattern for a short period when the stimulation is finished. After that, the first flicker is stored in short-term memory, which has a limited capacity. To put it clearly, it can hold about seven items for approximately 10 or 30 seconds at one time (Bauer, 2015). Once a memory is formed, it will be manipulated as a sort of filter and first stored in the sensory stage; then in short-term memory; and ultimately, for some memories, in long-term memory. The different phases of human memory function helps to protect us from the flood of information or too much information and retain only the important information in long-term memory.

Human memory is ultimately associative, meaning that a new piece of information is better recalled to be known information when associated with background knowledge. Known information is gradually transferred from short-term memory into long-term memory. The more the information is repeated, the more likely it is to be retained in long-term memory (Cowan, 2008).

Long-term memory is referred to the storage of information over an extended period (Shiffrin, & Atkinson, 1969). In fact, long-term memory is basically the way the mind stores information over a long period of time. From a practical perspective, anything that we remember from more than a few minutes ago is presently kept in our long-term memory. Short-term memory, however, operates in seconds, not minutes. Obviously, a general disagreement may occur that minutes are not considered as a long period. However, the information is stored in the same way that our memories from long time ago have been stored. Simply put, all of long-term memories are stored without being aware of it. They are also part of working memory, or things that can be recalled afterwards. The more certain information is emphasized, the easier it will be to recall that information from long-term memory. Short-term memories can become long-term memory via consolidation, in which we review what we have engaged in that memory and make significant associations between that information stored in long-term memory.

Unlike WM and short-term memory, which are limited and decline rapidly, long-term memory is able to store unlimited amount of information for an indefinite period (Hochreiter & Schmidhuber, 1997). It is generally accepted that people tend to easily manipulate and store known information since this kind of information has more meaning to them. Apart from that, it can be mentally connected to known information in their long-term memory.

1.4.2 Working Memory and Its Capacity

Working memory (WM) is an individual's ability to concurrently manipulate some information while retaining other information (Baddeley, 1986). In the notion of memory consolidation, WM is easily interrupted until it has been stored in long-term memory (Carruthers, 2013). Only a small number of WM memories are consolidated (Nadel & Hardt, 2011), and this depends on the level of stimulation and attention, all of which are related to the personal significance of the information. After consolidation process, it is able to stay permanently, although the ability to retain depends on several factors especially how often it is retrieved and recalled.

It is generally accepted that each individual may have a different personal limit to working memory capacity and it lies in one's power with age during childhood. To put it simply, adults may have a greater fixed capacity whereas young children may not. For instance, Sweeny, Wurnitsch, Gopnik, and Whitney (2015) showed that adults' capacities are estimated to almost double when compared to that of 4-year-old children. A precise activity may therefore be accomplished in direct association with an individual but exceed that of the others.

Furthermore, WM capacity increases with age during childhood. Young children typically have very small abilities that increase gradually until the teenage years, when adult capacities are reached that are more than double that of 4-year-old children. The growth curve of individuals with average and low WM capacities for their age is shown in Figure 1.1.

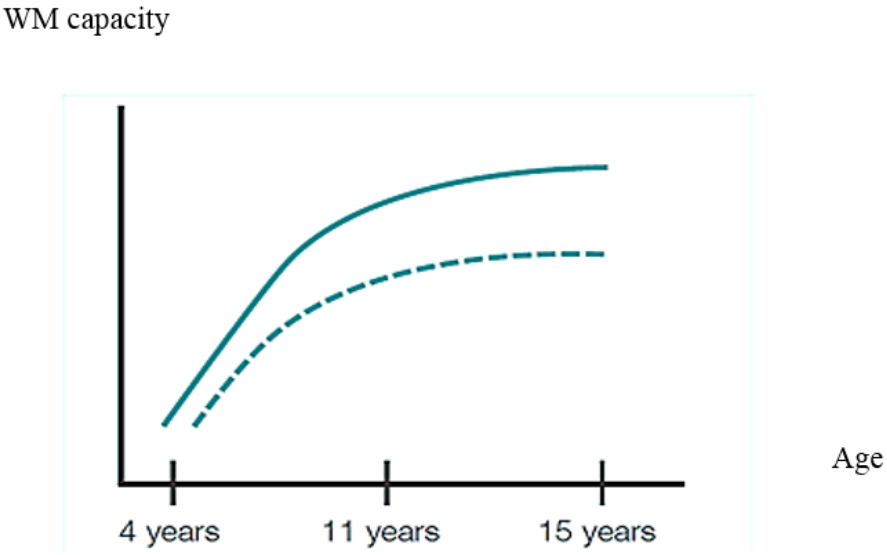


Figure 1.1 Changes in memory capacity with age

Note: This figure is adopted from Gathercole and Alloway (2007).

As shown above, the changes in working memory capacity with age for an average child are presented by the solid line. The broken line represents scores of a child with a low WM capacity.

The growth lines also indicate that, typically, individuals who have poor WM capacities in childhood do not catch up with those of their peers. Although their WM capacities increase with age, they do not demonstrate the same rate when compared to others. For this reason, when they grow older, they will lag behind.

Individual differences in working memory capacity appear to arise significantly between different children of the same age (Sarigiannidis, Crickmore, & Astle, 2016). According to their study, a typical class of 30 children aged 7 to 8 years exhibited poor performance in WM tasks. In agreement with a study of Fitamen, Blaye, and Camos (2019), to some extent, individuals who have poor WM capacities in childhood will not be able to catch up with those of their peers.

In terms of individual difference related to age, many studies indicate age-related declines in WM. For instance, a study of Bopp and Verhaeghen (2007) described moderate to large negative correlations between WM and age. WM rises steadily up to adolescence and then it begins to level off after the age of twenties (Lambek & Shevlin, 2011). The decline appears to be linear with a continuous rate beginning in the twenties, and provides compelling evidence that no sharp decline in old age (Borella et al., 2008).

However, no consensus in the field exists when it comes to the relationship between gender and WM performance. For example, Schmidt et al. (2009) found no difference in accuracy, speed and brain complexity between men and women when completing a verbal n-back task. In a study of Alloway, Gathercole, and Pickering (2006), they explored the structure of verbal and visuospatial short-term and working memory in children between ages 4 and 11 years using multiple tasks to measure memory components underlying WM and found no gender differences in any of the tasks. Their study is in good agreement with Nagel, Ohannessian, and Cummins (2007), in which they reported no difference at all between genders. In addition, Redick et al. (2012) indicated little to no evidence of gender difference found in a large sample analysis using automated complex span tasks. Their findings are in line with a study of Robert and Savoie (2006) that it is difficult to determine the difference between genders on WM performance. They argued that if a difference does exist, it would be most likely biological in origin.

To sum up, WM capacity increases throughout childhood and decreases after the age of twenties onwards. Such a growth is regarded as a major source of cognitive development and appears to be the root cause of the capacity limit of WM. Throughout childhood, different factors have been stated as the potential sources of WM

development. Consequently, changes in the speed of forgetting and of the size due to the focus of attention, acquisition, brain stimulation and maintenance of WM strategies have been suggested as in a study of Blasiman and Was (2018) in which the twenty-one factors influencing WM and may possibly underpin working memory development.

It would be beneficial to highlight that different techniques have been carried out to understand the neuronal mechanism behind WM capacity. Most of them are based on non-invasive neuroimaging modalities such as fNIRS, fMRI, EEG and MEG, which mainly employ each modality one at a time, called standalone processes. For instance, Aghajani, Garbey, and Omurtag (2017) measured mental workload with EEG and fNIRS and found different patterns between EEG and NIRS data during a working memory task. The results revealed that EEG results from the electrical activity of cortical and subcortical neurons with a submillisecond temporal resolution. On the other hand, NIRS yields local measures of changes in Hb.O2 and Hb.R concentration and is, therefore, an indicator of metabolic changes associated with neural activity. Furthermore, the physics of measurement behind EEG and NIRS are somewhat different; the property of EEG signal makes itself prone to blink and muscle artifacts whereas fNIRS is more tolerant to eyeblink artifacts.

In addition, Liu et al. (2017) used a 16-optode continuous wave fNIRS system developed at Drexel University covering the forehead and 28 EEG sensors at the standard 10/20 sites, with 16 participants performing a n-back task. They found significant correlations between working memory load and some EEG frequency band powers along with Hb.O2 and Hb.R.

1.5 Statement of the Problems

It is known from the literature that among the existing human neuroimaging techniques, some have higher spatial but lower temporal resolution whereas others have higher temporal but lower spatial resolution. Therefore, the integration of multiple measurement strategies known as a simultaneous EEG and fNIRS may have the potential to maximize both spatial and temporal information.

This measurement gains much research interest since both recording procedures share similar advantages as follows:

First, EEG and fNIRS technologies are robust against motion artifacts and do not impose remarkable physical constraints; therefore, being practical to use for a wide range of age such as from infants to elderly people (Quaresima, Bisconti, & Ferrari, 2012).

Second, EEG and fNIRS do not involve exposure to high-intensity magnetic fields (>1 T) (Chiarelli, Zappasodi, Di Pompeo, & Merla, 2017).

Third, their hardware costs are considerably lower when compared to those of other functional brain imaging modalities such as fMRI (Lystad & Pollard, 2009). Furthermore, regarding operating costs for patients in particular, both EEG and fNIRS are considered much cheaper when compared to fMRI (Zhang, Yao, Wang, Monaghan, & Mcalpin, 2019).

Finally, it is beneficial to integrate EEG and fNIRS recordings since these two methods are able to measure signals derived from brain activity without interfering with one another (Zama, Takahashi, & Shimada, 2019). A summary of fMRI, fNIRS and EEG brain signals' characteristics is shown in Table 1.1 below.

Table 1.1

Summary of fMRI, fNIRS and EEG Brain Signals' Characteristics

Signals	**EEG**	**fNIRS**	**fMRI**
Risk	low	low	low
Temporal resolution	high	low	low
Spatial resolution	low	mediate	high
Characteristic	electrical	optical	metabolic
Portability	high	high	low
Cost	low	low	high

Note: Table 1.1 is adopted from a study of Zhang, Yao, Wang, Monaghan, and Calpine (2019).

Although EEG and fNIRS seem promising and share some similarities as mentioned above, these two signals are somewhat different. It is generally accepted that fNIRS estimates brain hemodynamic fluctuations relying on spectroscopic measurements, whereas EEG captures the macroscopic temporal dynamics of brain electrical activity through passive voltages evaluations.

To put it clearly, on the one hand, fNIRS can assess the oxygenation status and hemodynamics of the brain non-invasively. Brain activity is therefore measured in real-time based on changes in blood oxygenation.

On the other hand, EEG is regarded a fast signal whereas NIRS is considered as a slow signal. Thus, EEG measures the electrical activity of the brain and provides high temporal resolution.

Despite the fact that a simultaneous measurement of the EEG and NIRS has generated recent research interest (Al-shargie, Tang, Badruddin, & Kiguchi, 2015), up to this date, only few studies have addressed the possibilities of recording NIRS with their EEG counterpart simultaneously.

The reason behind this may be due to the different characteristic of EEG and NIRS signals. Electrical brain activity and its hemodynamic counterpart may not have

a perfect spatiotemporal correspondence (Chiarelli, Zappasodi, Di Pompeo, & Merla, 2017).

Previous work has therefore preferred to only EEG or NIRS measurement and analysis despite using the same experimental paradigm. Up to that time, EEG and NIRS signals were calibrated and analysed using different methods due to the different scale of temporal resolution (Korhonen et al., 2014).

Moreover, regarding the measuring instrument in particular, there is the limitation to measure simultaneous EEG and NIRS signals using one single device.

The challenging stage of this study is the process of combining multiple brain monitoring techniques known as a simultaneous EEG and fNIRS, which is able to measure the fast EEG signal and the slow NIRS signals using a customized cap. EEG technology with international 10/20 system is required the positions to place the electrodes. These positions could generally overlap with the positions of the fNIRS optodes when measuring with the traditional devices. Consequently, instead of positioning these electrodes and optodes next to each other in different spots, this study aimed to measure the exact same spot or channel location.

With different perspectives as discussed above, a drive in the present study is to determine the potential of the use of simultaneous EEG and fNIRS for visual working memory and to examine the effectiveness of the application of multiscale entropy (MSE) for analysing brain activity in terms of entropy levels.

The contribution of this study can also bring an insight into brain complexity measurement and analysis, which increases accuracy on the neural measurement.

1.6 Research Objectives

The objectives of this study are as follows:

1. To determine the potential use of simultaneous EEG and fNIRS for recording brain activity.
2. To apply multiscale entropy (MSE) in analyzing brain activity for entropy levels or brain complexity levels.

1.7 Research Questions

Specifically, this study sought answers to the following questions:

1. Does simultaneous EEG and fNIRS have the potential use for recording brain activity?
2. Can the application of multiscale entropy (MSE) be applied in analyzing brain activity for entropy levels or complexity levels?

1.8 Research Hypothesis

The present study focuses on examining brain activity using simultaneous EEG-fNIRS data recorded during a behavioural task. Multiscale entropy (MSE) is then applied to analyse these signals in terms of entropy or brain complexity levels. Brain complexity is considered as interesting characteristic since the dynamics of brain activity can illustrate task-related functions.

In this study, a pooling of bioelectricity (EEG) and haemodynamic (fNIRS) signals was used to measure different perspectives of brain complexity. The scale of data measurement was also adjusted to be consistent with the entropy scale.

The main aim of the present study is to apply MSE as a new feature for EEG and fNIRS analysis in the aspects of brain complexity levels. A null hypothesis is formulated as follows:

H_0: there is no statistically significant difference in the participants' responses on pictures with visual stimuli between MSE analysis of EEG – fNIRS measurements.

1.9 Conceptual Framework

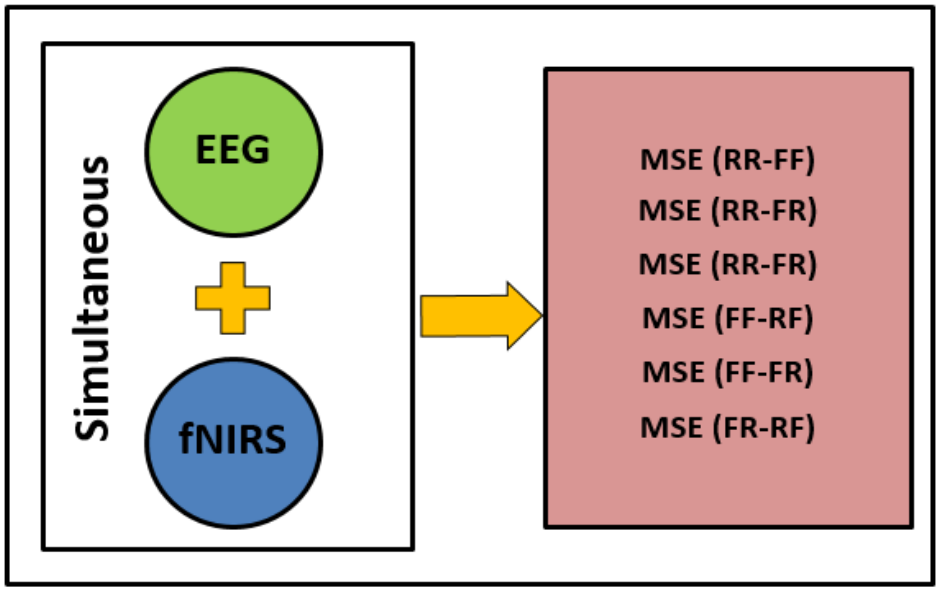


Figure 1.2 Conceptual Framework

The present study employed the Wilcoxon signed-rank test, a non-parametric statistical technique, to compare a repeated measurement in one sample group for determining a significant difference in mean rank of each pair (i.e., RR-FF, RR-FR, RR-RF, FF-FR, FF-RF, and FR-RF).

Sample size in this study is small (less than 30) so that an assumption of normal distribution is impossible to be met. For this case, the use of the Wilcoxon signed-rank

test, which is a substitution of paired sample t-test in parametric statistics, is therefore considered as a suitable method of data analysis.

As shown above, this study is based on two nominal variables, that is, whether the participants remembered or forgot each visual stimulus tasks (the experiment and the scene recognition test), and one measurement variable (simultaneous EEG and fNIRS). A level of difference in median was significant at zero ($W = 0$, $p < 0.05$).

CHAPTER 2

MATERIALS AND METHODS

2.1 Introduction

One of inspiring tasks in neuroscience is investigating the brain complexity. This task can be effectively addressed by applying various methods assimilated into a multimodal approach because each method has its pros and cons, but helps to explain certain aspects of brain complexity during processing information. These methods, for example, provide information about changes in electrical and hemodynamic activities.

In the present view, a simultaneous EEG and fNIRS is used to provide a better understanding of the mechanisms involved in cerebral activation. Materials and methods used in this study are described as follows.

2.2 Participants

The participants of this study were 12 males and 3 females aged from 20 to 30 years old males: (M=25.08, SD=2.19); females: (M=25.00, SD=1.00), all were students of different ethnicities (e.g. Japanese, Chinese, Thai and Indonesian). The participants had self-reported right handed, normal colour vision with no prior memory disorders and no history of mental illness or sustained physical illness. In line with the study of Alloway, Gathercole, and Pickering (2006), in which they reported that gender differences do not affect memory performance, this was not considered an exclusionary criterion.

Concerning the relationship between memory function and age, Lambek and Shevlin (2011), suggested that memory growth is constant and begins to level off at

the age of twenty. Memory function is also known to decline in later life. Thus, the participants within the age range of 20 to 30 years were considered for this study. The participants signed on the informed consent before the experiment and participated in this study voluntarily.

In compliance with ethics approval by the Faculty of Information Science and Electrical Engineering, Kyushu University (approval number: ISEE-H26-03), all participants were required to inform consent prior to engaging in the experiment.

The experimental period was two months with permission from the university. Careful experimental procedure is essential to the reliability of research. The participants were selected based on a purposive sampling method with the following criteria shown in Table 2.1.

Table 2.1
Selection criteria of participants

Criteria
1. Range of age between 20-30
2. Normal colour vision
3. No prior memory disorders
4. No history of mental illness or sustained physical illness

2.3 Experimental Paradigm

Prior to the experiment, the participants were given the task-specific instructions along with a brief practice session to minimise their bodily and eye movements from the start until after the response. In line with a study by Yoo and Chung (2005), the participants were seated in a comfortable height-adjustable chair,

which was at a distance of approximately 50 cm away from the centre of computer screen so that their eyes were positioned directly in front of the fixation cue. The participants put their index finger on numeric keypad buttons fixed to the right armrest. They were instructed to keep their eyes on the monitor and refrain as much as possible from moving their body throughout the data recording.

All stimuli were presented on a computer screen for 3 seconds surrounding fixation with black-colour background for 9 seconds. During this period, the participants were instructed to make a two-choice manual response using the index finger to each test stimulus. They were required to press the left button designated ‘‘Remember’’ when they believed the test item was part of the memory set and would like to remember, correspondingly, press the right button designated ‘‘Forget’’ when they believed the test item was not part of the memory set and would like to forget. The timing diagram and the sequence of stimuli was shown in Figure 2.1.

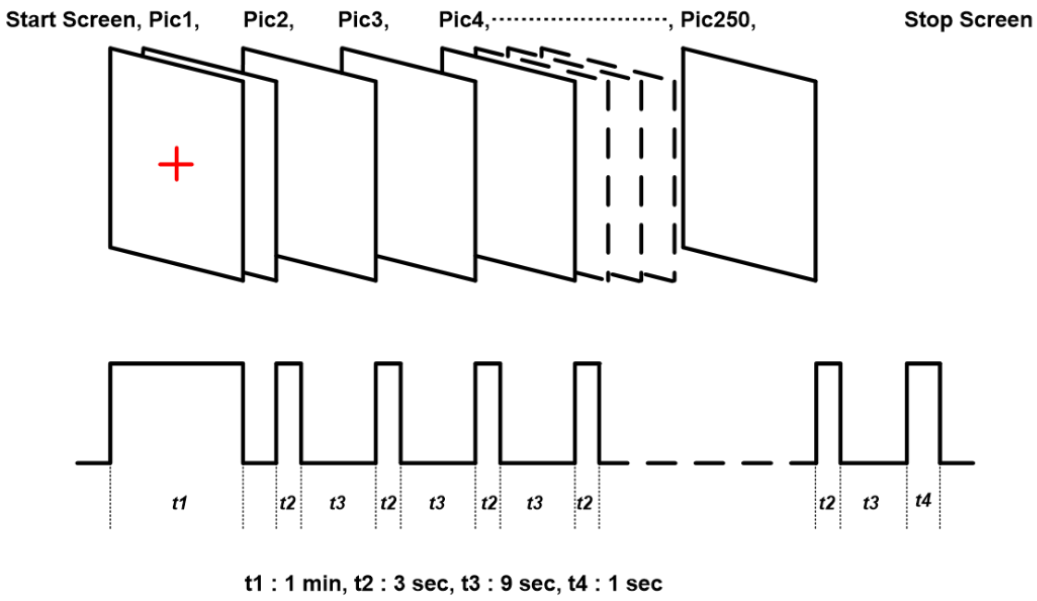


Figure 2.1 Timing diagram and the sequence of stimuli

In the continuous stimulus set, all participants were asked to look at the screen, in which 250 indoor/outdoor scenes from SUN database were randomly shown, and gave responses via mouse clicking (Xiao, Hays, Ehinger, Oliva, & Torralba, (2010).

As shown above, Figure 2.1 illustrates the sequential activities in the cognitive experiment and their timing. The period t1 is the pre-stimulus time before the experiment started. The EEG-NIRS signals with corrected baseline were then segmented into epochs; each of which includes the period t2, the time for visual stimulus, and t3, the time for receiving response from each participant.

2.4 Scene UNderstanding (SUN) Database

The SUN database is the first dataset with a large set of scene objects and regarded as a standard database for the scene recognition test.

In this study, a total of 500 image features from the database were randomly presented to each participant. These images were drawn randomly from the target categories (indoors and outdoors) and shown at a size of at least 200×200 pixels (Xiao, Ehinger, Hays, Torralba, & Oliva, 2016).

Examples of indoor and outdoor images are shown in Figure 2.2 below.



Figure 2.2 Examples of indoor and outdoor images from SUN database

2.5 Scene Recognition Test

After the measurement, the participants rested for 15-20 minutes and then performed a scene recognition test by identifying which of the 500 scenes they had previously seen in the experiment. The recognition test procedure comprises of 250 scenes from the previous experiment and 250 new ones from SUN database. The participants were instructed to decide, as truthfully as possible, whether each stimulus represented a picture of previously seen or unseen via mouse clicking “YES” or “NO”, respectively.

In terms of the scene recognition test, timing was not controllable. The collected EEG-NIRS data were subsequently pre-processed.

2.6 Customised Cap for Simultaneous EEG-fNIRS Measurement

A customised cap for simultaneous EEG-fNIRS measurement has been designed customarily, which contains 16-fNIRS sources or emitter and 16-fNIRS detectors with 30-EEG electrodes designed. The holders consisted of a rubber base fitted with optode sockets. The rubber base has been designed specifically at a fixed 3-cm distance between the source and the detector. In addition, simultaneous EEG-fNIRS recording and measurements with responses time-locked to the stimuli were applied at locations based on the international 10/20 system of electrode placement with the customised cap.

To put it clearly, 30 EEG electrodes were placed on the 30-brain location with a reference position at FCz and a ground position at AFz.

EEG data were recorded from 30 channels based on the extended 10/20 system (Fp1, Fp2, AF3, AF4, F3, F4, F5, F6, F7, F8, FC3, FC4, C4, C4, CP3, CP4, P3, P4, P5, P6, P7, P8, PO3, PO4, O1, O2, T7, T8, Fz and Cz) .

The NIRS source-detector combination was positioned on the whole scalp. The NIRS signals were acquired using 16 emitters and 16 detectors, which formed a combinational pair of 28 channels. The NIRS optodes were adjusted around the EEG electrodes in the exact same channel locations for simultaneous signal acquisition as shown in Figure 2.3.

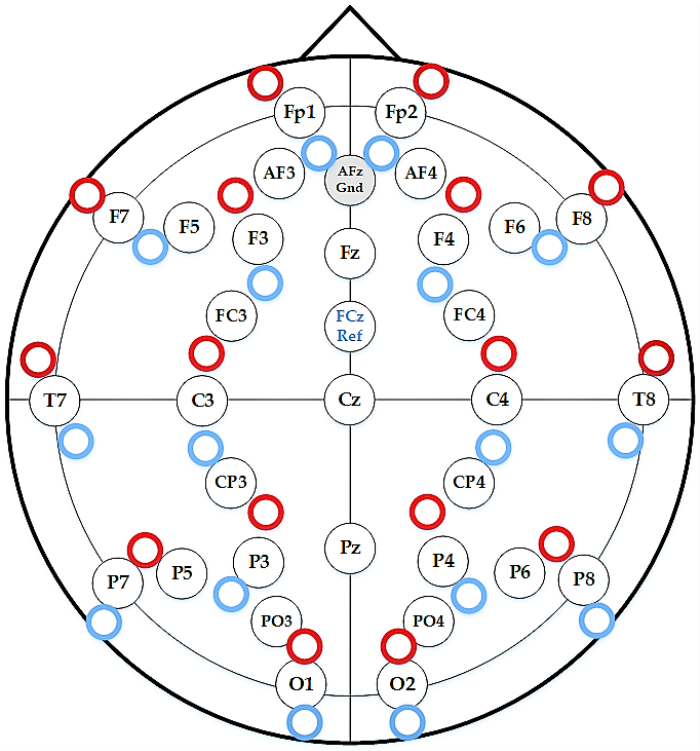


Figure 2.3 Customised cap for simultaneous EEG-fNIRS measurement

Figure 2.3 shows the customised cap for simultaneous EEG-fNIRS measurement. The red socket is the emitter and the blue socket is the receiver or detector. As shown in this figure, the cap was purposively designed to measure EEG and NIRS channels in the exact same positions.

Particularly, this cap was also designed specifically to have the adjustable inner drawstring or band for secure fit and to keep the hat in place during the process of measurement.

In conclusion, the EEG electrodes were positioned according to the international 10/20 system placement. The distance between Hb.O2 source and detector is approximately 3 cm, with each Hb.O2 source-detector pair forming a channel (Gagnon et al., 2012), resulting in 30 channels for EEG and 28 channels for fNIRS. For fNIRS, the scalp was covered with 16 emitters and 16 detectors.

A total of 28 NIRS channels are positioned on (pre)frontal (12 channels), motor (2 channels around C3 and C4), parietal (8 channels), occipital areas (4 channels around POz) and temporal (2 channels around T7 and T8).

A total of 30 EEG channels are positioned on (pre)frontal (13 channels), motor (3 channels around C3, C4 and Cz), parietal (8 channels), occipital areas (4 channels around POz) and temporal (2 channels around T7 and T8).

2.7 Brain Complexity

The human mind is primarily known as a complex phenomenon built on the physical scaffolding of the brain, which neuroscientific investigation is required to examine in detail. The brain, as a complex system, together with the dynamical features of neural population activity develop from the interactions of the neuro-anatomical networks, all of which is referred as brain complexity. It is true that mental states derive from the interaction between multiple physical and functional levels. According to Bassett and Gazzaniga (2011), the nature of the relationship between the mind and the brain is, however, far from discovered and understood.

For this reason, to understand the complexity in the human brain, Bassett and Gazzaniga (2011) argue that the brain can be understood as a complex system, in which mental states emerge from the interaction between multiple physical and functional levels.

Additionally, brain complexity is related to the involvement of networks of neurons, which are activated by well-defined stimuli and have close time domain relationships with each other. The electrical activity generated in response to these stimuli is described as a time-locked response. Evoked potentials are measured at the scalp surface and represented the involvement of neuronal populations activated by different types of generators that, depending on the activation status of the entire system, interact with each other (Norcia, Appelbaum, Ales, Cottereau, & Rossion, 2015). Synchronization changes must therefore be analysed for neural ensembles whose cell bodies are located in the grey matter (relatively close to the surface).

According to Kelso, Dumas, and Tognoli (2013), these phenomena interact with the system's resting synchronization status and represent the intimate integration mechanisms for the various subsystems constituting the brain response. Likewise, measurement of brain complexity requires synchronous activation of a large population of neurons.

In brief, brain complexity is a very interesting characteristic because the complexity of brain is able to show how the brain changes activity when stimulated by the task. In this study, a pooling of bioelectricity (EEG) and hemodynamic (fNIRS) was used to measure different perspectives of brain complexity. The scale of data measurement was also adjusted to be the same entropy scale.

2.7.1 Entropy

A key characteristic of the complex nonlinear behavior of human signals is predictability, which can be quantified by entropy (Raffalt, Denton, & Yentes, 2018). The concept of entropy is first introduced by Rudolph Clausius in the context of thermodynamics (Camacho & Martínez, 2015). It abides by the second law of thermodynamics, which states that the change of the entropy in the volume element is equal to the ratio of the heat state changes in temperature (Zhang, Cai, Skums and Zhang, 2018).

It is known from the literature that Boltzmann investigates the entropy from the perspective of molecular motion theory (Sharp, 2001; Sohrab, 2014). The relationship that between the entropy changes at the macroscopic level and the heat absorbed by the system is extended to a certain relationship between the entropy and the distribution of subsystems at the microscopic level of the system.

Underlying the microscopic interpretation of entropy by the Boltzmann formula, it is not only creates an opportunity for the generalization of entropy concept, but also supports the use of entropy in biomedical signal analysis.

It is also worth noting that C. E. Shannon, who is the father of information theory (Collins, 2002), first proposed the concept of information entropy in 1948. Shannon entropy is characterised by a degree of uncertainty associated with the occurrence of the result (Borowska, 2015); that is, the higher value of the entropy, the more uncertain the results will be.

Additionally, the Shannon entropy also reveals the average uncertainty of information sources. The higher level of uncertain information source, the more

misleading the information source will be (Khalaj, Pasha, Tavakkoli-Moghaddam, & Khalaj, 2018).

At present, the applications of entropy in biomedical signals have received extensive research attentions (Peng, Chen, Sun, Ser, & Lin, 2017; Wang, Zhao, Qu, & Chen, 2017). For instance, Pincus (1991) proposed the concept of approximate entropy to examine the changes of heart rate for infantile sudden illness. Approximate entropy is good at solving the problem of common signal with short noise in biomedical signals. Richman and Moorman (2000) developed the sample entropy. Sample entropy, compared with approximate entropy, shows better relative consistency and less dependence on data length (Liu, Jiang, Xu, & Xue, 2016; Richman, & Moorman, 2000; Yan et al., 2012).

In conclusion, entropy is a concept handling predictability, probability and randomness, with higher values of entropy always related to less system order and more randomness.

2.7.2 Multiscale Entropy (MSE)

A multiscale method for computing the entropy of biological signals was developed by Costa et al. (2002). This approach calculates the sample entropy on the original time series and on coarse-scaled series derived from the original signal. Since biological systems must be adaptable across multiple time scales, measurements of biological signals are likely to carry information across multiple scales. A multiscale estimation of the information content of EEG signals may reveal more information when compare to the entropy of the original signal.

Based on sample entropy with multiscale approach on temporal data, MSE has been widely applied for medical data analysis. This is pertinent given the complexity

and non-linearity of medical data. Shannon entropy has led to the development of various entropies such as Kolmogorov-Sinai entropy, Grassberger entropy and Approximate entropy. Approximate entropy (ApEn) has been commonly used to analyse biological data (Yentes et al., 2013). Furthermore, it has been developed into Sample entropy (SampEn) (Hornero, Abásolo, Escudero, & Gómez, 2008; Richman, & Moorman, 2000). In the vein of ApEn, SampEn divides the data into short sequences, called epochs, and then determines the sample entropy according to eq.(2.1).

$$\mathrm{SampEn}(m, r, N) = -\log\left(\frac{\sum A_i}{\sum B_i}\right) = -\log\frac{A}{B} \tag{2.1}$$

where m is template length, r is the tolerance for accepting matches, N is the number of data points, A_i is the number of matches of length $m+1$, and B_i is number of matches of length m.

To determine MSE, the data are coarse-graining by averaging in the range of a specified scale as shown in Figure 2.4. The scale 1 series is the original time series. The scale 2, two adjacent data points are averaged, thus the number of total data points is reduced to N/2 if there are originally N data points in total. Through the scaling process, the new data set can be expressed by eq. (2.2) (Costa, Goldberger, & Peng, 2005; Hornero, Abásolo, Escudero, & Gómez, 2008; Richman, & Moorman, 2000; Wu et al., 2013). Due to a large number of recording channels with a high sampling frequency, multi-scale analysis is required to obtain linear MSE graphs. Sample entropy was therefore selected to optimize efficiency in data processing (Richman, & Moorman, 2000).

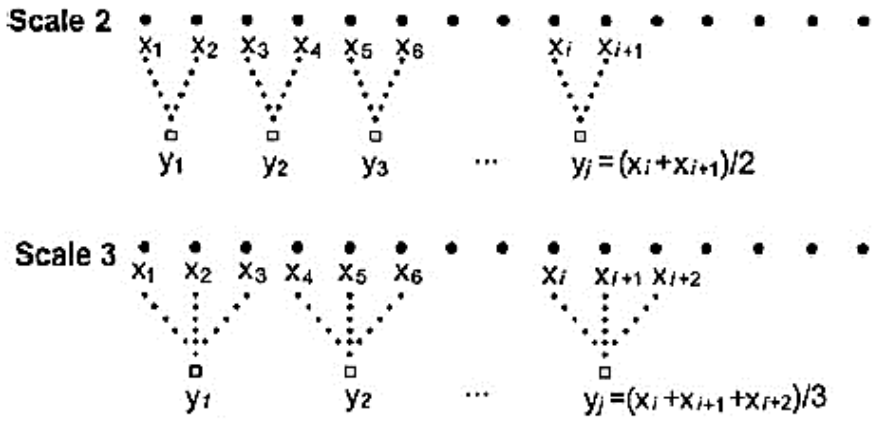


Figure 2.4 Schematic illustration of the coarse-graining procedure for scales 2 and 3.

$$y_j^{(\tau)} = \frac{1}{\tau} \sum_{i=j\tau-\tau+1}^{j\tau} x_i \, , 1 \leq j \leq \frac{N}{\tau} \tag{2}$$

where τ is the scale level, and x_i is the original data point then, the new data set is used to compute sample entropy in each scale.

Previous studies have shown that SampEn has the acceptable range for m= 2, r= 0.15 x SD of the time series (Catarino, Churches, Baron-Cohen, Andrade, & Ring, 2011; Richman, & Moorman, 2000). Adopting the method proposed by Catarino et al. (2011), we used m = 2, r = 0.15 x SD of the time series. For N, we calculated from the sampling frequency and epoch length used for quantitative analysis (12 seconds).

According to Richman and Moorman (2000), the appropriate N size for SampEn analysis must be a minimum of 10^m to 20^m, where m = 2; N should be at least 100 to 400 in each scale. When the scale increases, the number of N in each scale will decrease. For EEG sampling frequency at 500 Hz, when calculating, the size of N, N_{EEG} is equal to 500 Hz x 12 sec = 6000 data points. Considering the 20th scale, the size of the N_{EEG} is 300, which is still enough for SampEn analysis. With respect to

fNIRS, which has a sampling frequency of only 10 Hz. To calculate the size of *N*, N_{fNIRS} = 10 Hz x 12 sec = 60 data points, which is not enough to perform analysis with SampEn from Scale 1. Therefore, it is necessary to up-sample by a factor of 10 using the spline interpolation method to get N_{fNIRS} = 1200 data points, which is enough to analyse with SampEn up to Scale 12. For topographic rendering, the values of MSE EEG and MSE fNIRS at Scale 10 were used for analysis as the mean values with the sufficient size of *N*.

2.8 Statistical Analysis

2.8.1 Wilcoxon signed-rank test

This study uses the Wilcoxon signed-rank test, a non-parametric statistical technique, to compare a repeated measurement in one sample group for determining a significant difference in mean rank of each pair (i.e., RR-FF, RR-FR, RR-RF, FF-FR, FF-RF, and FR-RF).

As a rule, sample sizes equal to or greater than 30 are considered sufficient for the Central Limit Theorem, meaning that the distribution of the sample means is normally distributed. In other words, as long as the sample is based on 30, the sampling distribution of the mean can be safely assumed to be normal.

In this study, the sample size is less than 30 meaning that an assumption of normal distribution is impossible to be met. The use of the Wilcoxon signed-rank test, which is a substitution of paired sample t-test in parametric statistics, is therefore considered as an appropriate method of data analysis.

As mentioned previously, the Wilcoxon signed-rank test is used to test differences of paired data without the normal distribution assumption of the

differences that is required for the paired t-test. According to Leon, (1998), the procedure is as follows:

First, the difference between each pair of data is calculated. The differences are then ranked. Second, the ranks are assigned the sign (±) of the corresponding difference. Third, two sums are computed: the sum of the positive signed ranks (T+) and the sum of the absolute values of the negative signed ranks (T−).

The sum of the totals should be: $(T+) + (T-) = n(n + 1)/2$, where n is the number of nonzero differences.

If H_0 were true, one would expect about half of the differences to be positive and about half of the differences to be negative.

If so, the sum of positive ranks would be approximately equal to the sum of the negative ranks: $T+ \approx T- \approx 1/2 \cdot n(n + 1)/2$.

2.8.2 Pearson's correlation coefficient

Pearson's correlation coefficient is a statistical measure of the strength of a linear relationship between paired data. It is also recognised as a parametric correlation test because it depends to the distribution of the data and can be used when x and y are from normal distribution. The plot of y = f(x) is called the linear regression curve (Saad, Glen, Chen, Beauchamp, Desai, & Cox, 2009).

In this study, the number of 3,739 pictures were responded by the 15 participants. In fact, the exact number of pictures were 3,750. However, some participants failed to respond to some pictures by clicking "Remember" or "Forget" meaning that they missed 11 pictures for this task.

To sum up, the number of 3,739 pictures were used to analyse a Pearson's correlation coefficient. Since, the number is large (more than 30); an assumption of normal distribution is accepted. The use of Pearson correlation (r), which measures a linear dependence between two variables; that is, EEG and NIRS (Hb.O2) and NIRS (Hb.R) is therefore considered as an appropriate method of data analysis. Correlation coefficient is comprised between -1 and 1 as follows:

First, the result of -1 indicates a strong negative correlation: this means that every time x increases, y decreases.

Second, the result of 0 means that there is no association between the two variables (x and y). Third, the result of 1 indicates a strong positive correlation : this means that y increases with x. Interpretation of Pearson's correlation coefficient is shown in Figure 2.5 as follows.

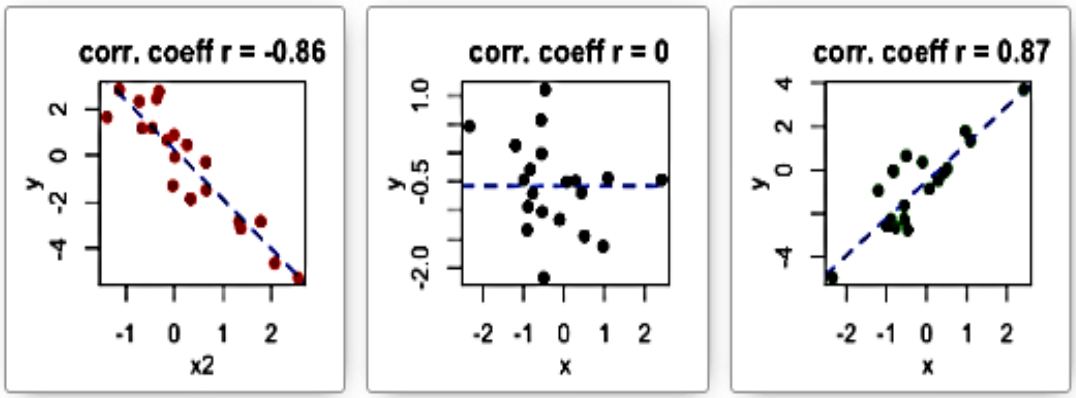


Figure 2.5 Interpretation of Pearson's correlation coefficient

Note: This figure is adopted from a study of Saad, Glen, Chen, Beauchamp, Desai, and Cox (2009).

2.9 Conclusion

Brain activation can be investigated with a number of techniques. Combining two or more of these techniques can yield additional insights, particularly if they provide complementary information (Debener et al., 2006).

Regarding fNIRS, a non-invasive imaging technique measuring the changes in concentration of oxygenated (Hb.O2) and deoxygenated hemoglobin (Hb.R) in cortical areas is considered as a promising alternative to fMRI.

In a nutshell, fNIRS has spatial resolution of a little less than a cm, temporal resolution of ms to tens of ms, light penetration of only about 1 cm into the superficial portions of the brain (Crosson et al., 2010). Accordingly, for superficial brain regions, it is a suitable complement to fMRI. Its portability, relatively low cost, ability to be used in a normal and unconfined environment, and non-invasiveness make it potentially beneficial clinically.

Since technology is developing day by day, it is possible to acquire the EEG and NIRS data simultaneously. Over the last decade, simultaneous EEG and fNIRS has been gaining more attention and gradually an increasing number of research approaches have focused on the use of simultaneous EEG and fNIRS.

As for fNIRS, is suitable for simultaneous and artifact-free recording with EEG because its near infrared light does not interfere with the electrical EEG measurement. These two techniques can also be combined for simultaneous acquisition in non-laboratory situations such as an incubator in an intensive care unit without causing major discomfort to the patient.

While EEG is very powerful to detect brief processes in the range of 100 ms and attached to the scalp surface, fNIRS provides integration over a comparable timeframe and a better localization. EEG and fNIRS are therefore complementary, as they allow simultaneous analysis with high temporal resolution of the neuronal and hemodynamic components of brain activation. A combining of EEG and fNIRS, is therefore complementary and useful for recording brain function analysis with more accurate than an individual modality alone.

For in depth understanding and insight of what is happening inside the human brain during the working memory process, both high spatial and high temporal resolution is essential and up until now the research studies in simultaneous EEG-fNIRS are scant. A handful of studies on visual working memory function using simultaneous EEG and fNIRS have been previously published. In this sense, it is believed that fNIRS should not be considered as a competitor of EEG, but a pooling modality for cases in which one technique cannot be used effectively.

This study is mainly focused on the visual memory function involving simultaneous EEG-NIRS data acquisition and analysis. It aims to highlight the application of multi-scale entropy (MSE) to analyse brain activity in terms of entropy levels or brain complexity levels and to determine the potential of using simultaneous EEG and fNIRS to measure visual working memory function and data processing.

CHAPTER 3

RESEARCH FINDINGS

3.1 Introduction

Specifically, this study aims to use simultaneous EEG and fNIRS for recording brain activity and to apply MSE in analyzing brain activity for entropy levels, and finally sought the answers to the following questions:

1. Does simultaneous EEG and fNIRS have the potential use for recording brain activity?
2. Can the application of multiscale entropy (MSE) be applied in analyzing brain activity for entropy levels or complexity levels?

As for Research Questions 1 and 2, simultaneous EEG and fNIRS was found to have the potential use for recording brain activity and the application of multiscale entropy (MSE) can be applied in analyzing brain activity for entropy levels or complexity levels. The results are presented as follows.

3.2 Demographic Information

As shown in Table 3.1, the participants in this study were 12 males and 3 females aged from 20 to 30 years old (males M= 25.08, SD =2.19; females M = 25.00, SD = 1.00). They were postgraduate students from different ethnicities such as Japanese, Chinese and Thai. From a total of 3,750 pictures, also called trials, there were 1,163 (31.01%) RR, 348 (9.28%) RF, 1,575 (42.00%) FR, 651 (17.36%) FF, and 13 (0.35%) no response. All epochs corresponding to the same category at each channel were analysed with the MSE approach. Note that, from the total of 3,750 trials,

only the complete trials were considered and the trials that the participants left blank or did not respond were eliminated from the study.

Table 3.1

Demographic information of participants

Participants ID	Gender	Age	RR	RF	FR	FF	No Response	Total
N0001	M	21	100	36	86	28	0	250
N0002	F	26	15	1	144	90	0	250
N0003	M	22	68	32	90	59	1	250
N0004	M	26	96	24	58	71	1	250
N0005	F	24	48	12	146	44	0	250
N0006	M	25	74	6	148	22	0	250
N0007	M	25	26	3	193	28	0	250
N0008	M	26	63	25	91	69	2	250
N0009	M	24	103	33	79	34	1	250
N0010	M	28	85	27	94	39	5	250
N0011	M	25	90	32	98	30	0	250
N0012	F	25	112	17	80	41	0	250
N0013	M	29	91	54	68	34	3	250
N0014	M	25	86	17	120	27	0	250
N0015	M	25	106	29	80	35	0	250
Total	M = 12 F = 3	Male (M=25.08, SD=2.19) Female (M=25.00, SD=1.00)	1163 31.01%	348 9.28%	1575 42.00%	651 17.36%	13 0.35%	3750 100%

Considering a total of 3,750 trials from 15 participants, regardless of whether they wished to remember or forget, the participants remembered 2,738 trials or 73.01% of all visual stimuli.

This suggests that the brain has the capacity to retain visual information in this experiment no matter how much an intentional mental state is involved. It indicates the large extent to which memory is under subconscious control.

As shown in Table 3.2, in terms of pictures viewed per participant, the cohort may be categorised into two groups: Group A (%R1 - %R3 at similar levels such as

N0001 and N0003); Group B (%R1 - %R3 at different levels such as N0002 and N0004).

By splitting the participants in this manner, this study aims to gain insights into the application of different strategies or memory-boosting mnemonics. As for %R1 to %R3, they were calculated from eq. (3.1) – (3.3) as follows.

$$\%R1 = \%RR/(RR+RF) \quad (3.1)$$

$$\%R2 = \%(RR+FR)/(RR+RF+FR+FF+\text{No response}) \quad (3.2)$$

$$\%R3 = \%FR/(FR+FF) \quad (3.3)$$

Table 3.2

Pictures viewed per participant

Participant ID	%R1	%R2	%R3	Group
N0001	73.53	74.40	75.44	A
N0002	93.75	63.60	61.54	B
N0003	68.00	63.20	60.40	A
N0004	80.00	61.60	44.96	B
N0005	80.00	77.60	76.84	A
N0006	92.50	88.80	87.06	A
N0007	89.66	87.60	87.33	A
N0008	71.59	61.60	56.88	B
N0009	75.74	72.80	69.91	A
N0010	75.89	71.60	70.68	A
N0011	73.77	75.20	76.56	A
N0012	86.82	76.80	66.12	B
N0013	62.76	63.60	66.67	A
N0014	83.50	82.40	81.63	A
N0015	78.52	74.40	69.57	A
Mean	79.07	73.01	70.11	A = 11
SD	8.92	8.98	11.45	B = 4

where %R1 = the percentage of memory efficiency
%R2 = the percentage of memory recall
%R3 = the percentage of accidental memory recall

3.3 EEG Results

The EEG data was recorded using Neurofax electroencephalograph EEG – 1100 (Nihonkoden, Japan) at a sampling rate of 500 Hz. EEG signals were acquired by band-pass filtering. The signals were processed in 0.5~30 Hz range. The EEG was recorded on the whole scalp according to the international 10/20 system. The skin was cleaned with alcohol and scrub gently with skinpure® to keep the impedance below 5 kOhms. For the same channel, the recording electrode was attached next to the optode.

Most notably, all EEG and NIRS signals were recorded simultaneously. For timing synchronization, triggers were sent to both EEG and NIRS equipment simultaneously via a serial port using MATLAB with Psychtoolbox and hemodynamic changes were recorded while the participants focused on the visual stimulation.

After that, all recorded EEG channels were arranged into a topographic map. Using MATLAB R2015b with the open source toolbox EEGLAB v12.0.2.5b, the raw EEG data were analyzed for independent component (Al-Shargie, Tang, Badruddin, & Kiguchi, 2015).

The components relating to eye blinking and eye movement artifacts were removed. Other noises were also removed through bandpass filter 0.5-30 Hz for EEG and Notch filter 60 Hz for power line noise. The pre-stimulus EEG data were used for baseline correction.

The EEG data were subsequently categorized into four groups: Remember-Remember, Remember-Forget, Forget-Remember, Forget-Forget followed by the process of MSE analysis as shown in Figure 3.1.

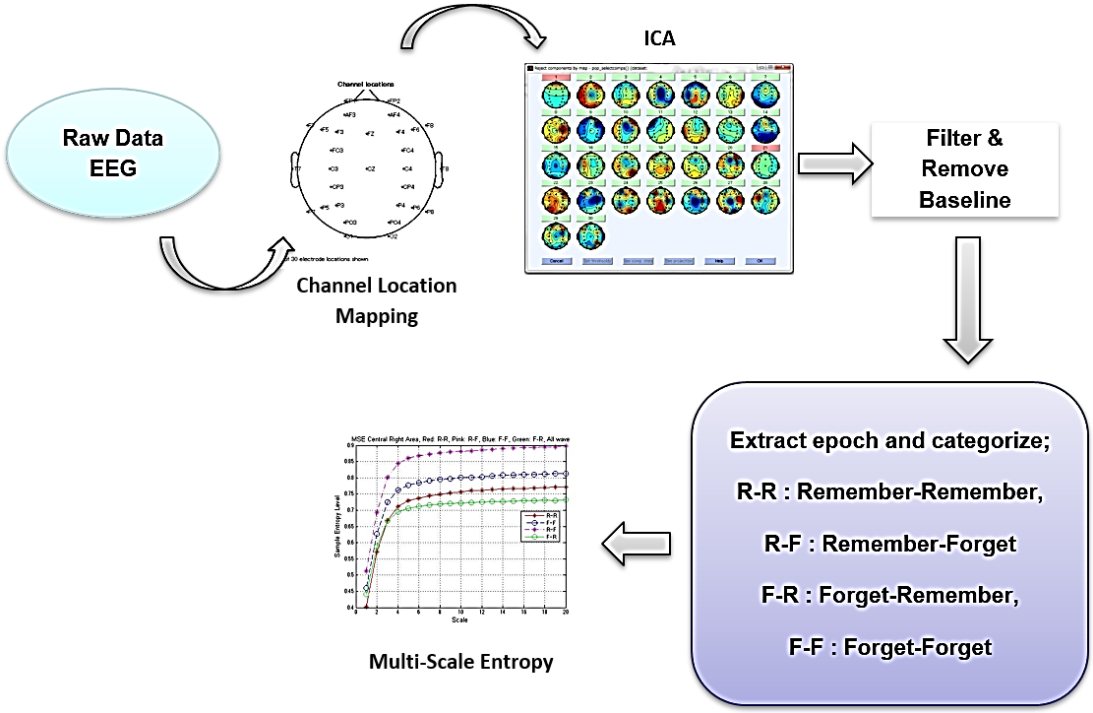


Figure 3.1 EEG recording and analysis

3.3.1 Pre-Processing Analysis

The purpose of pre-processing is to improve signal quality or signal conditioner. Undeniably, this process is necessary for ensuring the stability and overall quality of the recording for further signal analysis. In general, it starts with process of data acquisition or it gains incoming information. Sequential steps involved are as follows:

3.3.1 (a) Channel location mapping

The first step is channel location mapping, which is referred to the simulation of the position of EEG measurement by specifying the coordinates of position based on the international 10/20 standard system. This system is recognised as a method to apply the location of scalp electrodes in the context of EEG and also based on the

relationship between the location of an electrode and the underlying area of the brain, specifically the cerebral cortex.

The locations are systematically modelled using EEGLab toolbox for Independent Components Analysis (ICA) and Topography, respectively. The 30 of 30-electrode channel location is shown in Figure 3.2 below.

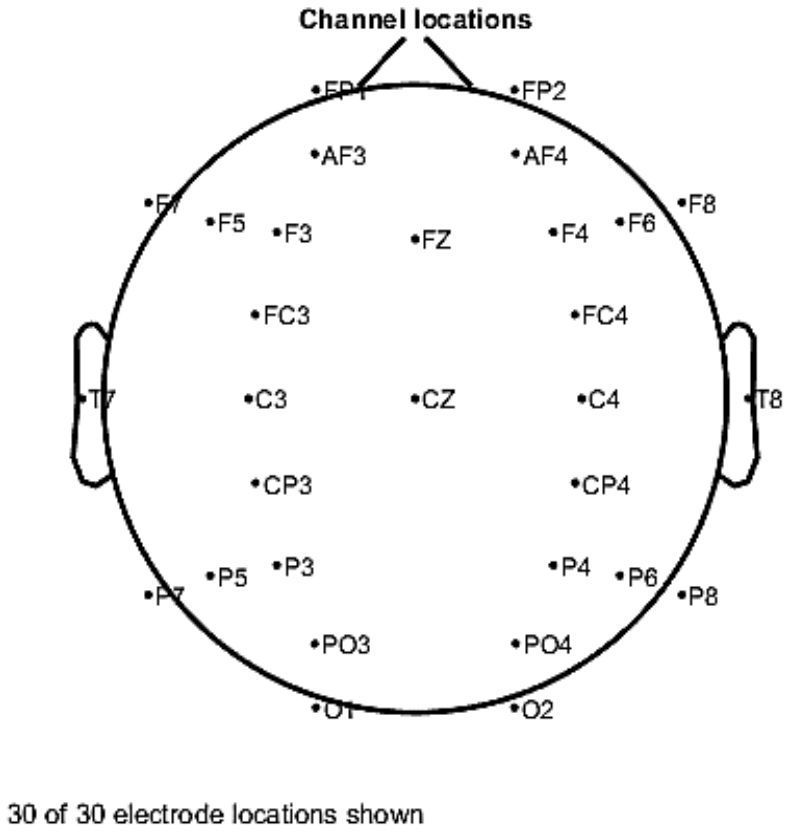


Figure 3.2 EEG channel location mapping

3.3.1 (b) Artifacts removal

The second step is to remove artifacts known as the main sources of interference encountered in small signals like EEG. These artifacts can lead to shape changes of the measured signals. For this reason, a comprehensive knowledge of the types of artifacts is requisite to remove the artifacts or noise efficiently. Removal of artifacts can be done in many ways, such as thresholding to intercept signals during artifacts.

This method seems practical and convenient, but it will cause signal loss throughout the artifact phase. In contrast to traditional artifact cancelling approaches, ICA is therefore a promising method used to remove artifacts from signals without losing signals during that time. Vigário, Sarela, Jousmiki, Hamalainen, and Oja (2000) indicated that ICA has been shown to be an efficient tool for artifact identification and extraction from EEG recordings. For EEG signals, ICA is commonly used to remove artifacts in two ways: eye blink artifacts and eye movement artifacts as shown in Figure 3.3.

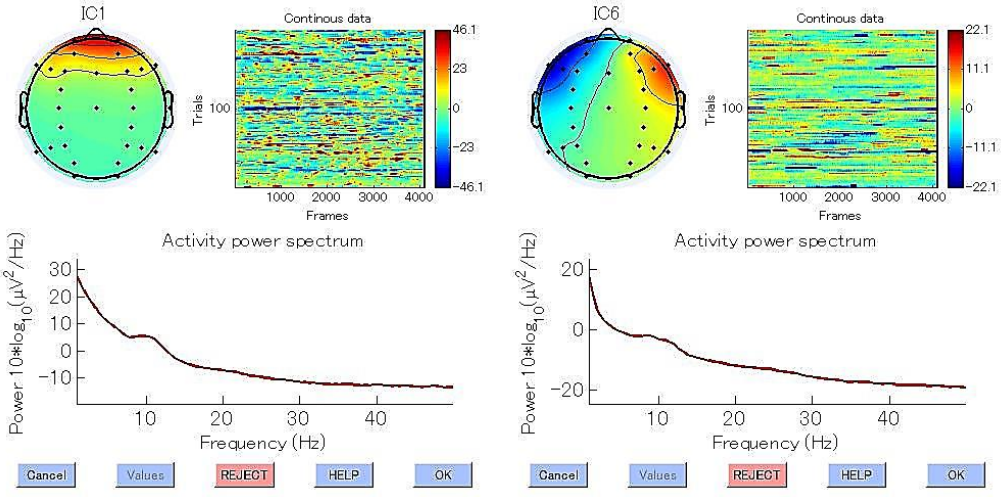
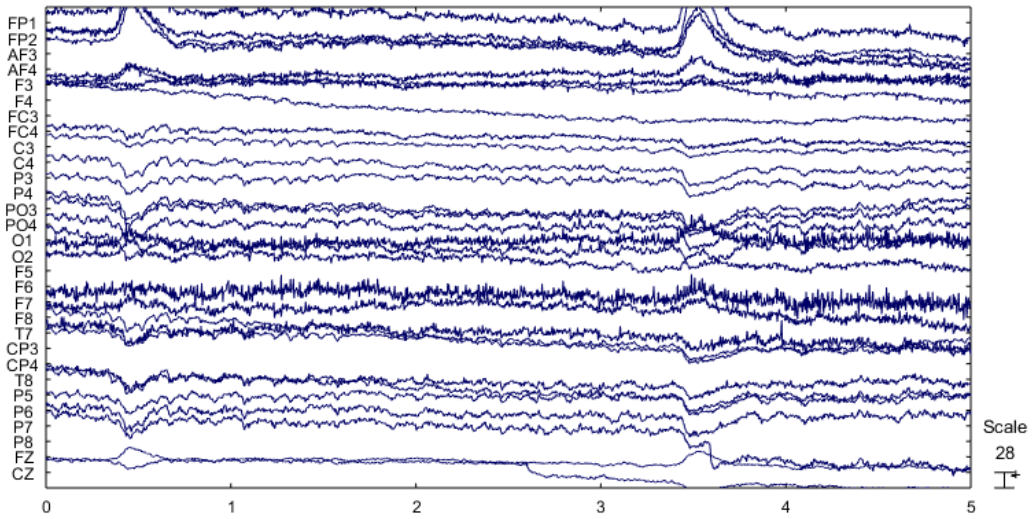
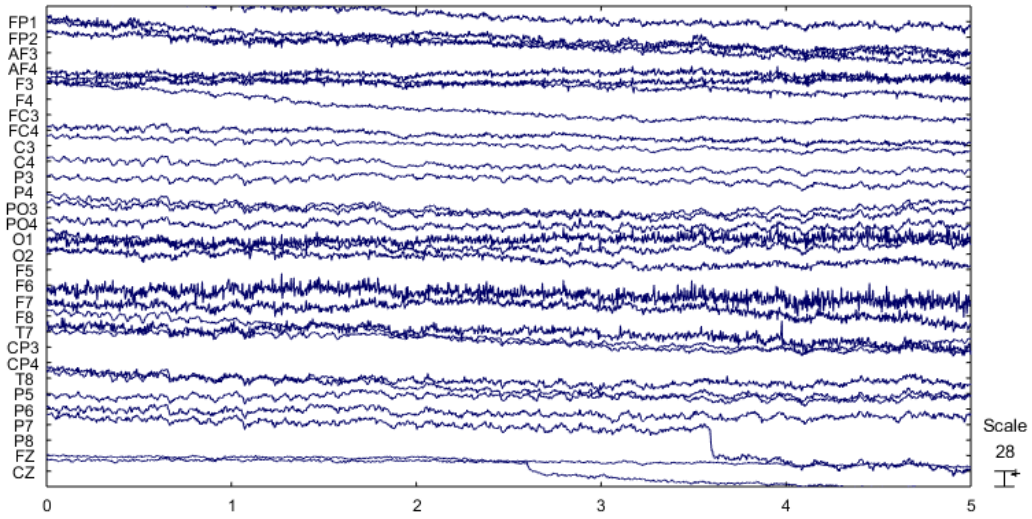


Figure 3.3 ICA: Eye blink & Eye Movement

As shown in Figure 3.4 below, A and B display the results of the EEG signal before and after the artifact removal using MATLAB EEGLab toolbox.



A: Before ICA



B: After ICA

Figure 3.4 EEG signal before and after the artifacts removal

3.3.1 (c) FIR Digital filter

After the process of artifacts removal, the next step is to eliminate small noise. For EEG, this kind of noise is considered as high frequency noise, which, in most cases, is caused by EMG and electrical signals inserted into the system.

To eliminate this noise, bandpass filtering is preferable, with frequency range of 0.5-30 Hz covering the range of brainwaves, from Delta, Theta, Alpha and Beta, respectively. Bandpass filter is developed with the purpose of the frequency response result and the signal cleaned by the filter using the MATLAB EEGLab toolbox in the FIR filter format as shown in Figure 3.5 below.

After artifact removal process, the EEG signal (Figure 3.4 B) is processed for noise reduction by using FIR bandpass filter. Subsequently, the EEG output is further analyzed by MSE. The EEG output is shown in Figure 3.6.

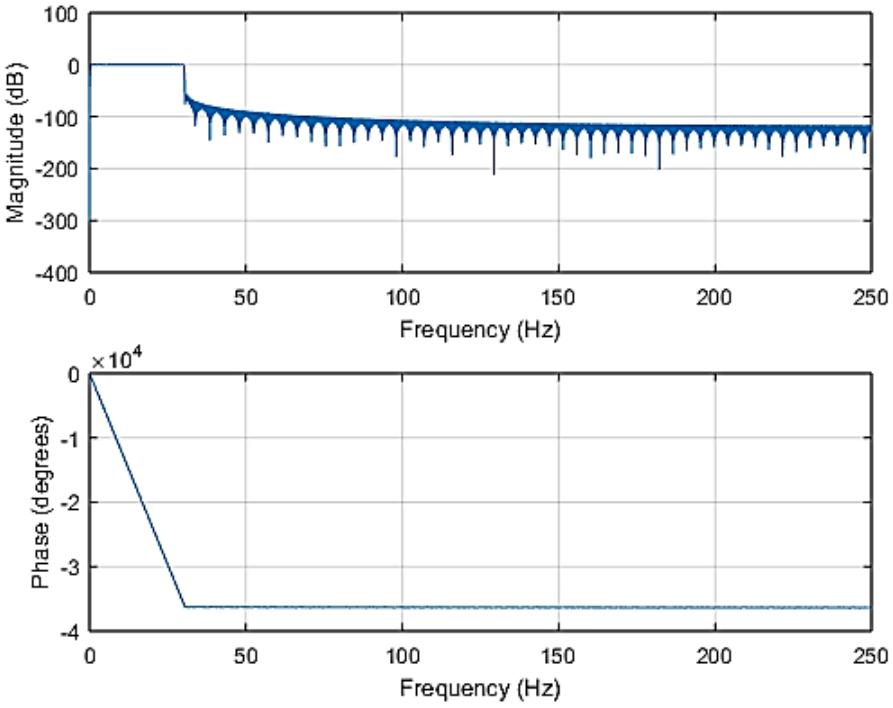


Figure 3.5 FIR digital bandpass filter, 0.5 – 30 Hz

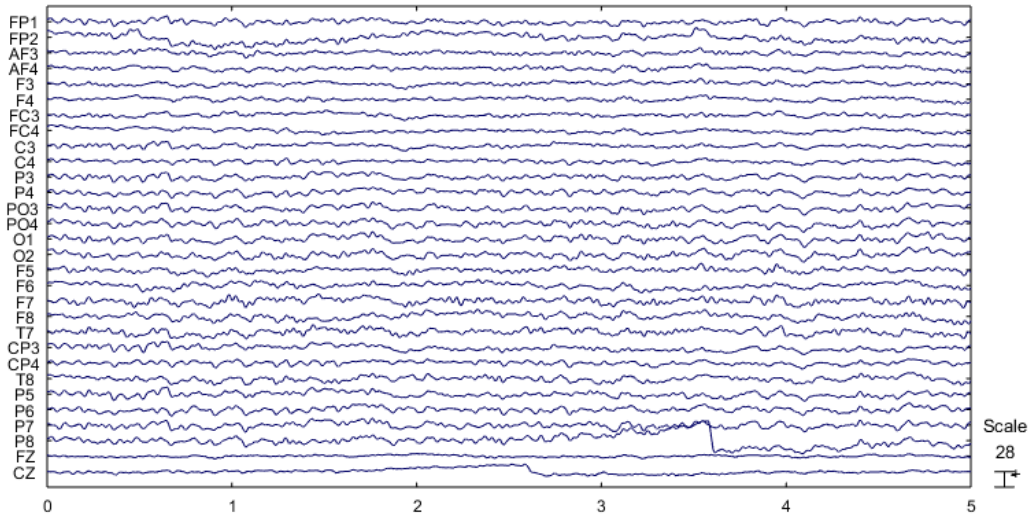


Figure 3.6 EEG output after bandpass filtering

3.3.2 EEG Complexity Analysis

In a single channel, each EEG epoch was converted into the level of complexity using MSE and displayed in accordance with a level of sample entropy from Scale 1 to Scale 20. On average, the results from the 15 participants are shown in Figure 3.7

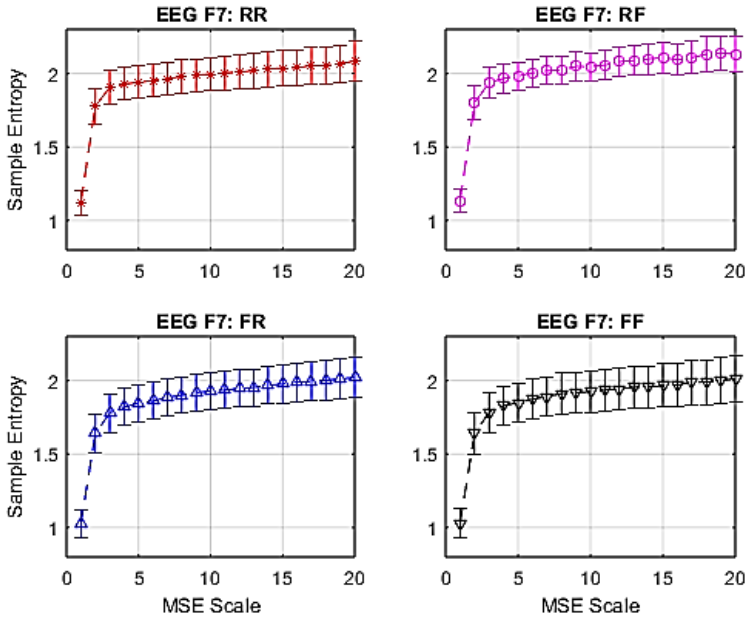


Figure 3.7 Comparison among MSE graphs

The results of comparison among the four MSE graphs are presented in Figure 3.7 with standard error (SE) at F7. In the frontal lope associated with memory function, there is a dramatically high slope from Scale 1 to Scale 3. After that, most of the acceleration is horizontal along a gradual slope.

Figure 3.8 presents a comparison among the four MSE graphs, RR – RF – FR – FF, at F7. The MSE EEG results revealed that, among the four groups (RR – RF – FR – FF), RF represents the highest level, followed by RR, FR, and FF respectively.

In comparison, as divided into two groups: 1 (RR and RF), and 2 (FR and FF), the results revealed that, with the attempts to remember (RR and RF), the brain activation when remembering measured by MSE EEG is higher.

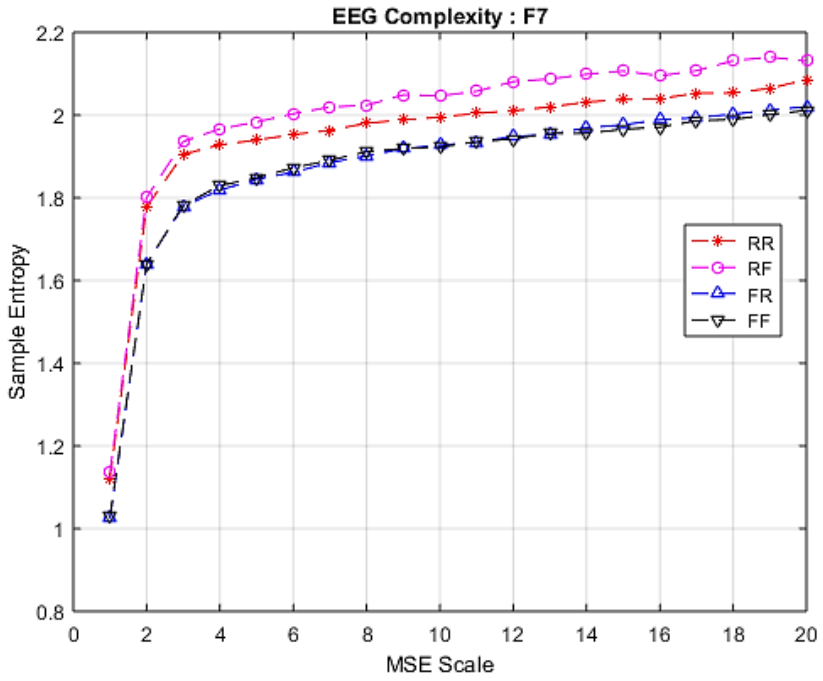


Figure 3.8 Comparison among MSE graphs, RR – RF – FR – FF, at F7

3.4 NIRS Results

Raw NIRS signals recorded from the fNIRS Hitachi EGT-7100 at 10 Hz sampling frequency. The data comprise 3 sets of data namely, Hb.O2, Hb.R and Total Hemoglobin (total Hb). Total Hb is referred to the sum of both hemoglobin NIRS data.

In this study, the analyzed data have been successfully converted from the light intensity to the concentration of hemoglobin by using a Modified Beer-Lambert.

Only Hb.O2 and Hb.R is restricted to be used in this study. In contrast to Hb.O2 and Hb.R, which directly demonstrate the brain activity, total Hb is not selected because it is not directly related to brain activity measurement.

Hb.O2 and Hb.R are used to improve signal quality to eliminate signal disturbances and adjust any DC offset by using Discrete Wavelet Transform.

The next step is to group the NIRS data into Remember-Remember, Remember-Forget, Forget-Remember, and Forget-Forget, respectively. Subsequently, each NIRS data set will further be analyzed with multiscale entropy as shown in Figure 3.9 below.

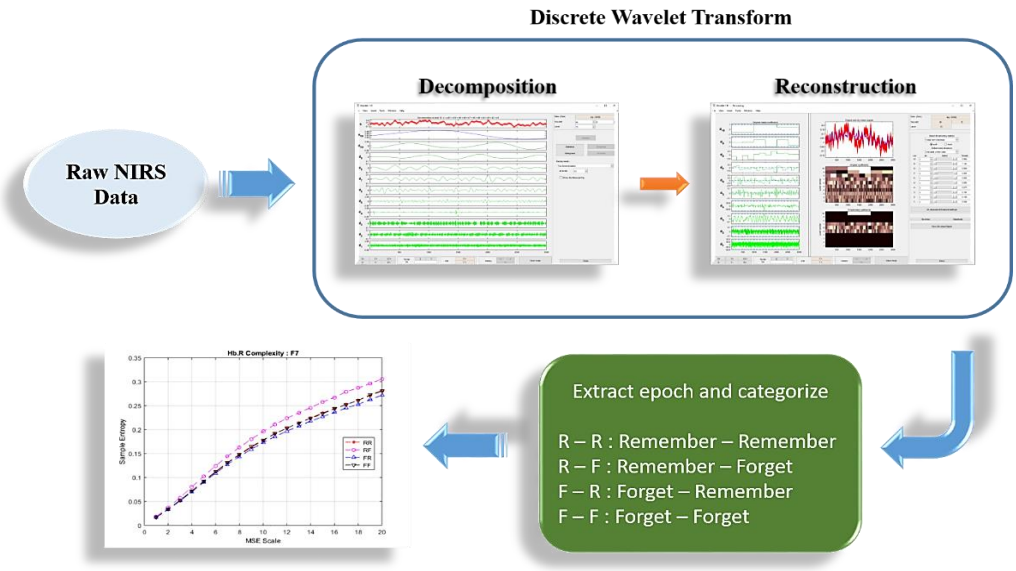


Figure 3.9 fNIRS recording and analysis

3.4.1 Pre-processing Results

3.4.1 (a) Discrete Wavelet Transform (DWT)

The pre-processing data of NIRS is similar to that of EEG pre-processing data; that is, to eliminate noise and adjust baseline. However, the NIRS interference is not only a high-frequency noise, but it is also a low-frequency noise.

Regarding fNIRS measurement, Hb.O2 is preferred due to its higher sensitivity to NIR based measurements than Hb. Despite its advantages, it is evident that there is the presence of low frequency noise (0.1 Hz) of both vascular (Hb, Hb.O2) and metabolic (cytocrhome-c-oxidase) responses to visual stimuli. The cause of these low frequency oscillations are not exactly known but are usually attributed to extracerebral activities such as respiration. Obrig et al. (2000) have found that these modulations are considerably expressed in the Hb.O2 responses.

In general, a commonly used method in pre-processing of NIRS is bandpass filtering with a frequency range of 0.1 – 0.3 Hz or using the means of data sets called a moving average window (Sai, Zhou, Ding, Fu, & Sang, 2014).

In this study, discrete wavelet transform (DWT) was applied to decompose the residual signal into different scales with corresponding frequency bands. This method is used to determine which frequency range is considered as signal or noise (Tsunashima, Yanagisawa, & Iwadate, 2012).

MATLAB r2015b was used in DWT analysis by using mother wavelet with respect to Daubechies (db). This is because they are similar in terms of biological signals. In this regard, db order 8 level 10 was used for signal separation.

Separation of signal components or Decomposition is known as the separation of the frequency components of original signals. The components are divided into 2 groups: Detail component and Approximate component. Using Db8 Level 10, the components can be separated into d1 - d10 and a10 as in Figure 3.10.

As shown in Figure 3.10 below, when the signal has been decomposed into various components, it will be separated into component data and noise. NIRS is considered as a slow wave. In addition, interference are present in both low and high frequency noise. The selection of the main signal components is therefore determined by the frequency of brain activation during the experiment, refer to (d6).

Since NIRS is a slow wave, there is a possibility that Lead-Lag signals may occur. For that reason, d5 and d7 components must be chosen as side components to prevent NIRS signal changes. After obtaining all the components required, reconstruction is then processed to combine the selected components, d5, d6, d7 and a10 back into the NIRS signal as shown in Figure 3.11.

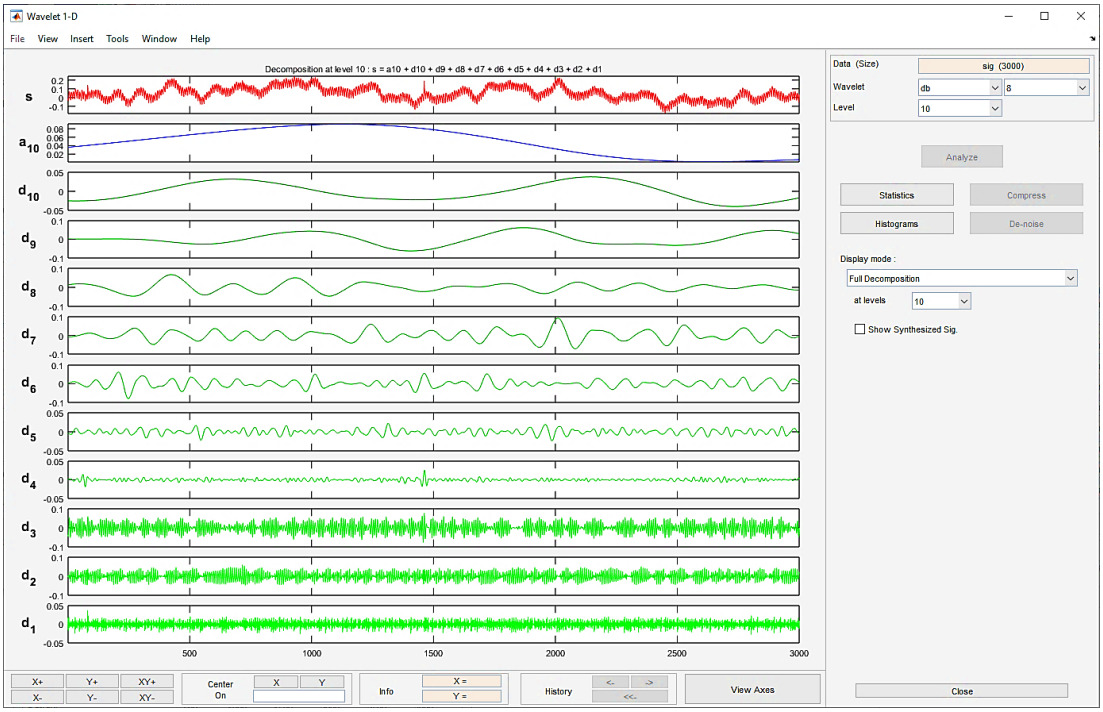


Figure 3.10 Decomposition of NIRS signal

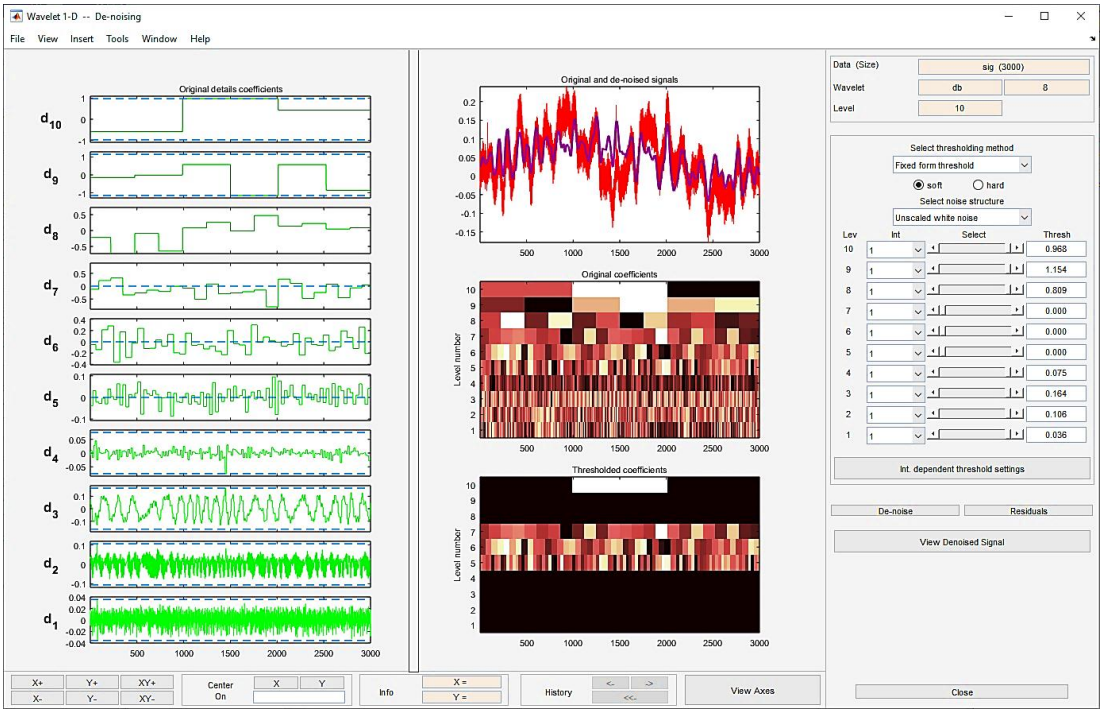


Figure 3.11 Reconstruction of NIRS signal

Figure 3.11 presents the reconstruction signals adjusted to zero offset in order to eliminate the oscillations caused by frequency-shifting or the amount of blood accumulation by removing the approximate component 10.

For further signal analysis, Figure 3.12 shows a comparison among the three signal types, namely raw signal, reconstruction signal and baseline correction signal, respectively.

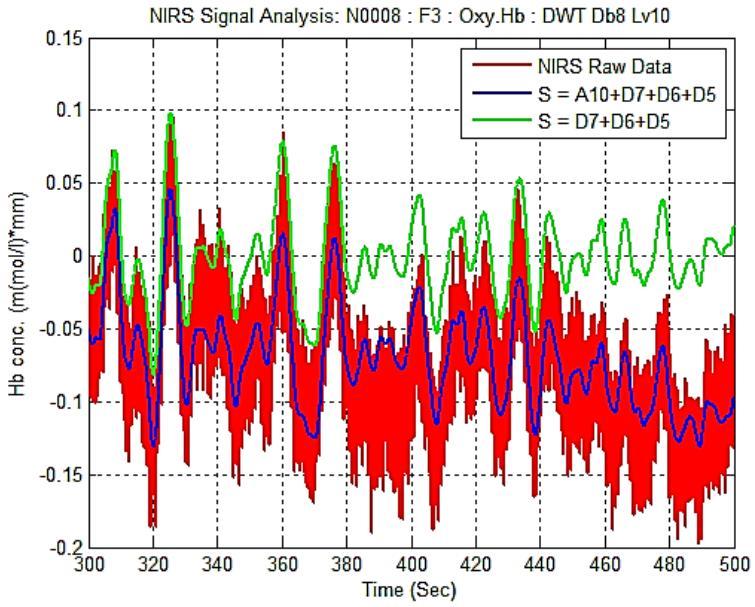
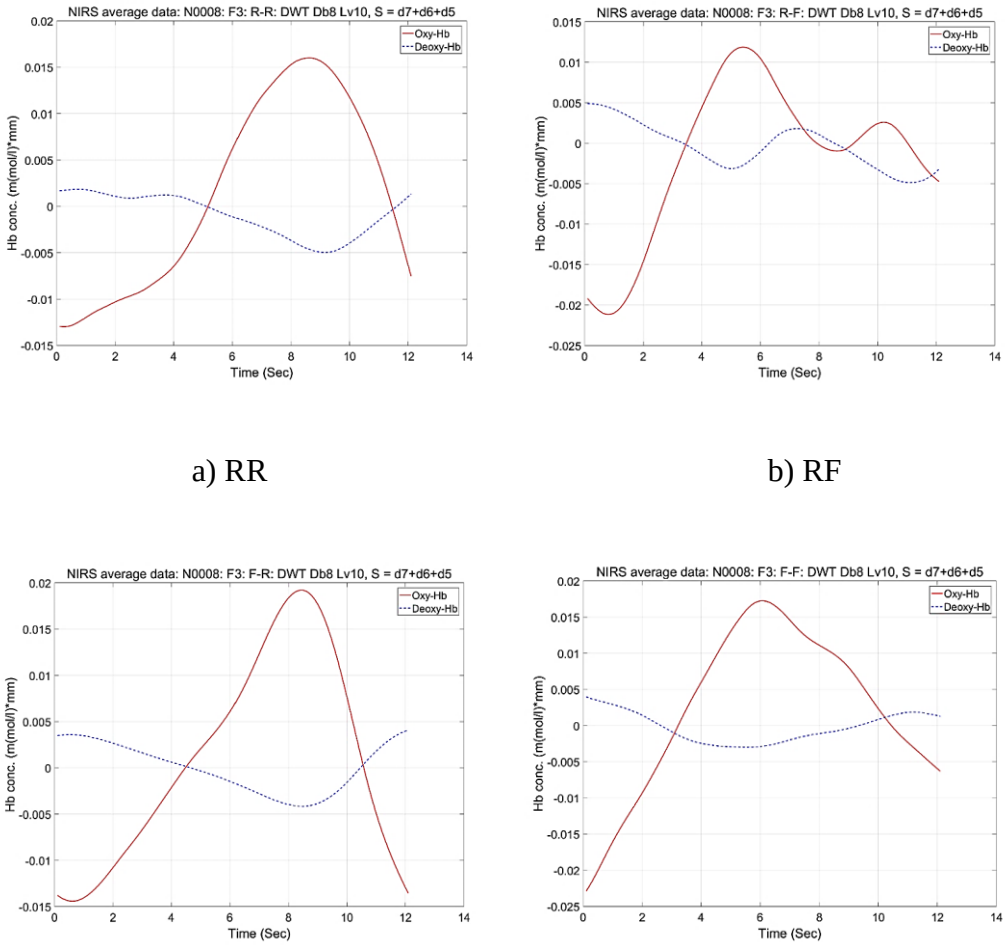


Figure 3.12 Comparison of raw signal, reconstruction signal and baseline correction signal

3.4.1 (b) Epoch Categorization

This step is to divide the NIRS data group that has been successfully eliminated the noise and adjusted baseline with DWT. NIRS data will be divided into 4 groups according to the decision-making and recall in the experiment and the scene recognition test, namely RR, RF, FR and FF, respectively. The mean of each group is shown in Figure 3.13.

From Figure 3.13, it can be seen that the graphs of both types of NIRS data are phase- reversed between Hb.O2 and Hb.R. Moreover, there are significantly different in each group, especially the RF group.



a) RR b) RF

c) FR d) FF

Figure 3.13 Comparison of NIRS data groups: RR, RF, FR, and FF

3.4.2 NIRS Complexity Analysis

In a similar way to EEG, the data from 28 fNIRS channels were converted into the level of complexity using MSE and displayed in terms of a level of sample entropy

from Scale 1 to Scale 20. In comparison, the results of Hb.O2 and Hb.R displayed in MSE fNIRS graphs are shown in Figure 3.14 – Figure 3.17.

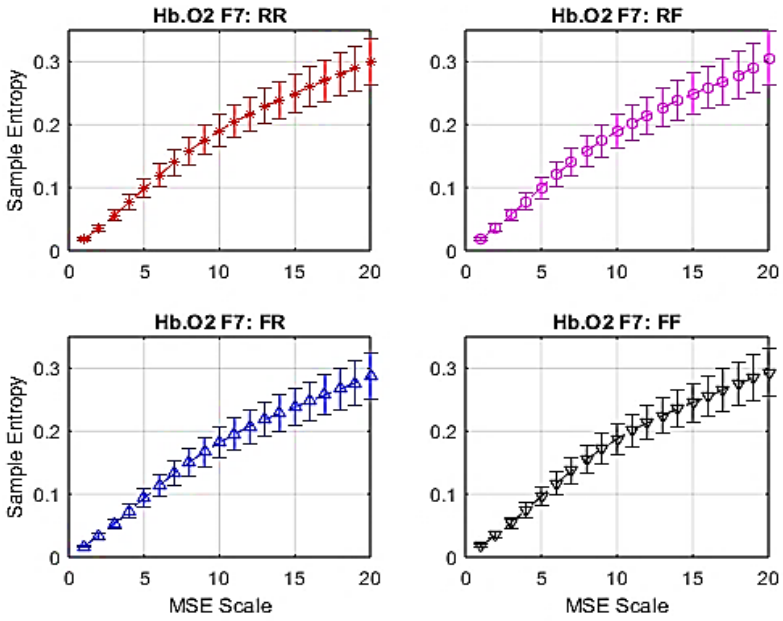


Figure 3.14 Results of Hb.O2 and Hb.R displayed in MSE fNIRS graphs

In line with MSE EEG, Figure 3.14 shows an example of MSE fNIRS graph with standard error (SE) at F7. As compared to MSE EEG, Hb.O2 of MSE fNIRS is more linear with a considerably low level of entropy due to the characteristic of fNIRS as a slow wave.

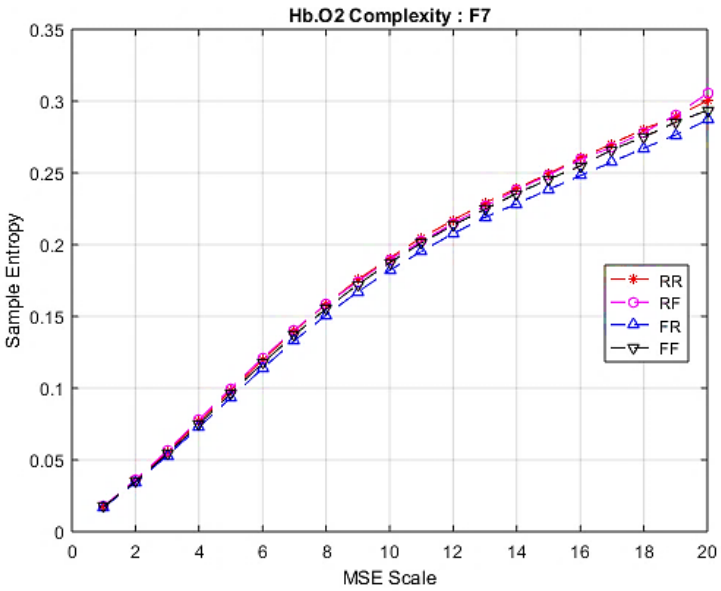


Figure 3.15 MSE fNIRS for Hb.O2

Figure 3.15 shows a graph of MSE fNIRS for Hb.O2. In terms of 4 MSE fNIRS in Hb.O2, there is a subtle difference among each of them. However, the results revealed that, with the intention to remember (RR and RF), the brain activation when remembering measured by MSE fNIRS is higher.

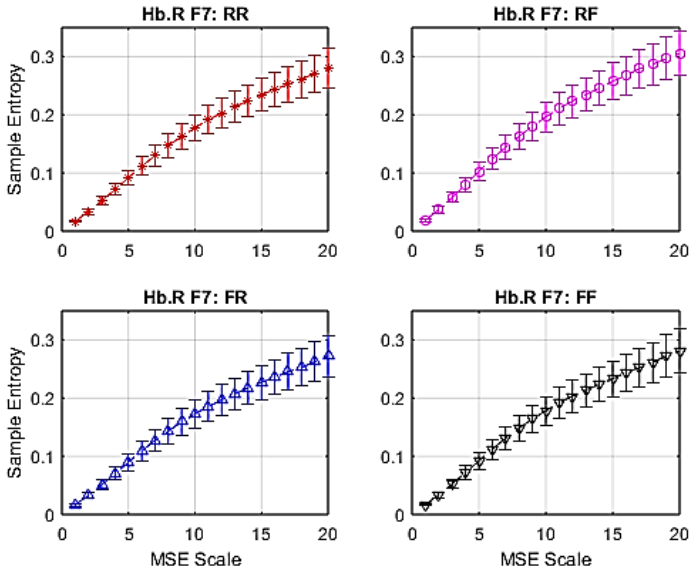


Figure 3.16 MSE fNIRS for Hb.R

Figure 3.16 shows a graph of MSE fNIRS for Hb.R. As compared to Hb.O2, both of them are similar in terms of a linearity and a level of entropy scale.

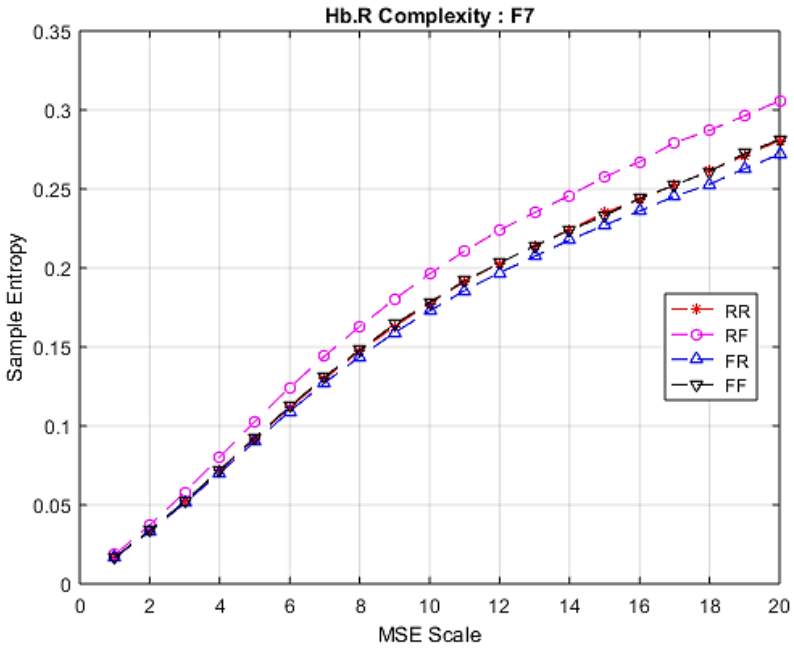


Figure 3.17 Comparison of MSE fNIRS in Hb.R at F7

Figure 3.17 shows a graph of 4 MSE fNIRS in Hb.R at F7 in comparison. The results revealed that RF or (remember but forget) is higher when compared to RR, FR, and FF, respectively.

3.5 MSE Topography and Statistical Analysis

3.5.1 MSE Topography

In order to present a detailed description of brain activity for a particular group, topography is used to show a 30 – channel for EEG and a 28 – channel for fNIRS as shown in Figure 3.18 – Figure 3.20.

From Scale 1 to Scale 20, the results of MSE taken from Scale 10 or the middle scale are shown in topography. In this study, Scale 10 is considered acceptable for sampling frequency in terms of both EEG and fNIRS.

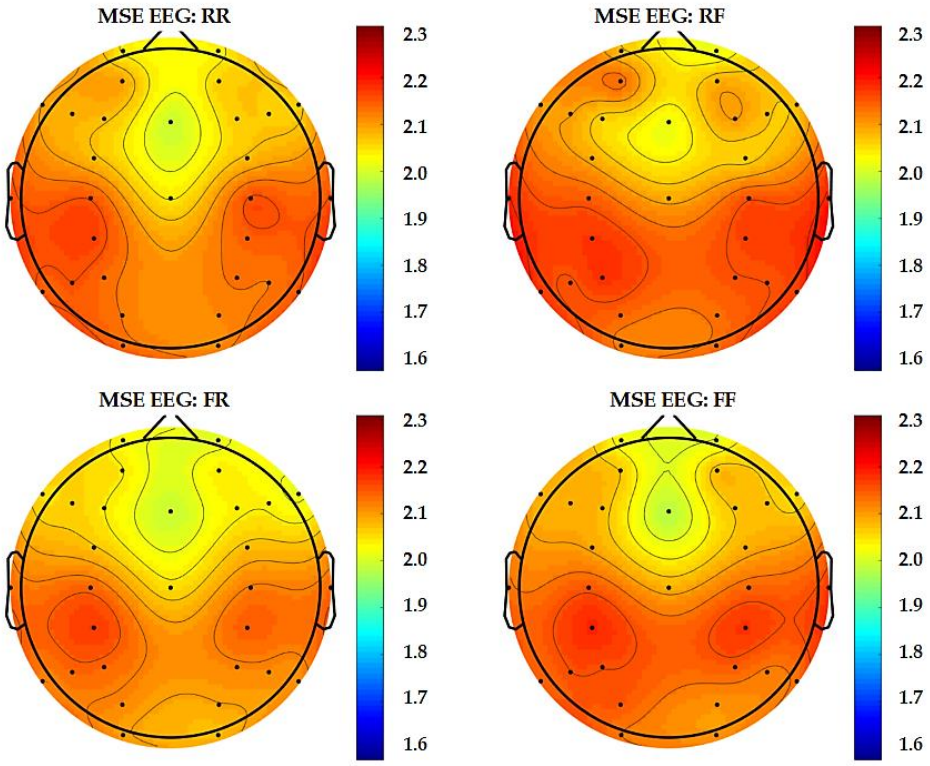


Figure 3.18 Topography of EEG

Figure 3.18 shows the brain activity presented in levels of entropy from 1.5 to 2.3. The results revealed that the brain activation measured in RR or (remember and remember) is higher when compared to RF, whereas FR and FF are indifferent.

Figure 3.19 and Figure 3.20 show the topography of fNIRS in Hb.O2 and Hb.R presented in levels of entropy from 0.1 to 0.32, respectively.

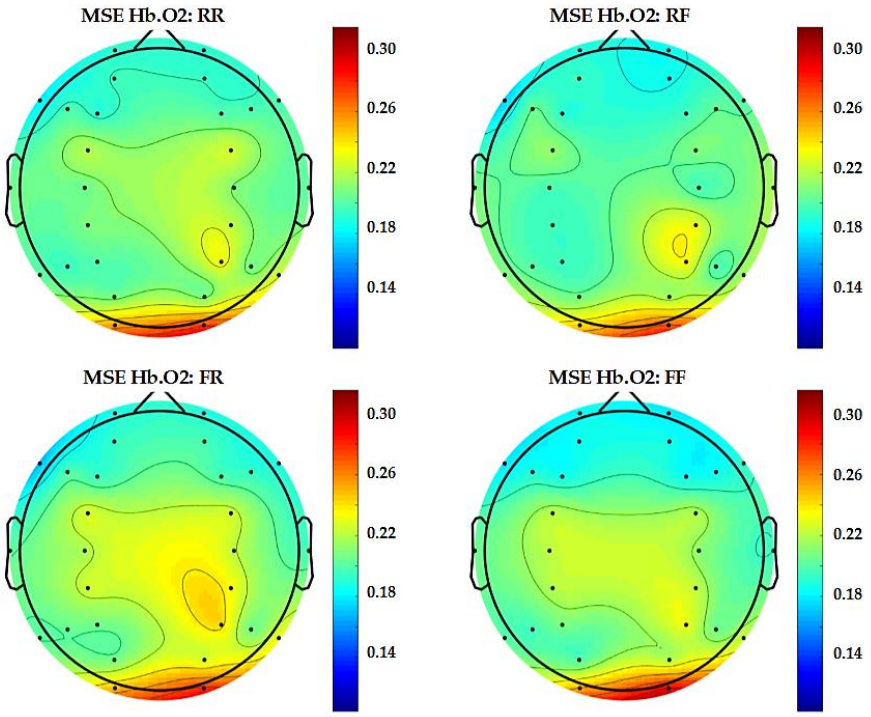


Figure 3.19 Topography of fNIRS in Hb.O2

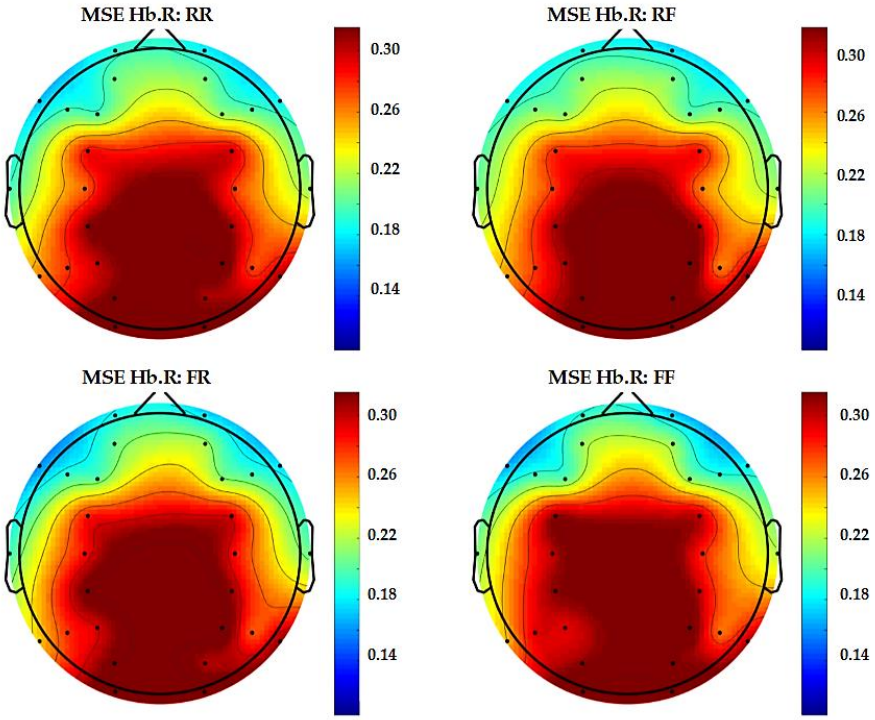


Figure 3.20 Topography of fNIRS in Hb.R

It was observed that, despite showing a more complexity level, there is indifferent among 4 fNIRS in Hb.R groups.

To better differentiate the brain complexity, the subtraction was used and presented into 6 groups, (RR and FF), (RR and FR), (RR and RF), (FR and FF), (RF and FR) and (RF and FF) as shown in Figure 3.21. – Figure 3.23.

In Figure 3.21 – 3.23, the differentiated results of MSE EEG, MSE Hb.O2, and MSE Hb.R are presented in accordance with levels of entropy (from -0.01 to 0.1 for EEG) and (from -0.02 to 0.02 for fNIRS). P values less than 0.05 presented with asterisks are shown in Table 3.3.

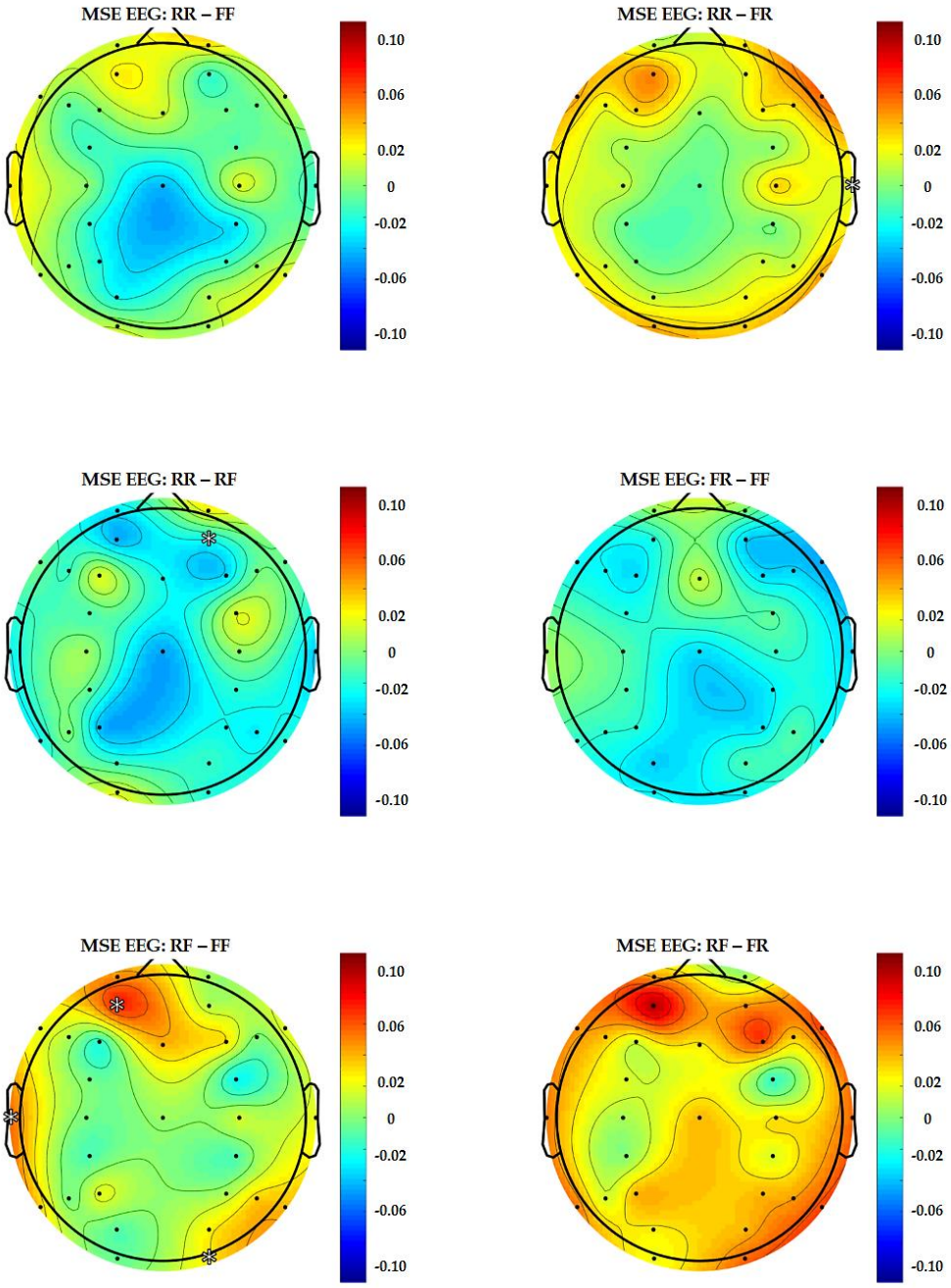


Figure 3.21 Topography of differential MSE EEG

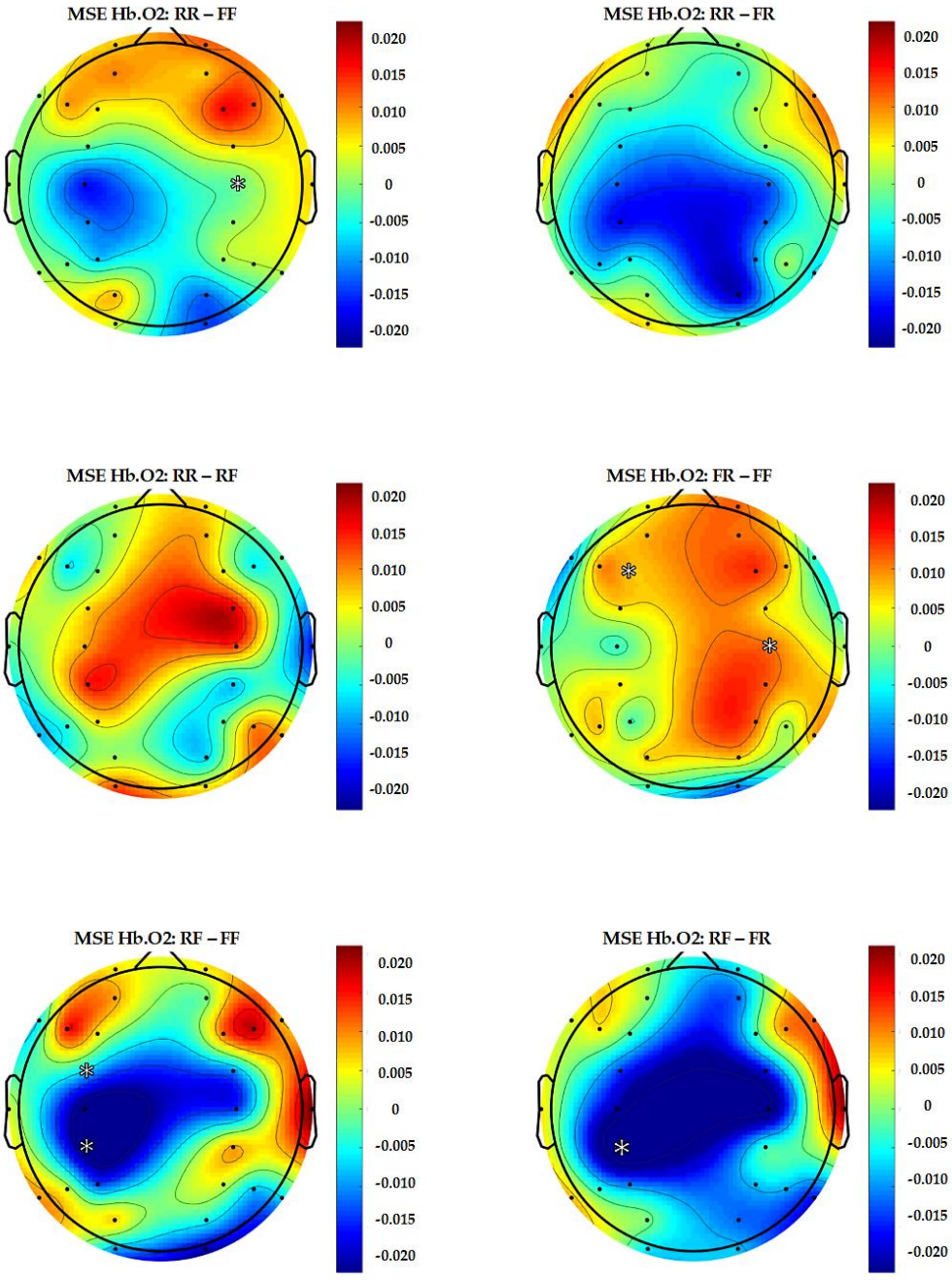


Figure 3.22 Topography of differential MSE Hb.O2

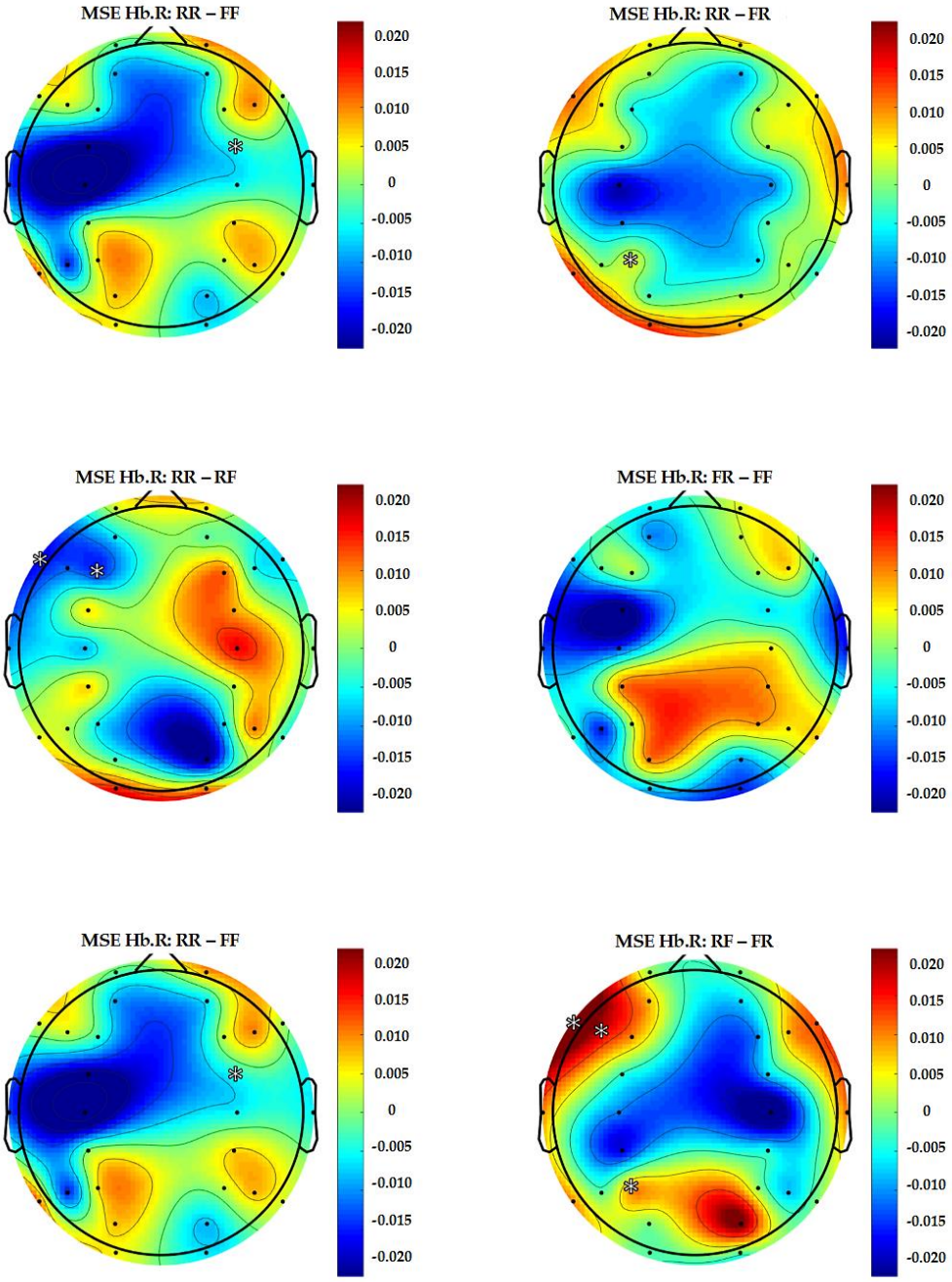


Figure 3.23 Topography of differential MSE Hb.R

3.5.2 Statistical Analysis: Wilcoxon signed-rank test

This section aims to present a significant difference in six pairs of the participants' responses on 30 channels in EGG, each of 28 channels in HbO2 and HbR measurements as follows.

1. The differential of MSE between RR and RF, (RR-RF)

2. The differential of MSE between RR and FR, (RR-FR)

3. The differential of MSE between RR and FF, (RR-FF)

4. The differential of MSE between RF and FR, (RF-FR)

5. The differential of MSE between RF and FF, (RF-FF)

6. The differential of MSE between FR and FF, (FR-FF)

An explanation of the results is divided into three main parts underlying on different types of measurements. Cohen's (1988) criterion of effect size which can be classified into three levels; (i) small; 0.1, (ii) 0.3; medium, and (iii) 0.5; large are used to determine an effect size in pair comparison.

The results of pair comparison with an insignificant difference can be found in Appendix X. The results of the Wilcoxon signed rank are reported as shown in Table 3.3 below.

Table 3.3

Results of the Wilcoxon Signed – Rank Test

Types of Measurements	Pairs		Median	Channels	Z	Asymp. Sig. (2-tailed)	*r*	Effect Size
EEG	1	RR	2.09	AF4	-2.07[b]	0.04	0.38	medium
		RF	2.11					
	2	RR	2.13	T8	-2.23[b]	0.03	0.41	medium
		FR	2.15					
	3	RF	2.13	AF3	-1.95[b]	0.05	0.36	medium
		FF	2.12					
	4	RF	2.09	O2	-2.21[b]	0.03	0.40	medium
		FF	2.09					
	5	RF	2.14	T7	-2.56[b]	0.01	0.47	medium
		FF	2.10					
Hb.O2	1	RR	0.23	C4	-1.95[b]	0.05	0.36	medium
		FF	0.21					
	2	RF	0.20	CP3	-2.05[c]	0.04	0.37	medium
		FR	0.21					
	3	RF	0.25	FC3	-2.29[b]	0.02	0.42	medium
		FF	0.23					
	4	RF	0.20	CP3	-2.21[c]	0.03	0.40	medium
		FF	0.20					
	5	FR	0.20	F3	-1.98[b]	0.05	0.36	medium
		FF	0.18					
	6	FR	0.22	C4	-2.10[b]	0.04	0.38	medium
		FF	0.21					
Hb.R	1	RR	0.20	F3	-2.14[c]	0.03	0.39	medium
		RF	0.20					
	2	RR	0.17	F7	-2.73[c]	0.01	0.50	large
		RF	0.22					
	3	RR	0.30	P3	-1.96[b]	0.05	0.36	medium
		FR	0.29					
	4	RR	0.31	FC4	-2.04[b]	0.04	0.37	medium
		FF	0.32					
	5	RF	0.32	P3	-2.34[b]	0.02	0.43	medium
		FR	0.29					
	6	RF	0.22	F5	-2.11[b]	0.04	0.39	medium
		FR	0.20					
	7	RF	0.18	F7	-2.51[b]	0.01	0.46	medium
		FR	0.17					
	8	RF	0.22	F5	-2.54[c]	0.01	0.46	medium
		FF	0.20					

Note. [b] Based on negative ranks; [c] Based on positive ranks.

Firstly, the results focuses on EGG measurement. There were five pairs showing a significant difference with a medium effect size whereby *p* value was equal to 0.05 or less than 0.05. The level of change in brain for the participants' responses in RF group (Md = 2.11) was significantly greater than that RR group (Md = 2.09) in channel 4, Z = -2.07, $p = 0.04$, r = 0.38. The participants' responses in RF group (Md = 2.14) also showed a significant greater increase as compared to the responses in FF group (Md = 2.10) in channel 21, Z = -2.56, $p = 0.01$, r = 0.47.

This is similar to the results in channel 3, it was revealed that level of change in brain on the responses in RF group (Md = 2.13) was significantly greater than that FF group (Md = 2.12), Z = -1.95, $p = 0.05$, r = 0.36. However, the level of change was not found in channel 16 in the pair comparison between RF (Md = 2.09) and FF (Md = 2.09) groups, $Z = -2.21$, $p = 0.03$, r = 0.40. Other than that, the findings showed that the participants' responses in FR group (Md = 2.15) manifested a significant increase in level of change in brain as compared to the responses in RR group (Md = 2.13) in channel 24, $Z = -2.23$, $p = 0.03$, r = 0.41.

Next, the second part emphasises on the results of HbO2 measurement. There were six pairs indicating a significant difference with a medium effect size whereby *p* value was equal to 0.05 or less than 0.05. Two pairs of the participants' responses in the comparisons between RF and FF groups as well as FR and FF groups showed a significant difference in two different channels. The results indicated that the responses in RF group (Md = 0.25) was significantly greater than that FF group (Md = 0.23) in channel 7, Z = -2.29, $p = 0.02$, r = 0.42. Nevertheless, the responses in RF and FF groups (Md = 0.20) in channel 22 showed a stable level in the participants' brain, Z = -2.21, $p = 0.03$. r = 0.40.

For the pair comparison of the participants' responses in RF and FF groups, the findings showed that level of change in brain for FR group (Md = 0.20) was significantly greater than that FF group in channel 5, Z = -1.98, p = 0.05, r = 0.36. In the same vein, the responses in FR group (Md = 0.22) manifested a significant increase in channel 10 as compared with the responses in FF group (Md = 0.21), Z = -2.10, p = 0.04, r = 0.38. The results also revealed that the responses in FR group (Md = 0.21) was significantly greater than that RF group (Md = 0.20) in channel 22, Z = -2.05, p = 0.04, r = 0 .37. Additionally to this, a significant increase in the participants' change in brain was found in a pair of the responses between RR (Md = 0.23) and FF (Md = 0.21) groups in channel 10, Z = -1.95, p = 0.05, r = 0.36.

In addition, the last part captures the results of HbR measurement. There were eight pairs illustrating a significant difference with a large effect size and a medium effect size whereby p value was equal to 0.05 or less than 0.05. Two pairs of the participants' responses in the comparisons between RR and RF groups as well as RR and FR groups showed a significant difference in two different channels. Four pairs of the participants' in the comparison between RF and FF groups demonstrated a significant difference in four different channels. The results of comparison with a large effect size was found in one pair of RF and RR groups in channel 19. The findings further indicated that the responses in RF group (Md = 0.22) was significantly greater than that RR group (Md = 0.17), Z = -2.73, p = 0.01, r = 0.50. On the other hand, level of change in the participants' brain in the comparison of the responses between RF and RR groups was equal (Md = 0.20) in channel 5, Z = -2.14, p = 0.03, r = 0.39.

Considering the responses in the pair comparison between RR and FR groups, the participants' responses in RR group (Md = 0.30) showed a significant increase as compared to the responses in FR group (Md = 0.29) in channel 8, Z = -1.96, p = 0.05,

r = 0.36. Contrary to this, the responses in RR group (Md = 0.31) manifested a significant decrease when comparing the responses with FF group (Md = 0.32), Z = -2.04, p = 0.04, r = 0.37.

As for the pair comparison of the participants' responses between FR and RF groups, the findings reported that the responses in RF group showed a significant increase in three different channels as compared to the responses in FR group, that is, (i) Channel 11; RF (Md = 0.32) and FR (Md = 0.29), Z = -2.34, p = 0.02, r = 0.43, (ii) Channel 17; RF (Md = 0.22) and FR (Md = 0.20), Z = -2.11, p = 0.04, r = 0.39, (iii) Channel 19; RF (Md = 0.18) and FR (Md = 0.17), Z = -2.51, p = 0.01, r = 0.46. Besides that, the responses in RF group (Md = 0.22) was significantly greater than that FF group (Md = 0.20) in channel 17, Z = -2.54, p = 0.01, r = 0.46.

The next step is to determine the relation between EEG and NIRS data by using Pearson Correlations Coefficient. The results are presented as follows.

3.5.3 Statistical Analysis: Correlations Coefficient

This section provides the results of the Pearson correlation in level of change in the participants' brain using three types of different measurements (i.e., EEG, Hb.O2, and Hb.R). The results of the correlations across different measurements were classified into four groups (i.e., RR, RF, FR, and FF) based on the participants' responses on pictures at first and second times in the experiment as follow Figure 3.24 – 3.27.

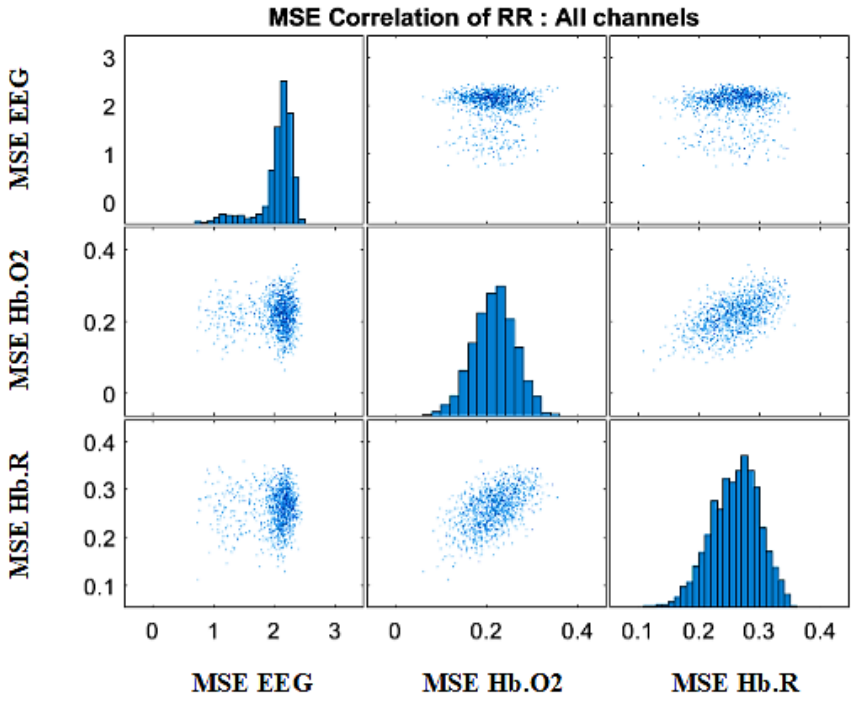


Figure 3.24 Scatter plot matrix for Correlation of RR group with sample size of 1,163 pictures

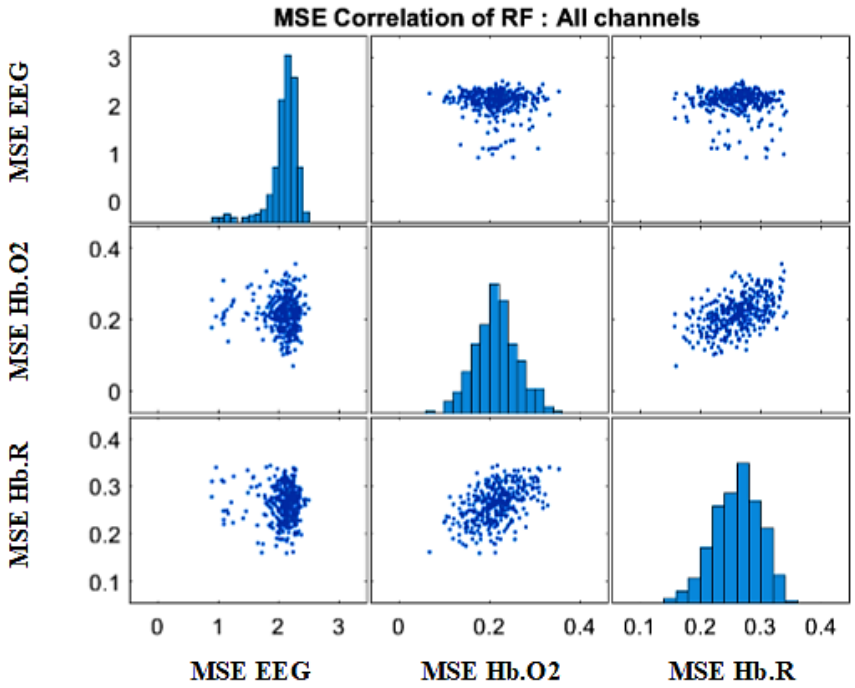


Figure 3.25 Scatter plot matrix for Correlation of RF group with sample size 348 pictures

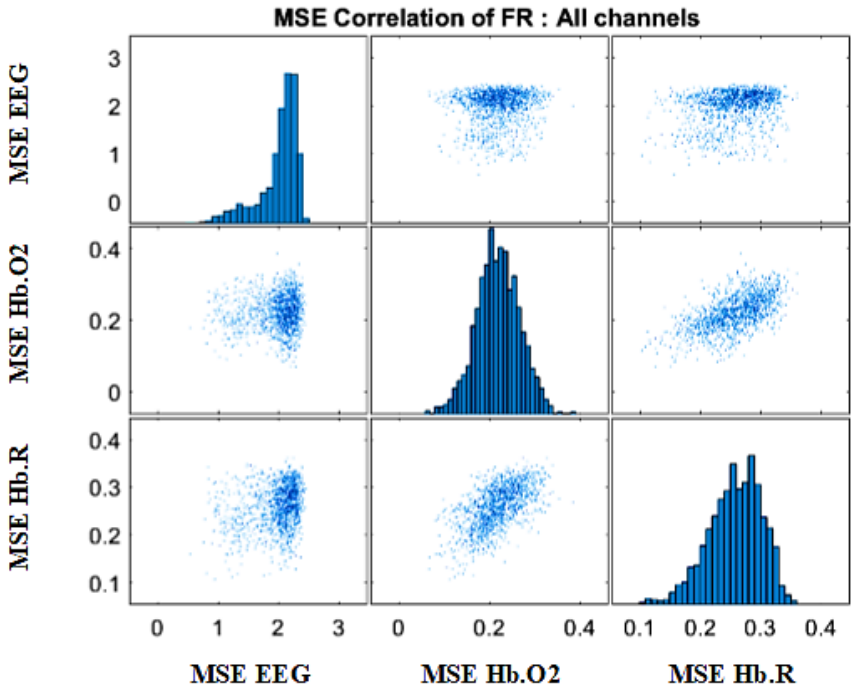


Figure 3.26 Scatter plot matrix for Correlation of FR group with sample size 1,577 pictures

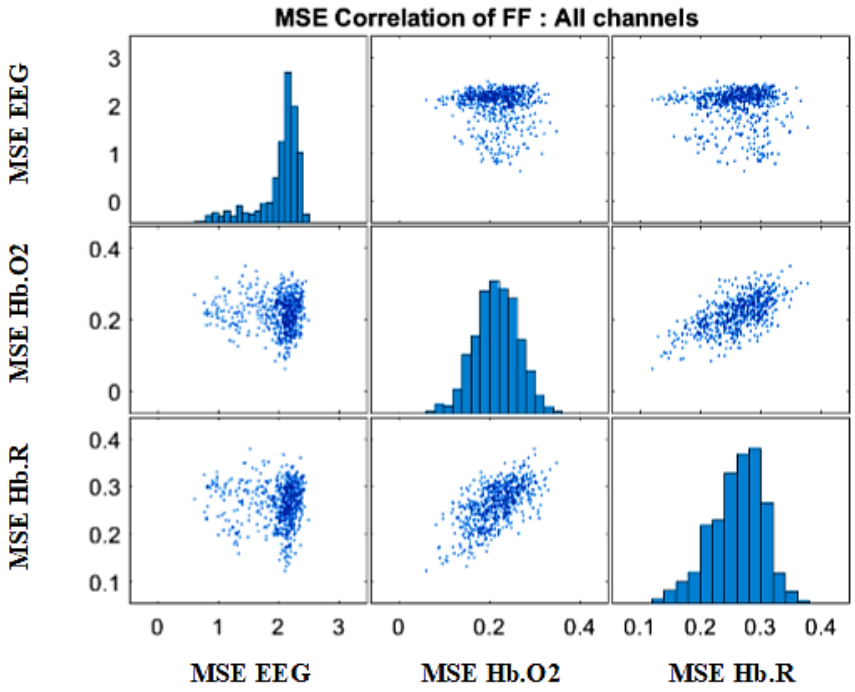


Figure 3.27 Scatter plot matrix for Correlation of FF group with sample size 651 pictures

The results of correlational analysis are presented in Table 3.4 which is accompanied with an account explaining the results in greater details.

Table 3.4

Results of the Pearson Correlation

Groups	Variables	Pearson Correlation (*r*)	Sig. (2-tailed)	Explained variance (%)	N***
RR	EEG−Hb.O2	0.021	0.469	0.04	1,163
	EEG−Hb.R	0.059*	0.044	0.35	
	Hb.O2−Hb.R	0.536**	0.000	28.73	
RF	EEG−Hb.O2	-0.039	0.471	0.15	348
	EEG−Hb.R	-0.070	0.193	0.49	
	Hb.O2−Hb.R	0.496**	0.000	24.60	
FR	EEG−Hb.O2	0.068**	0.007	0.46	1,577
	EEG−Hb.R	0.251**	0.000	6.30	
	Hb.O2−Hb.R	0.597**	0.000	35.64	
FF	EEG−Hb.O2	-0.049	0.211	0.24	651
	EEG−Hb.R	-0.022	0.582	0.05	
	Hb.O2−Hb.R	0.632**	0.000	39.94	

Note. * Correlation is significant at the 0.05 level (2-tailed).
** Correlation is significant at the 0.01 level (2-tailed).
*** N refers to numbers of pictures responded by 15 participants which were classified into four groups (i.e., RR, RF, FR, and FF).

A summary of the results is presented from one to another respective group. A criterion suggested by Evan (1996) was used to determine strengths of significant relationship with varying degrees, that is, 0.01 - 0.19; 'very weak', 0.20 - 0.39; 'weak', 0.40 - 0.59; 'moderate', 0.60 - 0.80; 'strong', and 0.90 - 1.00; 'very strong'. Firstly, the participants' responses on pictures in RR group showed a significant relationship in EEG and Hb.R measurements (i.e., r = 0.059, p = 0.04) and Hb.O2 and Hb.R measurements (i.e., r = 0.536, p = 0.00). A positive very weak strength was found in

the correlation between EEG and Hb.R measurements. Zero point three five per cent of the variance in EEG could explain the variance in the participants' responses in Hb.R Furthermore, a positive moderate strength was found in the correlation between Hb.O2 and Hb.R measurements. Approximately 29% of the variance in Hb.O2 could explain the variance in the participants' responses in Hb.R The findings in RR group pointed out that the responses in EEG and Hb.O2 measurements showed no significant relationship, r = 0.021, p = 0.46.

Secondly, the participants' responses on pictures in RF group showed a significant relationship in Hb.O2 and Hb.R measurements, r = 0.496, p = 0.00. This relationship showed a positive direction with moderate strength. Twenty four point six per cent of the variance in Hb.O2 could explain the variance in the participants' responses in Hb.R However, the relationships for the participants' responses which were measured with EEG and Hb.O2 and EEG and Hb.R were insignificantly negative, r = -0.039, p = 0.47 and r = -0.07, p = 0.19 respectively.

Next, the participants' responses on pictures in FR group exhibited a significant connection in EEG and Hb.O2 measurements (i.e., r = 0.068, p = 0.00), EEG and Hb.R (i.e., r = 0.251, p = 0.00) as well as Hb.O2 and Hb.R measurements (i.e., r = 0.597, p = 0.00). A positive very weak strength was found in the correlation between EEG and Hb.O2 measurements. Almost 0.5% of the variance in EEG could explain the variance in the participants' responses in Hb.O2 In addition, a positive weak strength was found in the correlation between EEG and Hb.R measurements. Approximately 6% of the variance in EEG could account for the variance in the participants' responses in Hb.R Other than that, a positive moderate strength was shown in the relationship between Hb.O2 and Hb.R measurements. More than 35% of the variance in Hb.O2 could explain the variance in the participants' responses in Hb.R.

Lastly, the participants' responses on pictures in FF group illustrated a significant relationship in Hb.O2 and Hb.R measurements, r = 0.632, p = 0.00. This correlation manifested a positive direction with strong strength. Almost 40% of the variance in Hb.O2 could explain the variance in the participants' responses in Hb.R However, the relationships for the participants' responses which were measured with EEG and Hb.O2 and EEG and Hb.R were insignificantly negative, r = -0.049, p = 0.21 and r = -0.02, p = 0.58 respectively.

CHAPTER 4

DISCUSSION AND CONCLUSION

This study has discussed the feasibility of using simultaneous EEG and fNIRS recordings, which extend the boundary of current measuring methodology and might be useful for creating novel understanding of neurophysiological phenomena such as those, which underlie brain complexity. EEG and fNIRS co-registration combining high temporal and spatial resolution may offer unique opportunities for brain function analysis. Consequently, a combination of these two techniques comprises the advantages of one technique while compensates for the limitations of the other.

While EEG measures electrical activity from the brain, providing high temporal resolution but low spatial resolution, fNIRS measures haemodynamic activity of the brain, with comparatively greater spatial resolution and poorer temporal resolution. These two signals complement each other's weaknesses, such that they may be combined in a common metric (e.g. MSE) to examine underlying cognitive processes.

This study has presented an application of simultaneous EEG and fNIRS recordings and utilising the metric of MSE to index brain complexity level. This approach may have prospects for the further investigation of other neurophysiological phenomena underlying brain complexity. Electroencephalography and fNIRS signal co-registration, combining high temporal and spatial resolution, provides a valuable opportunity for studying localised neurocognitive processes. The combination of these two techniques imparts the advantages of each, which compensate for the limitations of the other.

In this study, both EEG and fNIRS signals were converted to the same entropy scale to allow a comparison of brain activity in a common frame of reference. The maximum level of MSE EEG is approximately at 2.3, however the maximum level of MSE fNIRS is nearly 0.3. The level of MSE reveals characteristics of these two signals (e.g. non-linearity) that are considerably different. This analysis is considered to be more appropriate that addressing these signals separately in their native format.

Using neuroimaging to track patterns of brain activity as well as MSE to analyse the EEG, Hb.O2, and Hb.R data, the results revealed that RF shows the highest level followed by RR, FR, and FF, respectively. The brain is more active at (RR and RF) levels when compared to (FR and FF). In other words, the intention to remember things is likely to take more mental effort, and therefore show more brain activation than trying to forget them.

Our research findings agree with several studies, including Ang et al. (2014), in which brain is found to be more active during difficult tasks. In this study, (RF) may be associated with visual image difficulty. This is because some pictures are more difficult to classify, retrieve, and recall than others. Consequently, oxy-haemoglobin concentration during this task rises.

In this study, topography figures are used to display synchronized data from every channel. As shown in Figures 3.21 – 3.23, there are significant differences found in a number of pairs. However, regarding brain regions related to memory function (i.e. hits), taking this into consideration, there are significant differences between (RR and RF) at AF4 (EEG), F3 and F7 (Hb.R). As for (RR and FR), there are significant differences at P3 (Hb.R), (RR and FF) at FC4 (Hb.R), (RF and FR) at P3, F5 and F7

(Hb.R), (RF and FF) at AF3 (EEG), FC3 (Hb.O2) and F5 (Hb.R) as well as (FR and FF) at F3 (Hb.O2), $p < 0.05$ (two-tailed).

As shown in Table 3.3 and Figures 3.21 – 3.23, the brain activation mostly occurred in left ventrolateral prefrontal cortex (VLPFC), which has been associated with a diverse set of cognitive processes, including actively maintaining information in memory function (AF3, F3, F5, F7 and FC3).

Our findings appear to agree with Schroeter et al. (2004), who performed fNIRS during the Stroop task. They found differential haemodynamic responses in the left VLPFC correlated with age. It is worth mentioning that the investigations reported only fNIRS-measured prefrontal cortex activity, whereas the current study measures fast EEG (AF3 and AF4) and slower fNIRS (F3, F5, F7, FC3 and FC4) dominant sites simultaneously using a customized cap. These locations of the frontal lobes are closely related to memory functions, including short-term, working, and episodic long-term memory (N. A., Trans Cranial Technologies, 2012).

Aside from the prefrontal cortex, other areas related to memory functions were also monitored. For example, the primary somatosensory cortex (C4 and CP3), which is related to the sense of touch and finger proprioception caused by mouse clicking to respond whether the participants wished to remember or not in the experiment. The angular gyrus in the parietal lobe (P3) is associated with spatial focusing of attention (N. A., Trans Cranial Technologies, 2012), perhaps indicating that experiment required the participants' attention.

Moreover, the primary auditory cortex (T7) and middle temporal gyrus (T8) located in the temporal cortices may have been activated by operating noise of the fNIRS instrument during the experiment. Furthermore, the secondary visual cortex in

the occipital lobe (O2) was shown to be active while participants observed scenery on the display screen (N. A., Trans Cranial Technologies, 2012).

With responses time-locked to the stimuli, the participants demonstrated significantly higher activation in (RF) when compared to others in the frontal lobe, a region clearly associated with working memory systems and cognitive processing. In agreement with several neuroimaging studies (Cohen et al., 1997; Ma et al., 2012) the brain activation increased in the frontal area. In addition, a combination of all considerations suggests that simultaneous EEG and fNIRS should be preferred to only EEG or fNIRS. In particular, MSE EEG, MSE Hb.O2 and MSE Hb.R can be used for brain analysis.

Due to the complex and dynamic nature of conscious memory allocation, the participants may have employed unique strategies to memorise selected images. This could have resulted in memory processes overlapping across trials, whereby the participants continuously try to remember a previous stimulus. In this case, the presence of new trials could cause a distraction, which is known to diminish memory performance. The observations support the hypothesis that MSE EEG, MSE Hb.O2 and MSE Hb.R can be used to analyse neuronal activity. This remains a promising finding, and suggests that simultaneous multimodal brain signal recordings of EEG and fNIRS may be advantageous for brain analysis.

REFERENCES

Abásolo, D., Hornero, R., Espino, P., Alvarez, D., & Poza, J. (2006). Entropy analysis of the EEG background activity in Alzheimer's disease patients. *Physiological Measurement, 27*(3), 241-253.

Aboy, M., Cuesta-Frau, D., Austin, D., & Mico-Tormos, P. (2007) *Characterization of sample entropy in the context of biomedical signal analysis*. Paper presented at the 29th Annual International Conference of the IEEE Engineering in Medicine and Biology Society, Lyon, 22-26 August 2007, 5942-5945.

Aghajani, H., Garbey, M., & Omurtag, A. (2017). Measuring mental workload with EEG+fNIRS. *Frontiers in Human Neuroscience, 11*(359), 1-20. doi: 10.3389/fnhum.2017.00359

Al-Angari, H.M., & Sahakian, A.V. (2007) Use of sample entropy approach to study heart rate variability in obstructive sleep apnea syndrome. *IEEE Transactions on Biomedical Engineering*, *54*(10), 1900-1904.

Alloway, T. P., Gathercole, S. E., & Pickering, S. J. (2006). Verbal and visuospatial short-term and working memory in children: Are they separable?. *Child development, 77*(6), 1698-1716.

Al-shargie, F. M., Tang, T. B., Badruddin, N., & Kiguchi, M. (2015, December). Mental stress quantification using EEG signals. *In 2015 International Conference for Innovation in Biomedical Engineering and Life Sciences (pp. 15-19)*. Springer, Singapore.

Al-shargie, F., Tang, T. B., Badruddin, N., & Kiguchi, M. (2015, October). Simultaneous measurement of EEG-fNIRS in classifying and localizing brain activation to mental stress. *In 2015 IEEE International Conference on Signal and Image Processing Applications (ICSIPA) (pp. 282-286). IEEE.*

Alvarez, G. A., & Cavanagh, P. (2004). The capacity of visual short-term memory is set both by visual information load and by number of objects. *Psychological Science, 15*(2), 106-111.

Ang, K. K., Yu, J., & Guan, C. (2014, August). *Single-trial classification of NIRS data from prefrontal cortex during working memory tasks*. Paper presented at the 36th Annual International Conference of the IEEE Engineering in Medicine and Biology Society, Chicago, IL. doi: 10.1109/EMBC.2014.6944009

Araki, A., Ikegami, M., Okayama, A., Matsumoto, N., Takahashi, S., Azuma, H., & Takahashi, M. (2015). Improved prefrontal activity in AD/HD children treated with atomoxetine: A NIRS study. *Brain and Development, 37*(1), 76-87. doi: 10.1016/j.braindev.2014.03.011

Baddeley, A. (1992). Working memory. *Science, 255*(5044), 556-559.

Bashiri, M., Mumtaz, W., Malik, A. S., & Waqar, K. (2015, November). *EEG-based brain connectivity analysis of working memory and attention*. Paper presented at the IEEE Student Symposium in Biomedical Engineering & Sciences (ISSBES), Shah Alam, SGR.

Bassett, D. S., & Gazzaniga, M. S. (2011). Understanding complexity in the human brain. *Trends in cognitive sciences*, *15*(5), 200-209.

Basso Moro, S., Cutini, S., Ursini, M. L., Ferrari, M., & Quaresima, V. (2013). Prefrontal cortex activation during story encoding/retrieval: a multi-channel functional near-infrared spectroscopy study. *Frontiers in human neuroscience*, *7*(1), 925.

Bauer, P. J. (2015). Short-and Long-term Memory during Infancy and Early Childhood across Cultures. *International Encyclopedia of the Social & Behavioral Sciences (Second Edition)*, (pp. 896-900) USA: Elsevier. doi:10.1016/B978-0-08-097086-8.23064-X

Blasiman, R. N., & Was, C. A. (2018). Why is working memory performance unstable? *A review of 21 factors. Europe's journal of psychology*, 14(*1*), 188.

Blokland, Y., Spyrou, L., Lerou, J., Mourisse, J., Scheffer, G. J., van Geffen, G. J., ... & Bruhn, J. (2015). Detection of attempted movement from the EEG during neuromuscular block: proof of principle study in awake volunteers. *Scientific reports*, *5*(1), 12815.

Blokland, Y., Spyrou, L., Thijssen, D., Eijsvogels, T., Colier, W., Floor-Westerdijk, M., ... & Farquhar, J. (2013). Combined EEG-fNIRS decoding of motor attempt and imagery for brain switch control: an offline study in patients with tetraplegia. *IEEE transactions on neural systems and rehabilitation engineering*, *22*(2), 222-229.

Borowska, M. (2015). Entropy-based algorithms in the analysis of biomedical signals. Studies in Logic, *Grammar and Rhetoric*, *43*(1), 21-32.

Bortfeld, H., Wruck, E., & Boas, D. A. (2007). Assessing infants' cortical response to speech using near-infrared spectroscopy. *NeuroImage, 34*(1), 407-415. doi: 10.1016/j.neuroimage.2006.08.010

Bozkurt, A., Rosen, A., Rosen, H., & Onaral, B. (2005). A portable near infrared spectroscopy system for bedside monitoring of newborn brain. *BioMedical Engineering OnLine, 4*(29), 1-11. doi: 10.1186/1475-925X-4-29

Braver, T. S., Cohen, J. D., Nystrom, L. E., Jonides, J., Smith, E. E., & Noll, D. C. (1997). A parametric study of prefrontal cortex involvement in human working memory. *NeuroImage, 5*(1), 49-62. doi: 10.1006/nimg.1996.0247

Brooksby, B., Jiang, S., Dehghani, H., Pogue, B. W., Paulsen, K. D., Weaver, J., ... Poplack, S. P. (2005). Combining near-infrared tomography and magnetic resonance imaging to study in vivo breast tissue: Implementation of a Laplacian-type regularization to incorporate magnetic resonance structure. *Journal of Biomedical Optics*, *10*(5), 1-10. doi: 10.1117/1.2098627

Bruce, E. N., Bruce, M. C., & Vennelaganti, S. (2009). Sample entropy tracks changes in EEG power spectrum with sleep state and aging. *Journal of clinical neurophysiology: official publication of the American Electroencephalographic Societ*y, (4), 257.

Brunner, C., Delorme, A., & Makeig, S. (2013). Eeglab–An open source matlab toolbox for electrophysiological research. *Biomedical Engineering/Biomedizinische Technik*, 58(1), 1-2. doi:10.1515/bmt-2013-4182.

Bunce, S. C., Izzetoglu, M., Izzetoglu, K., Onaral, B., & Pourrezaei, K. (2006). Functional near-infrared spectroscopy. *IEEE engineering in medicine and biology magazine*, *25*(4), 54-62.

Buxton, R. B., Wong, E. C., & Frank, L. R. (1998). Dynamics of blood flow and oxygenation changes during brain activation: the balloon model. *Magnetic resonance in medicine*, *39*(6), 855-864.

Byun, S., Kim, A. Y., Jang, E. H., Kim, S., Choi, K. W., Yu, H. Y., & Jeon, H. J. (2019). Entropy analysis of heart rate variability and its application to recognize major depressive disorder: A pilot study. *Technology and Health Care*, (Preprint), 1-18.

Carruthers, P. (2013). Evolution of working memory. *Proceedings of the National Academy of Sciences*, *110(Supplement 2)*, 10371-10378.

Catarino, A., Churches, O., Baron-Cohen, S., Andrade, A., & Ring, H. (2011). Atypical EEG complexity in autism spectrum conditions: a multiscale entropy analysis. *Clinical neurophysiology*, *122*(12), 2375-2383.

Chen, J. E., & Glover, G. H. (2015). Functional magnetic resonance imaging methods. *Neuropsychology review*, *25*(3), 289-313.

Clapp, W. C., Rubens, M. T., & Gazzaley, A. (2009). Mechanisms of working memory disruption by external interference. *Cerebral Cortex*, *20*(4), 859-872.

Coffey, E. B. J., Brouwer, A., & Van Erp, J. B. F. (2012). Measuring workload using a combination of electroencephalography and near infrared spectroscopy. *Proceedings of the Human Factors and Ergonomics Society Annual Meeting*, *56*, 1822-1826. doi: 10.1177/1071181312561367

Cohen, J. D., Perlstein, W. M., Braver, T. S., Nystrom, L. E., Noll, D. C., Jonides, J., & Smith, E. E. (1997). Temporal dynamics of brain activation during a working memory task. *Nature*, *386*(6625), 604-608. doi: 10.1038/386604a0

Collins, G. P. (2002). *Claude E. Shannon: Founder of Information Theory*. Scientific American. < http://cispom. boisestate. edu/murli/links/ShannonSciAm. htm.

Cope, M. (1991). *The development of a near infrared spectroscopy system and its application for noninvasive monitoring of cerebral blood and tissue oxygenation in the newborn infants* (Doctoral dissertation, University of London).

Costa, M., Goldberger, A. L., & Peng, C. K. (2005). Multiscale entropy analysis of biological signals. *Physical Review E, 71*(2), 1-18. doi: 10.1103/PhysRevE.71.021906

Cowan, N. (2008). What are the differences between long-term, short-term, and working memory? *Progress in brain research*, *169*(1), 323-338.

Crosson, B., Ford, A., McGregor, K. M., Meinzer, M., Cheshkov, S., Li, X., ... & Briggs, R. W. (2010). Functional imaging and related techniques: an introduction for rehabilitation researchers. *Journal of rehabilitation research and development*, 47(2), 5-34.

Delgado-Bonal, A., & Marshak, A. (2019). Approximate entropy and sample entropy: A comprehensive tutorial. *Entropy*, *21*(6), 541.

Delorme, A., & Makeig, S. (2004). EEGLAB: An open source toolbox for analysis of single-trial EEG dynamics including independent component analysis. *Journal of Neuroscience Methods, 134*(1), 9-21. doi: 10.1016/j.jneumeth.2003.10.009

Diamantopoulou, S., Poom, L., Klaver, P., & Talsma, D. (2011). Visual working memory capacity and stimulus categories: a behavioral and electrophysiological investigation. *Experimental Brain Research, 209*(4), 501-513. doi: 10.1007/s00221-011-2536-z

Duann, J. R., Ide, J. S., Luo, X., & Li, C. S. R. (2009). Functional connectivity delineates distinct roles of the inferior frontal cortex and presupplementary motor area in stop signal inhibition. *Journal of Neuroscience*, *29*(32), 10171-10179.

Engle, R. W. (2002). Working memory capacity as executive attention. *Current Directions in Psychological Science, 11*(1), 19-23. doi: 10.1111/1467-8721.00160

Fazli, S., Mehnert, J., Steinbrink, J., Curio, G., Villringer, A., Müller, K. R., & Blankertz, B. (2012). Enhanced performance by a hybrid NIRS–EEG brain computer interface. *Neuroimage*, *59*(1), 519-529.

Ferrari, M., & Quaresima, V. (2012). A brief review on the history of human functional near-infrared spectroscopy (fNIRS) development and fields of application. *NeuroImage, 63*(2), 921-935. doi: 10.1016/j.neuroimage.2012.03.049

Flores Camacho, F., Ulloa Lugo, N., & Covarrubias Martínez, H. (2015). The concept of entropy, from its origins to teachers. *Revista mexicana de física E*, *61*(2), 69-80.

Fry, A. F., & Hale, S. (1996). Processing speed, working memory, and fluid intelligence: Evidence for a developmental cascade. *Psychological Science, 7*(4), 237-241. doi: 10.1111/j.1467-9280.1996.tb00366.x

Gathercole, S. E., & Alloway, T. P. (2007). *Understanding working memory: A classroom guide*. Lontoo: Harcourt Assessment.

Gevins, A., Smith, M. E., McEvoy, L., & Yu, D. (1997). High-resolution EEG mapping of cortical activation related to working memory: Effects of task difficulty, type of processing, and practice. *Cerebral Cortex, 7*(4), 374-385. doi: 10.1093/cercor/7.4.374

Haeussinger, F. B., Heinzel, S., Hahn, T., Schecklmann, M., Ehlis, A. C., & Fallgatter, A. J. (2011). Simulation of near-infrared light absorption considering individual head and prefrontal cortex anatomy: implications for optical neuroimaging. *PloS one*, *6*(10), e26377.

Herold, F., Wiegel, P., Scholkmann, F., & Mueller, N. G. (2018). Applications of functional near-infrared spectroscopy (fNIRS) neuroimaging in Exercise–Cognition science: a systematic, Methodology-Focused review. *Journal of clinical medicine*, *7*(12), 466.

Hirshfield, L. M., Chauncey, K., Gulotta, R., Girouard, A., Solovey, E. T., Jacob, R. J., ... Fantini, S. (2009). Combining electroencephalograph and functional near infrared spectroscopy to explore users' mental workload. In D. D. Schmorrow, I. V. Estabrooke, & M. Grootjen (Eds.), *Foundations of Augmented Cognition*: *Neurogonomics and Operational Neuroscience* (pp. 239-247). Berlin, Germany: Springer-Verlag. doi: 10.1007/978-3-642-02812-0_28

Hochreiter, S., & Schmidhuber, J. (1997). Long short-term memory. *Neural computation*, *9*(8), 1735-1780.

Hong, K. S., Khan, M. J., & Hong, M. J. (2018). Feature extraction and classification methods for hybrid fNIRS-EEG brain-computer interfaces. *Frontiers in Human Neuroscience, 12*(246), 1-25. doi: 10.3389/fnhum.2018.00246

Hornero, R., Abásolo, D., Escudero, J., & Gómez, C. (2008). Nonlinear analysis of electroencephalogram and magnetoencephalogram recordings in patients with Alzheimer's disease. *Philosophical Transactions of the Royal Society A: Mathematical, Physical and Engineering Sciences*, *367*(1887), 317-336.

Hu, X., Miller, C., Vespa, P., & Bergsneider, M. (2008). Adaptive computation of approximate entropy and its application in integrative analysis of irregularity of heart rate variability and intracranial pressure signals. *Medical engineering & physics*, *30*(5), 631-639.

Huppert, T. J., Diamond, S. G., Franceschini, M. A., & Boas, D. A. (2009). HomER: A review of time-series analysis methods for near-infrared spectroscopy of the brain. *Applied Optics, 48*(10), D280-D298. doi: 10.1364/AO.48.00D280

Khalaj, F., Pasha, E., Tavakkoli-Moghaddam, R., & Khalaj, M. (2018). Interval-Valued Uncertainty Based on Entropy and Dempster–Shafer Theory. *Journal of Statistical Theory and Applications*, *17*(4), 627-635.

Khan, M. J., Hong, M. J., & Hong, K. S. (2014). Decoding of four movement directions using hybrid NIRS-EEG brain-computer interface. *Frontiers in human neuroscience*, *8*(1), 244.

Kim, H. Y., Seo, K., Jeon, H. J., Lee, U., & Lee, H. (2017). Application of functional near-infrared spectroscopy to the study of brain function in humans and animal models. *Molecules and cells*, *40*(8), 523.

Korhonen, V., Hiltunen, T., Myllylä, T., Wang, X., Kantola, J., Nikkinen, J., ... & Kiviniemi, V. (2014). Synchronous multiscale neuroimaging environment for critically sampled physiological analysis of brain function: hepta-scan concept. *Brain connectivity*, *4*(9), 677-689.

Kumar, P. S., Arumuganathan, R., Sivakumar, K., & Vimal, C. (2008). Removal of ocular artifacts in the EEG through wavelet transform without using an EOG reference channel. Int. J. *Open Problems Compt. Math*, *1*(3), 188-200.

Lambek, R., & Shevlin, M. (2011). Working memory and response inhibition in children and adolescents: Age and organization issues. *Scandinavian Journal of Psychology*, *52*(5), 427-432.

Leon, A. C. (1998). Descriptive and inferential statistics. *In Comprehensive Clinical Psychology*; Bellack, A.S., Hersen, M., Eds.; Pergamon: Oxford, UK, 243–285.

Lin, P. Y., Lin, S. I., Penney, T., & Chen, J. J. (2009). Applications of near infrared spectroscopy and imaging for motor rehabilitation in stroke patients. *J Med Biol Eng*, *29*(5), 210-221.

Lin, Y. P., Wang, C. H., Jung, T. P., Wu, T. L., Jeng, S. K., Duann, J. R., & Chen, J. H. (2010). EEG-based emotion recognition in music listening. *IEEE Transactions on Biomedical Engineering*, *57*(7), 1798-1806. doi: 10.1109/TBME.2010.2048568

Lindenberger, U., & Baltes, P. B. (1994). Sensory functioning and intelligence in old age: A strong connection. *Psychology and Aging, 9*(3), 339-355. doi: 10.1037/0882-7974.9.3.339

Liu, X., Jiang, A., Xu, N., & Xue, J. (2016). Increment entropy as a measure of complexity for time series. *Entropy*, *18*(1), 22.

Liu, Y., Piazza, E. A., Simony, E., Shewokis, P. A., Onaral, B., Hasson, U., & Ayaz, H. (2017). Measuring speaker–listener neural coupling with functional near infrared spectroscopy. *Scientific Reports, 7*(43293), 1-13. doi: 10.1038/srep43293

Lystad, R. P., & Pollard, H. (2009). Functional neuroimaging: a brief overview and feasibility for use in chiropractic research. *The Journal of the Canadian Chiropractic Association*, *53*(1), 59.

Ma, L., Steinberg, J. L., Hasan, K. M., Narayana, P. A., Kramer, L. A., & Moeller, F. G. (2012). Working memory load modulation of parieto-frontal connections:

Evidence from dynamic causal modeling. *Human Brain Mapping, 33*(8), 1850-1867. doi: 10.1002/hbm.21329

Maturana-Candelas, A., Gómez, C., Poza, J., Pinto, N., & Hornero, R. (2019). EEG characterization of the Alzheimer's disease continuum by means of Multiscale Entropies. *Entropy, 21*(6), 544.

Mehta, R. K., & Parasuraman, R. (2013). Neuroergonomics: a review of applications to physical and cognitive work. *Frontiers in human neuroscience, 7*, 889.

Mirelman, A., Maidan, I., Bernad-Elazari, H., Nieuwhof, F., Reelick, M., Giladi, N., & Hausdorff, J. M. (2014). Increased frontal brain activation during walking while dual tasking: an fNIRS study in healthy young adults. *Journal of Neuroengineering and Rehabilitation, 11*(85), 1-7. doi: 10.1186/1743-0003-11-85

Molteni, E., Contini, D., Caffini, M., Baselli, G., Spinelli, L., Cubeddu, R., … Torriceli, A. (2012). Load-dependent brain activation assessed by time-domain functional near-infrared spectroscopy during a working memory task with graded levels of difficulty. *Journal of Biomedical Optics, 17*(5), 1-12. doi: 10.1117/1.JBO.17.5.056005

Morabito, F. C., Labate, D., La Foresta, F., Bramanti, A., Morabito, G., & Palamara, I. (2012). Multivariate multi-scale permutation entropy for complexity analysis of Alzheimer's disease EEG. *Entropy, 14*(7), 1186-1202. doi: 10.3390/e14071186

Moran, R. J., Campo, P., Maestu, F., Reilly, R. B., Dolan, R. J., & Strange, B. A. (2010). Peak frequency in the theta and alpha bands correlates with human working memory capacity. *Frontiers in Human Neuroscience, 4*(200), 1-12. doi: 10.3389/fnhum.2010.00200

Morris, N., & Jones, D. M. (1990). Memory updating in working memory: The role of the central executive. *British Journal of Psychology, 81*(2), 111-121. doi: 10.1111/j.2044-8295.1990.tb02349.x

N. A. Trans Cranial Technologies, *Cortical Functions Reference*, Wan Chai, Hong Kong: Trans Cranial Technologies ldt., 2012.

Nadel, L., & Hardt, O. (2011). Update on memory systems and processes. *Neuropsychopharmacology*, 36(*1*), 251.

Nagel B. J., Ohannessian A., & Cummins K. (2007). Performance dissociation during verbal and spatial working memory tasks. *Perceptual and Motor Skills, 105*(1), 243–250. doi:. 10.2466/pms.105.1.243-250

Norcia, A. M., Appelbaum, L. G., Ales, J. M., Cottereau, B. R., & Rossion, B. (2015). The steady-state visual evoked potential in vision research: a review. *Journal of vision, 15*(6), 4-4.

Peng, S., Chen, B., Sun, L., Ser, W., & Lin, Z. (2017). Constrained maximum correntropy adaptive filtering. *Signal Processing, 140*, 116-126.

Pincus, S. M. (1991, April). *Approximate entropy: A complexity measure for biological time series data*. Paper presented at the IEEE Seventeenth Annual Northeast Bioengineering Conference, Hartford, CT. doi: 10.1109/NEBC.1991.154568

Pincus, S. M., Mulligan, T., Iranmanesh, A., Gheorghiu, S., Godschalk, M., & Veldhuis, J. D. (1996). Older males secrete luteinizing hormone and testosterone more irregularly, and jointly more asynchronously, than younger males. *Proceedings of the National Academy of Sciences*, *93*(24), 14100-14105.

Putze, F., Hesslinger, S., Tse, C. Y., Huang, Y., Herff, C., Guan, C., & Schultz, T. (2014). Hybrid fNIRS-EEG based classification of auditory and visual perception processes. *Frontiers in Neuroscience, 8*(373), 1-13. doi: 10.3389/fnins.2014.00373

Quaresima, V., Bisconti, S., & Ferrari, M. (2012). A brief review on the use of functional near-infrared spectroscopy (fNIRS) for language imaging studies in human newborns and adults. *Brain and Language, 121*(2), 79-89. doi: 10.1016/j.bandl.2011.03.009

Raffalt, P. C., Denton, W., & Yentes, J. M. (2018). On the choice of multiscale entropy algorithm for quantification of complexity in gait data. *Computers in biology and medicine*, *103*(1), 93-100.

Ranger, M., Johnston, C. C., Limperopoulos, C., Rennick, J. E., & du Plessis, A. J. (2011). Cerebral Near-Infrared Spectroscopy as a Measure of Nociceptive Evoked Activity in Critically III Infants. *Pain Research and Management*, *16*(5), 331-336.

Redick T. S., Broadway J. M., Meier M. E., Kuriakose P. S., Unsworth N., Kane M. J., & Engle R. W. (2012). Measuring working memory capacity with automated complex span tasks. *European Journal of Psychological Assessment*, *28(*1*),* 164–171. doi:.10.1027/1015-5759/a000123

Richman, J. S., & Moorman, J. R. (2000). Physiological time-series analysis using approximate entropy and sample entropy. *American Journal of Physiology Heart and Circulatory Physiology, 278*(6), H2039-H2049. doi: 10.1152/ajpheart.2000.278.6.H2039

Robert M., & Savoie N. (2006). Are there gender differences in verbal and visuospatial working-memory resources? *European Journal of Cognitive Psychology*, *18*(1), 378–397. doi:. 10.1080/09541440500234104

Sai, L., Zhou, X., Ding, X. P., Fu, G., & Sang, B. (2014). Detecting concealed information using functional near-infrared spectroscopy. *Brain topography*, *27*(5), 652-662.

Sarigiannidis, I., Crickmore, G., & Astle, D. E. (2016). Developmental and individual differences in the precision of visuospatial memory. *Cognitive Development*, 39 (*1*), 1-12.

Sasabe, T., & Hagiwara, H. (2018, October). *Using NIRS to detect brain oxyHb changes during short-term memory tasks*. Paper presented at the IEEE 18th International Conference on Bioinformatics and Bioengineering (BIBE), Taichung, TG. doi: 10.1109/BIBE.2018.00067

Scheeringa, R., Petersson, K. M., Oostenveld, R., Norris, D. G., Hagoort, P., & Bastiaansen, M. C. M. (2009). Trial-by-trial coupling between EEG and BOLD identifies networks related to alpha and theta EEG power increases during working memory maintenance. *NeuroImage, 44*(3), 1224-1238. doi: 10.1016/j.neuroimage.2008.08.041

Schreppel, T., Egetemeir, J., Schecklmann, M., Plichta, M. M., Pauli, P., Ellgring, H., ... & Herrmann, M. J. (2008). Activation of the prefrontal cortex in working memory and interference resolution processes assessed with near-infrared spectroscopy. *Neuropsychobiology, 57*(4), 188-193. doi: 10.1159/000147473

Schroeter, M. L., Zysset, S., Wahl, M., & Von Cramon, D. Y. (2004). Prefrontal activation due to Stroop interference increases during development−An event-related fNIRS study. *NeuroImage, 23*(4), 1317-1325. doi: 10.1016/j.neuroimage.2004.08.001

Sharanreddy, P., & Kulkarni, P. K. (2013). EEG signal classification for epilepsy seizure detection using improved approximate entropy. *Int J Public Health Sci*, *2*(1), 23-32.

Shiffrin, R. M., & Atkinson, R. C. (1969). Storage and retrieval processes in long-term memory. *Psychological Review*, *76*(2), 179.

Shin, J., Von Lühmann, A., Kim, D. W., Mehnert, J., Hwang, H. J., & Müller, K. R. (2018). Simultaneous acquisition of EEG and NIRS during cognitive tasks for an open access dataset. *Scientific data*, *5(*1), 180003.

Sohrab, S. H. (2014). Boltzmann entropy of thermodynamics versus Shannon entropy of information theory. *Int. J. Mech*, *8*(1), 73-84.

Stergiou, N. (2016). *Nonlinear analysis for human movement variability*. CRC Press.

Sun, Y., Ayaz, H., & Akansu, A. N. (2015, December). *Neural correlates of affective context in facial expression analysis: A simultaneous EEG-fNIRS study*. Paper presented at the IEEE Global Conference on Signal and Information Processing (GlobalSIP), Orlando, FL.
doi: 10.1109/GlobalSIP.2015.7418311

Sweeny, T. D., Wurnitsch, N., Gopnik, A., & Whitney, D. (2015). Ensemble perception of size in 4–5-year-old children. *Developmental Science*, 18(*4*), 556-568.

Teng, C., Cheng, Y., Wang, C., Ren, Y., Xu, W., & Xu, J. (2018). Aging-related changes of EEG synchronization during a visual working memory task. *Cognitive Neurodynamics, 12*(6), 561-568. doi: 10.1007/s11571-018-9500-6

Tsunashima, H., Yanagisawa, K., & Iwadate, M. (2012). *Measurement of Brain Function Using Near-Infrared Spectroscopy (NIRS).* INTECH Open Access Publisher.

Ullah, K., Ali, M., Rizwan, M., & Imran, M. (2011, December). *Low-cost single-channel EEG based communication system for people with lock-in syndrome*. Paper presented at the IEEE 14th International Multitopic Conference, Karachi, SD. doi: 10.1109/INMIC.2011.6151455

Ungerleider, L. G., Courtney, S. M., & Haxby, J. V. (1998). A neural system for human visual working memory. *Proceedings of the National Academy of Sciences of the United States of America, 95*(3), 883-890. doi: 10.1073/pnas.95.3.883

Vigário, R., Sarela, J., Jousmiki, V., Hamalainen, M., & Oja, E. (2000). Independent component approach to the analysis of EEG and MEG recordings. *IEEE transactions on biomedical engineering, 47*(5), 589-593.

Wang, W., Zhao, J., Qu, H., & Chen, B. (2017). A correntropy inspired variable step-size sign algorithm against impulsive noises. *Signal Processing, 141*(1), 168-175.

Wu, S. D., Wu, C. W., Lin, S. G., Wang, C. C., & Lee, K. Y. (2013). Time series analysis using composite multiscale entropy. *Entropy, 15*(3), 1069-1084. doi: 10.3390/e15031069

Xiao, J., Hays, J., Ehinger, K. A., Oliva, A., & Torralba, A. (2010, June). *Sun database: Large-scale scene recognition from abbey to zoo*. Paper presented at the IEEE Computer Society Conference on Computer Vision and Pattern Recognition, San Francisco, CA. doi: 10.1109/CVPR.2010.5539970

Xue, G., Chen, C., Lu, Z. L., & Dong, Q. (2010). Brain Imaging Techniques and Their Applications in Decision-Making Research. *Xin li xue bao. Acta psychologica Sinica, 42*(1), 120-137.

Yan, J. J., Wang, Y. Q., Guo, R., Zhou, J. Z., Yan, H. X., Xia, C. M., & Shen, Y. (2012). Nonlinear analysis of auscultation signals in TCM using the combination of wavelet packet transform and sample entropy. *Evidence-Based Complementary and Alternative Medicine, 2012*.

Ye, J. C., Tak, S., Jang, K. E., Jung, J., & Jang, J. (2009). NIRS-SPM: Statistical parametric mapping for near-infrared spectroscopy. *NeuroImage, 44*(2), 428-447. doi: 10.1016/j.neuroimage.2008.08.036

Yentes, J. M., Hunt, N., Schmid, K. K., Kaipust, J. P., McGrath, D., & Stergiou, N. (2013). The appropriate use of approximate entropy and sample entropy with short data sets. *Annals of Biomedical Engineering, 41*(2), 349-365. doi: 10.1007/s10439-012-0668-3

Yoo, D. H., & Chung, M. J. (2005). A novel non-intrusive eye gaze estimation using cross-ratio under large head motion. *Computer Vision and Image Understanding, 98*(1), 25-51. doi: 10.1016/j.cviu.2004.07.011

Yücel, M. A., Selb, J. J., Huppert, T. J., Franceschini, M. A., & Boas, D. A. (2017). Functional near infrared spectroscopy: Enabling routine functional brain imaging. *Current opinion in biomedical engineering*, *4*(1), 78-86.

Zama, T., Takahashi, Y., & Shimada, S. (2019). Simultaneous EEG-NIRS Measurement of the Inferior Parietal Lobule During a Reaching Task With Delayed Visual Feedback. *Frontiers in human neuroscience*, *13*(1), 301.

Zhang, D., Zhao, H., Bai, W., & Tian, X. (2016). Functional connectivity among multi-channel EEGs when working memory load reaches the capacity. *Brain Research, 1631*(15), 101-112. doi: 10.1016/j.brainres.2015.11.036

Zhang, F., Cai, Z., Skums, P., & Zhang, S. (Eds.). (2018). Bioinformatics Research and Applications: 14th International Symposium, ISBRA 2018, Beijing, China, June 8-11, 2018, Proceedings (Vol. 10847). Springer.

APPENDIX A

Consent Form

Consent Form

As a researcher, I am asking you to participate in a research study titled

"Multiscale Entropy Analysis of Brain Complexity Using Simultaneous EEG and fNIRS"

This is because your qualifications unquestionably meet the criteria for this study. Please read this form carefully and feel free to ask any questions you may have before agreeing to participate in the study.

Purpose of the Study: The purpose of this study is to apply multi-scale entropy (MSE), a promising technique that is backboned of this study, for analysing brain activity in terms of entropy or brain complexity levels.

What the researcher will ask you to do: If you agree to participate in this study, you will be asked to participate in the experimental session. Prior to the experiment, you will be given task-specific instructions as well as a brief practice session for the visual memory task. Your accurate responses and the time spent in this experiment are highly respected and appreciated. It will take approximately 2 hours for the experiment and the recognition test. With your permission, the researcher would also like to have the simultaneous EEG-fNIRS data recorded**.**

Risks: The researchers do not anticipate any risks from participating in this study.

Benefits: The results from this study may benefit other people now or in the future especially in the area of neuroinformatics and brain function analysis

Compensation: You will receive a token of appreciation for your participation.

Your data will be kept confidential: Apart from that, in any sort of report in public, the researcher will not include any personal information that may identify you.

Taking part is voluntary: The participant's involvement is completely voluntary. You may refuse to participate before the study begins, discontinue at any time when you feel uncomfortable.

The researcher conducting this study is Mr. Thanate Angsuwatanakul, a Ph.D. student at Graduate School of Systems Life Sciences, Kyushu University. If you have any questions or concerns regarding your rights as a participant in this study, you can contact Mr. Thanate Angsuwatanakul at thanate.ang@gmail.com

****

Statement of Consent:

I have read the above information, and have received answers to any questions I asked.
I consent to participate in the study.

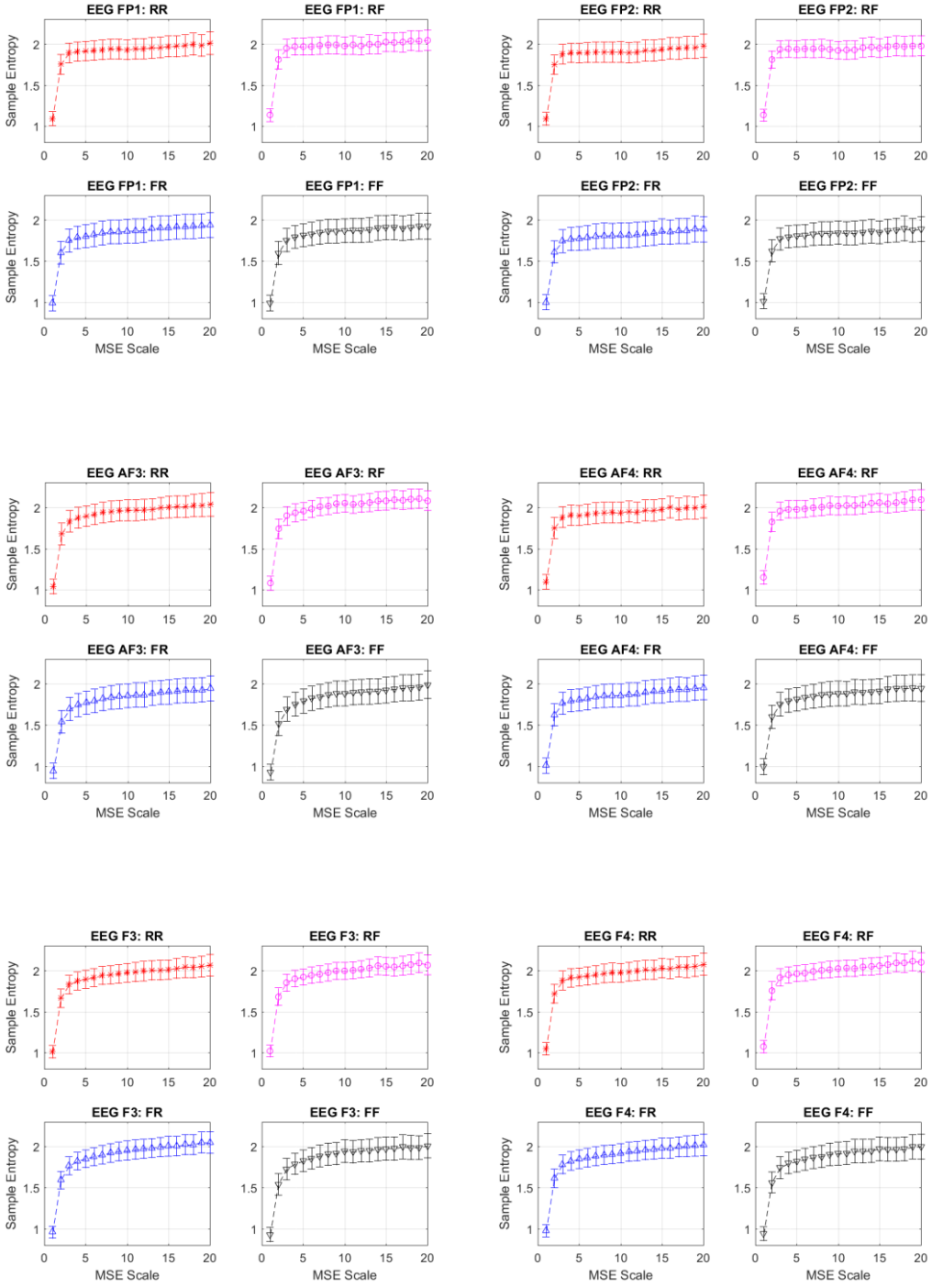
Signature _____Date _____

****

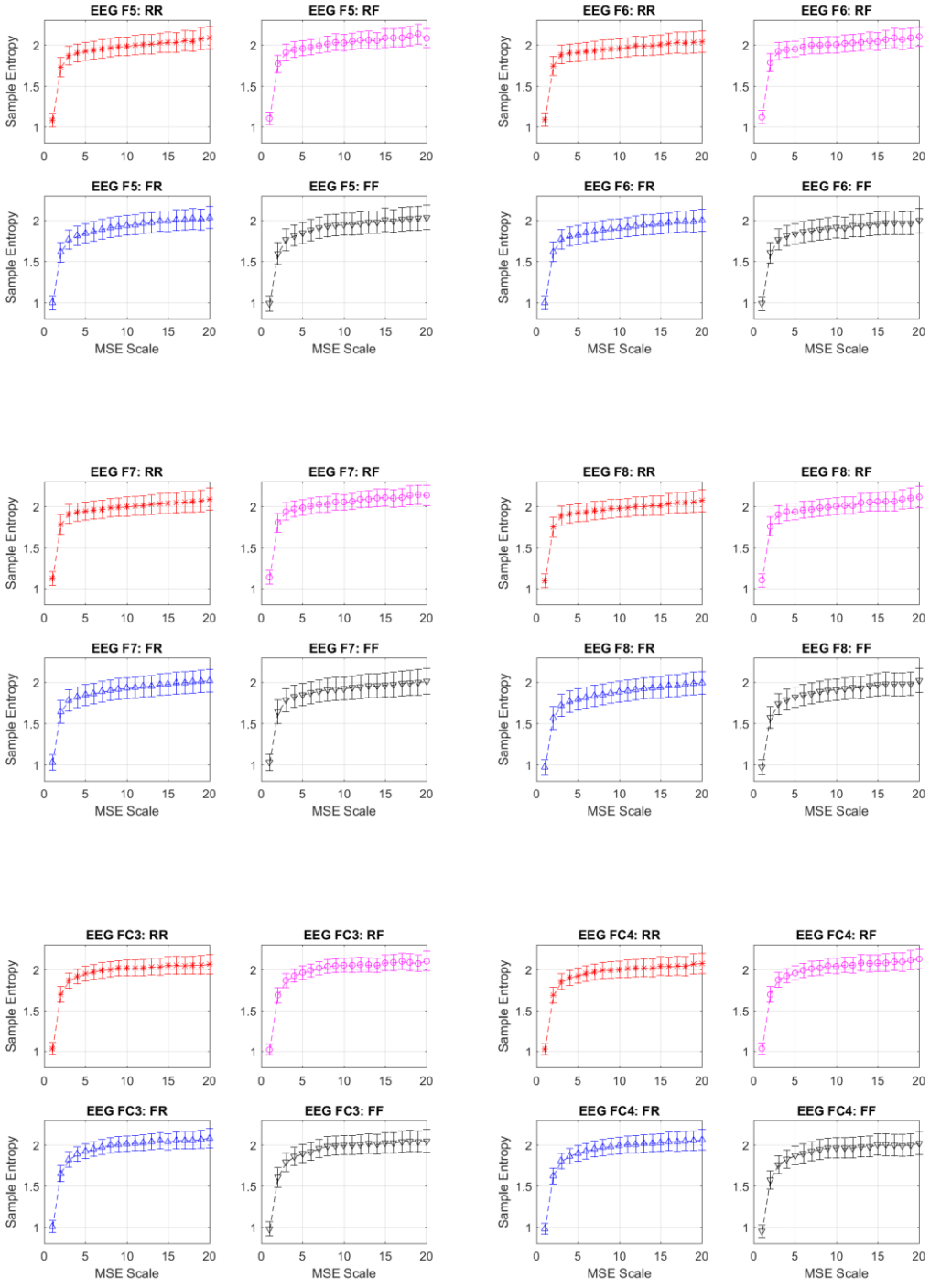
APPENDIX B

Averaging Graph of Multiscale Entropy Graph with Standard Error

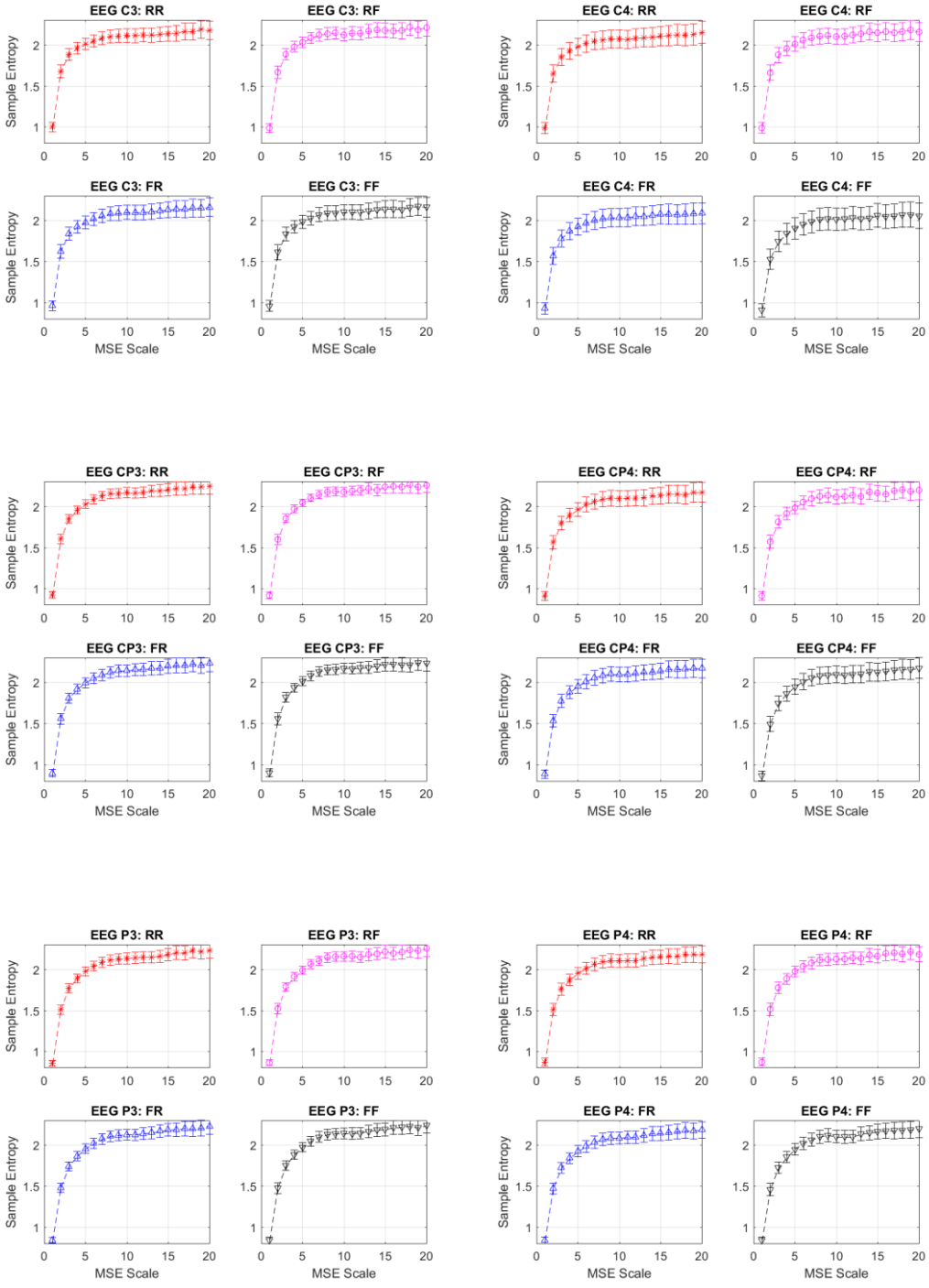
Averaging Multiscale Entropy of EEG Data



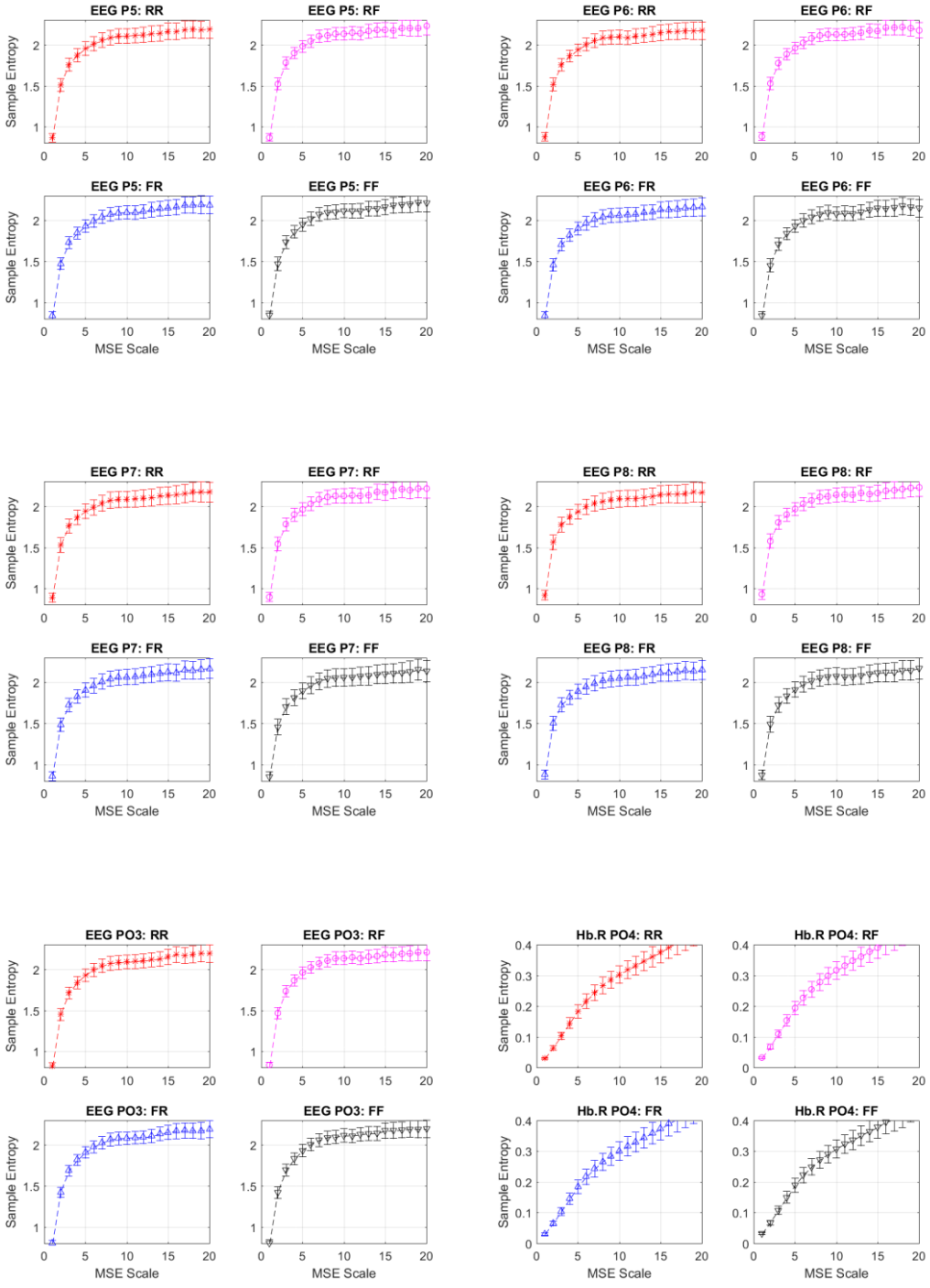
Averaging Multiscale Entropy of EEG Data



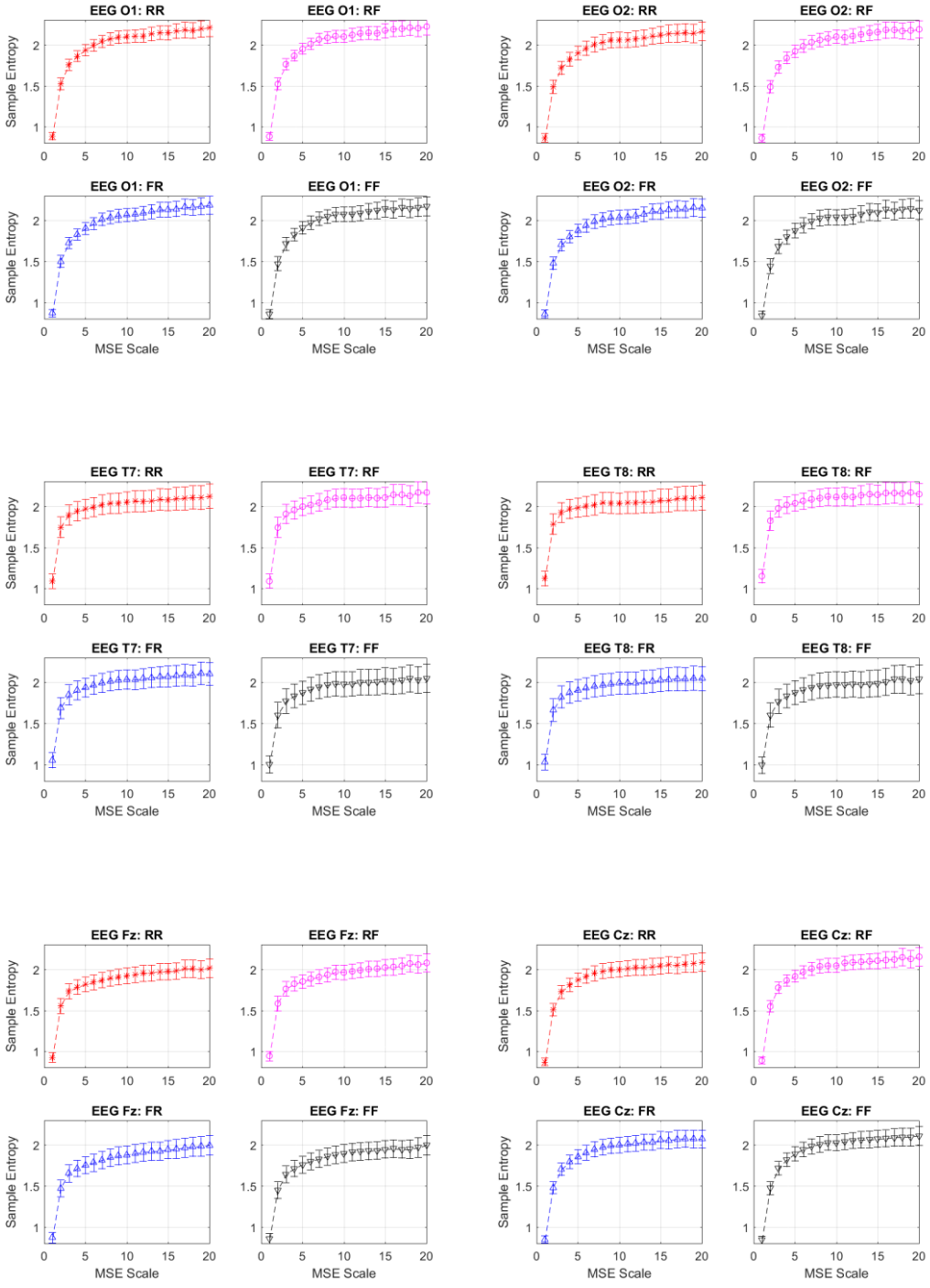
Averaging Multiscale Entropy of EEG Data



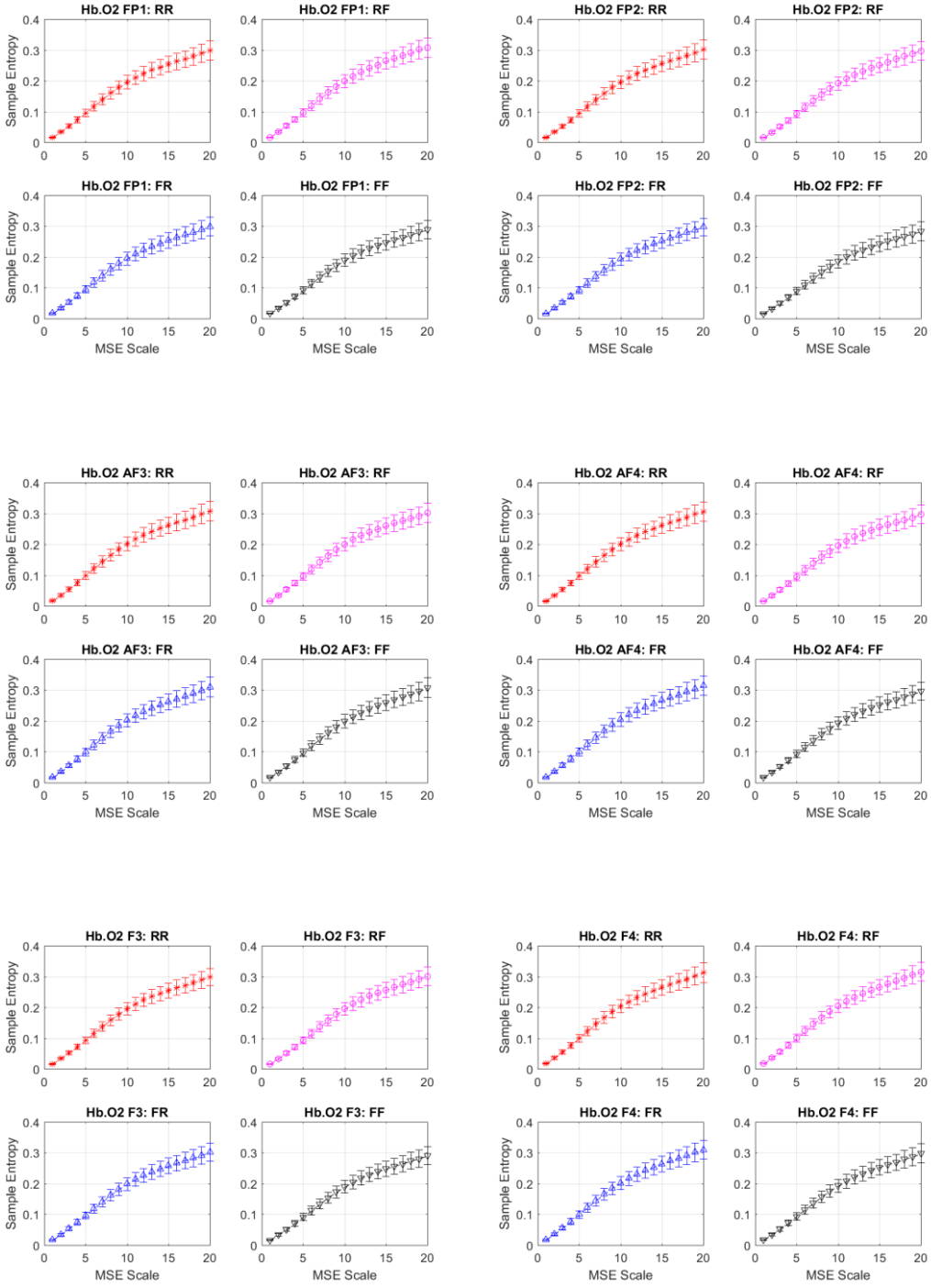
Averaging Multiscale Entropy of EEG Data



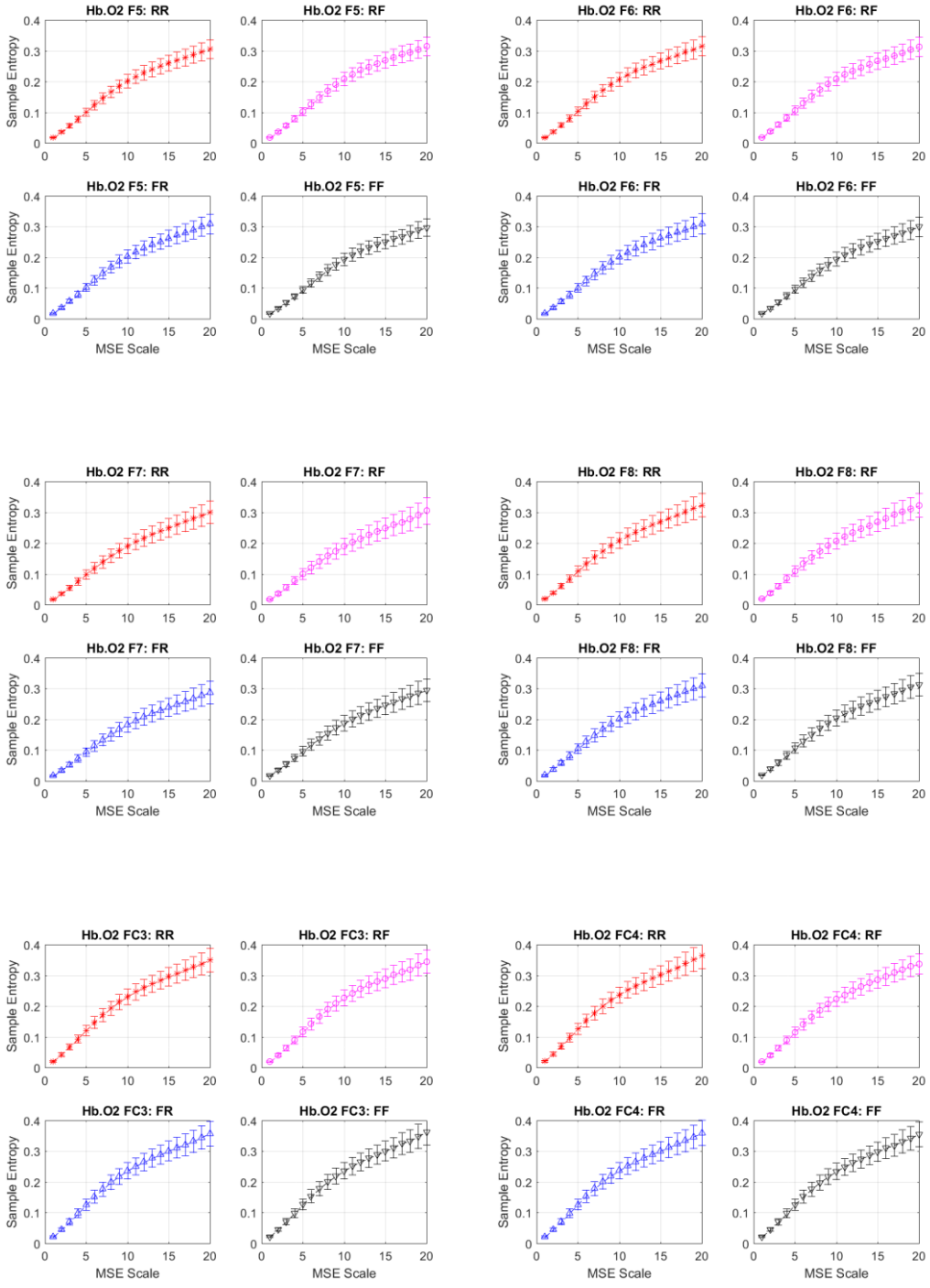
Averaging Multiscale Entropy of EEG Data



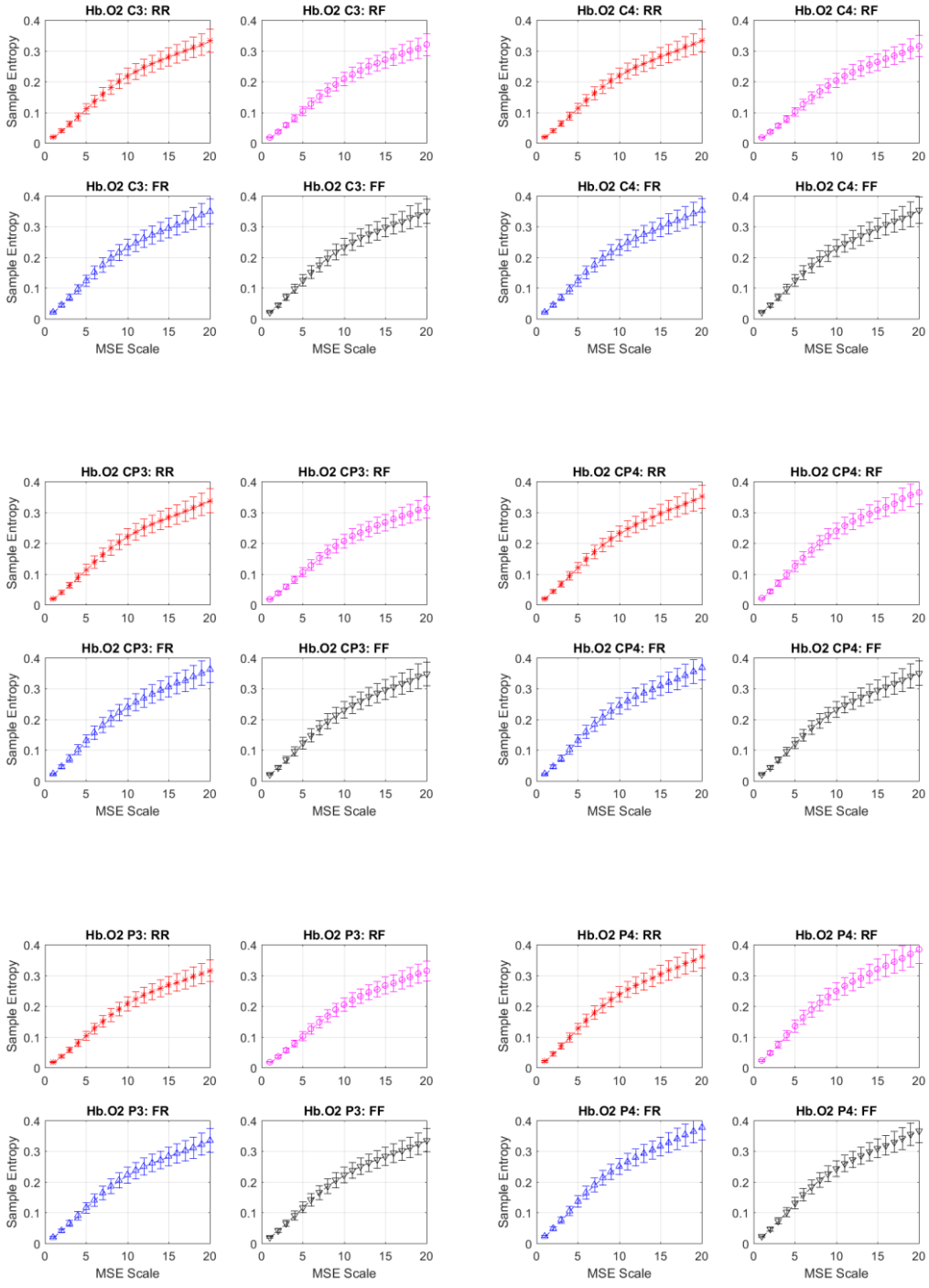
Averaging Multiscale Entropy of Hb.O2 Data



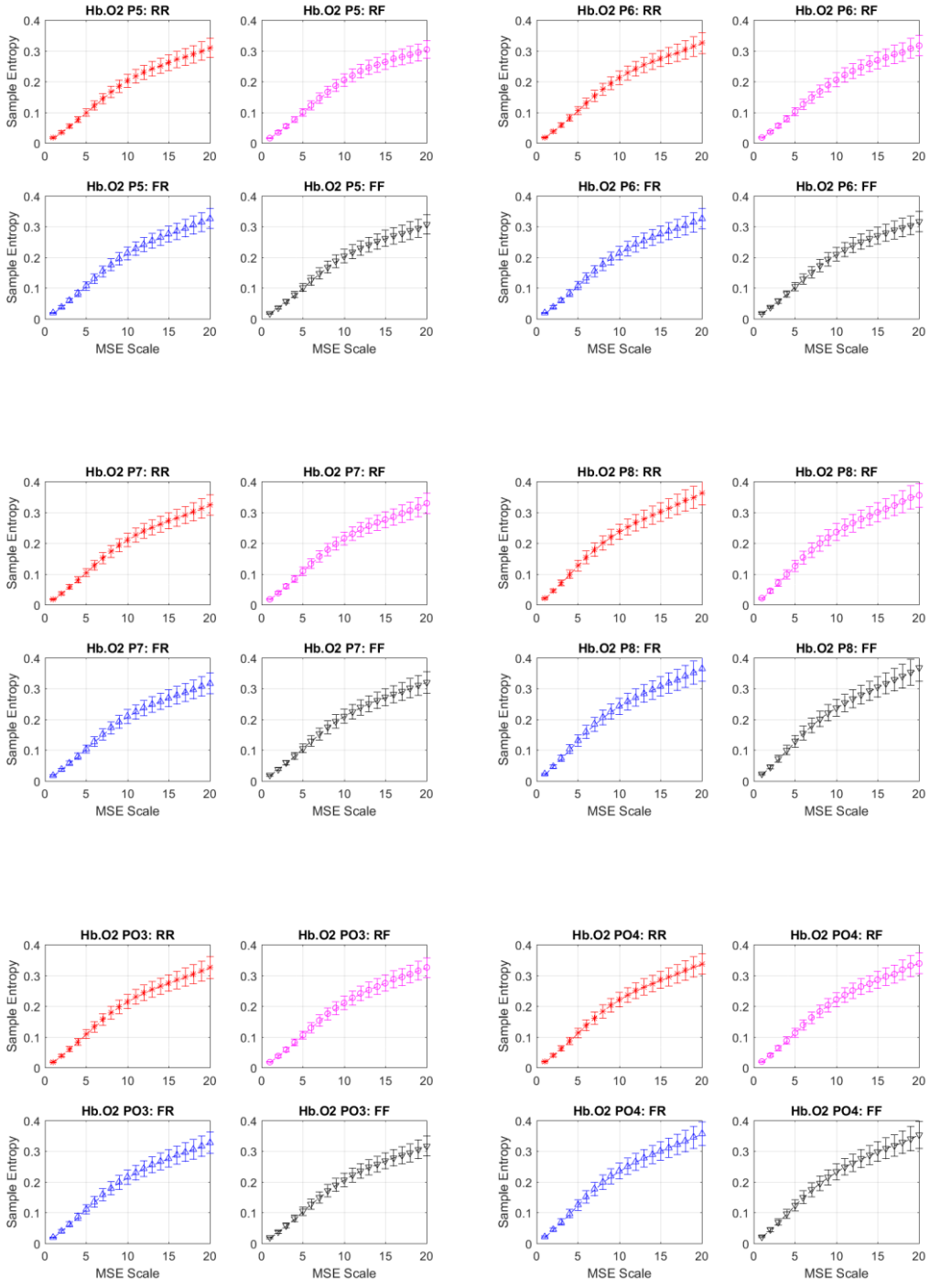
Averaging Multiscale Entropy of Hb.O2 Data



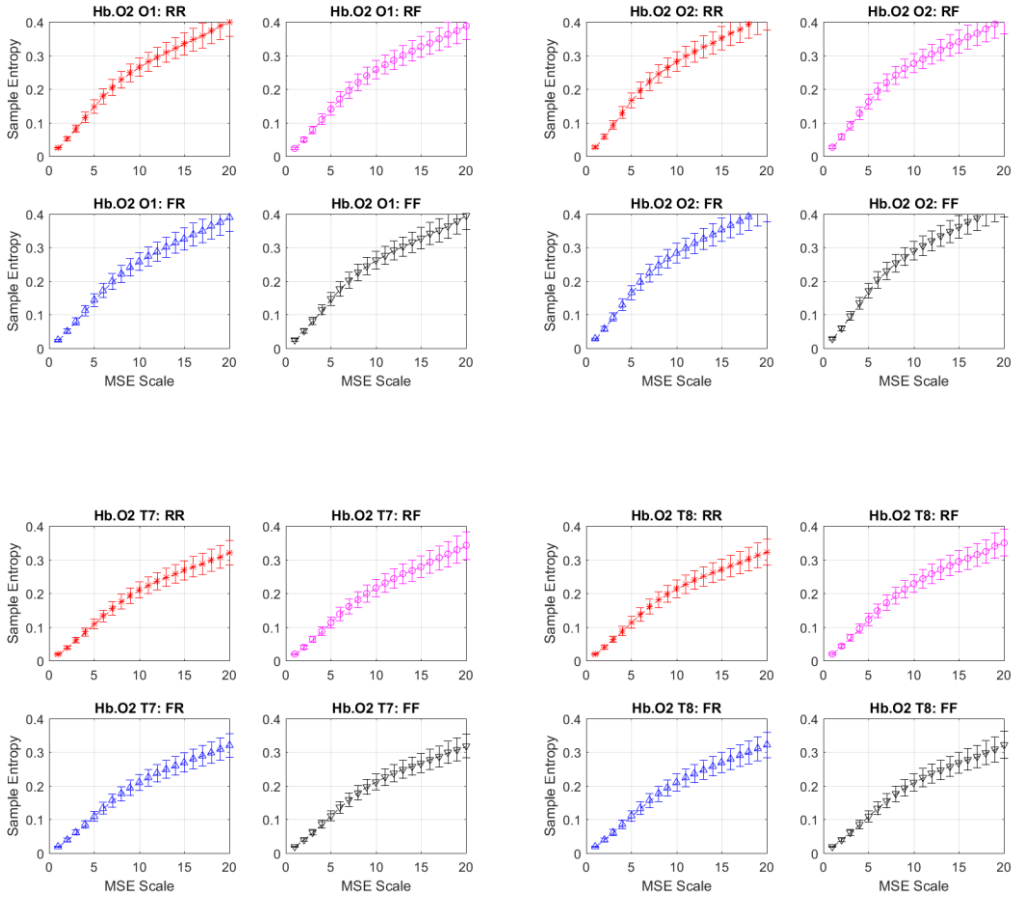
Averaging Multiscale Entropy of Hb.O2 Data



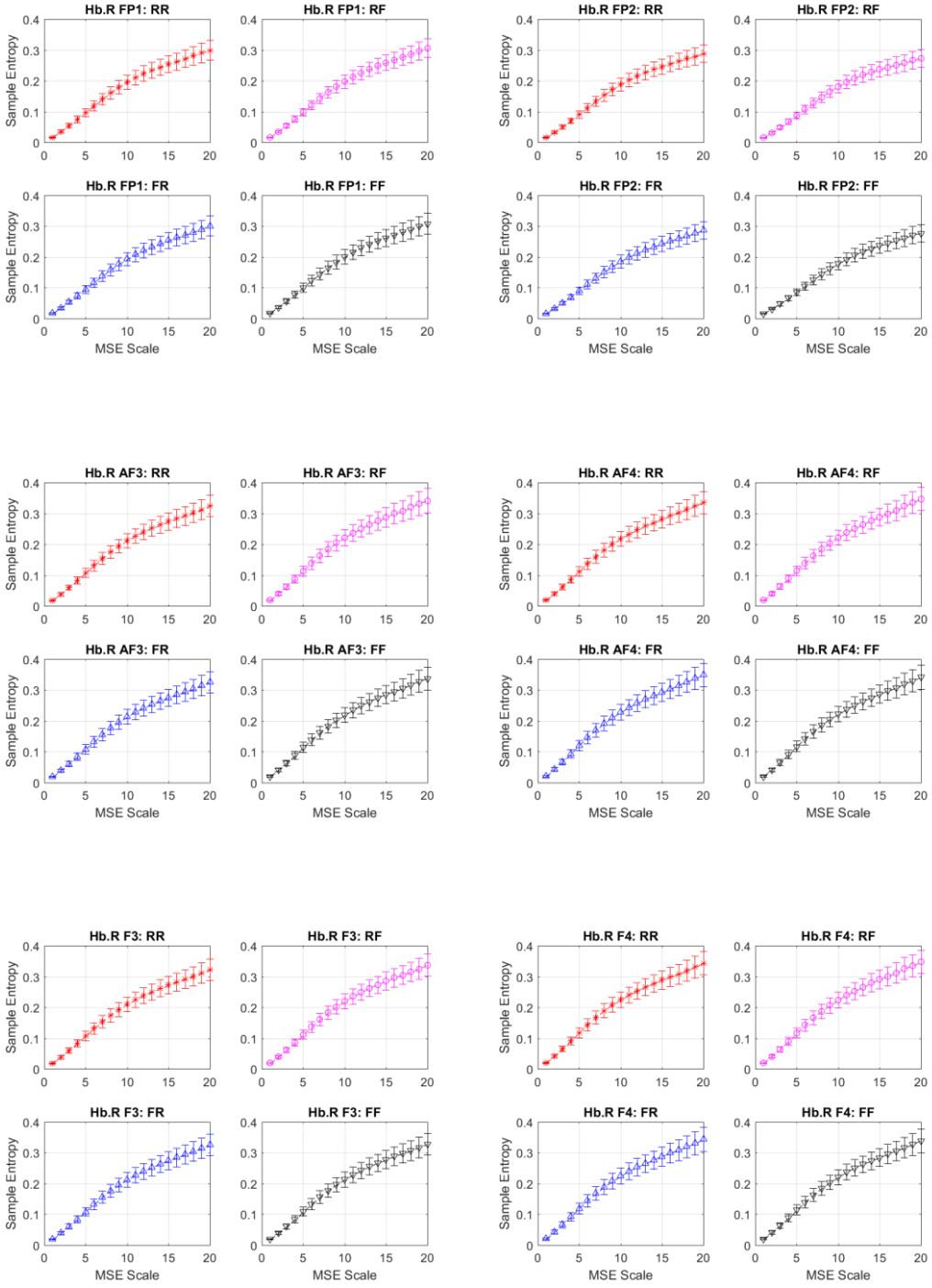
Averaging Multiscale Entropy of Hb.O2 Data



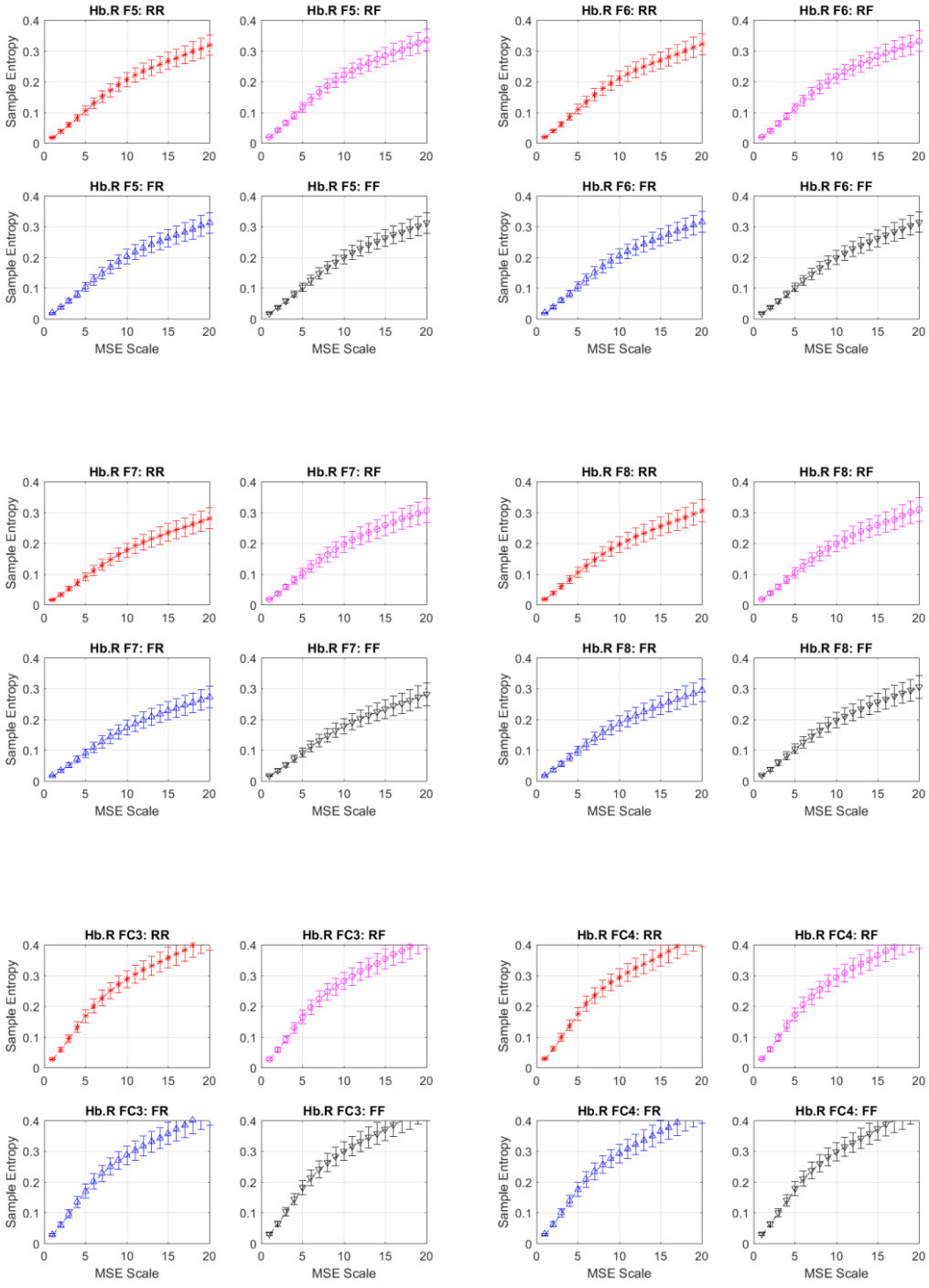
Averaging Multiscale Entropy of Hb.O2 Data



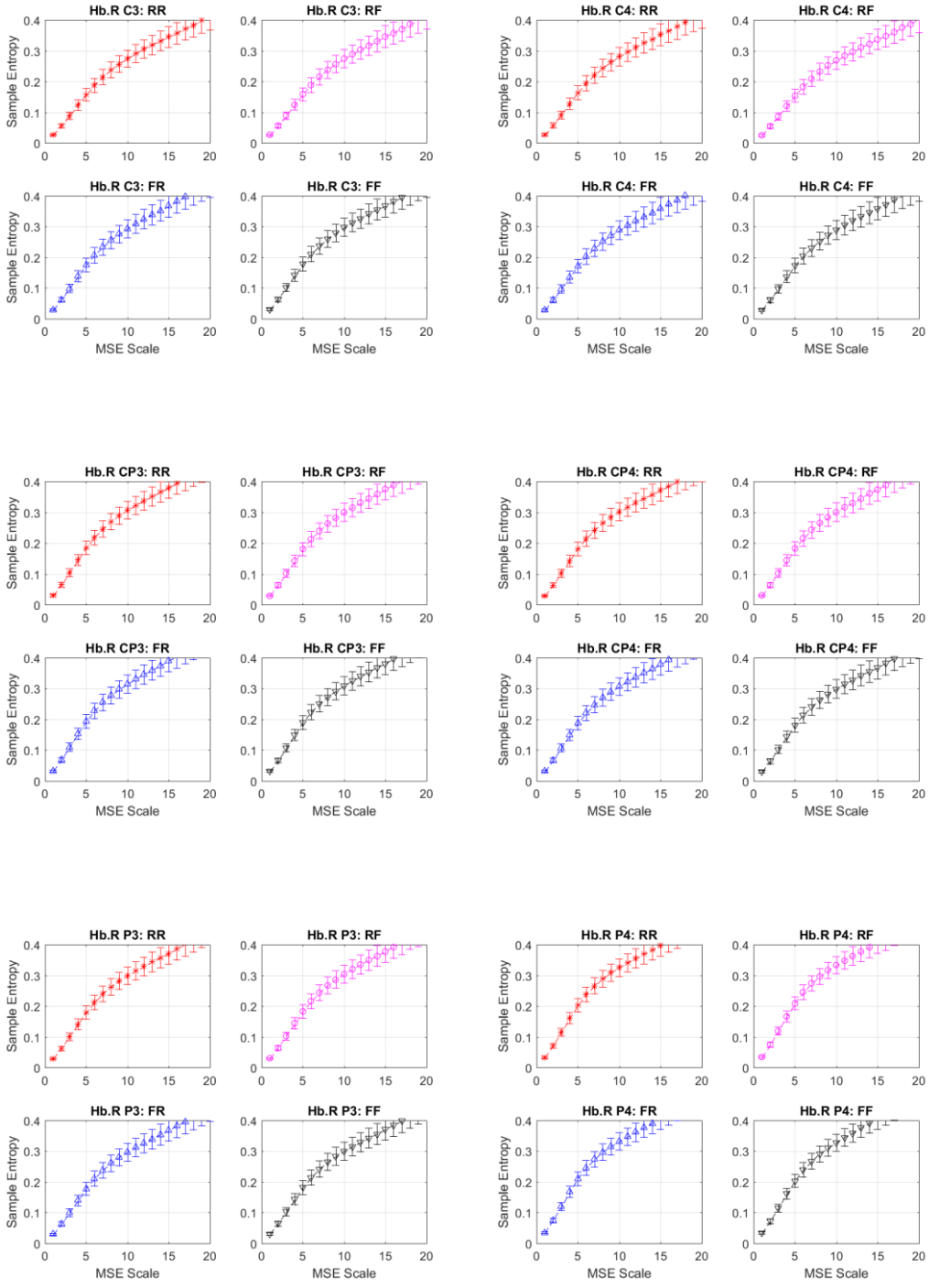
Averaging Multiscale Entropy of Hb.R Data



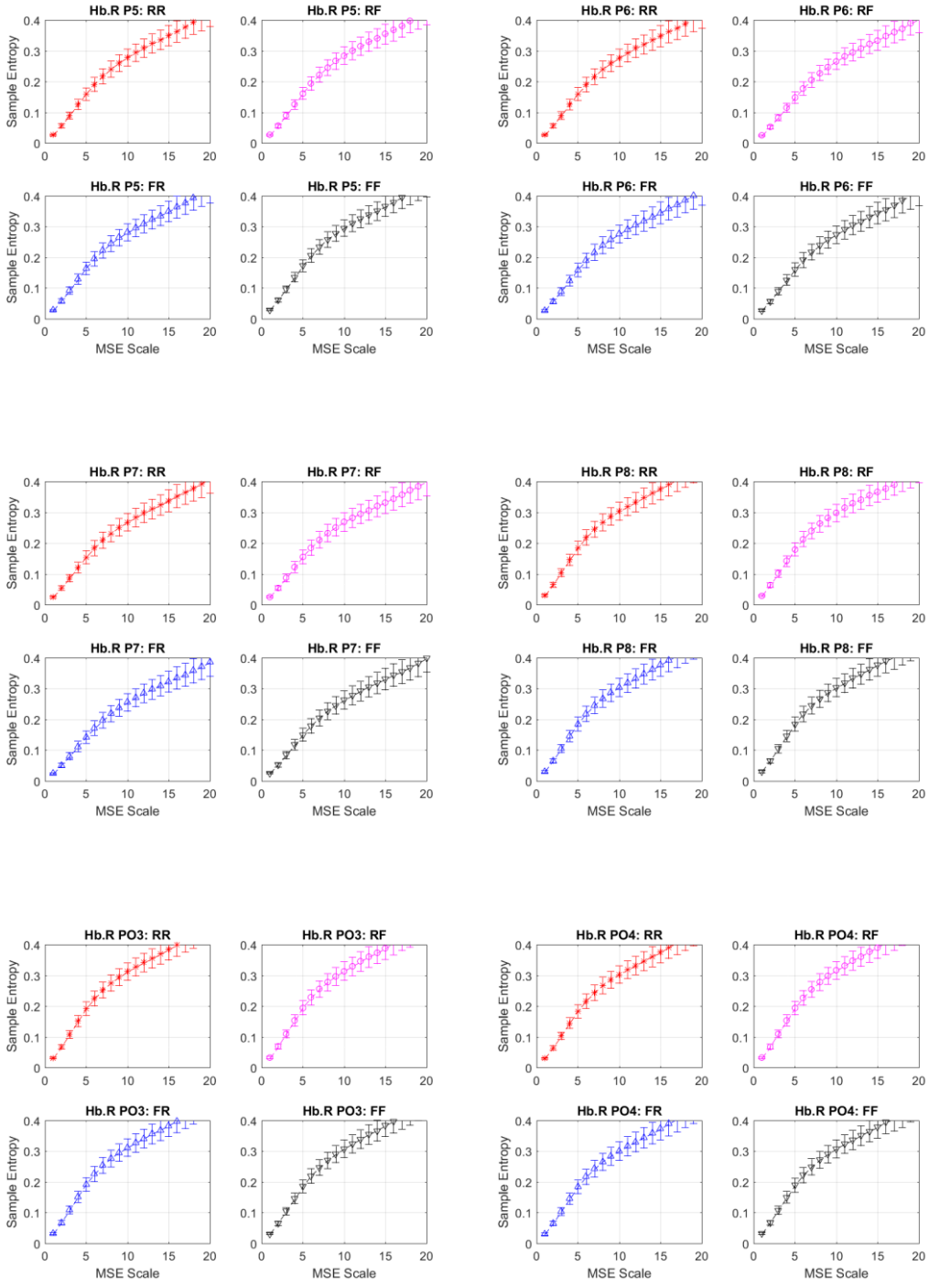
Averaging Multiscale Entropy of Hb.R Data



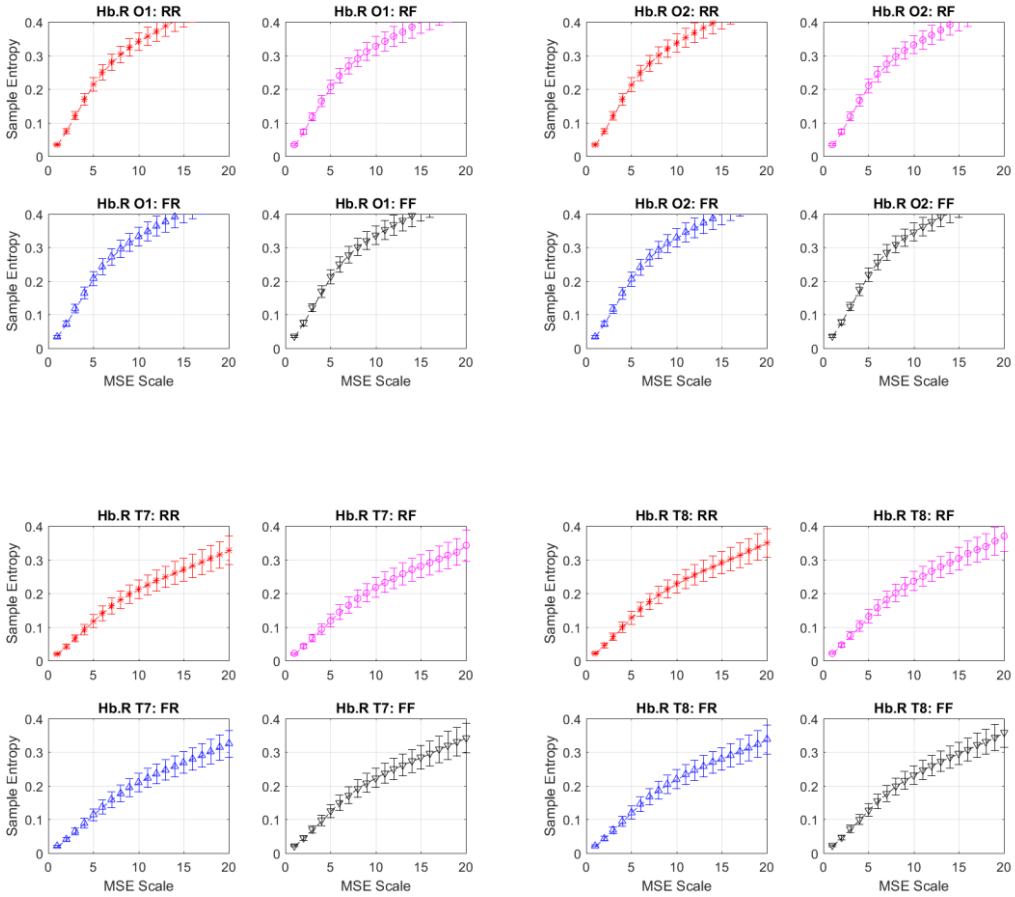
Averaging Multiscale Entropy of Hb.R Data



Averaging Multiscale Entropy of Hb.R Data



Averaging Multiscale Entropy of Hb.R Data

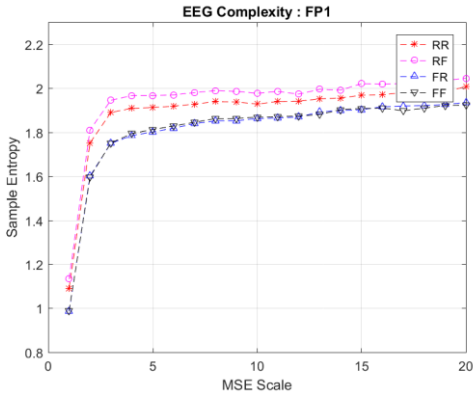


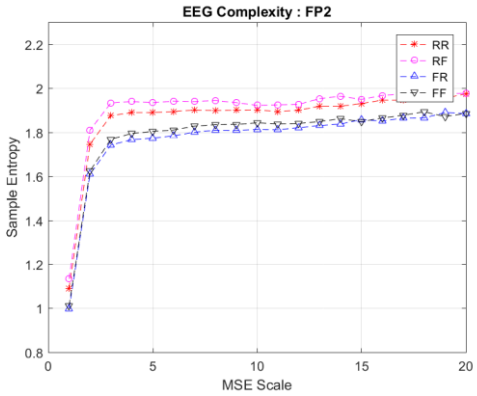
APPENDIX C

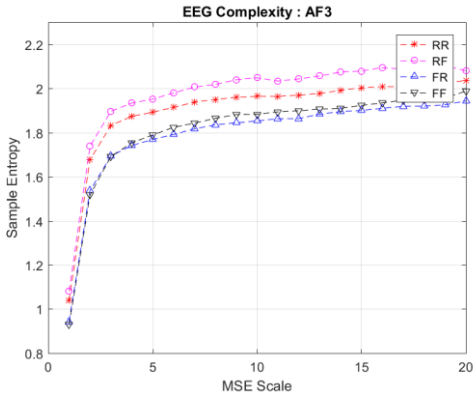
Comparison Multiscale Entropy Graph among four groups

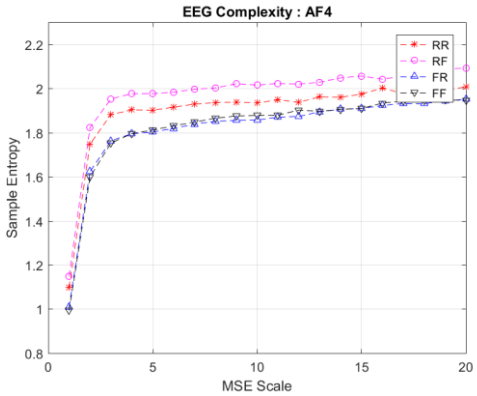
(RR, RF, FR, FF)

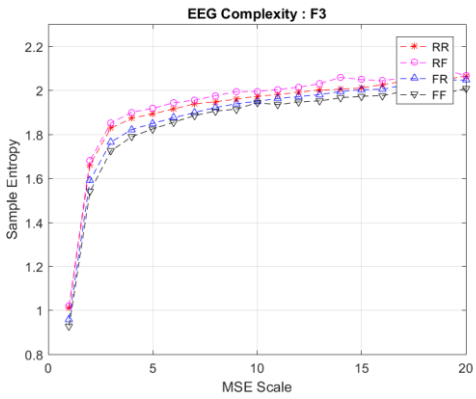
Comparison Multiscale Entropy of EEG Data

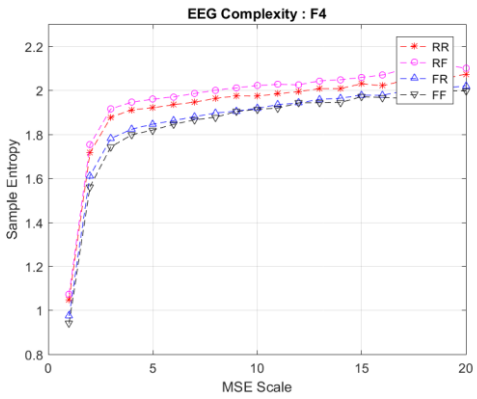




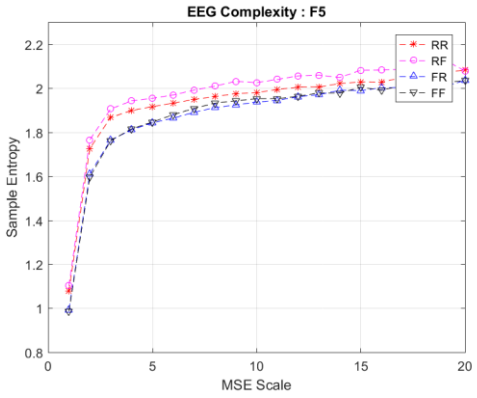


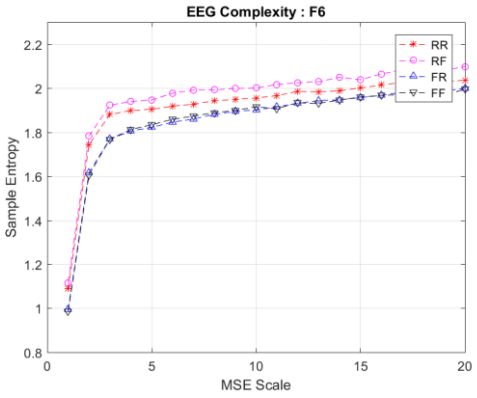


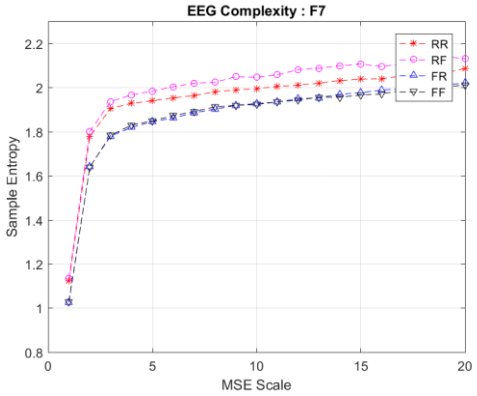


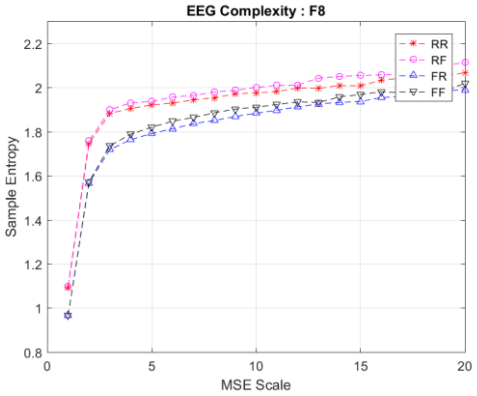


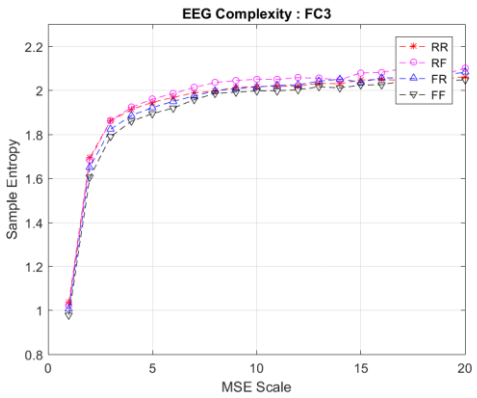
Comparison Multiscale Entropy of EEG Data

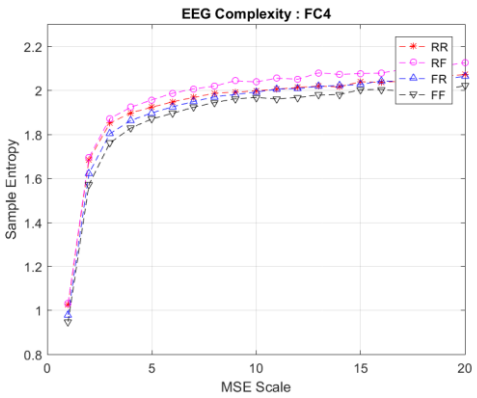




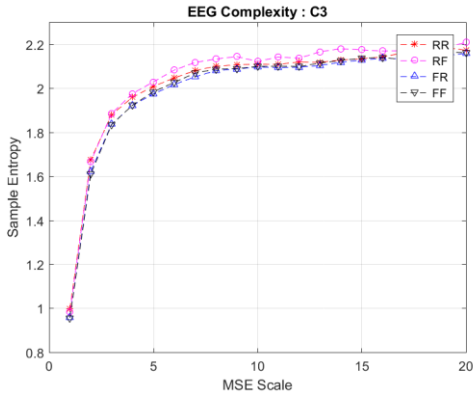


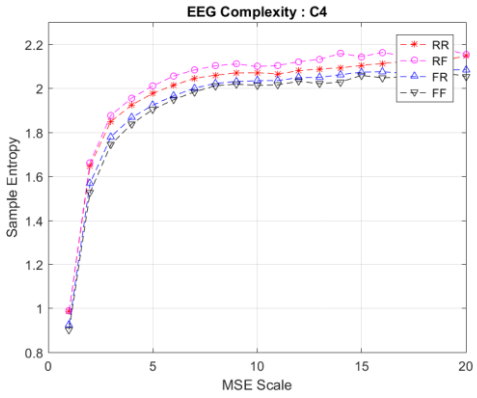


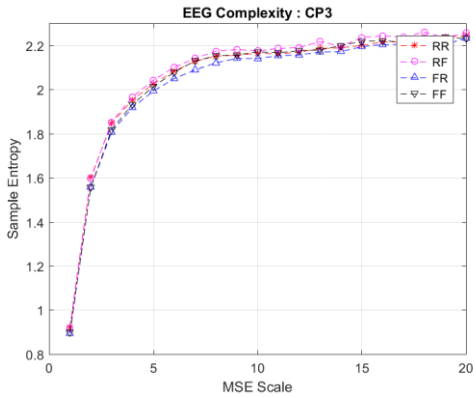


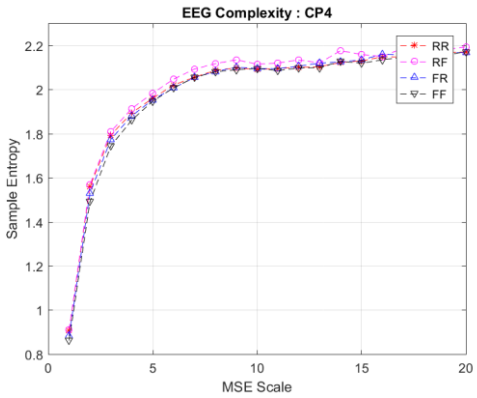


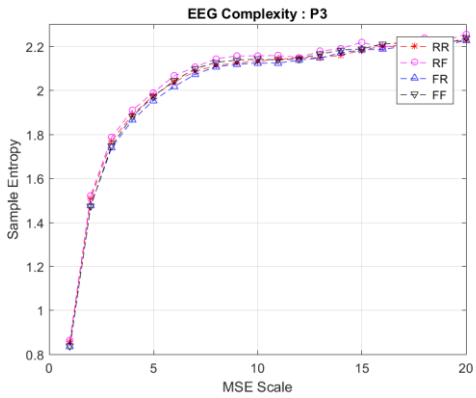
Comparison Multiscale Entropy of EEG Data

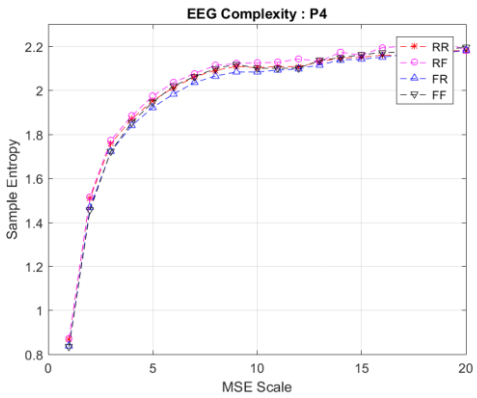




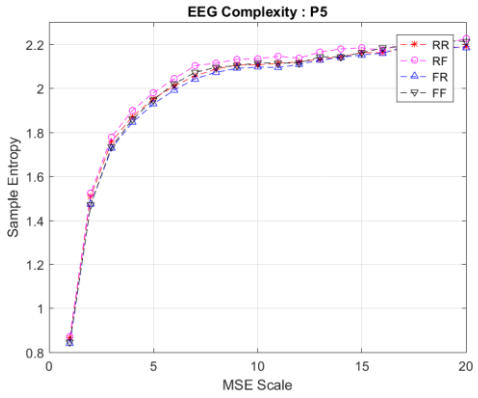


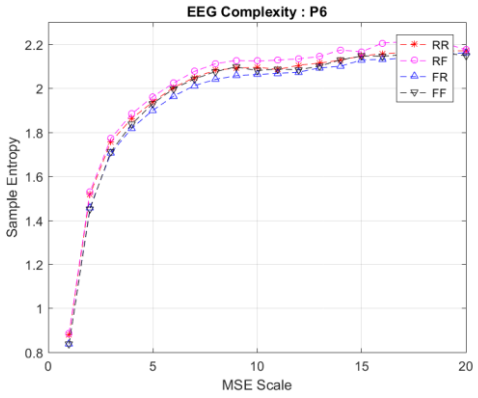


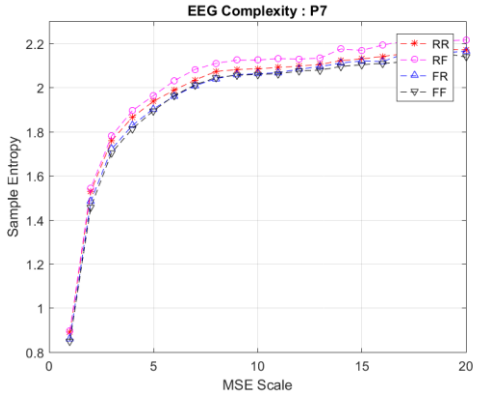


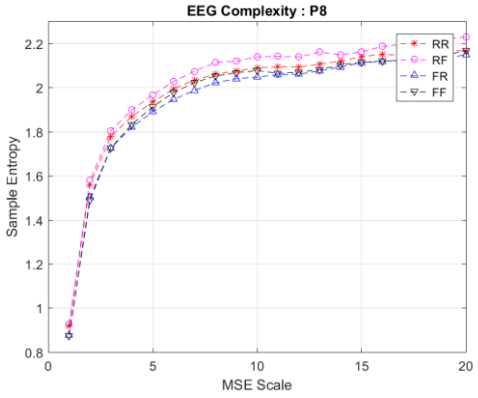


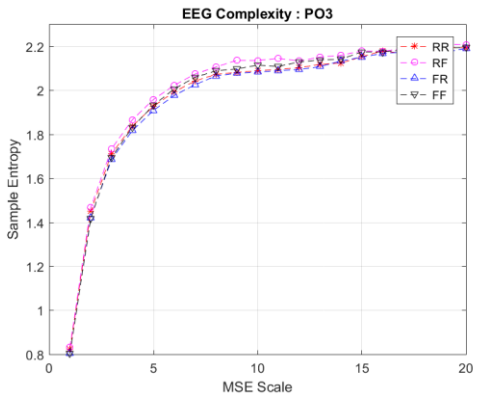
Comparison Multiscale Entropy of EEG Data

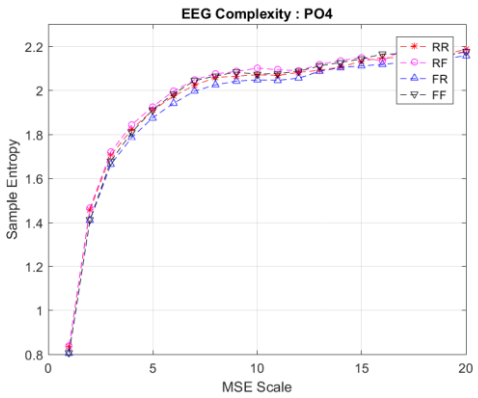




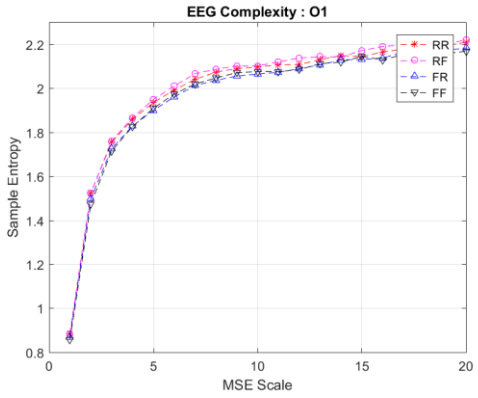


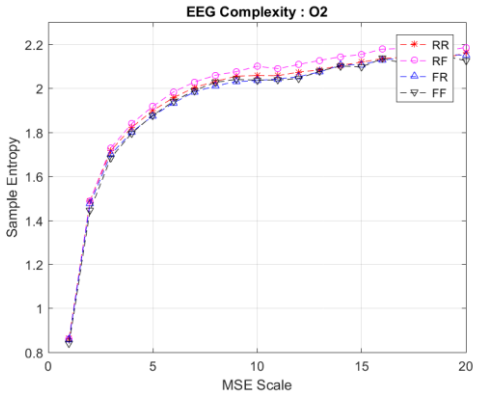


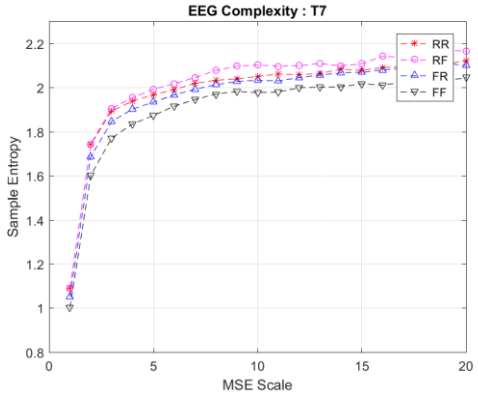


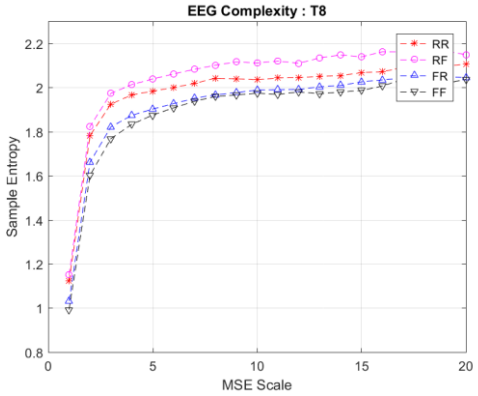


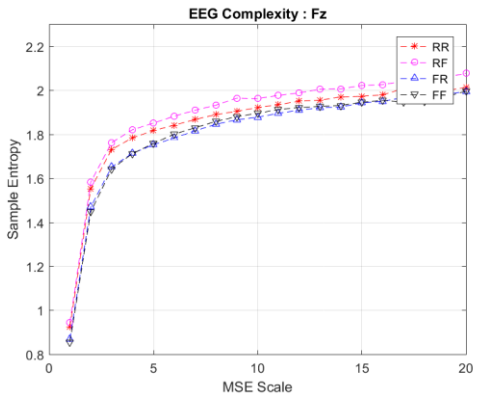
Comparison Multiscale Entropy of EEG Data

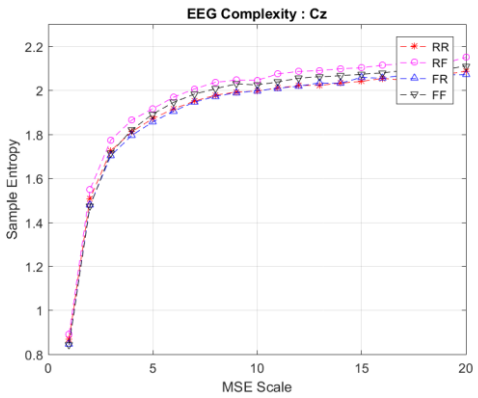




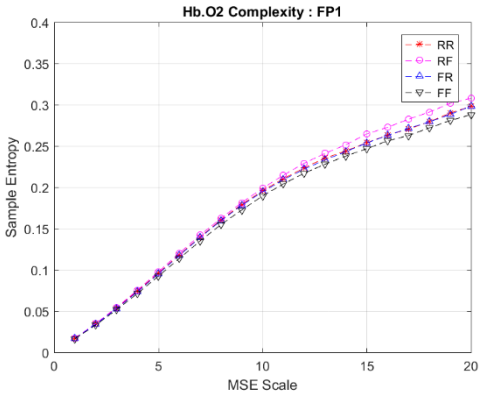


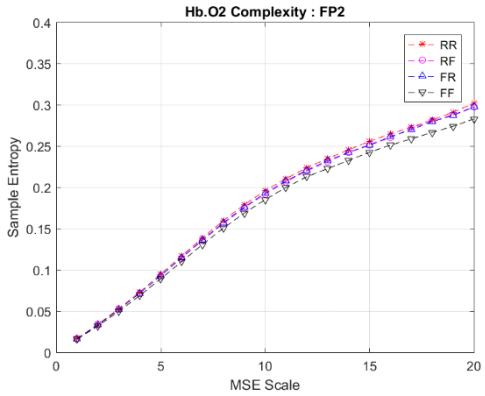


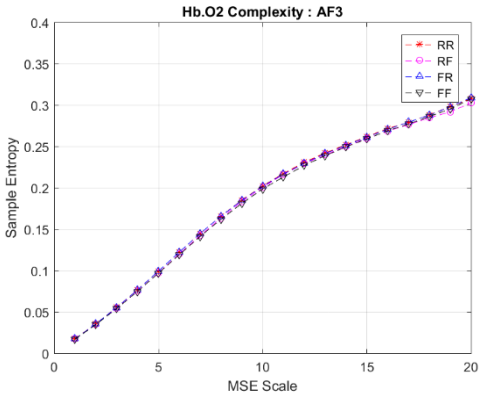


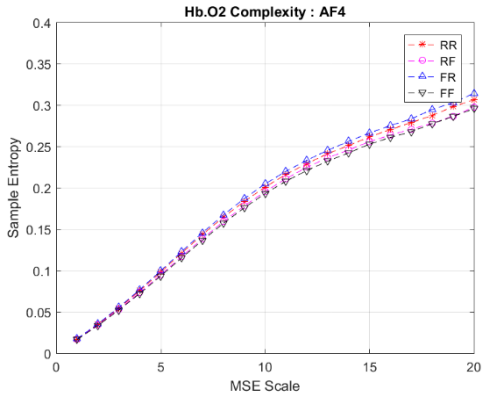


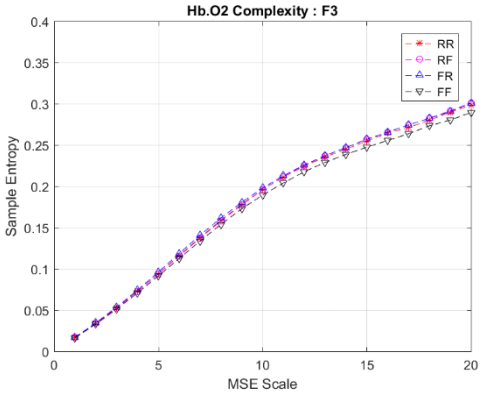
Comparison Multiscale Entropy of Hb.O2 Data

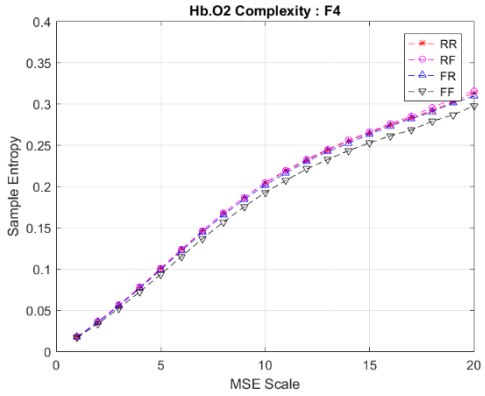




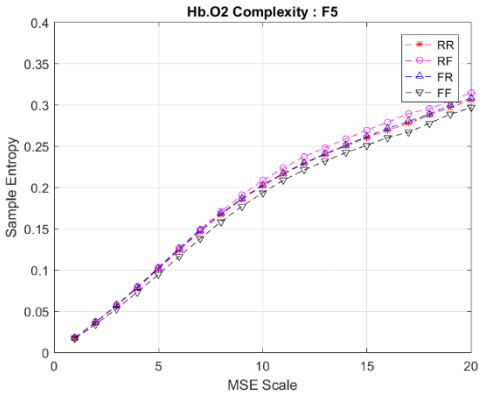


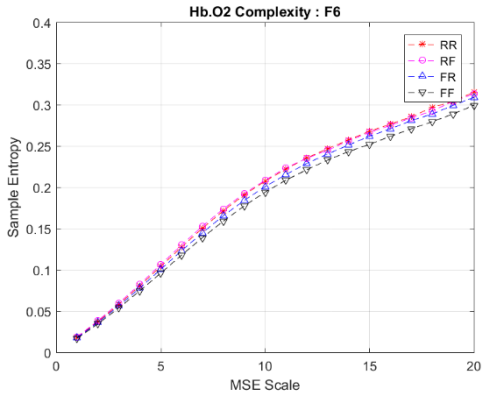


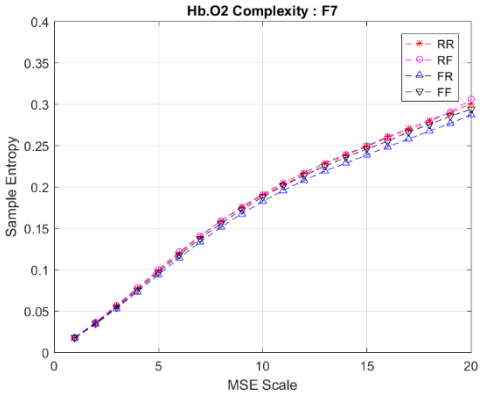


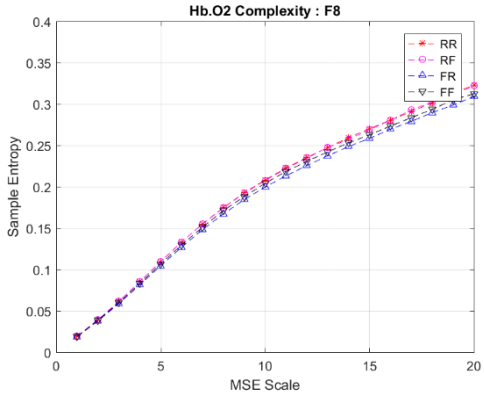


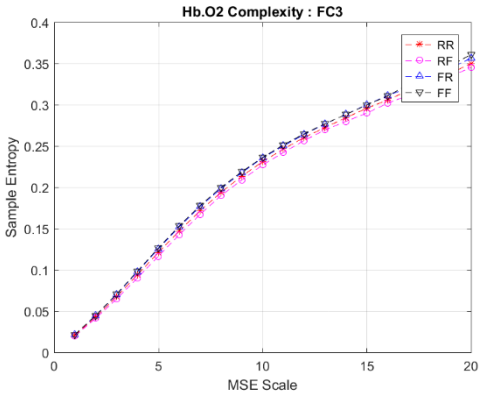
Comparison Multiscale Entropy of Hb.O2 Data

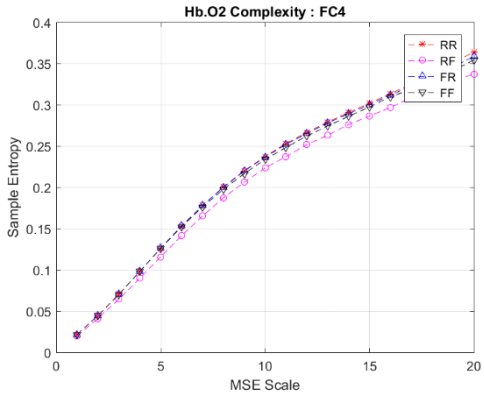




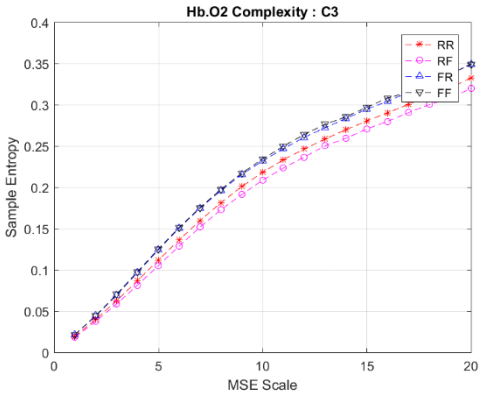


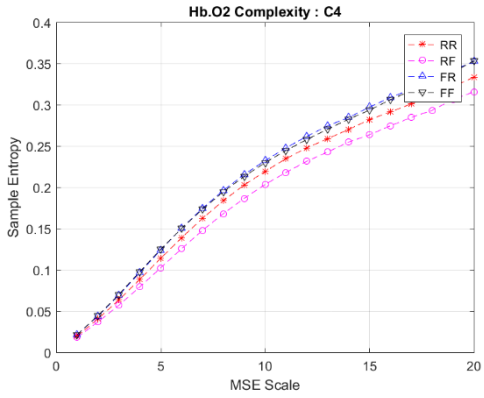


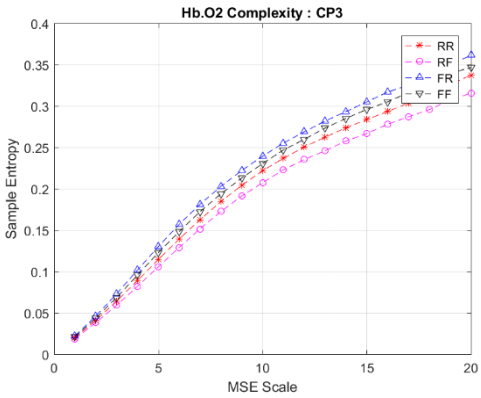


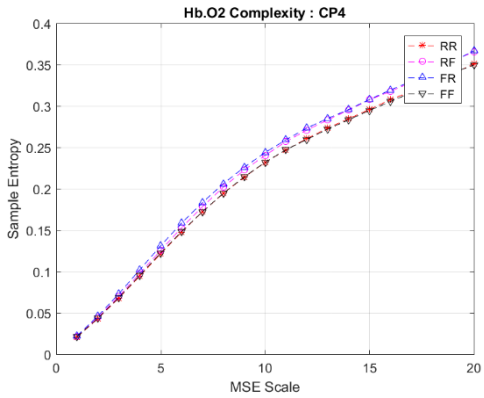


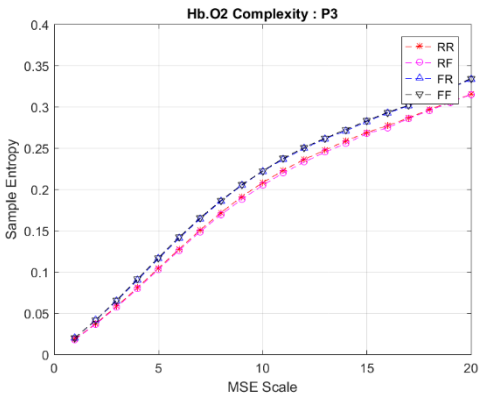
Comparison Multiscale Entropy of Hb.O2 Data

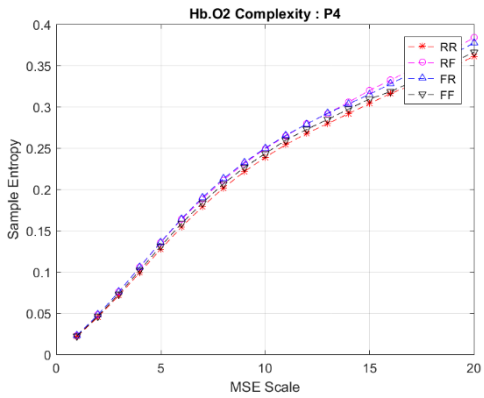




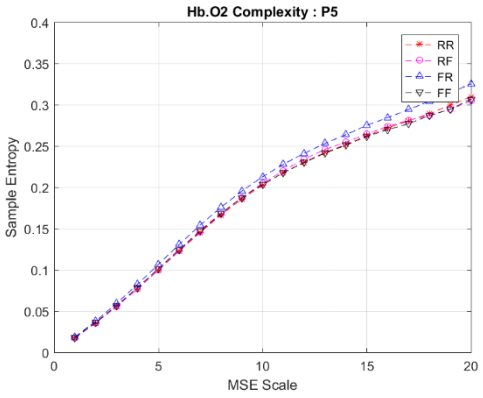


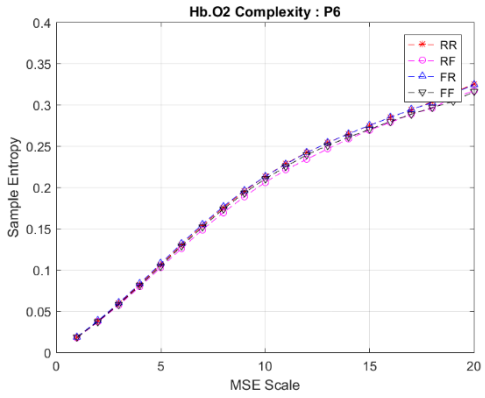


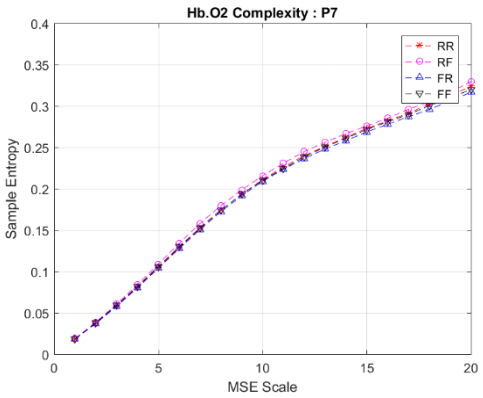


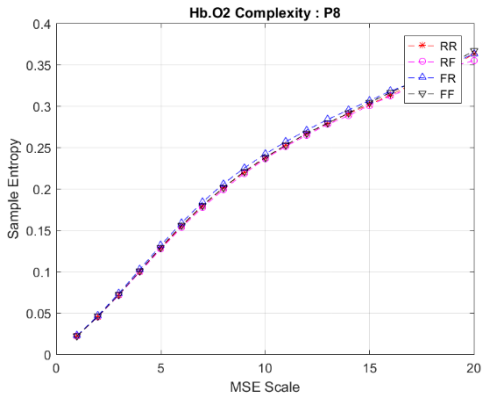


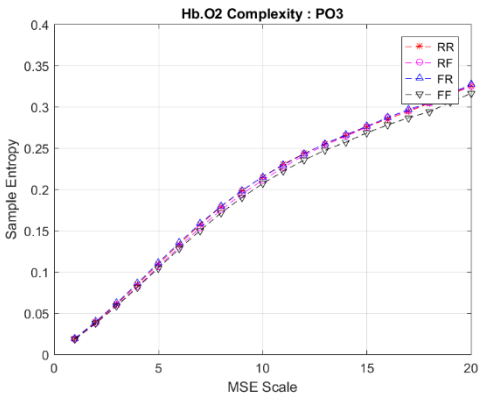
Comparison Multiscale Entropy of Hb.O2 Data

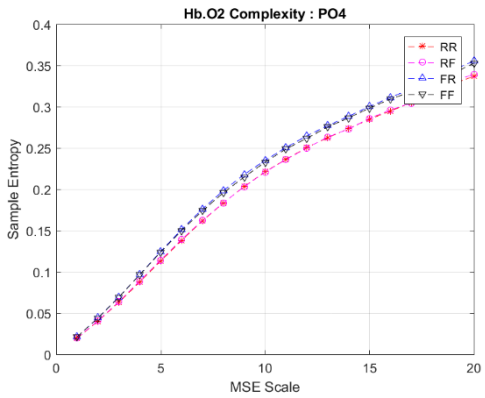




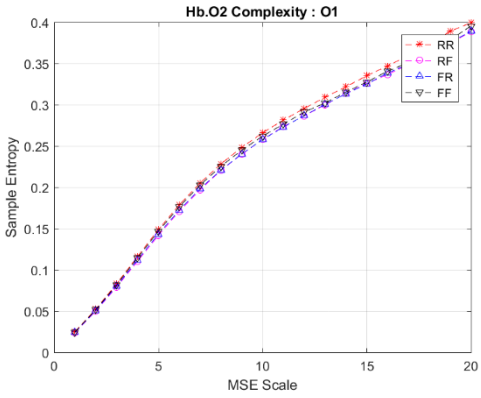


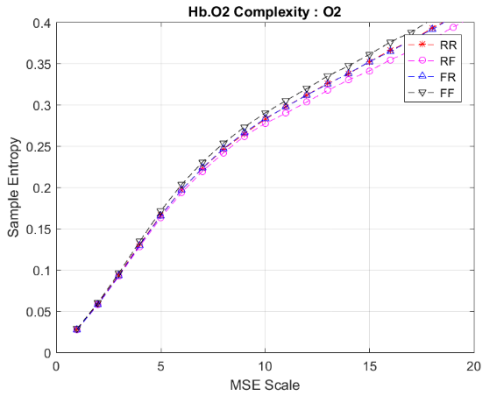


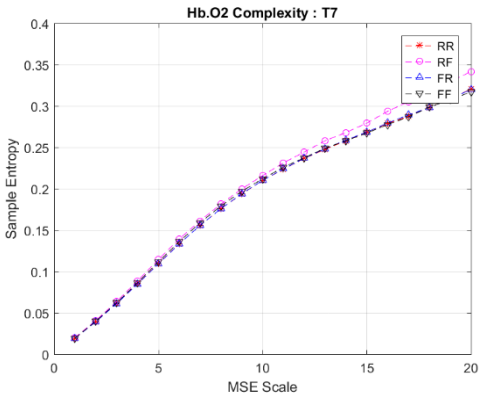


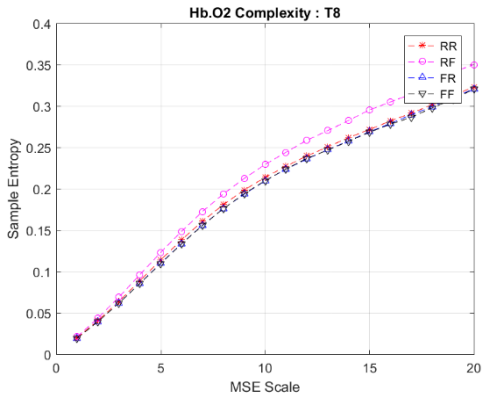


Comparison Multiscale Entropy of Hb.O2 Data

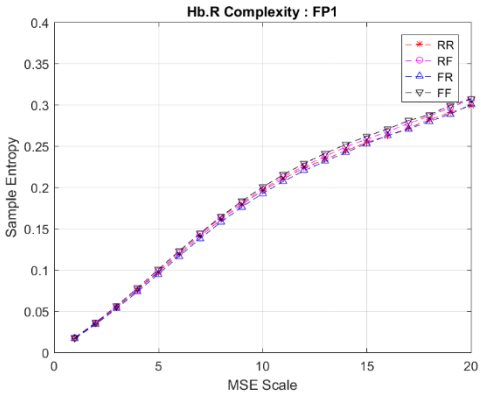


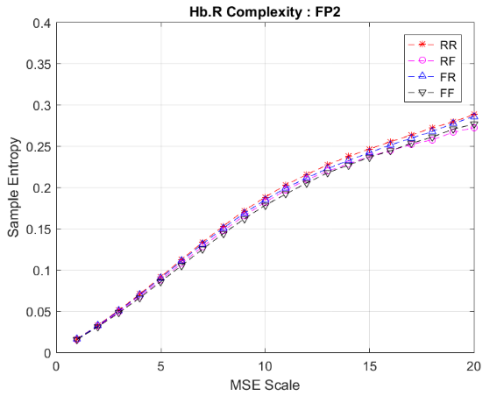


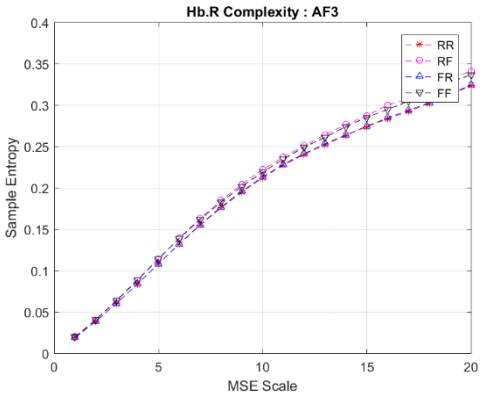


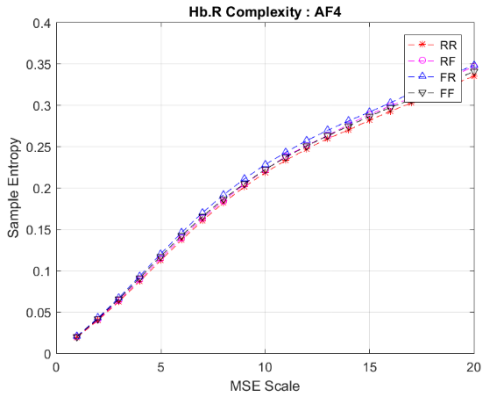


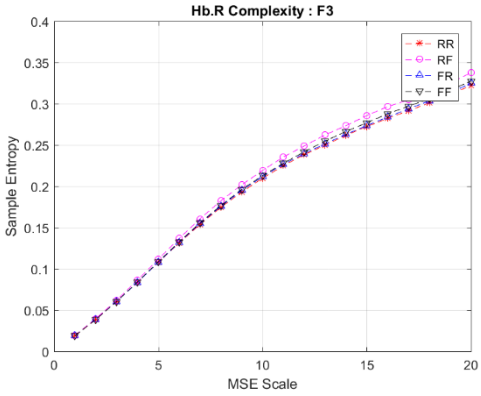
Comparison Multiscale Entropy of Hb.R Data

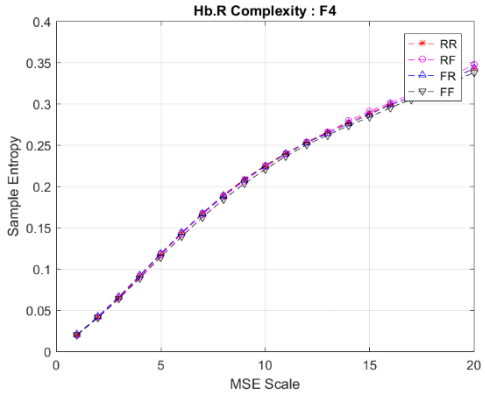




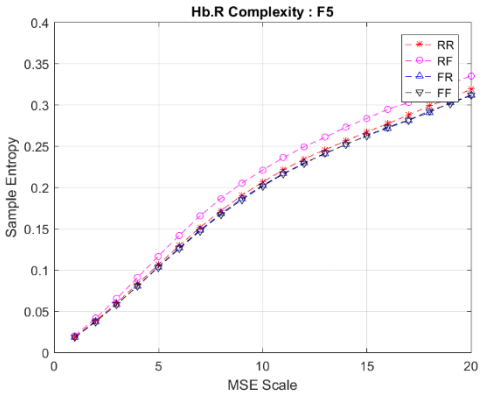


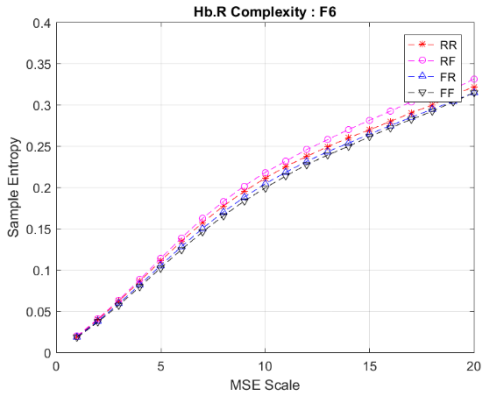


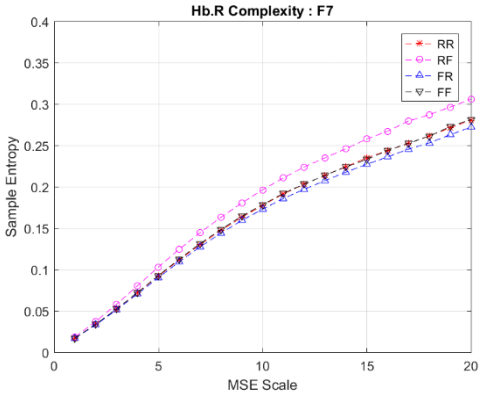


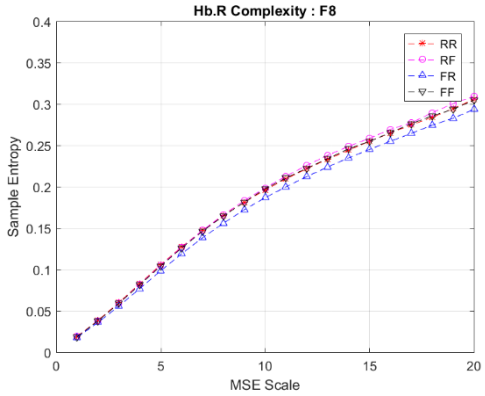


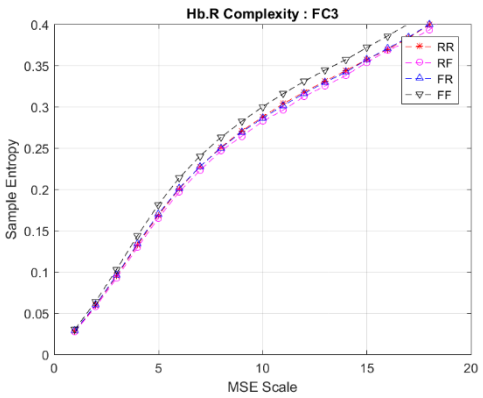
Comparison Multiscale Entropy of Hb.R Data

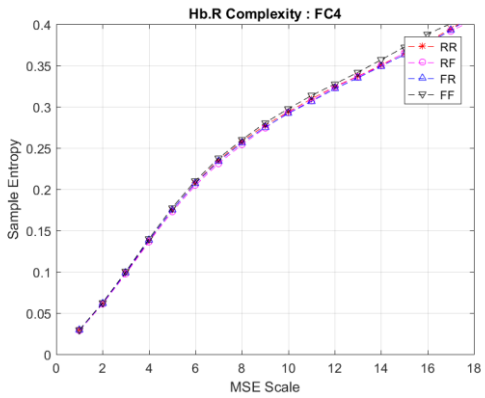




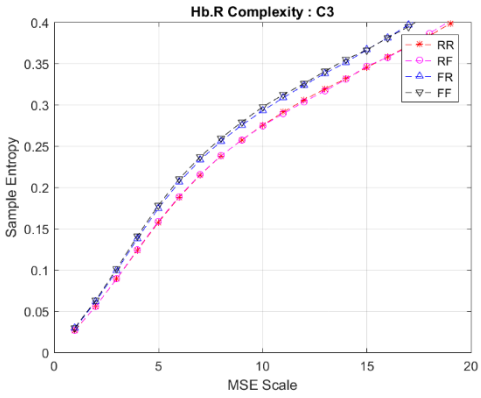


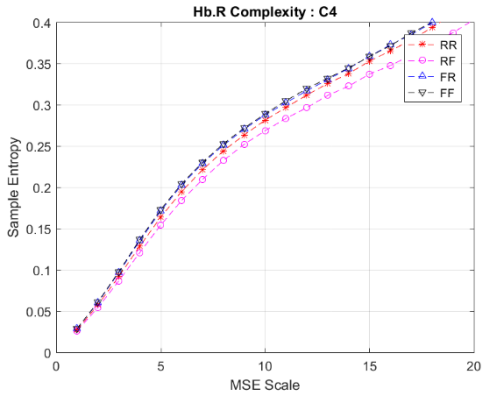


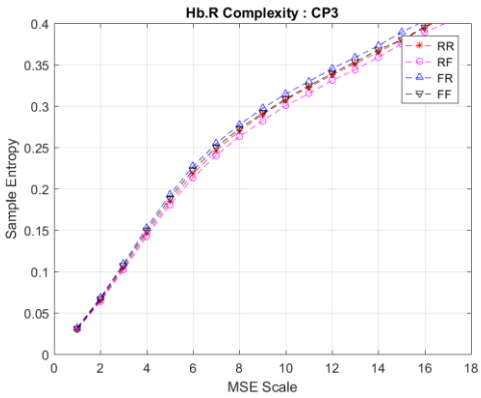


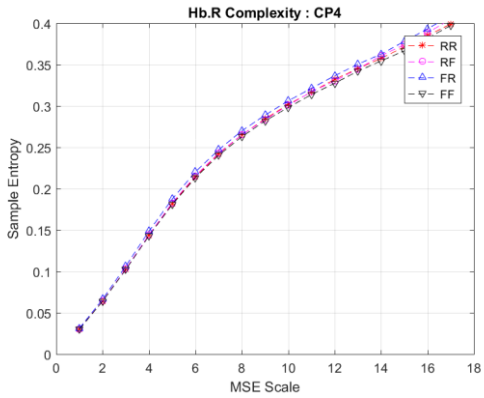


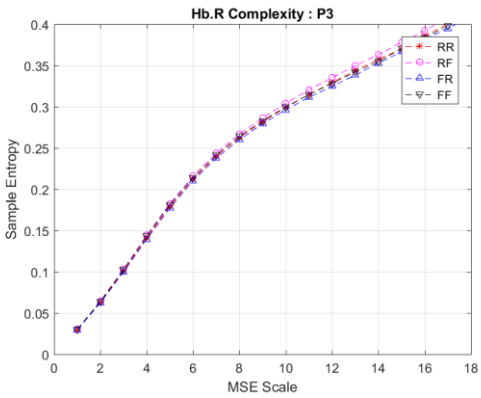
Comparison Multiscale Entropy of Hb.R Data

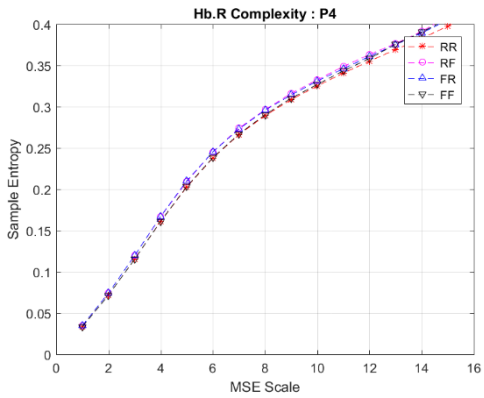




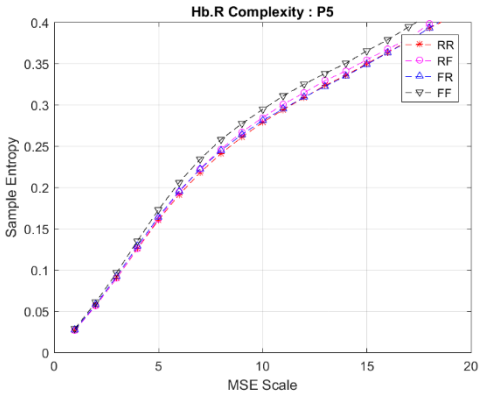


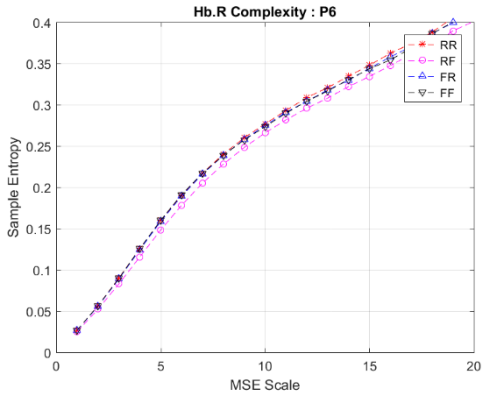


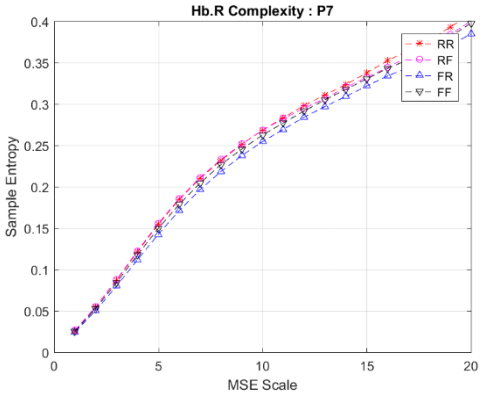


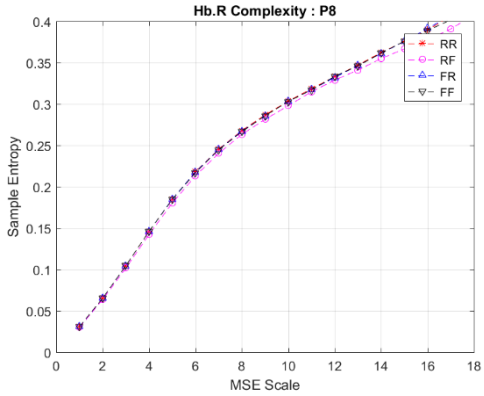


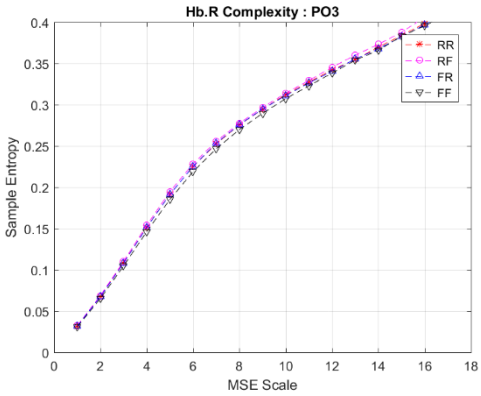
Comparison Multiscale Entropy of Hb.R Data

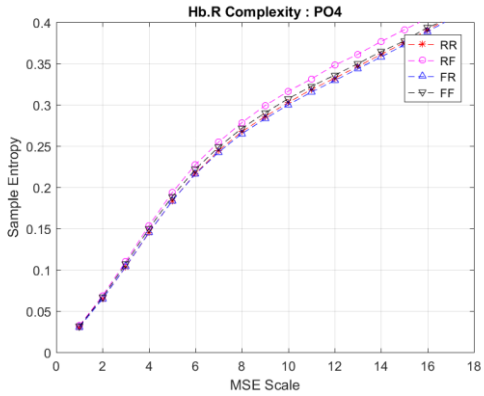




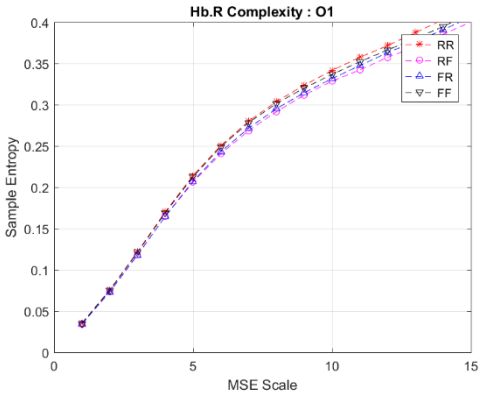


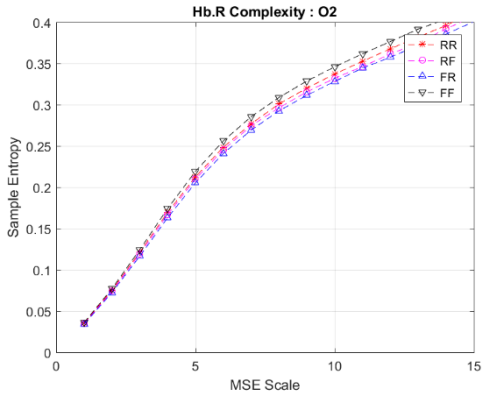


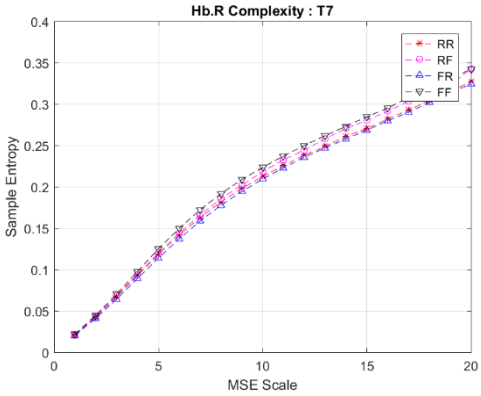


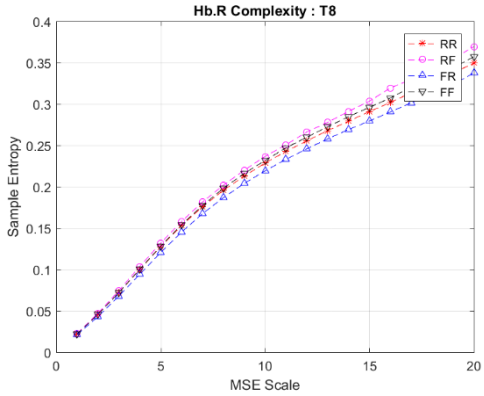


Comparison Multiscale Entropy of Hb.R Data





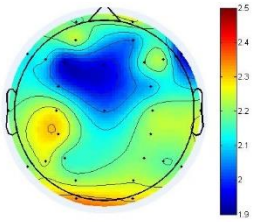
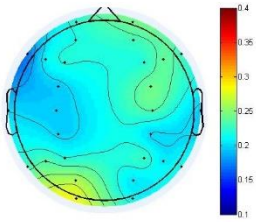
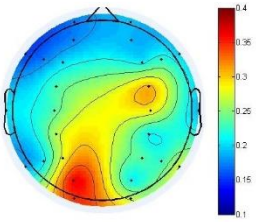
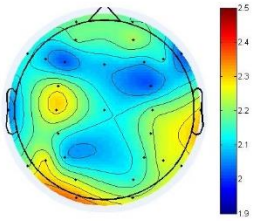
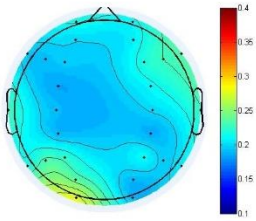
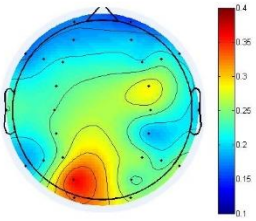
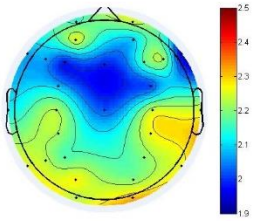
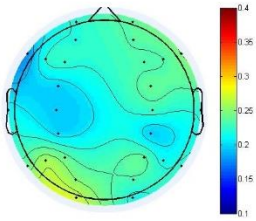
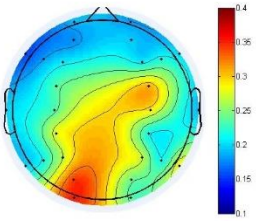
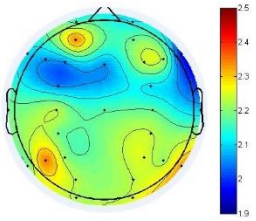
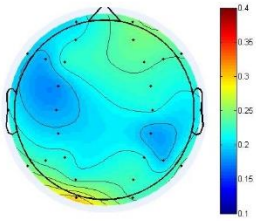
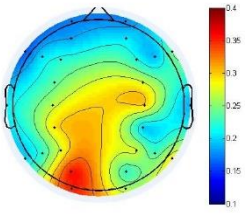


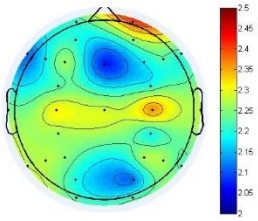
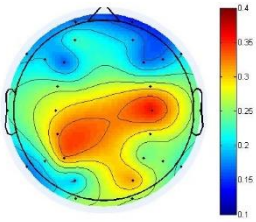
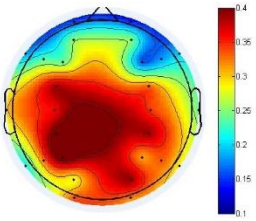
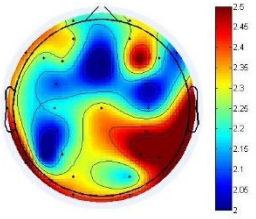
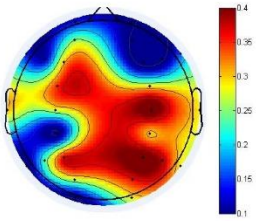
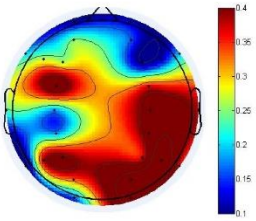
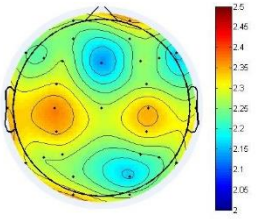
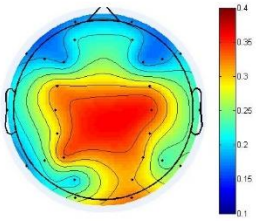
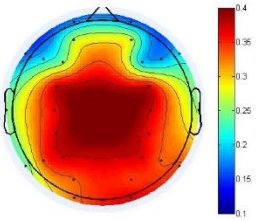
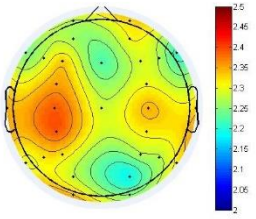
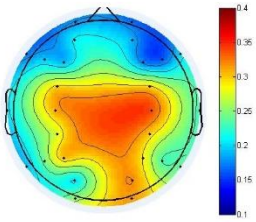
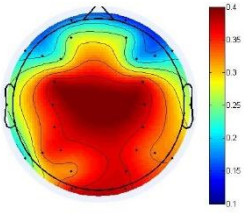


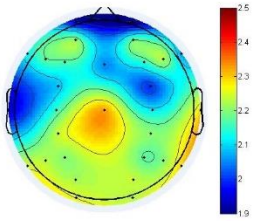
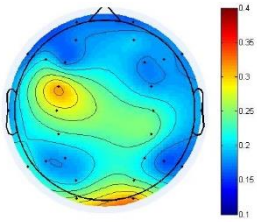
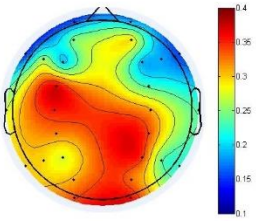
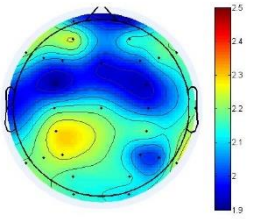
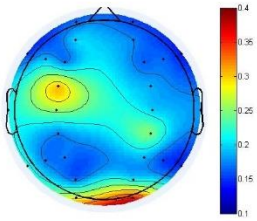
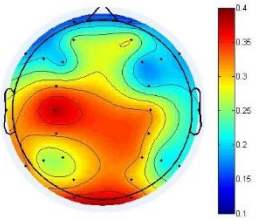
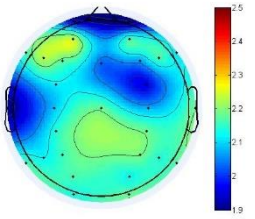
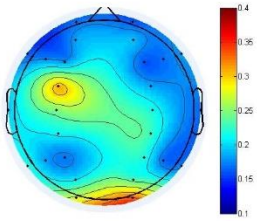
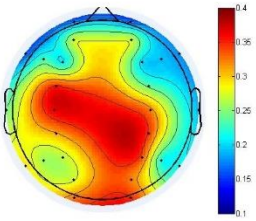
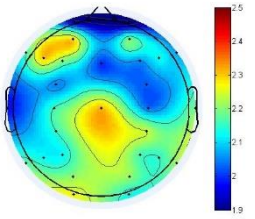
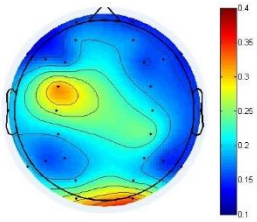
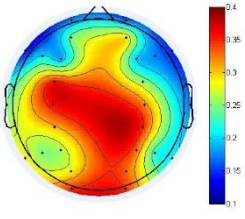
APPENDIX D

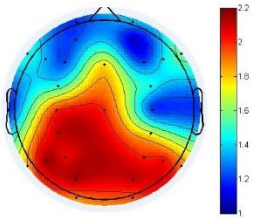
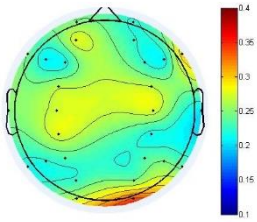
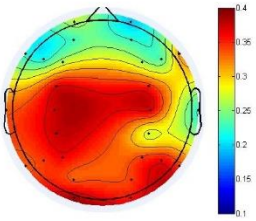
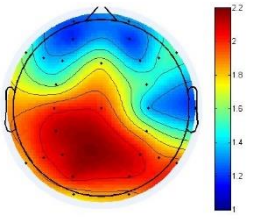
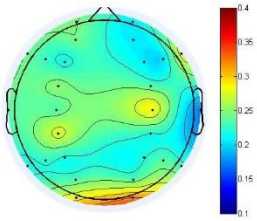
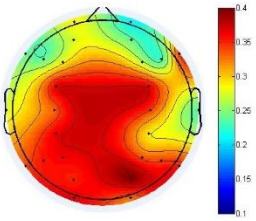
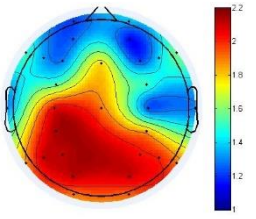
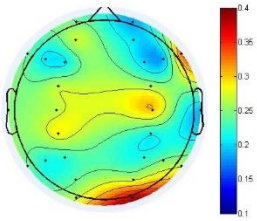
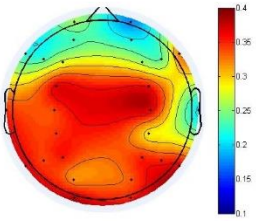
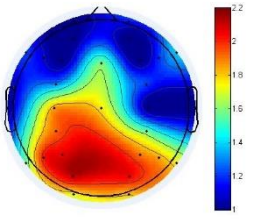
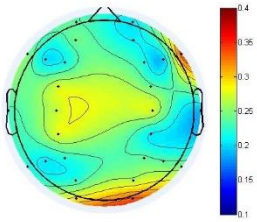
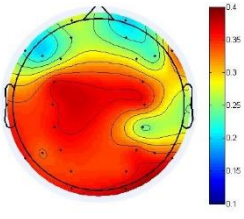
Participants' MSE Topography

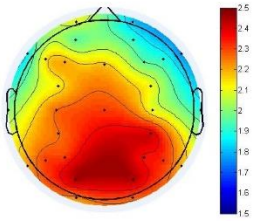
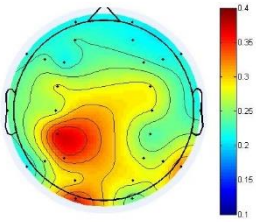
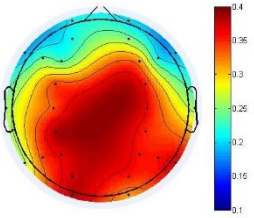
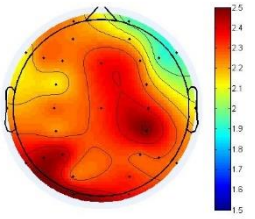
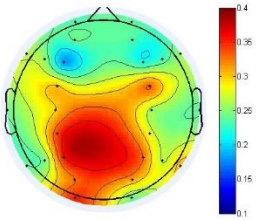
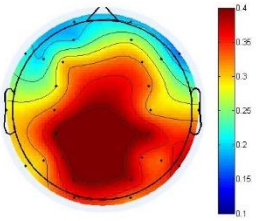
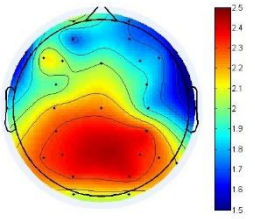
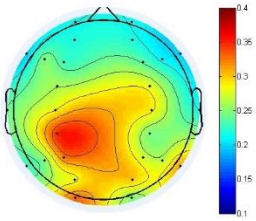
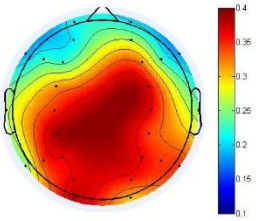
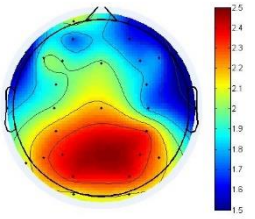
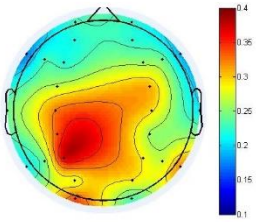
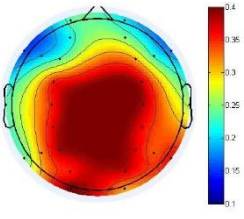
The Topography of average MSE at scale 10

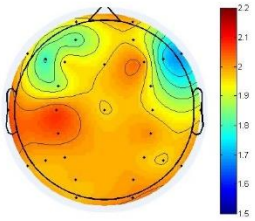
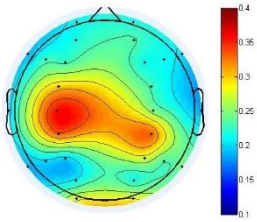
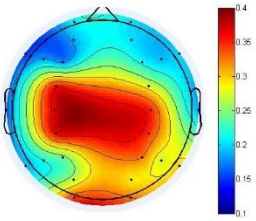
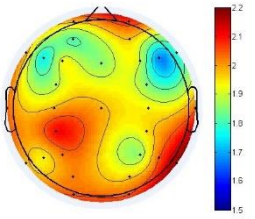
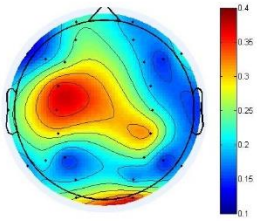
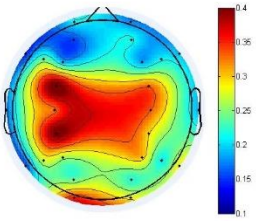
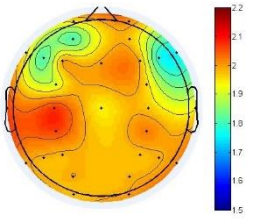
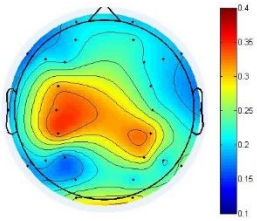
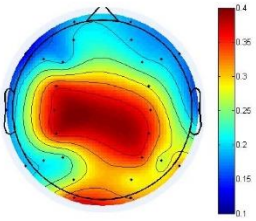
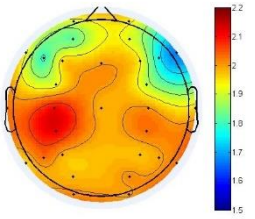
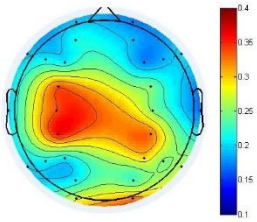
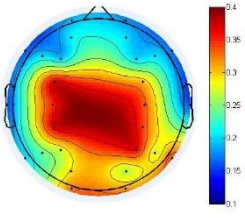
Participant 01	MSE EEG	MSE Hb.O2	MSE Hb.R
RR			
RF			
FR			
FF			

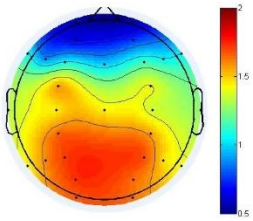
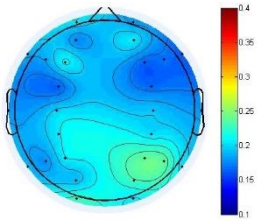
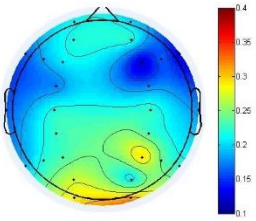
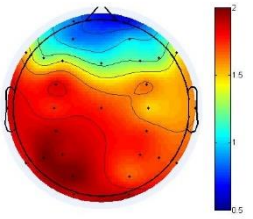
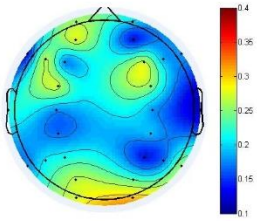
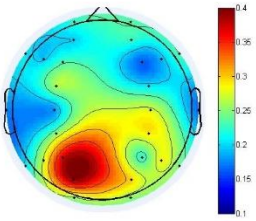
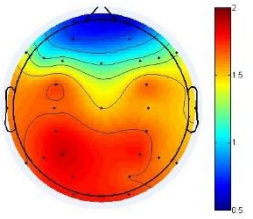
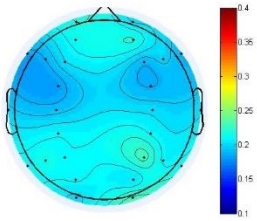
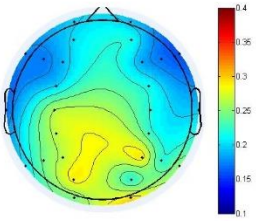
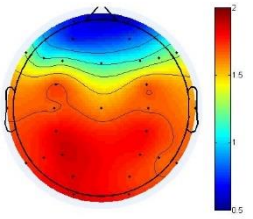
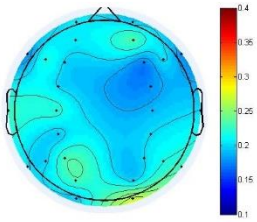
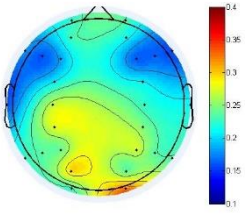
Participant 02	MSE EEG	MSE Hb.O2	MSE Hb.R
RR			
RF			
FR			
FF			

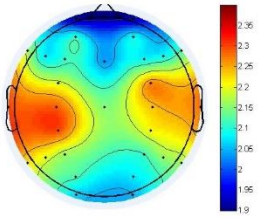
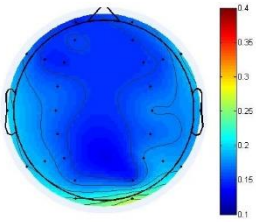
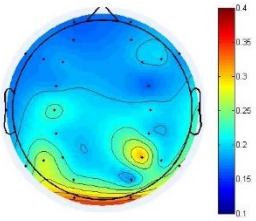
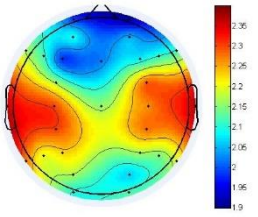
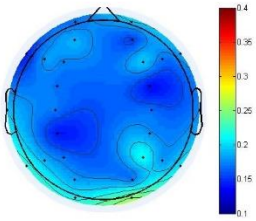
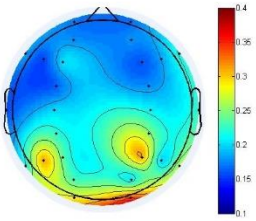
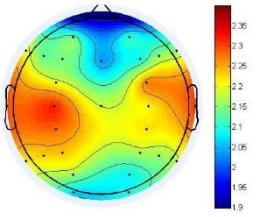
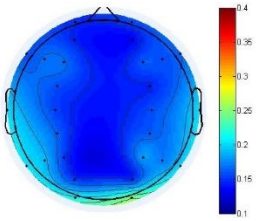
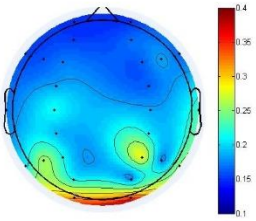
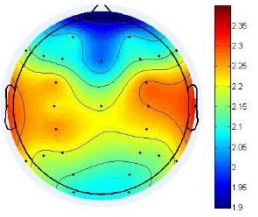
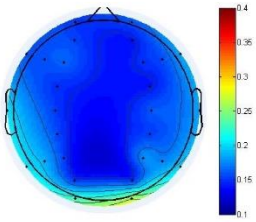
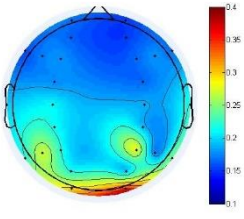
Participant 03	MSE EEG	MSE Hb.O2	MSE Hb.R
RR			
RF			
FR			
FF			

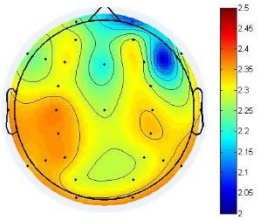
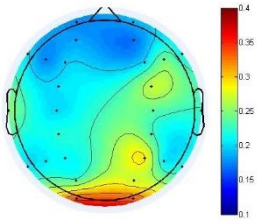
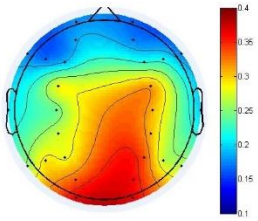
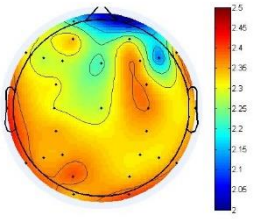
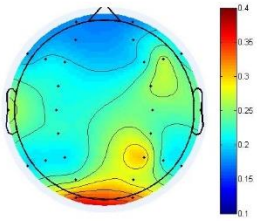
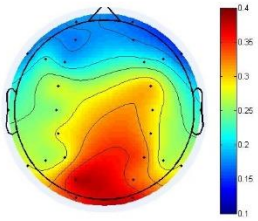
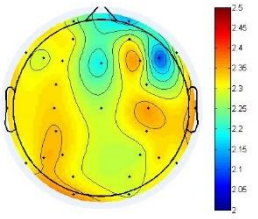
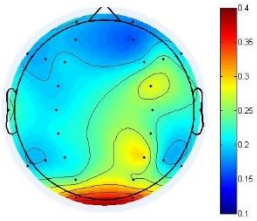
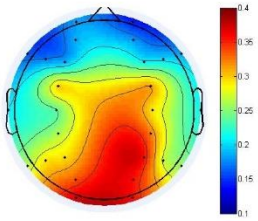
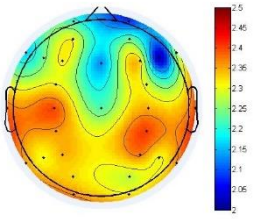
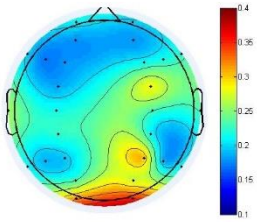
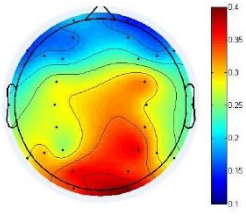
Participant 04	MSE EEG	MSE Hb.O2	MSE Hb.R
RR			
RF			
FR			
FF			

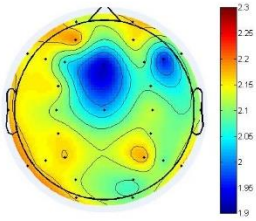
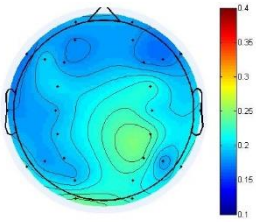
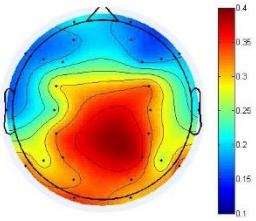
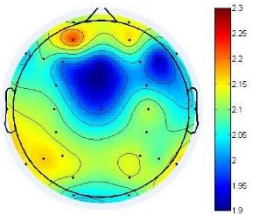
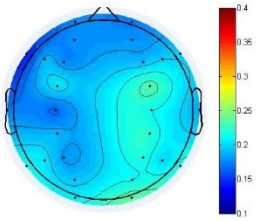
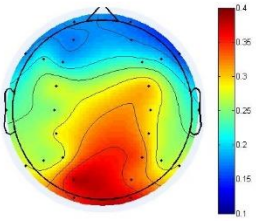
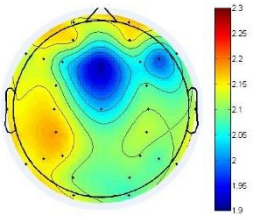
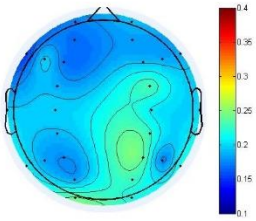
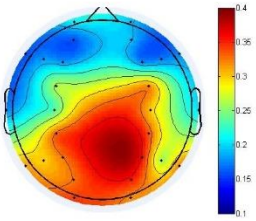
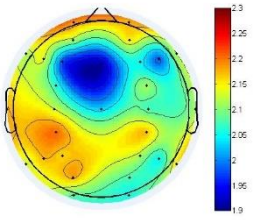
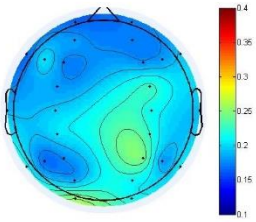
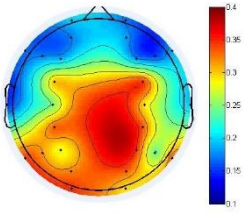
Participant 05	MSE EEG	MSE Hb.O2	MSE Hb.R
RR			
RF			
FR			
FF			

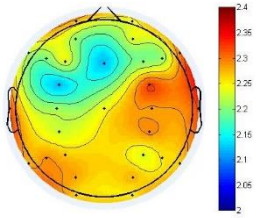
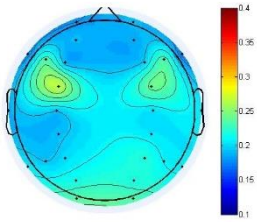
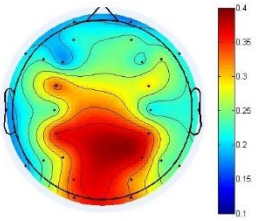
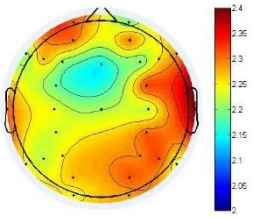
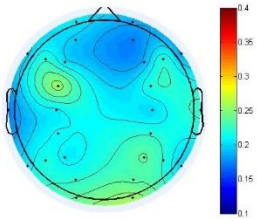
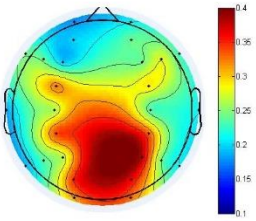
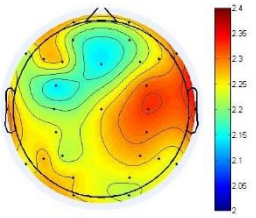
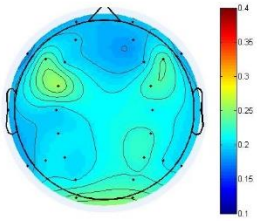
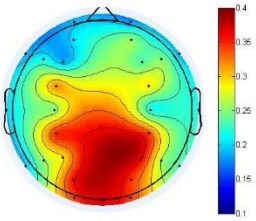
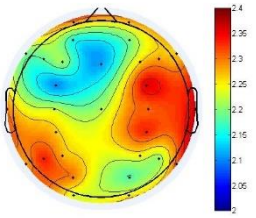
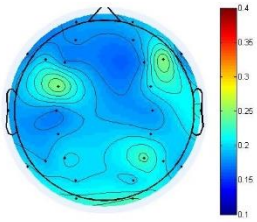
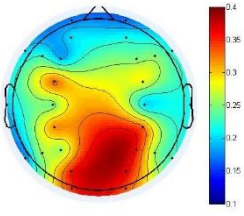
Participant 06	MSE EEG	MSE Hb.O2	MSE Hb.R
RR			
RF			
FR			
FF			

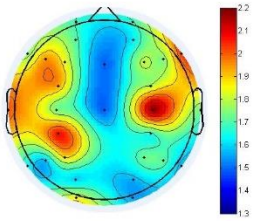
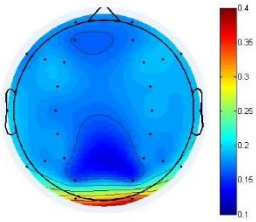
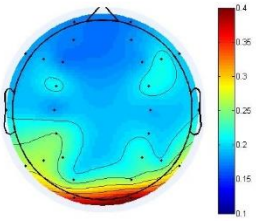
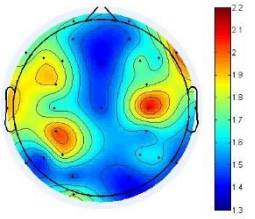
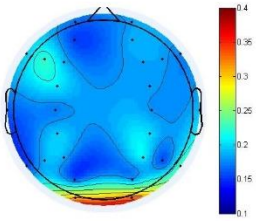
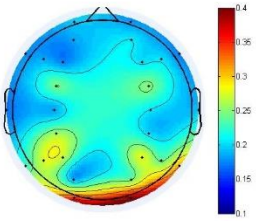
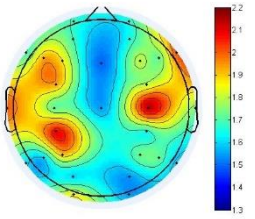
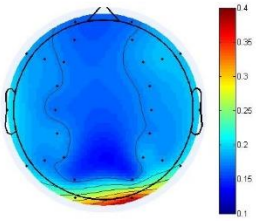
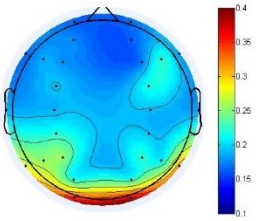
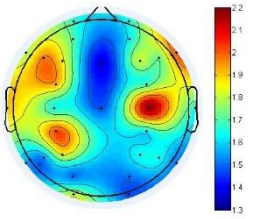
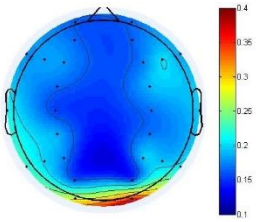
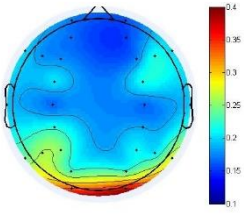
Participant 07	MSE EEG	MSE Hb.O2	MSE Hb.R
RR			
RF			
FR			
FF			

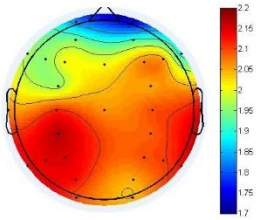
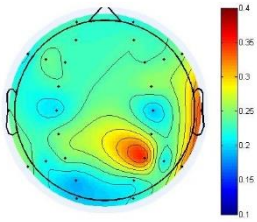
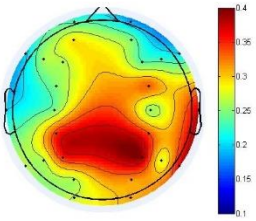
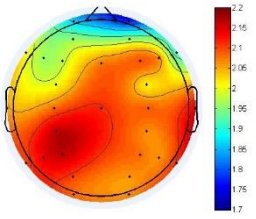
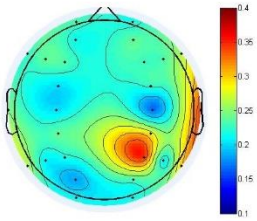
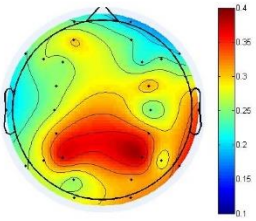
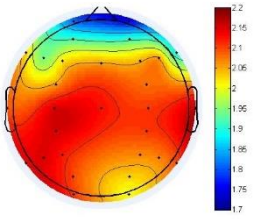
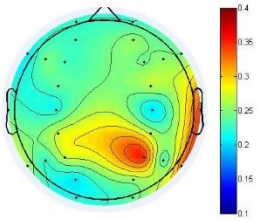
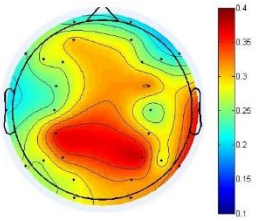
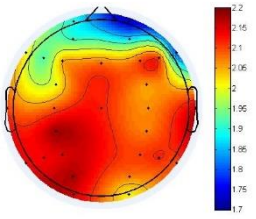
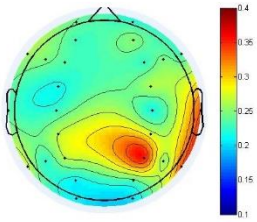
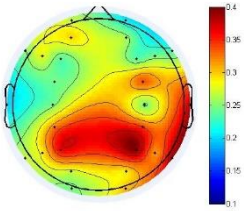
Participant 08	MSE EEG	MSE Hb.O2	MSE Hb.R
RR			
RF			
FR			
FF			

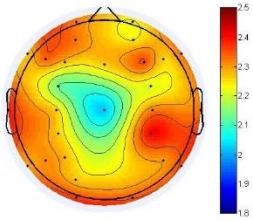
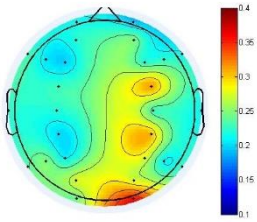
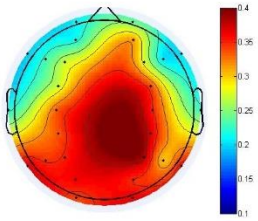
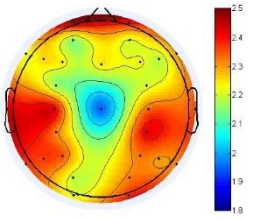
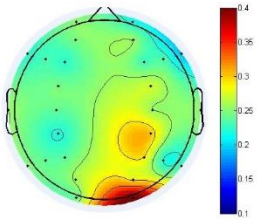
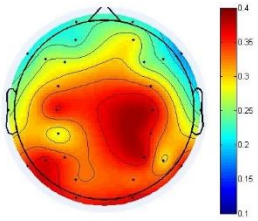
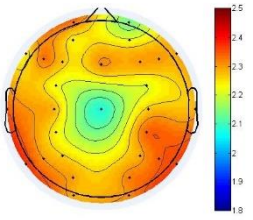
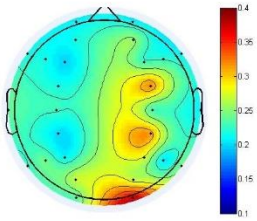
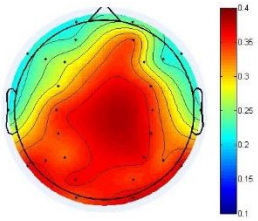
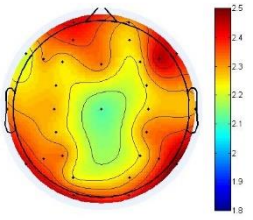
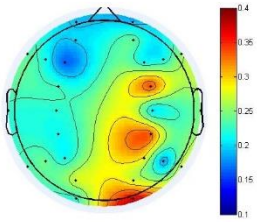
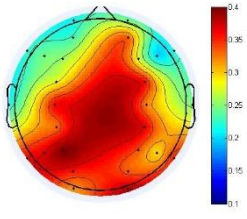
Participant 09	MSE EEG	MSE Hb.O2	MSE Hb.R
RR			
RF			
FR			
FF			

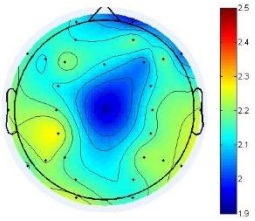
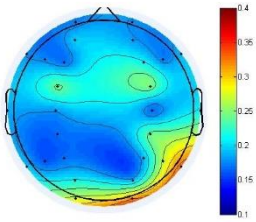
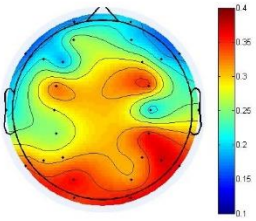
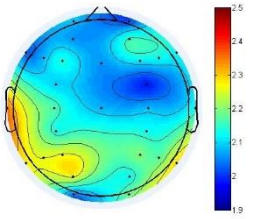
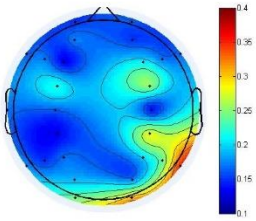
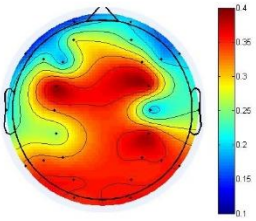
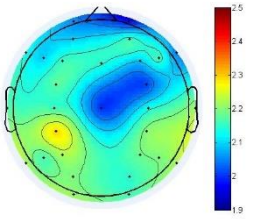
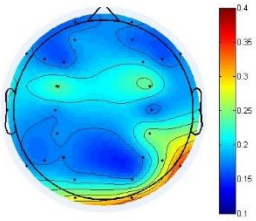
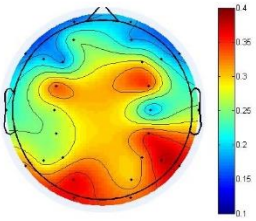
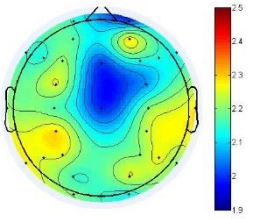
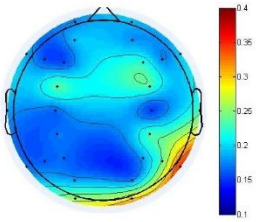
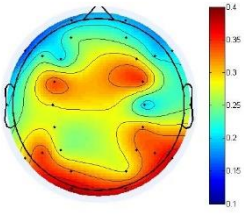
Participant 10	MSE EEG	MSE Hb.O2	MSE Hb.R
RR			
RF			
FR			
FF			

Participant 11	MSE EEG	MSE Hb.O2	MSE Hb.R
RR			
RF			
FR			
FF			

Participant 12	MSE EEG	MSE Hb.O2	MSE Hb.R
RR			
RF			
FR			
FF			

Participant 13	MSE EEG	MSE Hb.O2	MSE Hb.R
RR			
RF			
FR			
FF			

Participant 14	MSE EEG	MSE Hb.O2	MSE Hb.R
RR			
RF			
FR			
FF			

Participant 15	MSE EEG	MSE Hb.O2	MSE Hb.R
RR			
RF			
FR			
FF			

APPENDIX E

The Results of Wilcoxon's Signed Rank Test from SPSS

The results of Wilcoxon's signed rank test of MSE EEG

NPar Tests

Notes

Output Created		21-NOV-2019 00:47:57
Comments		
Input	Data	E:\P'Art\21-11-2019\DATA EGG.sav
	Active Dataset	DataSet0
	Filter	<none>
	Weight	<none>
	Split File	<none>
	N of Rows in Working Data File	15
Missing Value Handling	Definition of Missing	User-defined missing values are treated as missing.
	Cases Used	Statistics for each test are based on all cases with valid data for the variable(s) used in that test.
Syntax		NPAR TESTS /WILCOXON=C1RF C2RF C3RF C4RF C5RF C6RF C7RF C8RF C9RF C10RF C11RF C12RF C13RF C14RF C15RF C16RF C17RF C18RF C19RF C20RF C21RF C22RF C23RF C24RF C25RF C26RF C27RF C28RF C29RF C30RF WITH C1FF C2FF C3FF C4FF C5FF C6FF C7FF C8FF C9FF C10FF C11FF C12FF C13FF C14FF C15FF C16FF C17FF C18FF C19FF C20FF C21FF C22FF C23FF C24FF C25FF C26FF C27FF C28FF C29FF C30FF (PAIRED) /STATISTICS QUARTILES /MISSING ANALYSIS.
Resources	Processor Time	00:00:00.02
	Elapsed Time	00:00:00.03
	Number of Cases Allowed[a]	12098

a. Based on availability of workspace memory.

[DataSet0] E:\P'Art\21-11-2019\DATA EGG.sav

Descriptive Statistics

	N	Percentiles		
		25th	50th (Median)	75th
C1RF	15	1.8600	2.0800	2.2000
C2RF	15	1.7700	2.0000	2.1400
C3RF	15	1.8100	2.1300	2.2200
C4RF	15	1.9600	2.1100	2.2000
C5RF	15	1.8600	2.0000	2.2000
C6RF	15	1.9000	2.0300	2.2000
C7RF	15	1.8900	2.0400	2.1900
C8RF	15	1.8400	2.0200	2.1200
C9RF	15	1.9800	2.1700	2.2400
C10RF	15	1.9700	2.1200	2.2300
C11RF	15	2.0600	2.1600	2.2500
C12RF	15	1.9900	2.1500	2.2300
C13RF	15	2.0400	2.1400	2.2700
C14RF	15	2.0100	2.1100	2.1700
C15RF	15	2.0400	2.1000	2.2200
C16RF	15	2.0500	2.0900	2.2600
C17RF	15	1.8500	2.0800	2.1400
C18RF	15	1.6800	2.0600	2.1400
C19RF	15	1.9700	2.0300	2.2100
C20RF	15	1.8000	2.0000	2.1100
C21RF	15	1.9300	2.1400	2.3100
C22RF	15	2.0400	2.1300	2.2400
C23RF	15	1.9500	2.0900	2.2900
C24RF	15	1.9900	2.1400	2.3400
C25RF	15	2.0100	2.1400	2.2200
C26RF	15	2.0500	2.1500	2.2700
C27RF	15	1.9900	2.1500	2.2800
C28RF	15	2.0600	2.1800	2.2800
C29RF	15	1.8600	1.9300	2.1000
C30RF	15	1.9400	2.0700	2.1900
C1FF	15	1.8700	1.9600	2.1900
C2FF	15	1.6500	1.9500	2.1800
C3FF	15	1.7100	2.1200	2.1900
C4FF	15	1.6300	2.0900	2.2000
C5FF	15	1.9000	2.0500	2.2100
C6FF	15	1.8200	2.0500	2.2000
C7FF	15	1.9200	2.0000	2.2000

Descriptive Statistics

	N	Percentiles		
		25th	50th (Median)	75th
C8FF	15	1.7400	2.0600	2.2700
C9FF	15	2.0100	2.1300	2.2200
C10FF	15	2.0000	2.1400	2.3000
C11FF	15	2.0100	2.1500	2.2400
C12FF	15	1.9700	2.1200	2.2300
C13FF	15	2.0300	2.1500	2.2300
C14FF	15	2.0100	2.1100	2.1800
C15FF	15	2.0000	2.0800	2.2000
C16FF	15	2.0000	2.0900	2.2100
C17FF	15	1.9300	2.1200	2.1700
C18FF	15	1.7300	2.0200	2.1800
C19FF	15	1.7800	2.0700	2.1700
C20FF	15	1.6700	2.0200	2.2100
C21FF	15	1.8000	2.1000	2.3000
C22FF	15	2.1000	2.1800	2.2600
C23FF	15	2.0300	2.1700	2.2900
C24FF	15	1.6700	2.1100	2.3300
C25FF	15	2.0300	2.1500	2.2400
C26FF	15	1.9900	2.1200	2.2300
C27FF	15	1.9600	2.1200	2.2200
C28FF	15	2.0300	2.1200	2.3000
C29FF	15	1.8700	2.0000	2.1100
C30FF	15	1.9500	2.0600	2.1900

Wilcoxon Signed Ranks Test

Ranks

		N	Mean Rank	Sum of Ranks
C1FF - C1RF	Negative Ranks	9[a]	8.00	72.00
	Positive Ranks	5[b]	6.60	33.00
	Ties	1[c]		
	Total	15		
C2FF - C2RF	Negative Ranks	8[d]	9.31	74.50
	Positive Ranks	7[e]	6.50	45.50
	Ties	0[f]		
	Total	15		
C3FF - C3RF	Negative Ranks	11[g]	7.59	83.50
	Positive Ranks	3[h]	7.17	21.50
	Ties	1[i]		
	Total	15		
C4FF - C4RF	Negative Ranks	10[j]	9.10	91.00
	Positive Ranks	5[k]	5.80	29.00
	Ties	0[l]		
	Total	15		
C5FF - C5RF	Negative Ranks	4[m]	10.13	40.50
	Positive Ranks	10[n]	6.45	64.50
	Ties	1[o]		
	Total	15		
C6FF - C6RF	Negative Ranks	7[p]	9.14	64.00
	Positive Ranks	7[q]	5.86	41.00
	Ties	1[r]		
	Total	15		
C7FF - C7RF	Negative Ranks	7[s]	7.64	53.50
	Positive Ranks	6[t]	6.25	37.50
	Ties	2[u]		
	Total	15		
C8FF - C8RF	Negative Ranks	6[v]	9.08	54.50
	Positive Ranks	9[w]	7.28	65.50
	Ties	0[x]		
	Total	15		
C9FF - C9RF	Negative Ranks	7[y]	8.21	57.50
	Positive Ranks	8[z]	7.81	62.50
	Ties	0[aa]		
	Total	15		
C10FF - C10RF	Negative Ranks	6[ab]	7.25	43.50
	Positive Ranks	8[ac]	7.69	61.50

Ranks

		N	Mean Rank	Sum of Ranks
	Ties	1[ad]		
	Total	15		
C11FF - C11RF	Negative Ranks	9[ae]	8.56	77.00
	Positive Ranks	6[af]	7.17	43.00
	Ties	0[ag]		
	Total	15		
C12FF - C12RF	Negative Ranks	7[ah]	8.79	61.50
	Positive Ranks	7[ai]	6.21	43.50
	Ties	1[aj]		
	Total	15		
C13FF - C13RF	Negative Ranks	8[ak]	9.50	76.00
	Positive Ranks	7[al]	6.29	44.00
	Ties	0[am]		
	Total	15		
C14FF - C14RF	Negative Ranks	5[an]	8.50	42.50
	Positive Ranks	10[ao]	7.75	77.50
	Ties	0[ap]		
	Total	15		
C15FF - C15RF	Negative Ranks	9[aq]	8.00	72.00
	Positive Ranks	6[ar]	8.00	48.00
	Ties	0[as]		
	Total	15		
C16FF - C16RF	Negative Ranks	11[at]	7.95	87.50
	Positive Ranks	3[au]	5.83	17.50
	Ties	1[av]		
	Total	15		
C17FF - C17RF	Negative Ranks	6[aw]	10.58	63.50
	Positive Ranks	9[ax]	6.28	56.50
	Ties	0[ay]		
	Total	15		
C18FF - C18RF	Negative Ranks	3[az]	14.00	42.00
	Positive Ranks	12[ba]	6.50	78.00
	Ties	0[bb]		
	Total	15		
C19FF - C19RF	Negative Ranks	9[bc]	8.33	75.00
	Positive Ranks	5[bd]	6.00	30.00
	Ties	1[be]		
	Total	15		

Ranks

		N	Mean Rank	Sum of Ranks
C20FF - C20RF	Negative Ranks	7[bf]	10.57	74.00
	Positive Ranks	8[bg]	5.75	46.00
	Ties	0[bh]		
	Total	15		
C21FF - C21RF	Negative Ranks	13[bi]	8.08	105.00
	Positive Ranks	2[bj]	7.50	15.00
	Ties	0[bk]		
	Total	15		
C22FF - C22RF	Negative Ranks	5[bl]	10.00	50.00
	Positive Ranks	9[bm]	6.11	55.00
	Ties	1[bn]		
	Total	15		
C23FF - C23RF	Negative Ranks	4[bo]	10.63	42.50
	Positive Ranks	11[bp]	7.05	77.50
	Ties	0[bq]		
	Total	15		
C24FF - C24RF	Negative Ranks	10[br]	8.30	83.00
	Positive Ranks	5[bs]	7.40	37.00
	Ties	0[bt]		
	Total	15		
C25FF - C25RF	Negative Ranks	8[bu]	6.31	50.50
	Positive Ranks	5[bv]	8.10	40.50
	Ties	2[bw]		
	Total	15		
C26FF - C26RF	Negative Ranks	10[bx]	9.15	91.50
	Positive Ranks	5[by]	5.70	28.50
	Ties	0[bz]		
	Total	15		
C27FF - C27RF	Negative Ranks	10[ca]	9.00	90.00
	Positive Ranks	5[cb]	6.00	30.00
	Ties	0[cc]		
	Total	15		
C28FF - C28RF	Negative Ranks	8[cd]	8.69	69.50
	Positive Ranks	6[ce]	5.92	35.50
	Ties	1[cf]		
	Total	15		
C29FF - C29RF	Negative Ranks	8[cg]	8.00	64.00
	Positive Ranks	7[ch]	8.00	56.00

Ranks

		N	Mean Rank	Sum of Ranks
	Ties	0[ci]		
	Total	15		
C30FF - C30RF	Negative Ranks	6[cj]	9.67	58.00
	Positive Ranks	7[ck]	4.71	33.00
	Ties	2[cl]		
	Total	15		

a. C1FF < C1RF
b. C1FF > C1RF
c. C1FF = C1RF
d. C2FF < C2RF
e. C2FF > C2RF
f. C2FF = C2RF
g. C3FF < C3RF
h. C3FF > C3RF
i. C3FF = C3RF
j. C4FF < C4RF
k. C4FF > C4RF
l. C4FF = C4RF
m. C5FF < C5RF
n. C5FF > C5RF
o. C5FF = C5RF
p. C6FF < C6RF
q. C6FF > C6RF
r. C6FF = C6RF
s. C7FF < C7RF
t. C7FF > C7RF
u. C7FF = C7RF
v. C8FF < C8RF
w. C8FF > C8RF
x. C8FF = C8RF
y. C9FF < C9RF
z. C9FF > C9RF
aa. C9FF = C9RF
ab. C10FF < C10RF
ac. C10FF > C10RF
ad. C10FF = C10RF
ae. C11FF < C11RF

af. C11FF > C11RF

ag. C11FF = C11RF

ah. C12FF < C12RF

ai. C12FF > C12RF

aj. C12FF = C12RF

ak. C13FF < C13RF

al. C13FF > C13RF

am. C13FF = C13RF

an. C14FF < C14RF

ao. C14FF > C14RF

ap. C14FF = C14RF

aq. C15FF < C15RF

ar. C15FF > C15RF

as. C15FF = C15RF

Test Statistics[a]

	C1FF - C1RF	C2FF - C2RF	C3FF - C3RF	C4FF - C4RF	C5FF - C5RF
Z	-1.226[b]	-.828[b]	-1.949[b]	-1.762[b]	-.757[c]
Asymp. Sig. (2-tailed)	.220	.408	.051	.078	.449

Test Statistics[a]

	C6FF - C6RF	C7FF - C7RF	C8FF - C8RF	C9FF - C9RF	C10FF - C10RF
Z	-.723[b]	-.560[b]	-.313[c]	-.143[c]	-.565[c]
Asymp. Sig. (2-tailed)	.470	.576	.754	.887	.572

Test Statistics[a]

	C11FF - C11RF	C12FF - C12RF	C13FF - C13RF	C14FF - C14RF
Z	-.974[b]	-.566[b]	-.911[b]	-.997[c]
Asymp. Sig. (2-tailed)	.330	.571	.362	.319

Test Statistics[a]

	C15FF - C15RF	C16FF - C16RF	C17FF - C17RF	C18FF - C18RF
Z	-.685[b]	-2.205[b]	-.199[b]	-1.024[c]
Asymp. Sig. (2-tailed)	.493	.027	.842	.306

Test Statistics[a]

	C19FF - C19RF	C20FF - C20RF	C21FF - C21RF	C22FF - C22RF
Z	-1.414[b]	-.796[b]	-2.562[b]	-.157[c]
Asymp. Sig. (2-tailed)	.158	.426	.010	.875

Test Statistics[a]

	C23FF - C23RF	C24FF - C24RF	C25FF - C25RF	C26FF - C26RF
Z	-.997[c]	-1.309[b]	-.350[b]	-1.792[b]
Asymp. Sig. (2-tailed)	.319	.191	.726	.073

Test Statistics[a]

	C27FF - C27RF	C28FF - C28RF	C29FF - C29RF	C30FF - C30RF
Z	-1.708[b]	-1.071[b]	-.228[b]	-.875[b]
Asymp. Sig. (2-tailed)	.088	.284	.820	.381

a. Wilcoxon Signed Ranks Test

b. Based on positive ranks.

c. Based on negative ranks.

The results of Wilcoxon's signed rank test of MSE Hb.O2

NPar Tests

Notes

Output Created		21-NOV-2019 01:30:40
Comments		
Input	Data	E:\P'Art\HbO\HbO DATA.sav
	Active Dataset	DataSet0
	Filter	<none>
	Weight	<none>
	Split File	<none>
	N of Rows in Working Data File	15
Missing Value Handling	Definition of Missing	User-defined missing values are treated as missing.
	Cases Used	Statistics for each test are based on all cases with valid data for the variable(s) used in that test.
Syntax		NPAR TESTS /WILCOXON=C1RF C2RF C3RF C4RF C5RF C6RF C7RF C8RF C9RF C10RF C11RF C12RF C13RF C14RF C15RF C16RF C17RF C18RF C19RF C20RF C21RF C22RF C23RF C24RF C25RF C26RF C27RF C28RF WITH C1FF C2FF C3FF C4FF C5FF C6FF C7FF C8FF C9FF C10FF C11FF C12FF C13FF C14FF C15FF C16FF C17FF C18FF C19FF C20FF C21FF C22FF C23FF C24FF C25FF C26FF C27FF C28FF (PAIRED) /STATISTICS QUARTILES /MISSING ANALYSIS.
Resources	Processor Time	00:00:00.02
	Elapsed Time	00:00:00.02
	Number of Cases Allowed[a]	12892

a. Based on availability of workspace memory.

[DataSet0] E:\P'Art\HbO\HbO DATA.sav

Page 1

Descriptive Statistics

	N	Percentiles		
		25th	50th (Median)	75th
C1RF	15	.1700	.2100	.2300
C2RF	15	.1700	.1900	.2100
C3RF	15	.1800	.2000	.2400
C4RF	15	.1600	.1900	.2100
C5RF	15	.1800	.2000	.2200
C6RF	15	.1900	.2100	.2200
C7RF	15	.2000	.2500	.3000
C8RF	15	.1900	.2300	.2600
C9RF	15	.1700	.2100	.2600
C10RF	15	.1800	.2000	.2600
C11RF	15	.1700	.2100	.2200
C12RF	15	.2100	.2200	.3000
C13RF	15	.1800	.2200	.2600
C14RF	15	.1800	.2300	.2700
C15RF	15	.2100	.2700	.2900
C16RF	15	.2500	.3000	.3300
C17RF	15	.1800	.2000	.2300
C18RF	15	.1700	.2000	.2300
C19RF	15	.1400	.1800	.2200
C20RF	15	.1700	.1900	.2200
C21RF	15	.1700	.2200	.2500
C22RF	15	.1700	.2000	.2400
C23RF	15	.2000	.2400	.2900
C24RF	15	.1800	.2200	.2400
C25RF	15	.1900	.2100	.2300
C26RF	15	.1700	.2100	.2400
C27RF	15	.1800	.2100	.2200
C28RF	15	.2100	.2300	.2900
C1FF	15	.1600	.1900	.2100
C2FF	15	.1700	.1900	.2100
C3FF	15	.1800	.2000	.2200
C4FF	15	.1800	.1900	.2300
C5FF	15	.1700	.1800	.2100
C6FF	15	.1700	.1900	.2200
C7FF	15	.1800	.2300	.2700
C8FF	15	.1900	.2300	.2800
C9FF	15	.1800	.2200	.2700

Descriptive Statistics

	N	Percentiles		
		25th	50th (Median)	75th
C10FF	15	.1800	.2100	.2500
C11FF	15	.1800	.2100	.2300
C12FF	15	.2000	.2400	.2900
C13FF	15	.1900	.2100	.2300
C14FF	15	.2000	.2300	.2700
C15FF	15	.2200	.2600	.2900
C16FF	15	.2300	.2900	.3300
C17FF	15	.1700	.2000	.2200
C18FF	15	.1800	.2000	.2300
C19FF	15	.1700	.1800	.2000
C20FF	15	.1800	.2000	.2200
C21FF	15	.1900	.2000	.2300
C22FF	15	.1900	.2000	.2800
C23FF	15	.1900	.2200	.2800
C24FF	15	.1900	.2100	.2300
C25FF	15	.1900	.2000	.2200
C26FF	15	.1900	.2000	.2400
C27FF	15	.2000	.2100	.2200
C28FF	15	.2100	.2300	.2700

Wilcoxon Signed Ranks Test

Ranks

		N	Mean Rank	Sum of Ranks
C1FF - C1RF	Negative Ranks	10[a]	7.20	72.00
	Positive Ranks	4[b]	8.25	33.00
	Ties	1[c]		
	Total	15		
C2FF - C2RF	Negative Ranks	7[d]	4.43	31.00
	Positive Ranks	4[e]	8.75	35.00
	Ties	4[f]		
	Total	15		
C3FF - C3RF	Negative Ranks	8[g]	7.50	60.00
	Positive Ranks	4[h]	4.50	18.00
	Ties	3[i]		
	Total	15		
C4FF - C4RF	Negative Ranks	6[j]	5.92	35.50
	Positive Ranks	7[k]	7.93	55.50
	Ties	2[l]		
	Total	15		
C5FF - C5RF	Negative Ranks	9[m]	6.39	57.50
	Positive Ranks	4[n]	8.38	33.50
	Ties	2[o]		
	Total	15		
C6FF - C6RF	Negative Ranks	6[p]	6.00	36.00
	Positive Ranks	5[q]	6.00	30.00
	Ties	4[r]		
	Total	15		
C7FF - C7RF	Negative Ranks	9[s]	8.67	78.00
	Positive Ranks	4[t]	3.25	13.00
	Ties	2[u]		
	Total	15		
C8FF - C8RF	Negative Ranks	5[v]	7.10	35.50
	Positive Ranks	8[w]	6.94	55.50
	Ties	2[x]		
	Total	15		
C9FF - C9RF	Negative Ranks	6[y]	6.58	39.50
	Positive Ranks	8[z]	8.19	65.50
	Ties	1[aa]		
	Total	15		
C10FF - C10RF	Negative Ranks	7[ab]	7.00	49.00
	Positive Ranks	6[ac]	7.00	42.00

Ranks

		N	Mean Rank	Sum of Ranks
	Ties	2[ad]		
	Total	15		
C11FF - C11RF	Negative Ranks	5[ae]	4.70	23.50
	Positive Ranks	4[af]	5.38	21.50
	Ties	6[ag]		
	Total	15		
C12FF - C12RF	Negative Ranks	6[ah]	5.83	35.00
	Positive Ranks	5[ai]	6.20	31.00
	Ties	4[aj]		
	Total	15		
C13FF - C13RF	Negative Ranks	9[ak]	7.17	64.50
	Positive Ranks	4[al]	6.63	26.50
	Ties	2[am]		
	Total	15		
C14FF - C14RF	Negative Ranks	7[an]	7.79	54.50
	Positive Ranks	6[ao]	6.08	36.50
	Ties	2[ap]		
	Total	15		
C15FF - C15RF	Negative Ranks	6[aq]	7.08	42.50
	Positive Ranks	6[ar]	5.92	35.50
	Ties	3[as]		
	Total	15		
C16FF - C16RF	Negative Ranks	9[at]	8.33	75.00
	Positive Ranks	6[au]	7.50	45.00
	Ties	0[av]		
	Total	15		
C17FF - C17RF	Negative Ranks	10[aw]	7.60	76.00
	Positive Ranks	4[ax]	7.25	29.00
	Ties	1[ay]		
	Total	15		
C18FF - C18RF	Negative Ranks	5[az]	6.00	30.00
	Positive Ranks	8[ba]	7.63	61.00
	Ties	2[bb]		
	Total	15		
C19FF - C19RF	Negative Ranks	4[bc]	8.38	33.50
	Positive Ranks	11[bd]	7.86	86.50
	Ties	0[be]		
	Total	15		

Ranks

		N	Mean Rank	Sum of Ranks
C20FF - C20RF	Negative Ranks	4[bf]	6.00	24.00
	Positive Ranks	6[bg]	5.17	31.00
	Ties	5[bh]		
	Total	15		
C21FF - C21RF	Negative Ranks	7[bi]	7.21	50.50
	Positive Ranks	5[bj]	5.50	27.50
	Ties	3[bk]		
	Total	15		
C22FF - C22RF	Negative Ranks	3[bl]	3.67	11.00
	Positive Ranks	9[bm]	7.44	67.00
	Ties	3[bn]		
	Total	15		
C23FF - C23RF	Negative Ranks	10[bo]	7.15	71.50
	Positive Ranks	3[bp]	6.50	19.50
	Ties	2[bq]		
	Total	15		
C24FF - C24RF	Negative Ranks	6[br]	6.17	37.00
	Positive Ranks	5[bs]	5.80	29.00
	Ties	4[bt]		
	Total	15		
C25FF - C25RF	Negative Ranks	8[bu]	7.50	60.00
	Positive Ranks	4[bv]	4.50	18.00
	Ties	3[bw]		
	Total	15		
C26FF - C26RF	Negative Ranks	8[bx]	5.13	41.00
	Positive Ranks	4[by]	9.25	37.00
	Ties	3[bz]		
	Total	15		
C27FF - C27RF	Negative Ranks	6[ca]	6.42	38.50
	Positive Ranks	7[cb]	7.50	52.50
	Ties	2[cc]		
	Total	15		
C28FF - C28RF	Negative Ranks	6[cd]	5.25	31.50
	Positive Ranks	6[ce]	7.75	46.50
	Ties	3[cf]		
	Total	15		

a. C1FF < C1RF

b. C1FF > C1RF

c. C1FF = C1RF

d. C2FF < C2RF
e. C2FF > C2RF
f. C2FF = C2RF
g. C3FF < C3RF
h. C3FF > C3RF
i. C3FF = C3RF
j. C4FF < C4RF
k. C4FF > C4RF
l. C4FF = C4RF
m. C5FF < C5RF
n. C5FF > C5RF
o. C5FF = C5RF
p. C6FF < C6RF
q. C6FF > C6RF
r. C6FF = C6RF
s. C7FF < C7RF
t. C7FF > C7RF
u. C7FF = C7RF
v. C8FF < C8RF
w. C8FF > C8RF
x. C8FF = C8RF
y. C9FF < C9RF
z. C9FF > C9RF
aa. C9FF = C9RF
ab. C10FF < C10RF
ac. C10FF > C10RF
ad. C10FF = C10RF
ae. C11FF < C11RF
af. C11FF > C11RF
ag. C11FF = C11RF
ah. C12FF < C12RF
ai. C12FF > C12RF
aj. C12FF = C12RF
ak. C13FF < C13RF

al. C13FF > C13RF

am. C13FF = C13RF

an. C14FF < C14RF

ao. C14FF > C14RF

ap. C14FF = C14RF

aq. C15FF < C15RF

ar. C15FF > C15RF

as. C15FF = C15RF

Test Statistics[a]

	C1FF - C1RF	C2FF - C2RF	C3FF - C3RF	C4FF - C4RF	C5FF - C5RF
Z	-1.232[b]	-.179[c]	-1.671[b]	-.708[c]	-.844[b]
Asymp. Sig. (2-tailed)	.218	.858	.095	.479	.399

Test Statistics[a]

	C6FF - C6RF	C7FF - C7RF	C8FF - C8RF	C9FF - C9RF	C10FF - C10RF
Z	-.269[b]	-2.289[b]	-.708[c]	-.826[c]	-.249[b]
Asymp. Sig. (2-tailed)	.788	.022	.479	.409	.803

Test Statistics[a]

	C11FF - C11RF	C12FF - C12RF	C13FF - C13RF	C14FF - C14RF
Z	-.119[b]	-.179[b]	-1.335[b]	-.634[b]
Asymp. Sig. (2-tailed)	.905	.858	.182	.526

Test Statistics[a]

	C15FF - C15RF	C16FF - C16RF	C17FF - C17RF	C18FF - C18RF
Z	-.279[b]	-.859[b]	-1.484[b]	-1.097[c]
Asymp. Sig. (2-tailed)	.781	.390	.138	.273

Test Statistics[a]

	C19FF - C19RF	C20FF - C20RF	C21FF - C21RF	C22FF - C22RF
Z	-1.516[c]	-.359[c]	-.913[b]	-2.209[c]
Asymp. Sig. (2-tailed)	.130	.719	.361	.027

Test Statistics[a]

	C23FF - C23RF	C24FF - C24RF	C25FF - C25RF	C26FF - C26RF
Z	-1.840[b]	-.359[b]	-1.705[b]	-.157[b]
Asymp. Sig. (2-tailed)	.066	.719	.088	.875

Test Statistics[a]

	C27FF - C27RF	C28FF - C28RF
Z	-.496[c]	-.593[c]
Asymp. Sig. (2-tailed)	.620	.553

a. Wilcoxon Signed Ranks Test

b. Based on positive ranks.

c. Based on negative ranks.

The results of Wilcoxon's signed rank test of MSE Hb.R

NPar Tests

Notes

Output Created		21-NOV-2019 02:10:39
Comments		
Input	Data	E:\P'Art\HbR\DATA HbR.sav
	Active Dataset	DataSet0
	Filter	<none>
	Weight	<none>
	Split File	<none>
	N of Rows in Working Data File	15
Missing Value Handling	Definition of Missing	User-defined missing values are treated as missing.
	Cases Used	Statistics for each test are based on all cases with valid data for the variable(s) used in that test.
Syntax		NPAR TESTS /WILCOXON=C1RF C2RF C3RF C4RF C5RF C6RF C7RF C8RF C9RF C10RF C11RF C12RF C13RF C14RF C15RF C16RF C17RF C18RF C19RF C20RF C21RF C22RF C23RF C24RF C25RF C26RF C27RF C28RF WITH C1FF C2FF C3FF C4FF C5FF C6FF C7FF C8FF C9FF C10FF C11FF C12FF C13FF C14FF C15FF C16FF C17FF C18FF C19FF C20FF C21FF C22FF C23FF C24FF C25FF C26FF C27FF C28FF (PAIRED) /STATISTICS QUARTILES /MISSING ANALYSIS.
Resources	Processor Time	00:00:00.03
	Elapsed Time	00:00:00.03
	Number of Cases Allowed[a]	12892

a. Based on availability of workspace memory.

[DataSet0] E:\P'Art\HbR\DATA HbR.sav

Descriptive Statistics

	N	Percentiles		
		25th	50th (Median)	75th
C1RF	15	.1700	.1900	.2200
C2RF	15	.1600	.1800	.2100
C3RF	15	.1800	.2000	.2500
C4RF	15	.1800	.2300	.2400
C5RF	15	.1900	.2000	.2600
C6RF	15	.1600	.2100	.2600
C7RF	15	.2400	.2800	.3600
C8RF	15	.2500	.3100	.3300
C9RF	15	.2000	.2600	.3300
C10RF	15	.2300	.2900	.3400
C11RF	15	.2700	.3200	.3700
C12RF	15	.3100	.3400	.3700
C13RF	15	.2600	.3400	.3600
C14RF	15	.2400	.3300	.3800
C15RF	15	.2900	.3400	.3500
C16RF	15	.3100	.3300	.3700
C17RF	15	.2000	.2200	.2400
C18RF	15	.1900	.2000	.2300
C19RF	15	.1700	.1800	.2100
C20RF	15	.1800	.1900	.2200
C21RF	15	.1700	.2000	.2600
C22RF	15	.2500	.2800	.3400
C23RF	15	.2900	.3000	.3600
C24RF	15	.2000	.2200	.2400
C25RF	15	.2600	.2900	.3300
C26RF	15	.2200	.2700	.3400
C27RF	15	.1900	.2600	.3300
C28RF	15	.2600	.3100	.3500
C1FF	15	.1700	.1900	.2200
C2FF	15	.1600	.1800	.2000
C3FF	15	.1700	.2100	.2400
C4FF	15	.1800	.2100	.2500
C5FF	15	.1900	.2000	.2400
C6FF	15	.1800	.2200	.2700
C7FF	15	.2400	.3000	.3500
C8FF	15	.2500	.3200	.3400
C9FF	15	.2500	.2800	.3600

Descriptive Statistics

	N	Percentiles		
		25th	50th (Median)	75th
C10FF	15	.2000	.2900	.3300
C11FF	15	.2600	.2800	.3600
C12FF	15	.2800	.3500	.3600
C13FF	15	.2900	.3200	.3500
C14FF	15	.2400	.3300	.3500
C15FF	15	.3200	.3500	.3600
C16FF	15	.3200	.3400	.3700
C17FF	15	.1800	.2000	.2200
C18FF	15	.1800	.2000	.2200
C19FF	15	.1500	.1600	.2000
C20FF	15	.1700	.1900	.2100
C21FF	15	.1900	.2000	.2300
C22FF	15	.2700	.3200	.3600
C23FF	15	.2500	.3300	.3500
C24FF	15	.1900	.2200	.2500
C25FF	15	.2500	.2900	.3300
C26FF	15	.2300	.2800	.3200
C27FF	15	.2100	.2400	.3000
C28FF	15	.2500	.3200	.3500

Wilcoxon Signed Ranks Test

Ranks

		N	Mean Rank	Sum of Ranks
C1FF - C1RF	Negative Ranks	6[a]	4.75	28.50
	Positive Ranks	6[b]	8.25	49.50
	Ties	3[c]		
	Total	15		
C2FF - C2RF	Negative Ranks	6[d]	6.67	40.00
	Positive Ranks	6[e]	6.33	38.00
	Ties	3[f]		
	Total	15		
C3FF - C3RF	Negative Ranks	5[g]	7.20	36.00
	Positive Ranks	7[h]	6.00	42.00
	Ties	3[i]		
	Total	15		
C4FF - C4RF	Negative Ranks	7[j]	7.43	52.00
	Positive Ranks	6[k]	6.50	39.00
	Ties	2[l]		
	Total	15		
C5FF - C5RF	Negative Ranks	9[m]	7.50	67.50
	Positive Ranks	4[n]	5.88	23.50
	Ties	2[o]		
	Total	15		
C6FF - C6RF	Negative Ranks	2[p]	8.75	17.50
	Positive Ranks	9[q]	5.39	48.50
	Ties	4[r]		
	Total	15		
C7FF - C7RF	Negative Ranks	7[s]	7.57	53.00
	Positive Ranks	6[t]	6.33	38.00
	Ties	2[u]		
	Total	15		
C8FF - C8RF	Negative Ranks	7[v]	6.21	43.50
	Positive Ranks	7[w]	8.79	61.50
	Ties	1[x]		
	Total	15		
C9FF - C9RF	Negative Ranks	5[y]	4.80	24.00
	Positive Ranks	9[z]	9.00	81.00
	Ties	1[aa]		
	Total	15		
C10FF - C10RF	Negative Ranks	7[ab]	6.29	44.00
	Positive Ranks	4[ac]	5.50	22.00

Ranks

		N	Mean Rank	Sum of Ranks
	Ties	4[ad]		
	Total	15		
C11FF - C11RF	Negative Ranks	12[ae]	7.50	90.00
	Positive Ranks	3[af]	10.00	30.00
	Ties	0[ag]		
	Total	15		
C12FF - C12RF	Negative Ranks	6[ah]	9.83	59.00
	Positive Ranks	9[ai]	6.78	61.00
	Ties	0[aj]		
	Total	15		
C13FF - C13RF	Negative Ranks	8[ak]	5.94	47.50
	Positive Ranks	4[al]	7.63	30.50
	Ties	3[am]		
	Total	15		
C14FF - C14RF	Negative Ranks	9[an]	7.89	71.00
	Positive Ranks	4[ao]	5.00	20.00
	Ties	2[ap]		
	Total	15		
C15FF - C15RF	Negative Ranks	6[aq]	5.17	31.00
	Positive Ranks	6[ar]	7.83	47.00
	Ties	3[as]		
	Total	15		
C16FF - C16RF	Negative Ranks	6[at]	7.25	43.50
	Positive Ranks	7[au]	6.79	47.50
	Ties	2[av]		
	Total	15		
C17FF - C17RF	Negative Ranks	11[aw]	7.41	81.50
	Positive Ranks	2[ax]	4.75	9.50
	Ties	2[ay]		
	Total	15		
C18FF - C18RF	Negative Ranks	9[az]	7.44	67.00
	Positive Ranks	4[ba]	6.00	24.00
	Ties	2[bb]		
	Total	15		
C19FF - C19RF	Negative Ranks	10[bc]	8.00	80.00
	Positive Ranks	4[bd]	6.25	25.00
	Ties	1[be]		
	Total	15		

Ranks

		N	Mean Rank	Sum of Ranks
C20FF - C20RF	Negative Ranks	6[bf]	7.33	44.00
	Positive Ranks	6[bg]	5.67	34.00
	Ties	3[bh]		
	Total	15		
C21FF - C21RF	Negative Ranks	7[bi]	6.93	48.50
	Positive Ranks	5[bj]	5.90	29.50
	Ties	3[bk]		
	Total	15		
C22FF - C22RF	Negative Ranks	7[bl]	6.07	42.50
	Positive Ranks	6[bm]	8.08	48.50
	Ties	2[bn]		
	Total	15		
C23FF - C23RF	Negative Ranks	7[bo]	9.43	66.00
	Positive Ranks	7[bp]	5.57	39.00
	Ties	1[bq]		
	Total	15		
C24FF - C24RF	Negative Ranks	6[br]	8.08	48.50
	Positive Ranks	7[bs]	6.07	42.50
	Ties	2[bt]		
	Total	15		
C25FF - C25RF	Negative Ranks	7[bu]	7.86	55.00
	Positive Ranks	6[bv]	6.00	36.00
	Ties	2[bw]		
	Total	15		
C26FF - C26RF	Negative Ranks	7[bx]	7.14	50.00
	Positive Ranks	6[by]	6.83	41.00
	Ties	2[bz]		
	Total	15		
C27FF - C27RF	Negative Ranks	4[ca]	10.38	41.50
	Positive Ranks	11[cb]	7.14	78.50
	Ties	0[cc]		
	Total	15		
C28FF - C28RF	Negative Ranks	7[cd]	5.71	40.00
	Positive Ranks	6[ce]	8.50	51.00
	Ties	2[cf]		
	Total	15		

a. C1FF < C1RF

b. C1FF > C1RF

c. C1FF = C1RF

d. C2FF < C2RF

d. C2FF < C2RF
e. C2FF > C2RF
f. C2FF = C2RF
g. C3FF < C3RF
h. C3FF > C3RF
i. C3FF = C3RF
j. C4FF < C4RF
k. C4FF > C4RF
l. C4FF = C4RF
m. C5FF < C5RF
n. C5FF > C5RF
o. C5FF = C5RF
p. C6FF < C6RF
q. C6FF > C6RF
r. C6FF = C6RF
s. C7FF < C7RF
t. C7FF > C7RF
u. C7FF = C7RF
v. C8FF < C8RF
w. C8FF > C8RF
x. C8FF = C8RF
y. C9FF < C9RF
z. C9FF > C9RF
aa. C9FF = C9RF
ab. C10FF < C10RF
ac. C10FF > C10RF
ad. C10FF = C10RF
ae. C11FF < C11RF
af. C11FF > C11RF
ag. C11FF = C11RF
ah. C12FF < C12RF
ai. C12FF > C12RF
aj. C12FF = C12RF
ak. C13FF < C13RF

al. C13FF > C13RF

am. C13FF = C13RF

an. C14FF < C14RF

ao. C14FF > C14RF

ap. C14FF = C14RF

aq. C15FF < C15RF

ar. C15FF > C15RF

as. C15FF = C15RF

Test Statistics[a]

	C1FF - C1RF	C2FF - C2RF	C3FF - C3RF	C4FF - C4RF	C5FF - C5RF
Z	-.833[b]	-.079[c]	-.241[b]	-.457[c]	-1.581[c]
Asymp. Sig. (2-tailed)	.405	.937	.810	.648	.114

Test Statistics[a]

	C6FF - C6RF	C7FF - C7RF	C8FF - C8RF	C9FF - C9RF	C10FF - C10RF
Z	-1.399[b]	-.526[c]	-.568[b]	-1.800[b]	-.982[c]
Asymp. Sig. (2-tailed)	.162	.599	.570	.072	.326

Test Statistics[a]

	C11FF - C11RF	C12FF - C12RF	C13FF - C13RF	C14FF - C14RF
Z	-1.718[c]	-.057[b]	-.670[c]	-1.793[c]
Asymp. Sig. (2-tailed)	.086	.954	.503	.073

Test Statistics[a]

	C15FF - C15RF	C16FF - C16RF	C17FF - C17RF	C18FF - C18RF
Z	-.633[b]	-.141[b]	-2.540[c]	-1.514[c]
Asymp. Sig. (2-tailed)	.527	.888	.011	.130

Test Statistics[a]

	C19FF - C19RF	C20FF - C20RF	C21FF - C21RF	C22FF - C22RF
Z	-1.746[c]	-.396[c]	-.749[c]	-.211[b]
Asymp. Sig. (2-tailed)	.081	.692	.454	.833

Test Statistics[a]

	C23FF - C23RF	C24FF - C24RF	C25FF - C25RF	C26FF - C26RF
Z	-.856[c]	-.213[c]	-.669[c]	-.317[c]
Asymp. Sig. (2-tailed)	.392	.832	.503	.751

Test Statistics[a]

	C27FF - C27RF	C28FF - C28RF
Z	-1.064[b]	-.387[b]
Asymp. Sig. (2-tailed)	.287	.698

a. Wilcoxon Signed Ranks Test

b. Based on negative ranks.

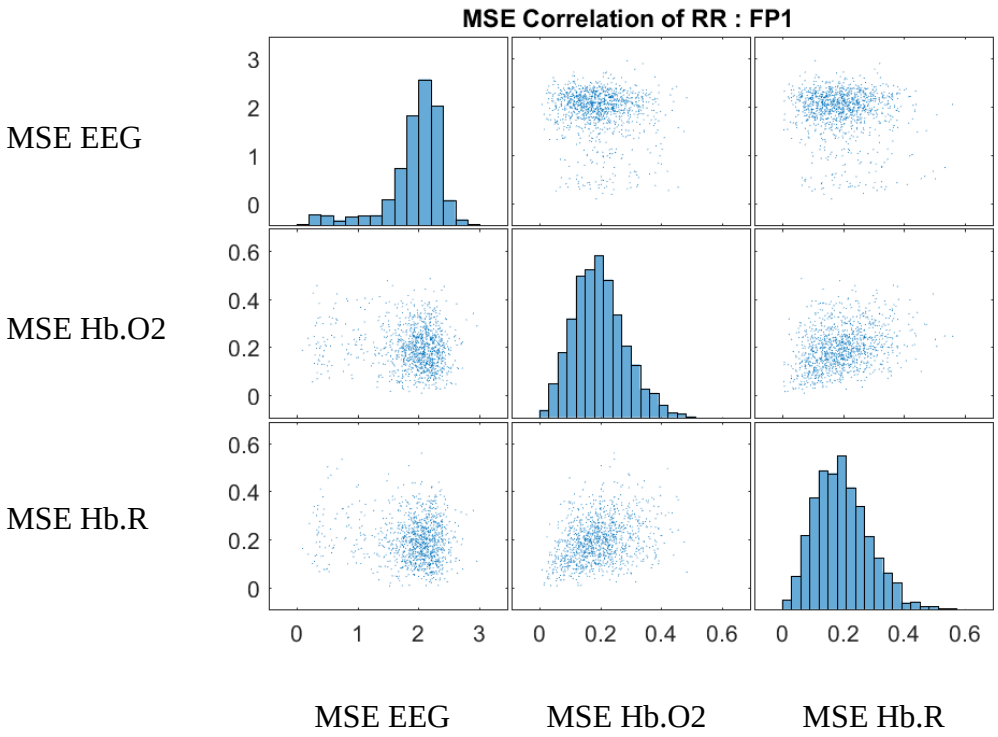
c. Based on positive ranks.

APPENDIX F

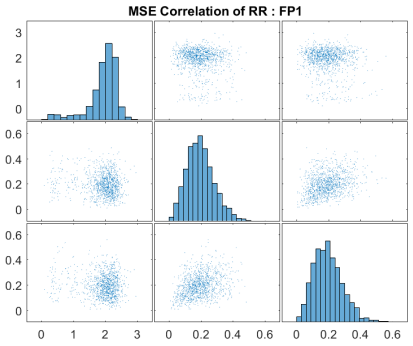
The Scatter Plot Matrix of the Correlation

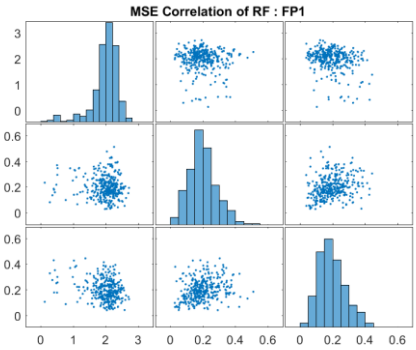
The scatter plot matrix for correlation of MSE EEG, MSE Hb.O2 and MSE Hb.R

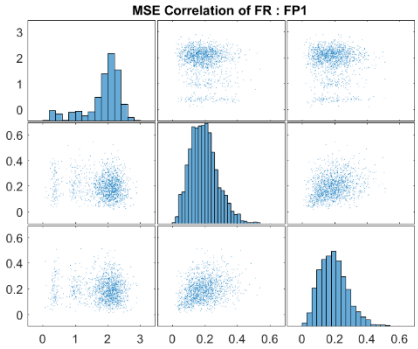
RR 1,163 pictures, RF 348 pictures, FR 1,577 pictures and FF 651 pictures

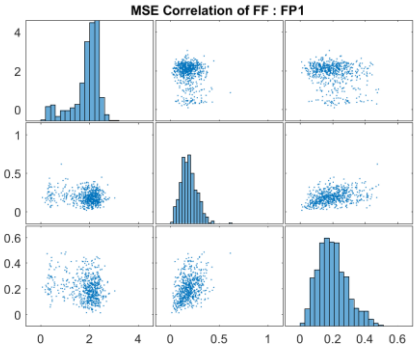


Fp1

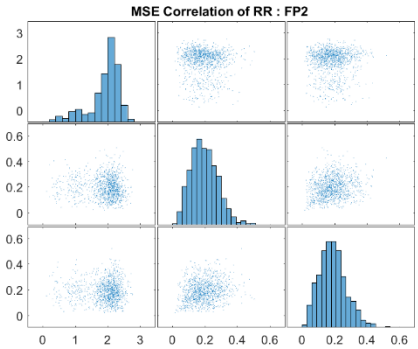

MSE Correlation of RR : FP1

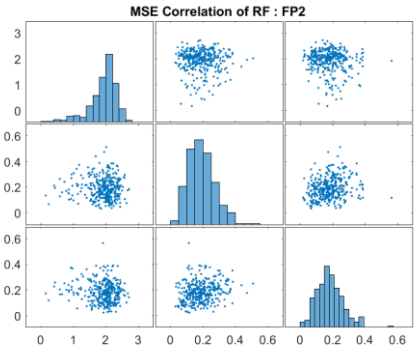

MSE Correlation of RF : FP1

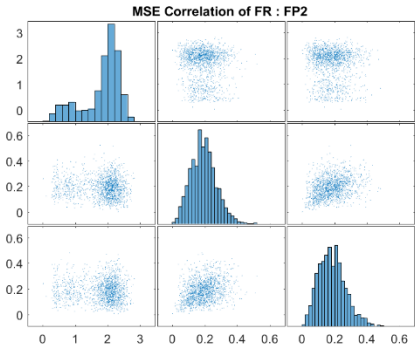

MSE Correlation of FR : FP1

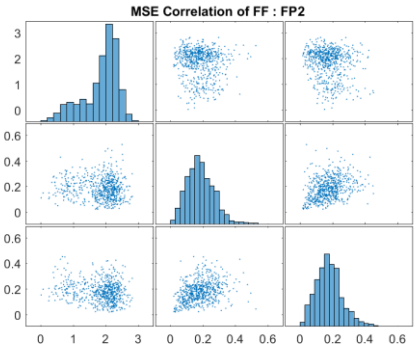

MSE Correlation of FF : FP1

Fp2

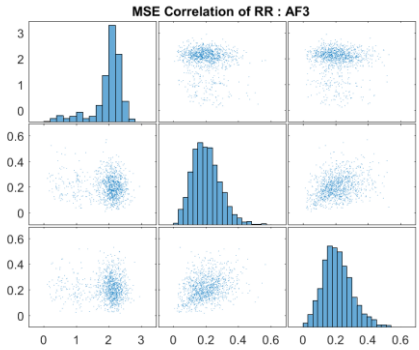

MSE Correlation of RR : FP2

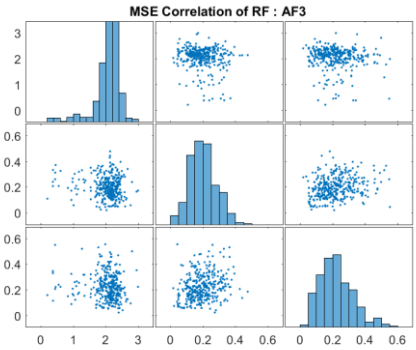

MSE Correlation of RF : FP2

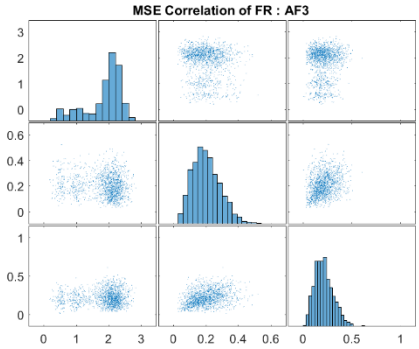

MSE Correlation of FR : FP2

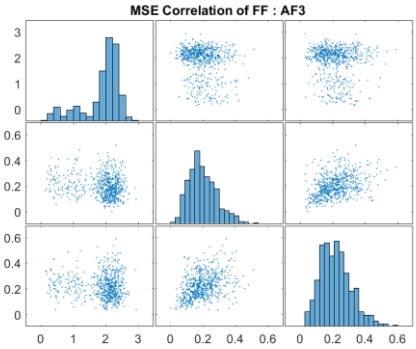

MSE Correlation of FF : FP2

AF3

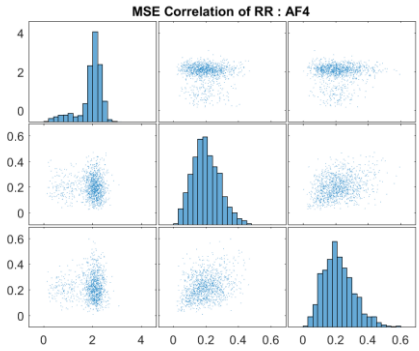

MSE Correlation of RR : AF3

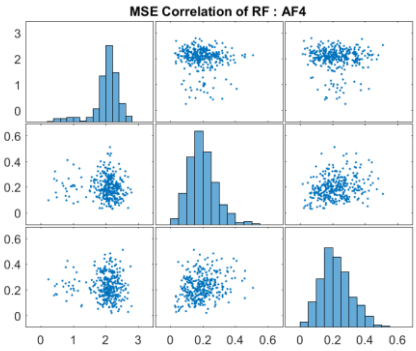

MSE Correlation of RF : AF3

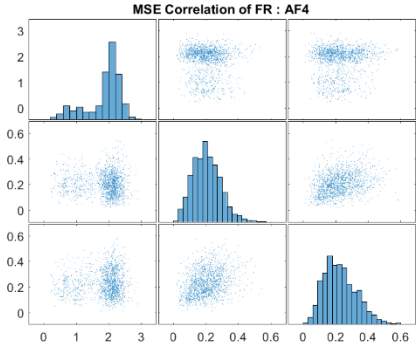

MSE Correlation of FR : AF3

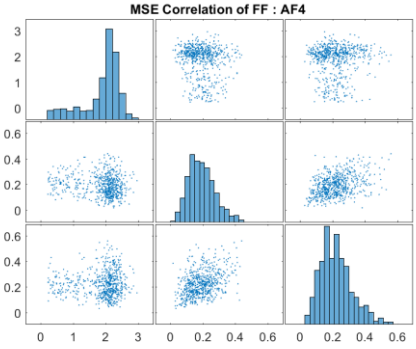

MSE Correlation of FF : AF3

AF4

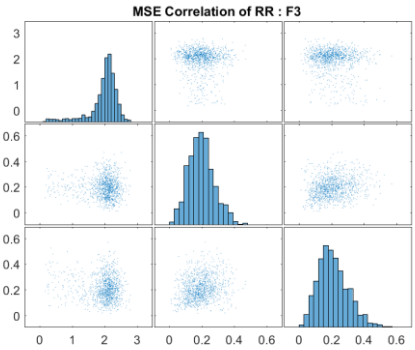

MSE Correlation of RR : AF4

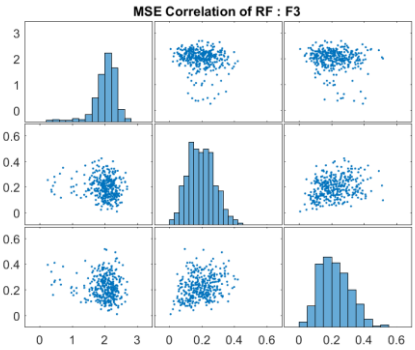

MSE Correlation of RF : AF4

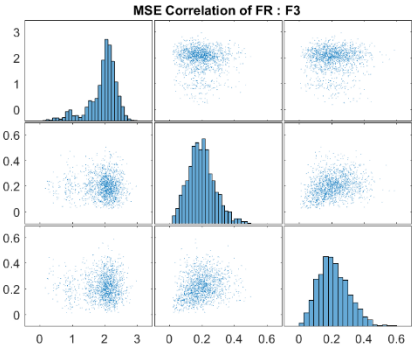

MSE Correlation of FR : AF4

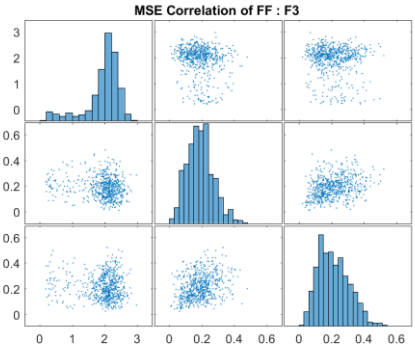

MSE Correlation of FF : AF4

F3

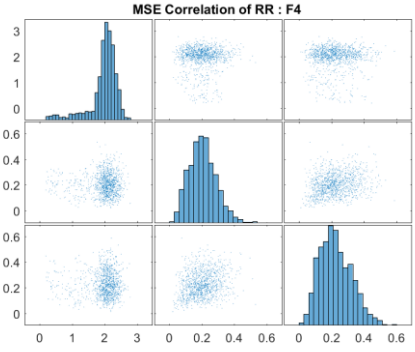

MSE Correlation of RR : F3

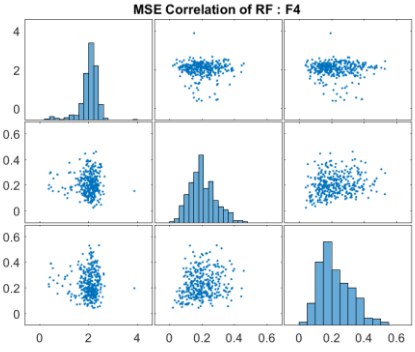

MSE Correlation of RF : F3

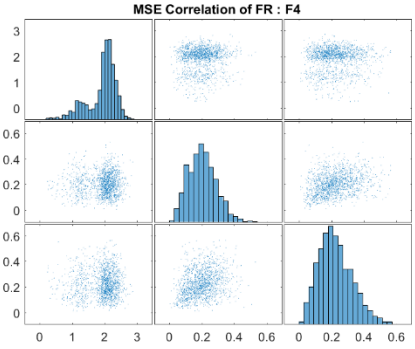

MSE Correlation of FR : F3

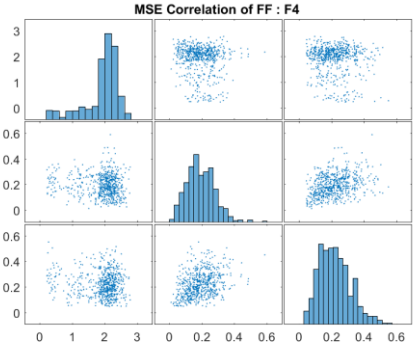

MSE Correlation of FF : F3

F4

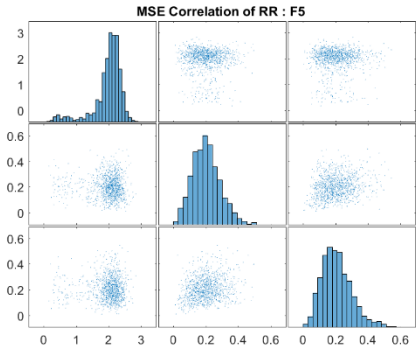

MSE Correlation of RR : F4

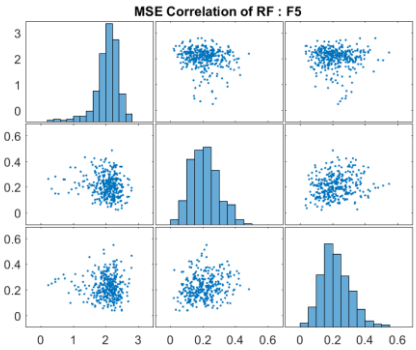

MSE Correlation of RF : F4

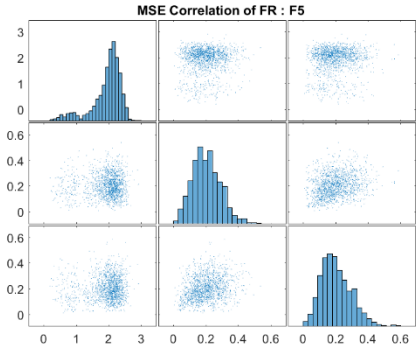

MSE Correlation of FR : F4

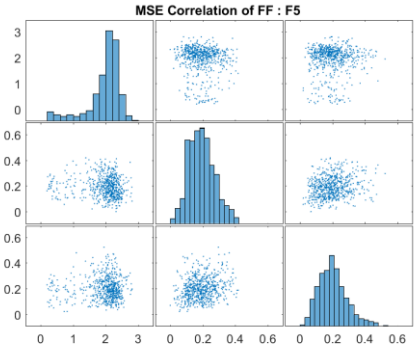

MSE Correlation of FF : F4

F5

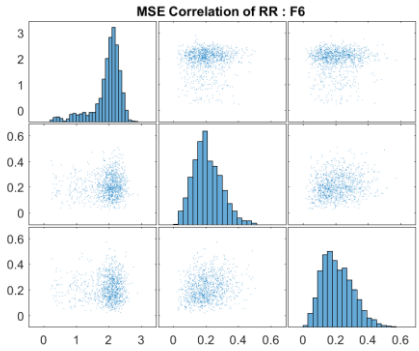

MSE Correlation of RR : F5

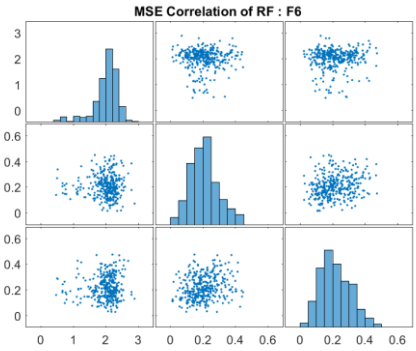

MSE Correlation of RF : F5

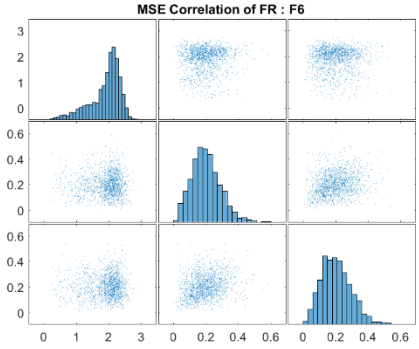

MSE Correlation of FR : F5

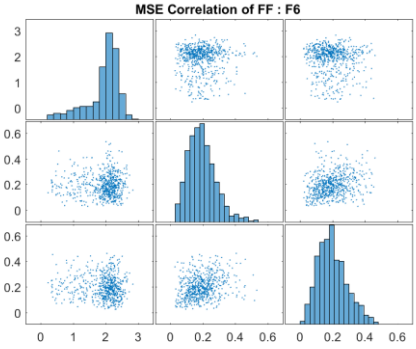

MSE Correlation of FF : F5

F6

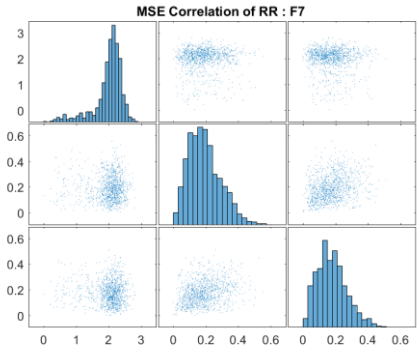

MSE Correlation of RR : F6

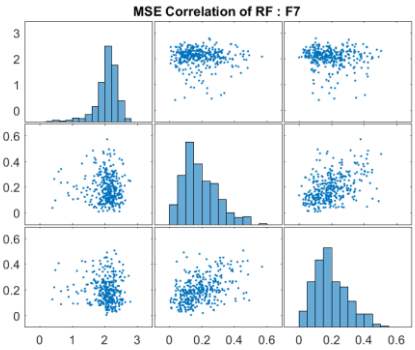

MSE Correlation of RF : F6

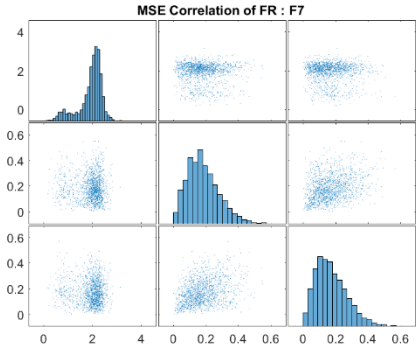

MSE Correlation of FR : F6

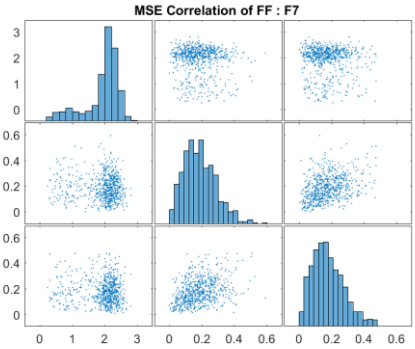

MSE Correlation of FF : F6

F7

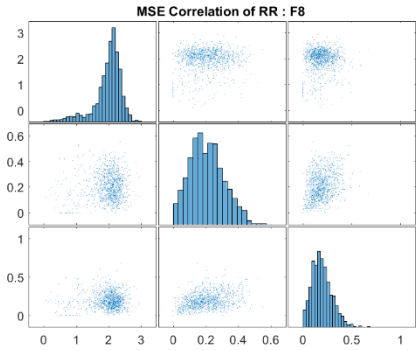

MSE Correlation of RR : F7

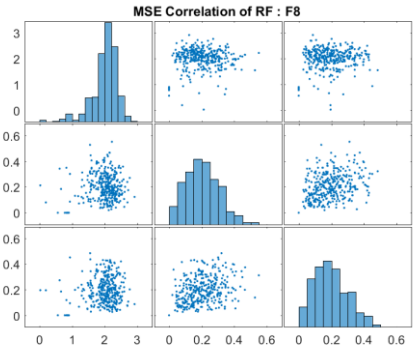

MSE Correlation of RF : F7

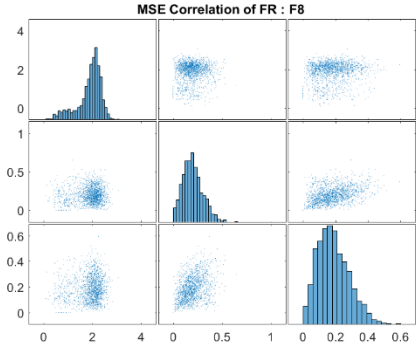

MSE Correlation of FR : F7

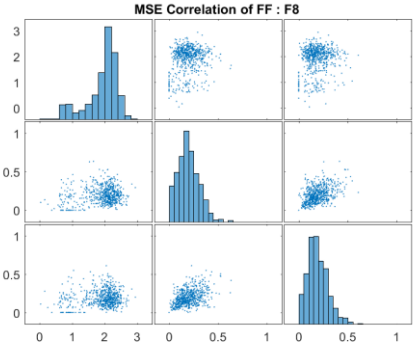

MSE Correlation of FF : F7

F8

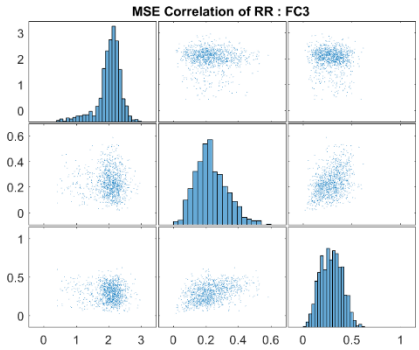

MSE Correlation of RR : F8

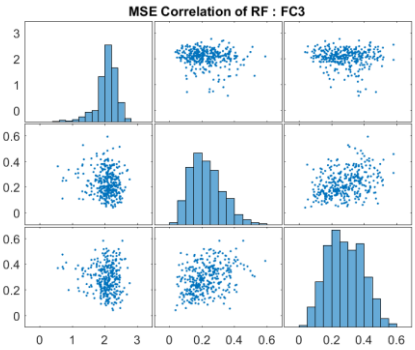

MSE Correlation of RF : F8

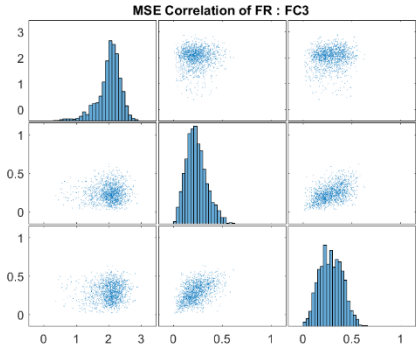

MSE Correlation of FR : F8

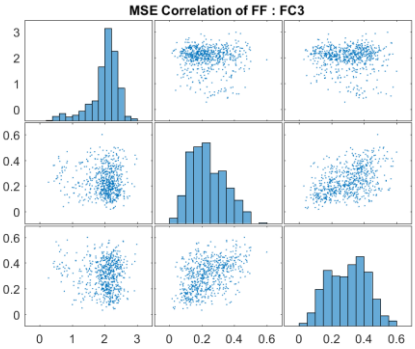

MSE Correlation of FF : F8

FC3

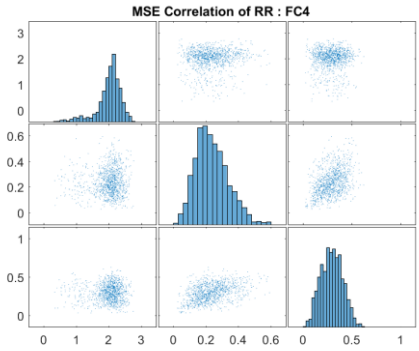

MSE Correlation of RR : FC3

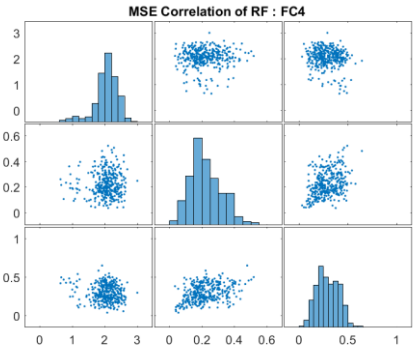

MSE Correlation of RF : FC3

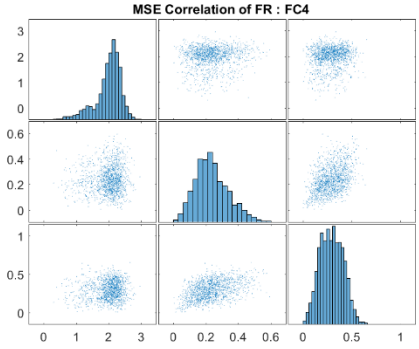

MSE Correlation of FR : FC3

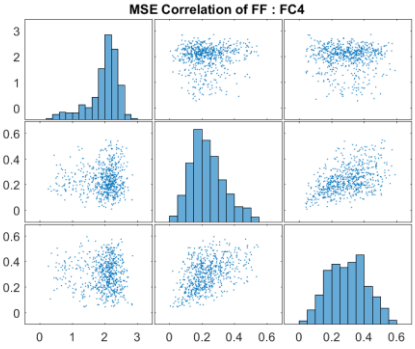

MSE Correlation of FF : FC3

FC4

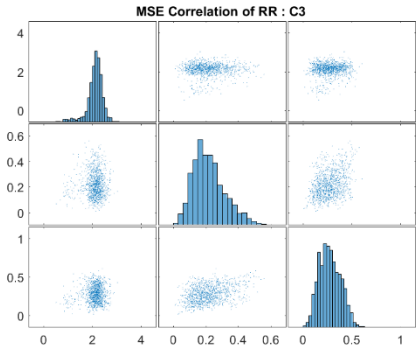

MSE Correlation of RR : FC4

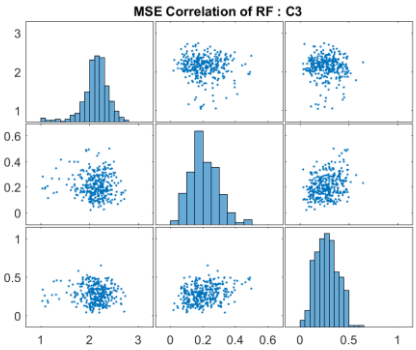

MSE Correlation of RF : FC4

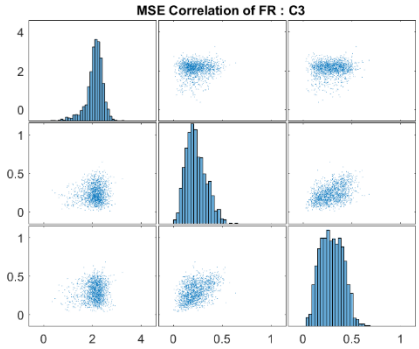

MSE Correlation of FR : FC4

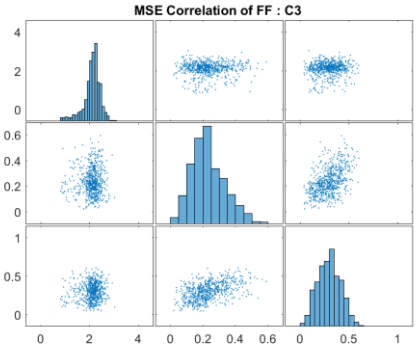

MSE Correlation of FF : FC4

C3

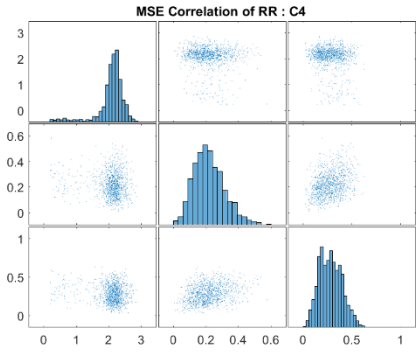

MSE Correlation of RR : C3

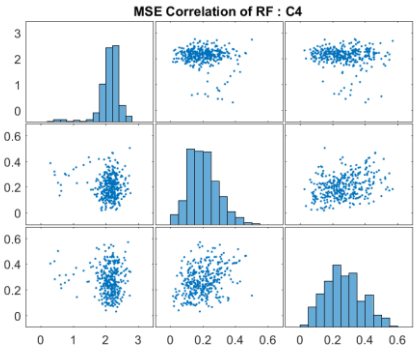

MSE Correlation of RF : C3

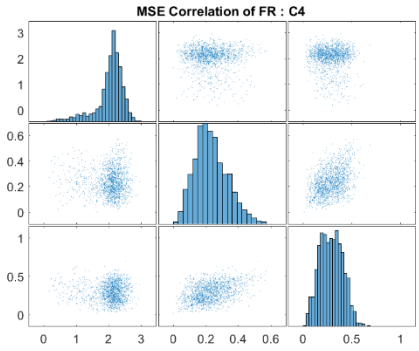

MSE Correlation of FR : C3

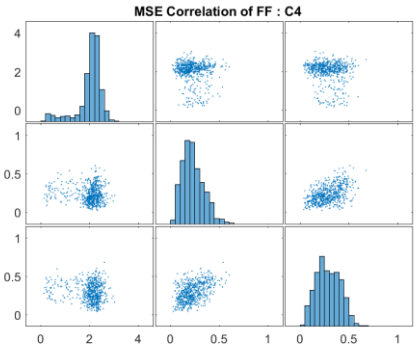

MSE Correlation of FF : C3

C4

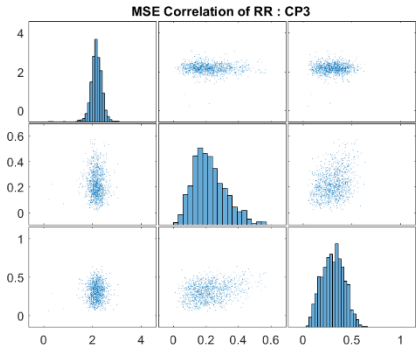

MSE Correlation of RR : C4

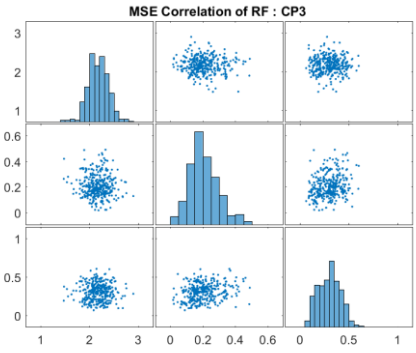

MSE Correlation of RF : C4

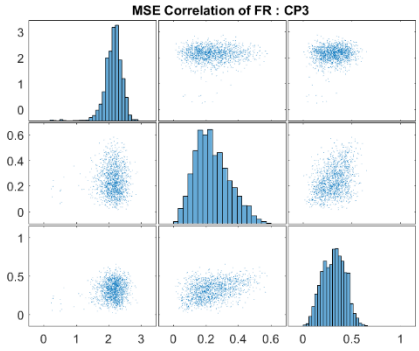

MSE Correlation of FR : C4

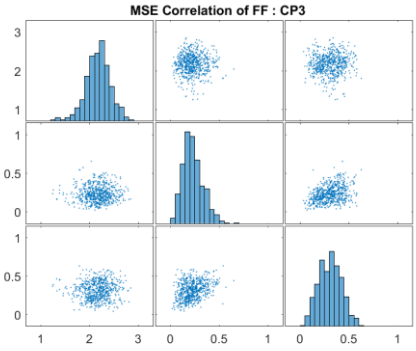

MSE Correlation of FF : C4

CP3

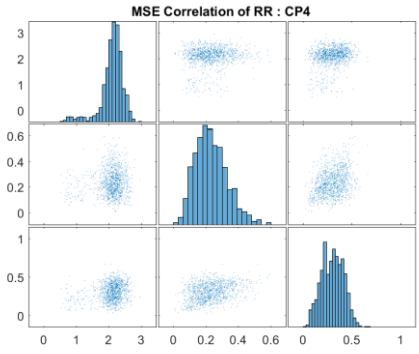

MSE Correlation of RR : CP3

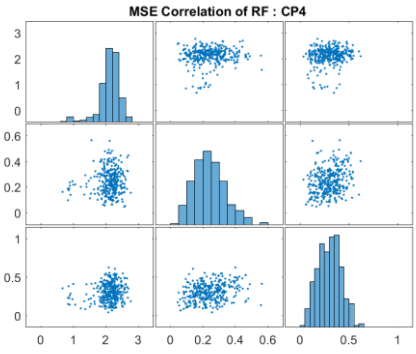

MSE Correlation of RF : CP3

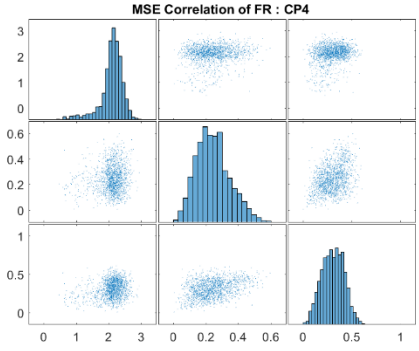

MSE Correlation of FR : CP3

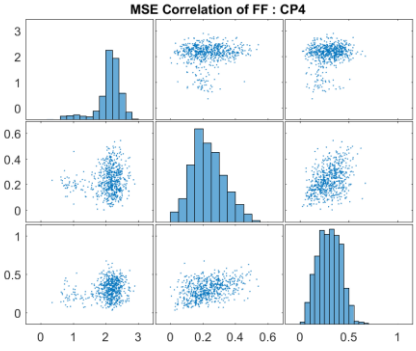

MSE Correlation of FF : CP3

CP4

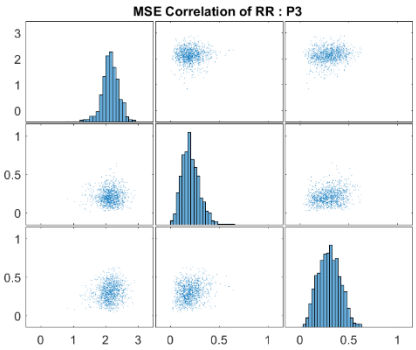

MSE Correlation of RR : CP4

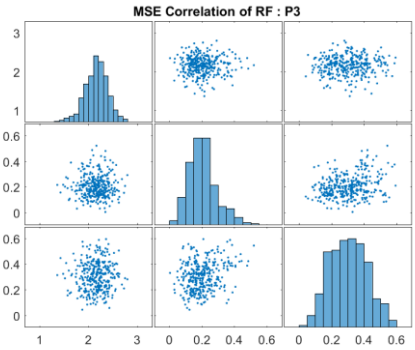

MSE Correlation of RF : CP4

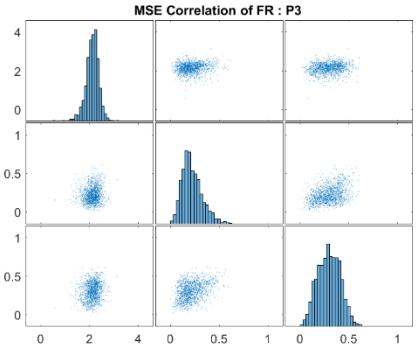

MSE Correlation of FR : CP4

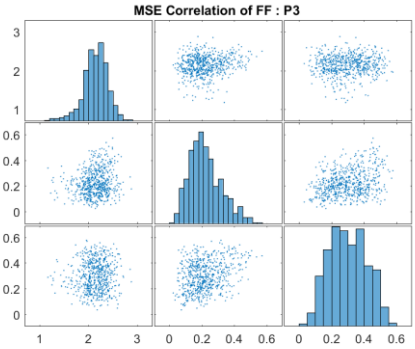

MSE Correlation of FF : CP4

P3

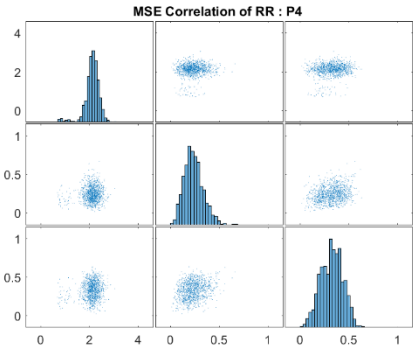

MSE Correlation of RR : P3

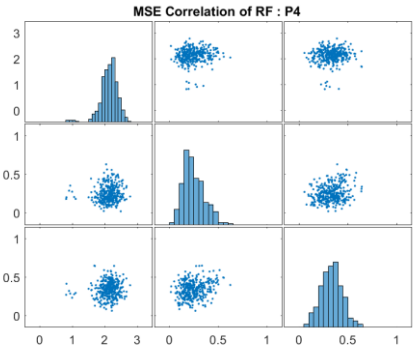

MSE Correlation of RF : P3

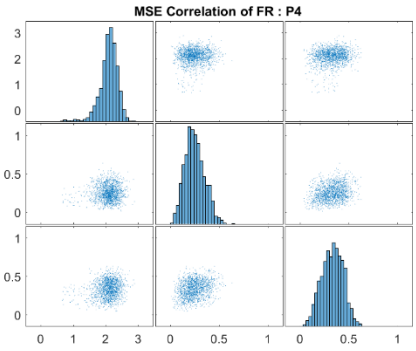

MSE Correlation of FR : P3

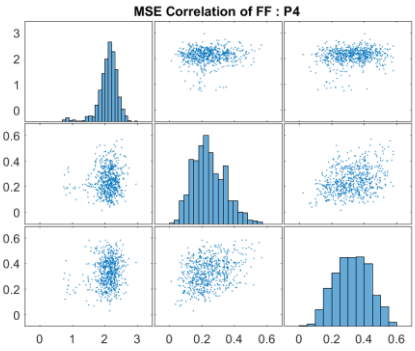

MSE Correlation of FF : P3

P4

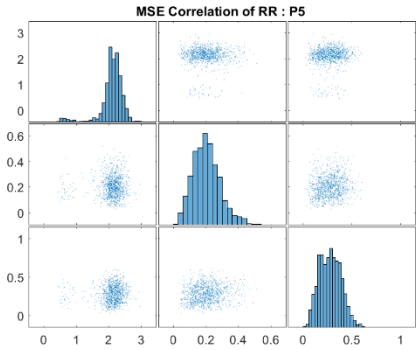

MSE Correlation of RR : P4

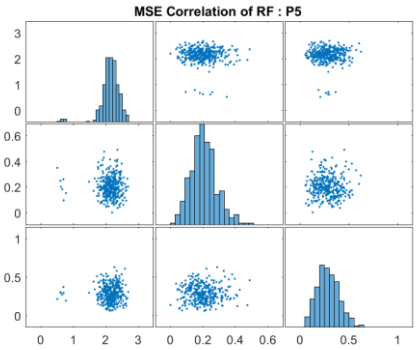

MSE Correlation of RF : P4

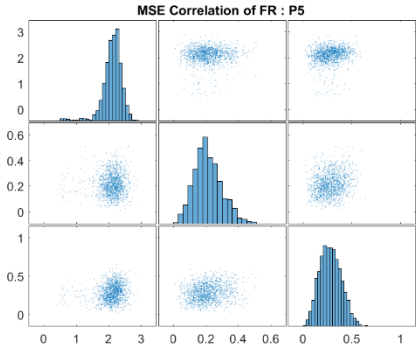

MSE Correlation of FR : P4

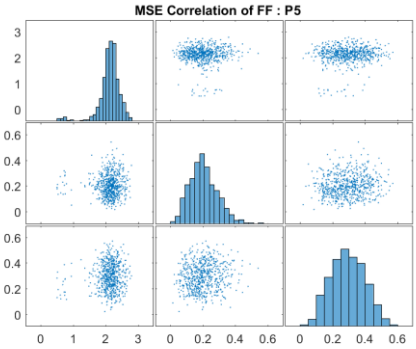

MSE Correlation of FF : P4

P5

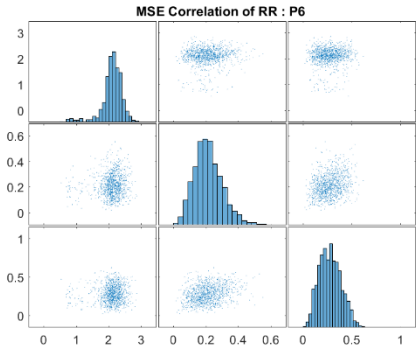

MSE Correlation of RR : P5

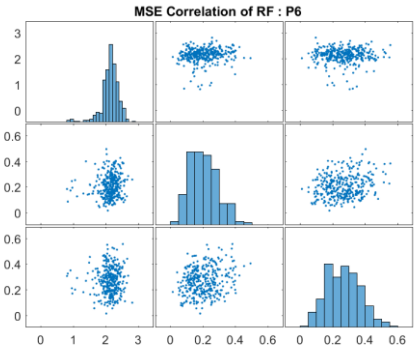

MSE Correlation of RF : P5

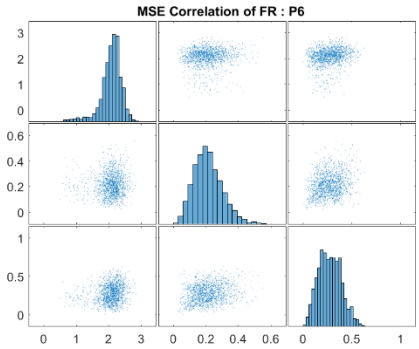

MSE Correlation of FR : P5

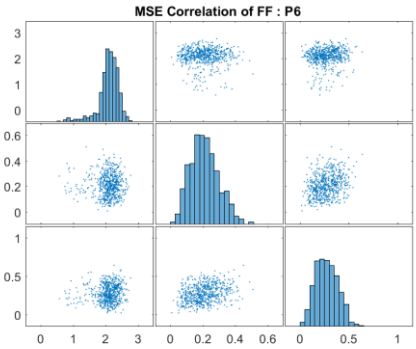

MSE Correlation of FF : P5

P6

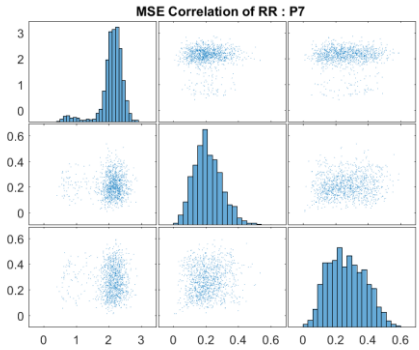

MSE Correlation of RR : P6

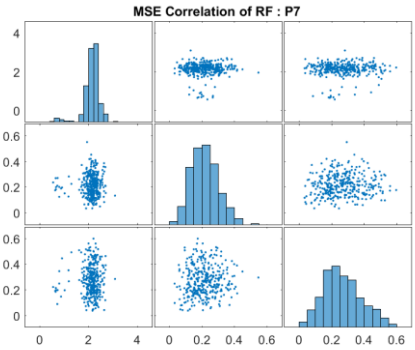

MSE Correlation of RF : P6

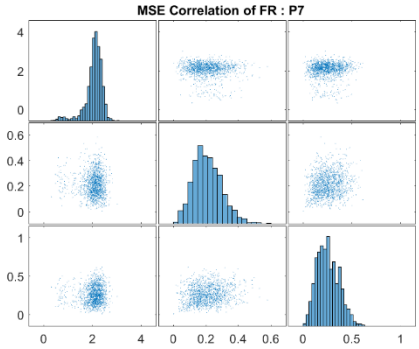

MSE Correlation of FR : P6

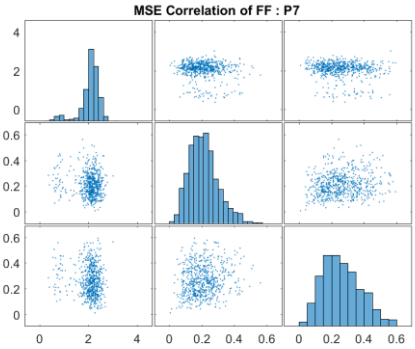

MSE Correlation of FF : P6

P7

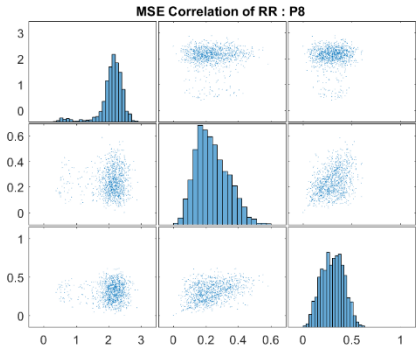

MSE Correlation of RR : P7

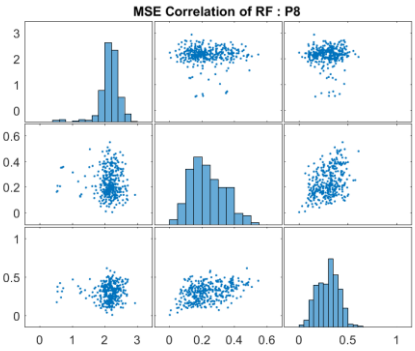

MSE Correlation of RF : P7

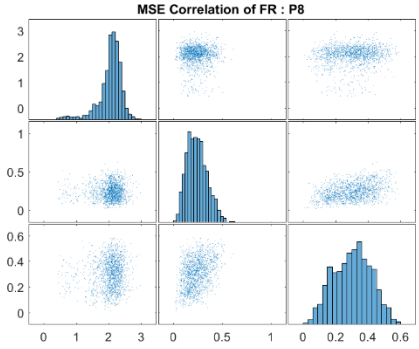

MSE Correlation of FR : P7

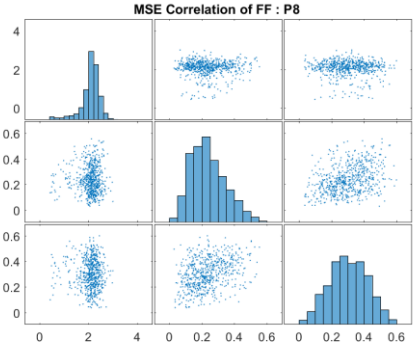

MSE Correlation of FF : P7

P8

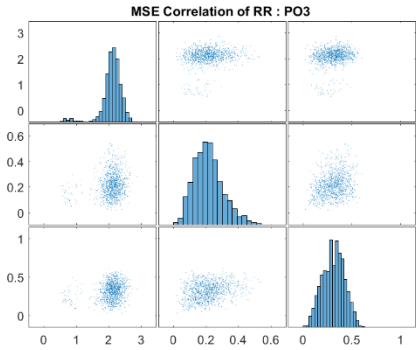

MSE Correlation of RR : P8

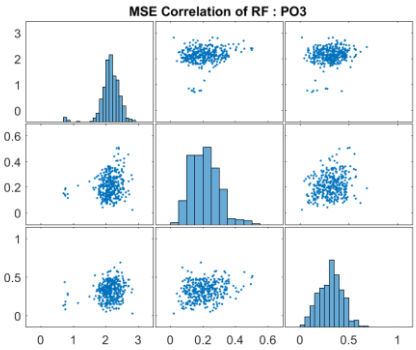

MSE Correlation of RF : P8

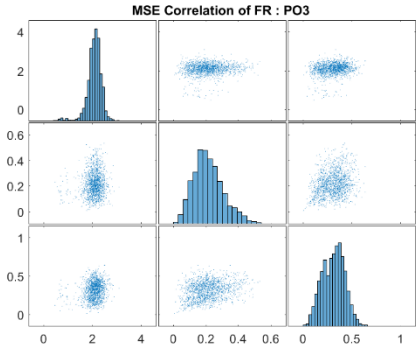

MSE Correlation of FR : P8

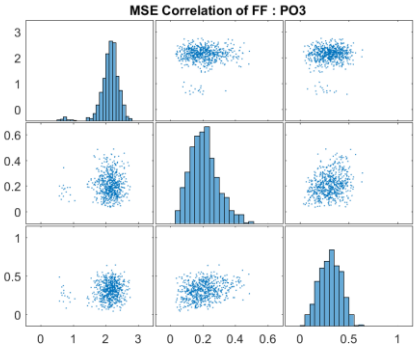

MSE Correlation of FF : P8

PO3

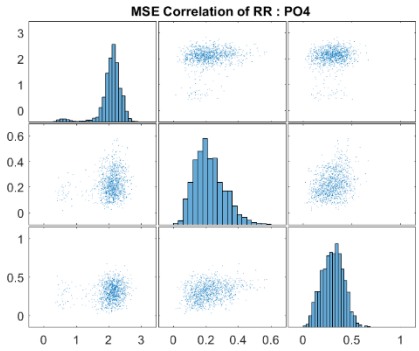

MSE Correlation of RR : PO3

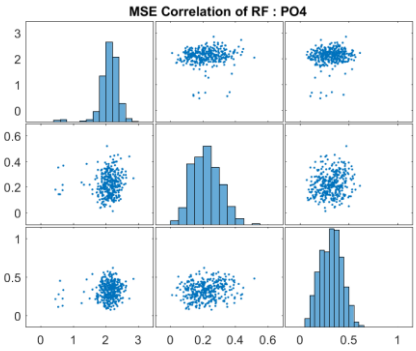

MSE Correlation of RF : PO3

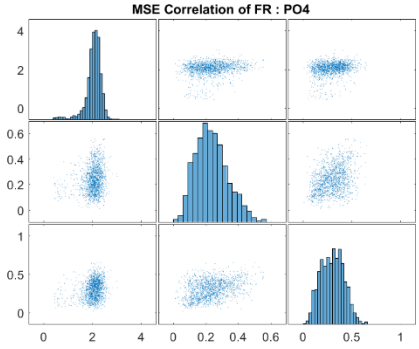

MSE Correlation of FR : PO3

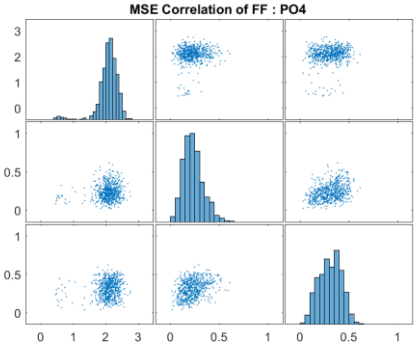

MSE Correlation of FF : PO3

PO4

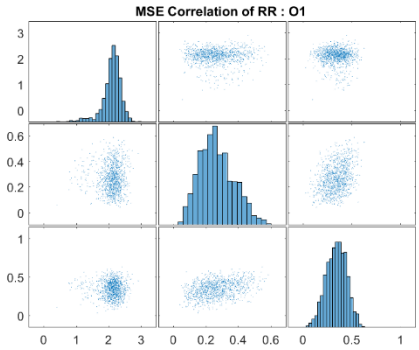

MSE Correlation of RR : PO4

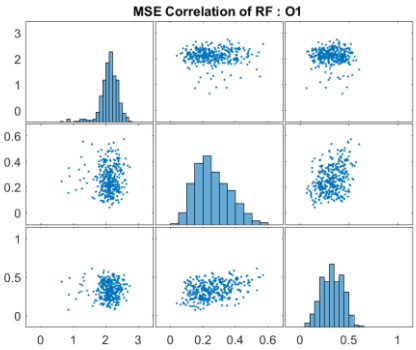

MSE Correlation of RF : PO4

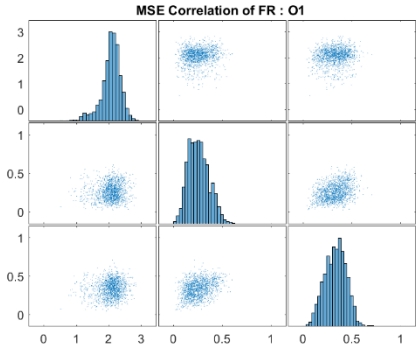

MSE Correlation of FR : PO4

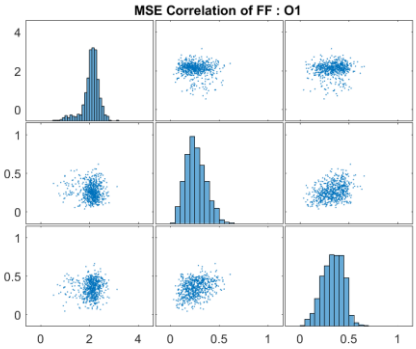

MSE Correlation of FF : PO4

O1

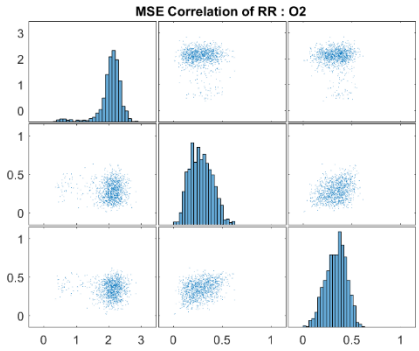

MSE Correlation of RR : O1

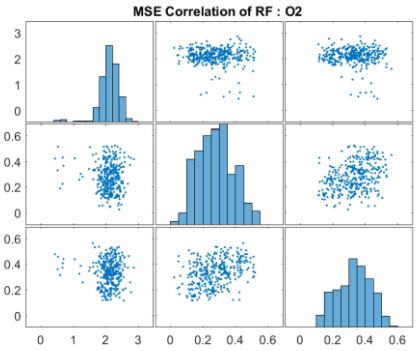

MSE Correlation of RF : O1

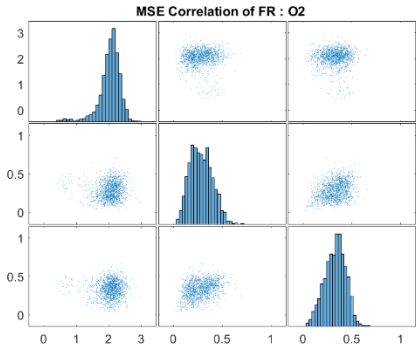

MSE Correlation of FR : O1

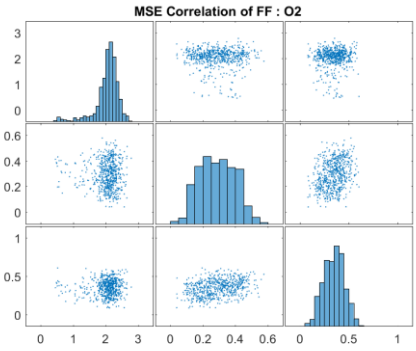

MSE Correlation of FF : O1

O2

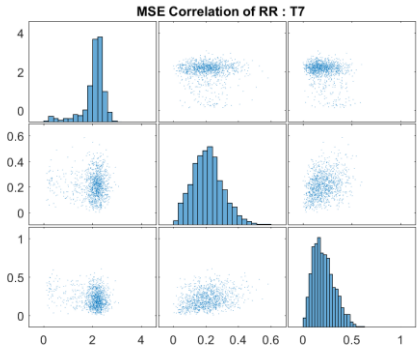

MSE Correlation of RR : O2

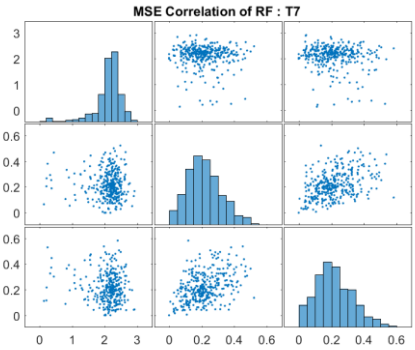

MSE Correlation of RF : O2

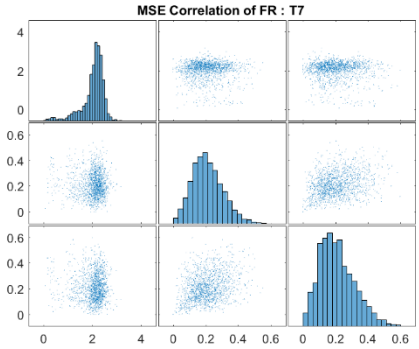

MSE Correlation of FR : O2

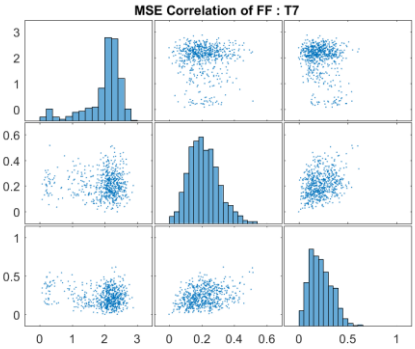

MSE Correlation of FF : O2

T7

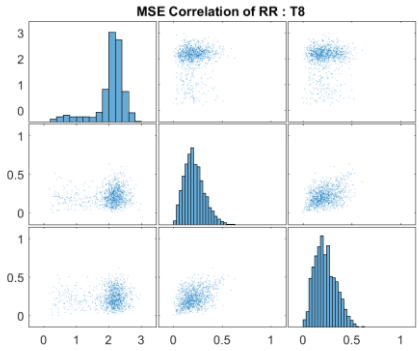

MSE Correlation of RR : T7

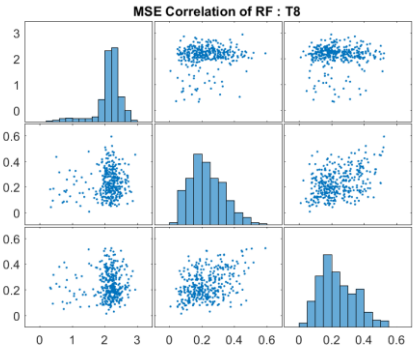

MSE Correlation of RF : T7

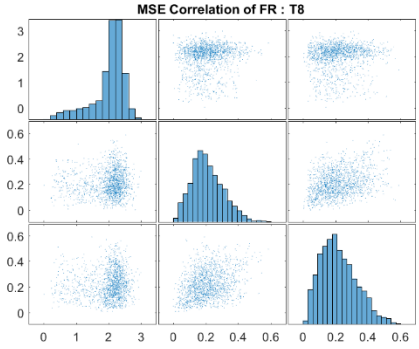

MSE Correlation of FR : T7

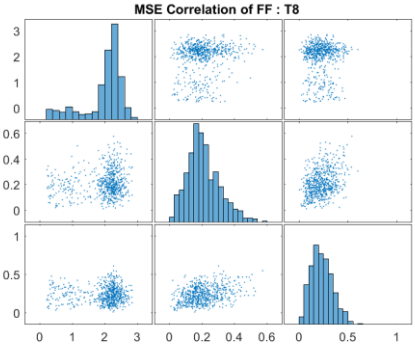

MSE Correlation of FF : T7

T8


MSE Correlation of RR : T8


MSE Correlation of RF : T8

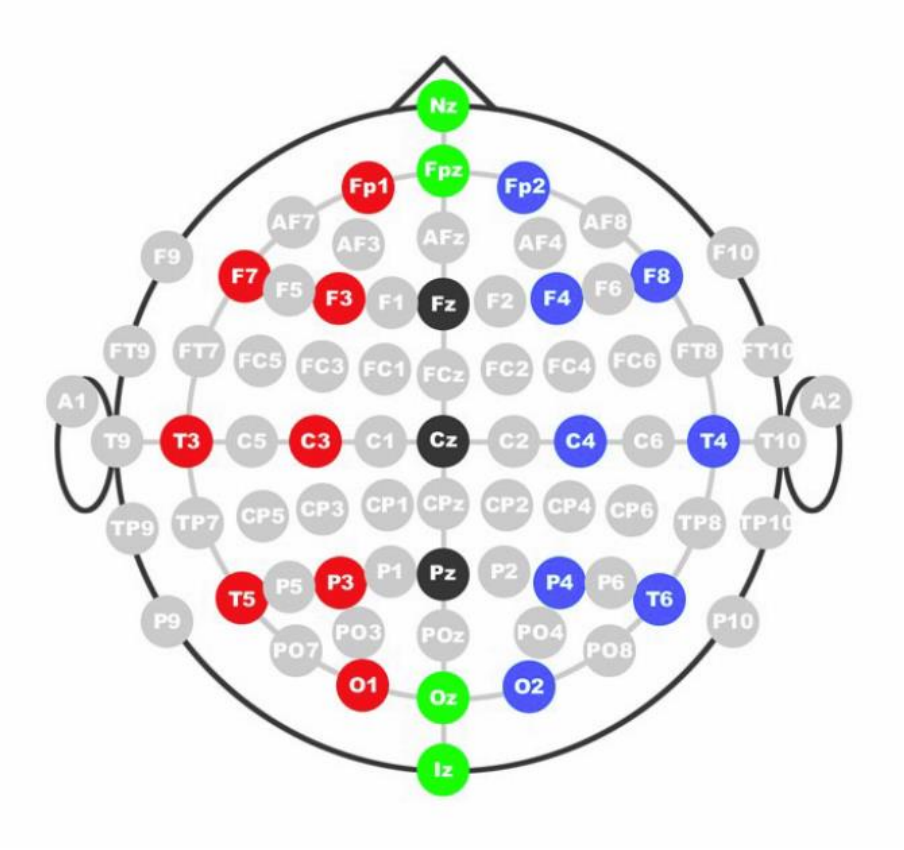

MSE Correlation of FR : T8


MSE Correlation of FF : T8

APPENDIX G

Brain Areas and Brain Functions

10/10 and 10/20 Electrode Positions



Corresponding Brodmann Areas

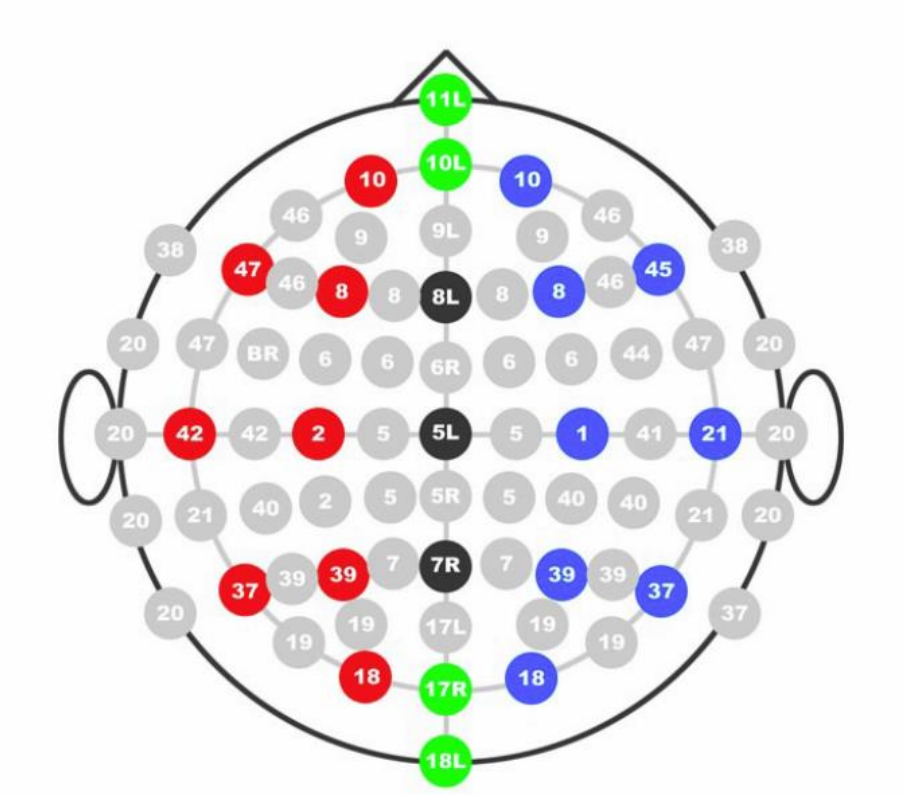


Table Appendix F

10/20 System	Brodmann Area	Brain Functions
AF3, AF4	9	Motor planning, WM, short-term memory, Memory encoding and recognition, Memory retrieval
F3	8	Eye movements, visuospatial function, WM, perceptual priming, visuospatial and visuomotor attention
F5	47	Language and emotion, WM, Episodic long-term memory
F7	38	Multimodal memory retrieval, Language functions, Self /other distinction
FC3, FC4	6	Sequencing/planning, visuospatial function, WM, Episodic long – term memory, visuospatial and visuomotor attention
C4	1	The sense of touch, Finger proprioception
CP3	2	The sense of touch, Finger proprioception
P3	39	Calculation, Reading, Spatial focusing of attention, Processing a sequence of actions
O2	18	Detection of light intensity, tracking visual motion patterns, visual priming, attention in visual processing
T8	21	Prosodic integration, processing complex sounds

Ref: N. A. Trans Cranial Technologies, *Cortical Functions Reference*, Wan Chai, Hong Kong: Trans Cranial Technologies ldt., 2012.